Aus dem Institut für Molekulare Medizin I

der Heinrich-Heine-Universität Düsseldorf

Elimination of chemotherapeutic-resistant tumors by natural product-induced cell death

Dissertation

zur Erlangung des Grades eines *Doctor rerum medicarum (Dr. rer. med.)*

der Medizinischen Fakultät der Heinrich-Heine-Universität Düsseldorf

vorgelegt von

Laura Schmitt

2023

Als Inauguraldissertation gedruckt mit Genehmigung der Medizinischen Fakultät der Heinrich-Heine-Universität Düsseldorf.

Gez.:

Dekan:	Prof. Dr. Nikolaj Klöcker
Gutachter/in:	Prof. Dr. Sebastian Wesselborg, Prof. Dr. Gerhard Fritz,
	Prof. Dr. Verena Jendrossek

Dedication

Without research, there is no hope

Without hope, there is no cure

–

Unknown

Nature itself is the best physician

–

Hippocrates

Publications

The following parts of this dissertation were published:

The mycotoxin viriditoxin induces leukemia- and lymphoma-specific apoptosis by targeting mitochondrial metabolism

Stuhldreier F*, **Schmitt L***, Lenz T, Hinxlage I, Zimmermann M, Wollnitzke P, Schliehe-Diecks J, Liu Y, Jäger P, Geyh S, Teusch N, Peter C, Bhatia S, Haas R, Levkau B, Reichert A, Stühler K, Proksch P, Stork B, Wesselborg S. The mycotoxin viriditoxin induces leukemia- and lymphoma-specific apoptosis by targeting mitochondrial metabolism. *Cell Death and Disease*. 2022, *equally contributing first authors, doi: 10.1038/s41419-022-05356-w [1]

40 Years of research on polybrominated diphenyl ethers (PBDEs) – A historical overview and newest data of a promising anticancer drug

Schmitt L, Hinxlage I, A Cea P, Gohlke H, Wesselborg S. 40 Years of research on polybrominated diphenyl ethers (PBDEs) – A historical overview and newest data of a promising anticancer drug. *Molecules*. 2021, doi: 10.3390/molecules26040995 [2]

Zusammenfassung

Die außergewöhnliche chemische Vielfalt der Natur macht Naturprodukte zu einer wertvollen Quelle für bioaktive Verbindungen mit therapeutischem Potenzial. Diese Arbeit konzentriert sich auf die Untersuchung zytotoxischer Naturstoffe und halbsynthetischer Substanzen als potenzielle Krebsmedikamente für Leukämie und Lymphome. Dazu wurden zwei Naturstoffe, Viriditoxin (VDT) und Bromoxib, sowie die halbsynthetischen Meriolin-Derivate Meriolin 16 und 36, als Substanzen mit vielversprechenden krebsbekämpfenden Eigenschaften identifiziert und auf ihre molekularen Mechanismen hin untersucht.

Die Bioaktivität des Mykotoxins VDT wurde in dieser Arbeit im Rahmen der umfassenden Überarbeitung eines Manuskripts untersucht. In diesem Manuskript wurde gezeigt, dass VDT eine ausgeprägte Wirkung auf Leukämie- und Lymphomzellen hat und Apoptose induziert, indem es direkt den intrinsischen mitochondrialen Todesweg aktiviert, selbst in Anwesenheit von anti-apoptotischem Bcl-2-Protein. Die mitochondriale Toxizität von VDT wurde durch die Hemmung der mitochondrialen Atmung, den Abbau des mitochondrialen Membranpotenzials, die Freisetzung von mitochondrialem Cytochrom c, die Bildung reaktiver Sauerstoffspezies und die anschließende Degradierung von Mitochondrien bestätigt. Zur Target-Identifizierung mittels des *thermal-proteome-profiling* wurden 20 mitoribosomale Proteine nach VDT-Behandlung ermittelt. Daher wurde in dieser Arbeit die Wirkung von VDT auf die mitoribosomale Translation weiter untersucht, konnte aber nicht bestätigt werden. Insgesamt könnte die gezielte Beeinflussung der mitochondrialen Atmung durch VDT einen vielversprechenden therapeutischen Ansatz für die Behandlung von Leukämie und Lymphomen darstellen.

Bromoxib gehört zur Verbindungsklasse der polybromierten diphenylether (PBDEs), und die Autorin dieser Dissertation hat im Rahmen eines umfassenden Übersichtartikels über PBDEs eine erste Struktur-Aktivitäts-Beziehungsanalyse für Bromoxib vorgelegt. In früheren Studien wurde Bromoxib als ein Naturprodukt mit therapeutischer Bedeutung für Leukämiepatienten identifiziert, da es im Gegensatz zu gesunden Zellen vor allem leukämische Zellen angreift. Diese Ergebnisse machten Bromoxib zu einem interessanten Kandidaten, der im Rahmen dieser Arbeit hinsichtlich seines molekularen Mechanismus weiter untersucht wurde. Bromoxib wirkt selektiv auf Lymphome, indem es den intrinsischen mitochondrialen Apoptoseweg aktiviert. In dieser Arbeit wurde Bromoxib als Protonophor identifiziert, das den sofortigen Kollaps des mitochondrialen Membranpotenzials induziert und den intrazellulären ATP-Spiegel durch Hemmung der oxidativen Phosphorylierung und durch Reduktion der Glykolyse senkt. Dadurch wird ein Zusammenbruch der Zellatmung ausgelöst, der zu einer energetischen Katastrophe innerhalb der Krebszelle führt. Darüber hinaus wurde festgestellt,

dass dieses energetische Desaster durch den verstärkten Abbau von Fettsäuren kompensiert wird. Es wurde gezeigt, dass Bromoxib ausgewählte Proteine der mitochondrialen Fettsäure-β-Oxidation stabilisiert, um ATP aus dem Abbau von Fettsäuren zu generieren, als schneller Rettungsmechanismus. Schließlich wurde festgestellt, dass die anhaltende Schädigung durch Bromoxib die intrinsische mitochondrien-abhängige Apoptose aktiviert. Zusammenfassend lässt sich sagen, dass Bromoxib in der vorliegenden Arbeit als ein potenzielles Therapeutikum identifiziert wurde, das auf den *‘deregulierten Zellstoffwechsel‘* von Lymphomen abzielt.

Die halbsynthetischen Verbindungen, Meriolin 16 und 36, haben sich in dieser Arbeit als multifunktionale Krebsmedikamente erwiesen, die auf verschiedene Krebsmerkmale abzielen. Merioline sind hochgradig zytotoxisch und aktivieren den intrinsischen mitochondrialen Apoptoseweg selbst in Gegenwart von anti-apoptotischem Bcl-2-Protein. Diese Substanzen sind nicht nur potente Apoptoseinduktoren, sondern auch wirksame Kinaseinhibitoren, insbesondere der CMGC-Familie (CDKs, MAPKs, GSK3s und CLKs). Es wurde gezeigt, dass Merioline den Zellzyklus hemmen, die Proliferation verringern und wichtige regulatorische Proteine des Zellzyklus verändern. Darüber hinaus induzieren sie DNA-Schäden und verringern die *de novo* RNA-Synthese. Viele der molekularen Signalwege, auf die die Merioline abzielen, sind in chemotherapieresistenten Tumoren verändert. Die untersuchten unterschiedlichen Effektormechanismen, die durch Merioline induziert werden, unterstreichen somit ihr therapeutisches Potenzial für die Behandlung von Leukämie und Lymphomen.

Zusammenfassend lässt sich sagen, dass die enorme chemische Vielfalt der Natur noch immer eine wertvolle Ressource an bioaktiven Verbindungen mit therapeutischem Potenzial bietet, um eine der weltweit häufigsten Todesursachen – Krebs – zu bekämpfen.

Summary

The exceptional chemical diversity in nature provides natural products as a valuable source of bioactive compounds with therapeutic potential. This work focuses on the investigation of cytotoxic natural products and semisynthetic substances as potential anticancer drugs in leukemia and lymphoma. The aim of the present work as a subproject of the Research Training Group 2158 (RTG 2158) was the identification and characterization of natural products in order to eliminate chemotherapeutic-resistant tumors by natural product-induced cell death. For this objective, two natural products, Viriditoxin (VDT) and Bromoxib, and the semisynthetic Meriolin derivatives, Meriolin 16 and 36, were identified as substances with promising anticancer properties and investigated concerning their molecular mechanisms.

The bioactivity of the mycotoxin VDT was investigated within this thesis in context of the comprehensive revision of a manuscript. In this manuscript it was shown, that VDT exhibited a pronounced effect on leukemia and lymphoma cells and induces apoptosis by directly targeting the intrinsic mitochondrial death pathway even in the presence of anti-apoptotic Bcl-2 proteins. The breakdown of mitochondrial membrane potential and respiration, the generation of reactive oxygen species and the release of cytochrome c with fragmentation of the mitochondria confirmed the mitochondrial toxicity of VDT. For target-identification, the thermal proteome profiling approach rendered 20 mitoribosomal proteins upon VDT treatment. Consequently, within this thesis the effect of mitoribosomal translation was further investigated but could not be confirmed. Taken together, the treatment of leukemia and lymphoma by targeting the mitochondrial respiration with VDT, might be a promising therapeutic approach.

Bromoxib belongs to the compound class of polybrominated diphenyl ethers (PBDEs) and the author of this thesis presented within an extensive literature review of PBDEs, a first structure-activity-relationship analysis for Bromoxib. In previous studies, Bromoxib was identified as a natural product of therapeutic relevance for patients with leukemia, since it affected primarily leukemic cells in contrast to their healthy counterparts. These results rendered Bromoxib as an interesting candidate for further investigation in this thesis in terms of its molecular mechanism. Bromoxib targets selectively lymphomas, by activating the intrinsic mitochondrial apoptosis pathway. In this thesis, Bromoxib was discovered as a protonophore, inducing the rapid breakdown of mitochondrial membrane potential, reducing intracellular ATP-levels by inhibiting oxidative phosphorylation and impairing glycolysis, thereby inducing a breakdown of cellular respiration leading to an energetic disaster within the cancer cell. Moreover, this energetic disaster was found to be compensated by increased degradation of fatty acids during mitochondrial β-oxidation. Bromoxib was found to stabilize selected proteins of the mitochondrial fatty acid β-oxidation in order to generate ATP from fatty acids as a rapid rescue

mechanism. Finally, the prolonged damage was found to activate intrinsic mitochondria dependent apoptosis. In summary, Bromoxib was identified in the present work as a small molecule targeting the hallmark of *'deregulated cellular metabolism'* in lymphoma.

The semisynthetic compounds Meriolin 16 and 36 were proven in this thesis to be multifunctional drugs targeting different hallmarks of cancer. Meriolins exhibit a high level of cytotoxicity and trigger the intrinsic mitochondrial apoptosis pathway, despite the presence of anti-apoptotic Bcl-2 protein. These substances are not only potent apoptosis inducers but also effective kinase inhibitors, especially of the CMGC family (CDKs, MAPKs, GSK3s and CLKs). Meriolins were shown to inhibit the cell cycle, reduce proliferation and alter key regulatory proteins of the cell cycle. Moreover, they induce DNA damage and reduce *de novo* RNA synthesis. Many of the molecular pathways targeted by Meriolins are altered in chemotherapeutic-resistant tumors. Thus, the investigated different effector mechanisms induced by Meriolins underscores their therapeutic potential for the treatment of leukemia and lymphoma.

In conclusion, the utilization of the vast chemical diversity found in nature still offers a valuable resource of bioactive compounds with therapeutic potential in order to fight one of the world's leading causes of death – cancer.

Abbreviations, Prefixes, Units

ACADVL	Acyl-CoA dehydrogenase very long chain
ACSL	Acyl-CoA syntethase long chain
ADP	Adenosine diphosphate
AIF	Apoptosis inducing factor
ALDO	Fructose biphosphate aldolase
ALL	Acute lymphoblastic leukemia
AML	Acute myeloid leukemia
ANT	Adenine nucleotide translocator
ASSP	Apoptosis-stimulating protein of p53
ATF	Activating transcription factor
ATM	Ataxia telangiectasia mutated
ATP	Adenosine triphosphate
ATR	Ataxia telangiectasia and Rad3 related protein
APAF	Apoptotic protease activating factor
APC/C	Anaphase-promoting complex/cyclosome
APEX	Apurinic apyrimidinic endonuclease
BAD	Bcl-2 associated agonist of cell death protein
BAK	Bcl-2 antagonist killer 1
BAX	Bcl-2-associated x protein
Bcl-2	B cell lymphoma 2
Bcl-$_w$	Bcl-2 like protein 2
Bcl-$_{XL}$	Bcl-2-related gene long isoform
BER	Base excision repair
BH3	Bcl-2 homology (BH) domain
BID	BH3-interactig death domain agonist
BIM	Bcl-2 interacting mediator of cell death
BIRC2	Baculoviral IAP repeat-containing protein 2
BMF	Bcl-2 modifying factor
BOK	Bcl-2-related ovarian killer
BRCA	Breast cancer type 1 susceptibility protein
Ca^{2+}	Calcium
CACT	Carnitine/acyl-carnitine translocase
CAD	Caspase-activated DNase
CAP	Chloramphenicol
Caspase/Casp	Aspartate-specific cysteine protease
CARD	Caspase recruitment domain
CCCP	Carbonyl cyanide m-chlorophenyl hydrazone
CD95	Cluster of differentiation 95
CDK	Cyclin-dependent kinase
CE	Cholesterylester
c-FLIP	Casp8 and FADD-like apoptosis regulator
caMK	Calmodulin-dependent protein kinase
CDC	Cell division control
CHK	Checkpoint kinase
CHX	Cycloheximide
c-IAP	Cellular inhibitor of apoptosis protein
CLK	CDC-like kinase
CLN	Cardiolipin
CoA	Coenzyme A
COX	Cytochrome c oxidase
CMGC family	CDKs, MAPKs, GSKs and CLKs
CPT	Carnitine palmitoyl transferase
CsA	Cyclosporine A
CTD	C-terminal domain
CTZ	Clotrimazol
CypD	Cyclophilin D
DD	Death domain
DDR	DNA damage response
DDRNA	DNA damage response RNA
DRP(1)	Dynamin-related protein 1
DRP	DNA repair pathways
DED	Death effector domain
DG	Diglyceride
DIABLO	Direct IAP binding protein with low PI
DICER	Endoribonuclease Dicer
dilncRNA	Damage-induced long non-coding RNA
DISC	Death-inducing signaling complex
DSB	Double strand break
DMSO	Dimethyl sulfoxide
DNA	Deoxyribonucleic acid
DNA-PK	DNA-dependent protein kinase
DR	Death receptor
DROSHA	RNAse III Drosha
DRP	Dynamin-related protein
ECH	Enoyl-CoA hydratase
ENDOG	Endonuclease G
ENO	Phosphopyruvate hydratase
ER	Endoplasmic Reticulum
ERK	Extracellular signal-regulated protein kinase
ETC	Electron transport chain
ETO/ETOPO	Etoposide
EXO	Exonuclease

FA	Fatty acid
FAO	Fatty acid β-oxidation
FADD	FAS-associated death domain protein
$FAD/FADH_2$	Flavin-adenine dinucleotide
FeS	Iron-sulfur
FFA	Free fatty acid
FIS	Fission protein
FMN	Flavin mononucleotide
FOXM	Forkhead box protein M
G-3-P	Glucose-3-phosphate
G-6-P	Glucose-6-phosphate
GADD	Growth-arrest- and DNA-damage inducible gene
GAPDH	Glyceraldehyde-3-phosphate dehydrogenase
GG-NER	General-genome nucleotide excision repair
GLUT	Glucose transporter
GRSF	G-rich sequence factor
GSK	Glycogen synthase kinase
HADHA/B	Hydroxyacyl-CoA dehydrogenase trifunctional multi-enzyme complex subunit α/β
HK	Hexokinase
HIF	Hypoxia-inducible factor
HR	Homologous recombination
HRK	Harakiri Bcl-2 interacting protein
HN	Hypodiploid nuclei
IAP	Inhibitor of apoptosis
ICL	Inter-strand crosslinks
IDH	Isocitrate dehydrogenase
ICR	Interstrand crosslink repair
IMM	Inner mitochondrial membrane
IMS	Intermembrane space
IR	Ionizing radiation
IP_3R	Inositol triphosphate receptor
IRE	Inositol-requiring enzyme
JNK	c-Jun N-terminal kinase
KSRP	KH-type splicing regulatory protein
LDH	Lactate dehydrogenase
lncRNA	Long non coding RNA
Loni	Lonidamine
LRPPRC	Leucine-rich PPR motif-containing protein
LPC	Lisophosphatidylcholine
MAM	Mitochondria associated membrane
MAPK	Mitogen-activated protein kinase
MAPL	Mitochondria-associated SUMO E3 protein ligase
MCL	Myeloid cell leukemia
MERC	Mitochondria-ER-contact site
MFF	Mitochondrial fission factor
MFN	Mitofusin
MGMT	6-O-methylguanine-DNA methyltransferase
MLH	MutL Homolog
MMR	Mismatch repair
MOMP	Mitochondrial outer membrane permeabilization
mPTP	Mitochondrial permeability transition pore
MRN	MRE11-RAD50-NBS1 complex
MRP	Mitoribosomal protein
MSH	MutS Homolog protein
mtDNA	Mitochondrial DNA
NAC	N-Acetylcysteine
NAD/NADH	Nicotinamide adenine dinucleotide
NER	Nucleotide excision repair
NHEJ	Non-homologous end-joining
NOD	Nucleotide-binding and oligomerization region
NOS	Nitric oxygen species
NOXA	Phorbol-12-myristate-13-acetate induced protein 1
NSCLC	Non-small cell lung cancer
O_2	Oxygen
OCR	Oxygen consumption rate
OMA	Metalloendopeptidase OMA
OMI	Serine protease HTRA2
OMM	Outer mitochondrial membrane
OPA	Optic atrophy 1 protein
OXPHOS	Oxidative phosphorylation
p53	Tumor antigen p53
PARP	Poly ADP ribose polymerase
PBDE	Polybrominated diphenyl ether
PC	Phosphatidylcholine
PCNA	Proliferating cell nuclear antigen
PDH	Pyruvate dehydrogenase
PE	Phosphatidylethanolamine
PERP	p53 apoptosis effector related to PMP 22
PFK	Phosphofructokinase
PGI	Glucose-6-phosphate isomerase
PGK	Phosphoglycerate kinase
PGM	Phosphoglycerate mutase
PI	Phosphatidylinositol
PIKK	Phosphatidylinositol 3-kinase (PI_3K) like kinases

PK	Pyruvate kinase
PKA	Protein kinase A
PLK	Serine/threonine-protein kinase
PPP	Pentose-phosphate pathway
PS	Phosphatidylserine
P-TEFb	Positive transcription elongation factor
PTEN	Phosphatase and tensin homolog
PUMA	p53 upregulated modulator of apoptosis
QVD	Q-VD-OPh (broad-range caspase inhibitor)
RAD	DNA repair protein RAD51 homolog 1
Rb	Retinoblastoma protein
Rb1	Retinoblastoma-associated protein
RDDR	RNA-dependent DNA repair
RER	Rough Endoplasmic Reticulum
RG	Research group
RNA pol II	RNA polymerase II
ROCK1	Rho-kinase 1
ROS	Reactive oxygen species
RPA	Replication protein A
RTG	Research training group
SD	Standard deviation
Ser	Serine
SER	Smooth endoplasmic reticulum
SERCA	Sarco- and endoplasmic reticulum Ca^{2+}-ATPase
siRNA	Small interfering RNA
SMAC	Second mitochondria derived activator of caspases
sncRNA	Small non-coding RNA
SNP	Single-nucleotide polymorphism
SRC	Spare respiratory capacity
SSB	Single strand break
STS	Staurosporine
TBP	TATA-binding protein
TCA	Tricarboxylic acid cycle
TC-NER	Transcription-coupled nucleotide excision repair
TERT	Telomerase reverse transcriptase
TF	Transcription factor
TG	Triglyceride
Thr	Threonine
TIG	Tigecycline
TLS	Translesion synthesis
TNF	Tumor necrosis factor
TPI	Triosephosphate isomerase
TPP	Thermal proteome profiling
TRAIL	TNF-related apoptosis-inducing ligand
UPR	Unfolded protein response
UV	Ultraviolet
VDAC	Voltage-dependent anion channel
VDT	Viriditoxin
γh2ax	Histone variant H2A.X
YME1L1	YME1 like 1 ATPase
3-BP	3-Bromopyruvate
53BP1	P53-binding protein 1

IC_{50}	Half maximal inhibitory concentration
ΔΨm	Mitochondrial membrane potential
kilo (k)	10^{3}
micro (µ)	10^{-6}
milli (m)	10^{-3}
nano (n)	10^{-9}
A	Ampere
Da	Dalton
g	Gram
g	Gravitational field strength
h	Hour
l	Liter
m	Meter
M	Molar
min	Minute
rpm	Revolutions per minute
s	Second
V	Volt

1 Introduction

In our unique world, everything is balanced in the circle of proliferation, birth, life and death. This thesis presents an interdisciplinary work composed of a molecular analysis of potential anticancer therapeutics of natural or semisynthetic origin aiming to overcome therapy resistance in cancer. Selective hallmarks of cancer will be targeted with the therapeutics, therefore the topics of controlled cell death, cell cycle regulation, deoxyribonucleic acid (DNA) damage and repair and cellular metabolism will be introduced in detail below.

1.1 Apoptosis

In multicellular organisms, a regulated form of cell death is essential for many homeostasis ensuring processes, such as embryogenesis, development and tissue homeostasis [3, 4]. Apoptosis is an evolutionarily conserved programmed form of cell death that is tightly regulated and executed through strictly controlled signaling pathways [5]. The regulated destruction of a cell ensures the degradation and disposal of potentially damaged and oncogenic cells, of pathogen-infected cells and normal cell turnover [3, 4]. The term apoptosis was introduced in 1972 by John Kerr, Alastair Curie and Andrew Wylie and it originates from the Greek terms ‘apo’ and ‘ptosis’, meaning ‘falling off’ like fruits or leaves falling from a tree in autumn [6]. Apoptosis is characterized by many morphological and biochemical features, such as chromatin condensation (pyknosis; irreversible process in the nucleus [7]) , subsequent nuclear fragmentation (karyorrhexis), protein cleavage and cytoplasmic shrinkage [6]. These processes are followed by membrane blebbing and nuclear fragmentation with separation of membrane enclosed cell fragments into apoptotic bodies [3] and the externalization of phosphatidylserine [8], Annexin I [9, 10] or calreticulin [11] to the surface of apoptotic cells as a signal (‘eat me’) for other cells to clear the apoptotic cells [8]. The charm of this process is, that the cells dying by apoptosis will be phagocytosed and digested by macrophages, phagocytes or neighboring cells without the release of the cellular content which prevents an inflammatory response and thus without inflicting any harm to surrounding tissues [12, 13].

Finally, the pro-active decision for programmed self-destruction can be triggered by neighboring cells or decided by the condemned cell itself [3, 4]. Two major pathways have been described to regulate apoptosis and will be further distinguished as extrinsic and intrinsic apoptosis pathway. Both forms of apoptosis rely on the activation of evolutionary conserved members of the aspartate-specific cysteine protease (caspase) family [14]. The name originates from cysteine-aspartic protease, which means, that they always carry a cysteine residue in their active center and cleave their substrates after an aspartic acid residue [15]. Caspases are present in cells as inactive zymogens and get activated by proteolytic processing. Once they

are activated they are involved in the execution of apoptosis by cleaving proteins required for cell degradation, such as signal transduction proteins, nuclear matrix and cytoskeletal proteins, DNA repair proteins and chromatin modifying proteins such as PARP1 (poly (ADP ribose) polymerase 1) [3, 16, 17]. Dependent on the function of the caspase, they are divided into two groups, initiator caspases (caspase-2, -8, -9,-10) and effector caspases (caspase-3, -6, -7) [18]. The main function of initiator caspases is to activate effector caspases, while the effector caspases are mainly responsible for the partial proteolysis of apoptosis substrates to either generate a gain-of-function or induce a loss-of-function [19], resulting in cell death.

Another feature of initiator caspases is, that they contain specific protein interaction domains (caspase recruitment domain (CARD) or death effector domains (DED)) at the N-terminus, which are indispensable for the recruitment and multimerization of the inactive monomeric procaspases [18]. Within the heteromeric complex, initiator caspases are activated by induced proximity [20]. In contrast to initiator caspases, the effector caspases are not activated by dimerization, they get activated by the initiator caspases via cleavage between the small and the large subunit, this results in a conformational change. Thereby, the two active sites are exposed to spatial proximity and can form an active effector caspase. A pro-apoptotic amplification loop is generated by the fact that active effector caspases can also activate other effector caspases as well as initiator caspases [21]. As main function, effector caspases (caspase-3 and -7) cleave a variety of substrates, preferably at the recognition sequence of aspartic acid - glutamic acid - valine - aspartic acid (amino acid code: DEVD), which is also present in PARP1 [17] as one of the best characterized caspase substrates [22]. Caspase-6 cleaves preferably at the sequence amino acid code VEHD [23].

The substrates of effector caspases can be divided into two groups, (i) proteins that are involved in pro-survival signaling or high energy consuming processes, such as DNA repair and (ii) proteins which are directly promoting the execution of apoptosis. Examples for the first group are PARP1 (involved in DNA repair) and the retinoblastoma-associated protein (Rb) [19, 24] or the DNA-dependent protein kinase (DNA-PK), the latter two are involved in proliferation [25]. Examples for the second group are caspase-activated DNase (CAD), which is an endonuclease facilitating DNA breakup [26], Rho-kinase 1 (ROCK1) which is a key regulator of membrane blebbing [27], α-fodrin an actin-binding cytoskeletal protein [28] and others [3, 19, 22, 24, 29]. The two major apoptosis signaling pathways differ in their way of activation and execution – the signaling of extrinsic and intrinsic apoptosis will be introduced in the following.

1.2 Extrinsic apoptosis pathway

The extrinsic pathway of apoptosis is important for regulating cell death in a variety of cell types, including neurons and immune cells [3]. In the immune system, the extrinsic pathway is critical for eliminating infected or damaged cells, and for the regulation of immune cell populations [30]. In neurons, the extrinsic pathway is involved in regulating programmed cell death during development. It can also be activated in response to injury or disease, leading to the elimination of damaged or dysfunctional neurons [31]. In multiple cell types, the extrinsic pathway of apoptosis plays a crucial role in signaling, ensuring tissue homeostasis, and controlling cell populations.

The extrinsic signaling pathway is activated via the binding of death receptor ligands to their respective death receptors, which results in the intracellular activation of the signaling cascade leading to execution of apoptosis (**Figure 1**). In more detail, a pro-apoptotic ligand, named death ligand, secreted by immunocompetent cells (macrophages, dendritic cells or T cells) binds to its receptor, named death receptor (DR) [32, 33]. Well characterized DRs and their ligands are tumor necrosis factor (TNF, formerly named TNF-α) binding to tumor necrosis factor receptor 1 (TNFR1), TNF-related apoptosis-inducing ligand (TRAIL) binding to death receptor 4 (DR4, TRAIL-R1) or death receptor 5 (DR5, TRAIL-R1) and cluster of differentiation 95 ligand (CD95L, FASL, APO1L), binding to (CD59, FAS or APO1) [34-37]. After transmission of the extracellular signal via the transmembrane receptor into the cell, caspase-8 gets activated resulting in the activation of the effector caspases [14, 38]. The CD95 pathway is the best characterized mechanism of death receptor dependent activation of caspase-8. The binding of CD95L to its receptor induces the formation of receptor trimers, resulting in a conformational change leading to the exposition of their death domains (DD). The DDs function as binding site for the cytosolic adapter protein, whose N-terminal death-effector domain (DED) builds the recruitment site for procaspase-8, which binds to the adapter proteins DED via its own DED site [14, 38]. In the CD95 pathway, the only adapter protein required for the recruitment of procaspase-8 to CD95 is the FAS-associated death domain protein (FADD) that comprises a DD and a DED [39]. Via dimerization of the DED, FADD associates with procaspase-8, thereby forming the death-inducing signaling complex (DISC) [40]. The local enrichment of procaspase-8 in this multi-protein complex is composed of death receptor, adapter protein and procaspase-8, and leads to the autoproteolytic caspase activation according to the so-called '*induced proximity model*' [32]. A stoichiometric study showed that six procaspase-8 molecules bind on average to one single FADD protein [41]. This activation process is tightly regulated, since inhibitory proteins such as Baculoviral IAP repeat-containing protein 2 (known as BIRC2 or CIAP1) and caspase-8 and FADD-like apoptosis regulator (known as CFLAR or c-FLIP) can be recruited to the DISC, thereby inhibiting procaspase-8 activation [42, 43]. The inhibitory protein

BIRC2 causes a higher CFLAR expression, which in turn directly inhibits procaspase-8 processing at the DISC [14, 44]. Once caspase-8 is activated, it cleaves the downstream effector caspases resulting in apoptotic cell death [14]. The effector caspase, caspase-3 is a dimeric protein that gets activated by cleavage – in the extrinsic pathway by cleavage of caspase-8 between the large and small subunit [14]. Another caspase-8-substrate is BH3-interacting death domain agonist (BID), which gets cleaved by caspase-8 (truncated BID, t-BID) and translocates to the mitochondria. There, tBID causes an amplification of the apoptotic signal by causing the release of pro-apoptotic factors and the cytochrome c dependent activation of procaspase-9 [45, 46]. To which extent this lateral axis mediating a crosstalk between extrinsic and intrinsic apoptosis is indispensable or only supportive for the extrinsic apoptosis pathway induced by the death ligand depends on the cell type [38]. In **Figure 1** the extrinsic and intrinsic apoptosis pathway are depicted schematically.

1.3 Intrinsic apoptosis pathway

Mitochondria are known to have a dual role, one as cellular powerhouse and another as signaling organelle (**Figure 1**). The organelle is surrounded by two membranes, the inner mitochondrial membrane (IMM) and the outer mitochondrial membrane (OMM) that can be distinguished by different composition and function [47]. The intrinsic apoptosis pathway can be induced by a multitude of non-receptor-mediated stimuli activating intracellular signals, acting directly on targets within the cell – the mitochondria – in more detail, acting on the OMM [3]. Thus, intrinsic apoptosis is also referred to as mitochondria-dependent apoptosis pathway, since central initiation steps of this pathway are located in the mitochondria. However, the OMM is the place, where anti- and pro-apoptotic signals get integrated upon stimuli, deciding the cell's destiny (**Figure 1**).

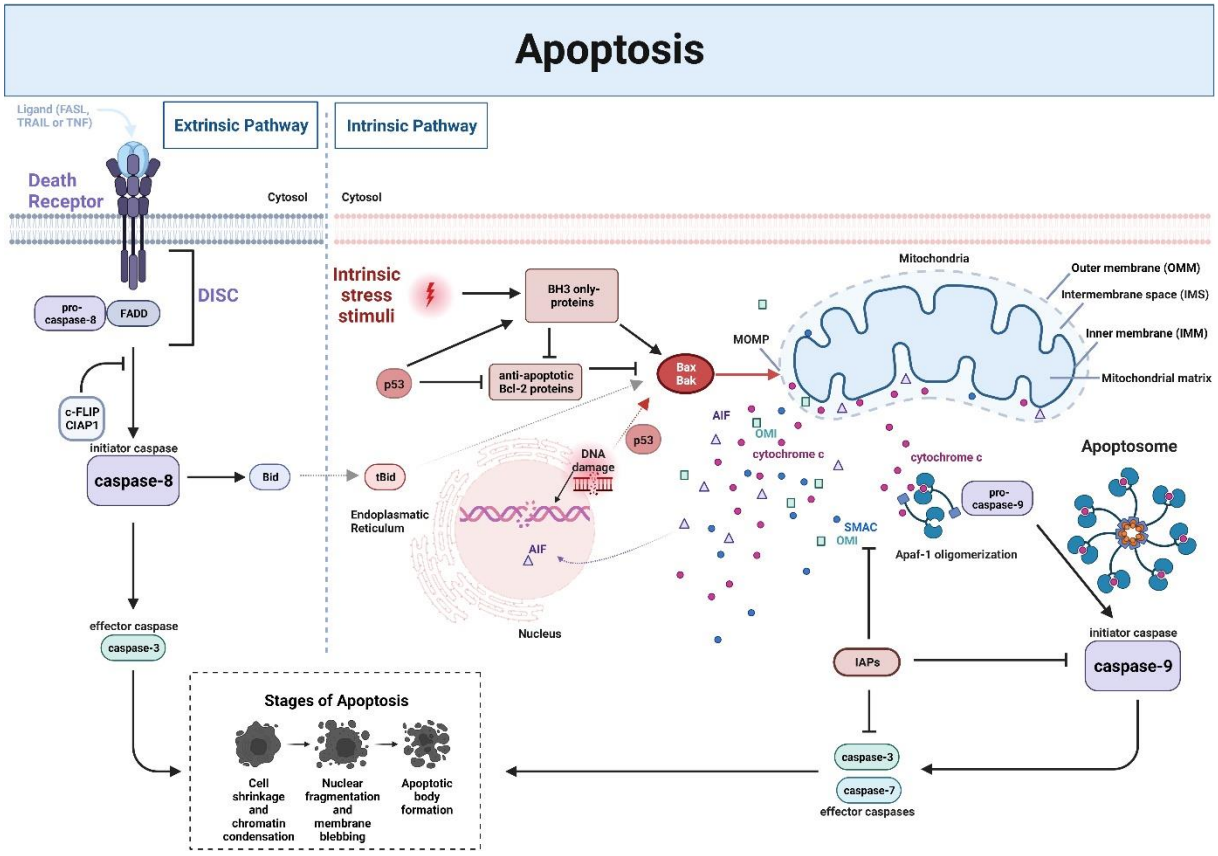

Figure 1 Apoptosis is a form of programmed cell death, it is distinguished between the extrinsic and intrinsic apoptosis pathway. The main signaling pathways of apoptosis are the death receptor (DR) dependent extrinsic pathway and the mitochondria dependent intrinsic pathway, differing in the either external or internal trigger and the proteins executing the apoptosis signaling. The DR pathway is activated upon binding of a ligand to the corresponding death receptor, such as binding of CD95L to the receptor CD95 or TRAIL to TRAIL-R. This binding induces a trimerization of the receptor, allowing the adaptor protein FADD to bind to the receptor, thereby building a platform for the recruitment of the main initiator caspase of the DR pathway, procaspase-8, which forms the so-called DISC (death inducing signaling complex). The enrichment of procaspase-8 at the DR leads to its autoproteolytic activation, which can be inhibited by c-FLIP or CIAP1. The intrinsic mitochondria dependent pathway gets activated upon intrinsic stress stimuli, for example ER stress, DNA damage, mitochondrial damage or growth factor depletion. With the mitochondria mostly being the primary target of intrinsic cellular damage, the main platform for the integration of internal stress signals is the outer mitochondrial membrane (OMM). As soon as a certain level of damage occurs, mitochondrial outer membrane permeabilization (MOMP) and/or mitochondrial permeability transition pore (mPTP) is formed regulated by the interconnected network of BH3-only proteins with pro- and anti-apoptotic BCL2 proteins. The BH3-only proteins activate Bax and Bak which oligomerize in the OMM forming the MOMP. This process can be inhibited by anti-apoptotic Bcl-2 proteins. When DNA damage occurs as intrinsic stimulus, tumor antigen p53 (p53) gets activated, which promotes MOMP formation by acting on BH3-only proteins, inhibiting anti-apoptotic Bcl-2 proteins or directly acting on Bax and Bak. The formation of the apoptotic pore, MOMP, leads to the release of pro-apoptotic factors from the mitochondrial intermembrane space (IMS), such as AIF, cytochrome c, SMAC or OMI. Once in the cytosol, cytochrome c assembles with dATP and Apaf-1 forming the so-called apoptosome, a multi-protein complex, which has the main function to activate initiator caspase-9 of the intrinsic pathway to further enhance the caspase cascade. The pro-apoptotic proteins SMAC and OMI counteract the IAPs function in inhibiting initiator caspase-9 and effector caspase-3 and -7. Both pathways, extrinsic as intrinsic, culminate in the activation of effector caspases (-3 and/or -7), which ultimately lead to the destruction of the cell accompanied by cell shrinkage, chromatin condensation, nuclear fragmentation, membrane blebbing and formation of apoptotic bodies. (This figure was created with Biorender.com, according to information in [3, 16, 48]).

Once the pro-apoptotic signals prevail, mitochondrial outer membrane permeabilization (MOMP) takes place, leading to a release of second messengers, such as cytochrome c from

the mitochondrial intermembrane space (IMS) into the cytosol [49]. Other pro-apoptotic molecules, that get sequestered into the cytosol are SMAC/DIABLO [50] or the serine protease HtrA2/OMI [51]. SMAC for example enhances apoptotic signaling by inhibiting anti-apoptotic proteins of the inhibitor of apoptosis (IAP) family such as XIAP [52]. However, irreversible induction of MOMP or mPTP induces the breakdown of the mitochondrial inner membrane potential ($\Delta\Psi m$), subsequent inhibition of mitochondrial respiration and $\Delta\Psi m$-driven ATP production. Along with these mitochondria-limited effects, also energy-dependent protein transport processes are inhibited. With activation of the caspase-cascade, a suicidal amplification loop is created with the release of pro-apoptotic factors from the mitochondria IMS interconnecting the mitochondria with the nucleus: Apoptosis-inducing factor (AIF) [53] and endonuclease G (ENDOG) [54] translocate into the nucleus where they activate caspase-independent DNA-fragmentation.

Finally, the mitochondrial key molecule for intrinsic apoptosis, cytochrome c, once released into the cytosol, binds and activates the apoptotic protease activating factor 1 (Apaf-1), together with deoxyadenosine triphosphate (dATP) and activates procaspase-9, forming the so-called apoptosome [55, 56]. The apoptosome is a multi-molecular wheel-shaped heptameric complex with sevenfold symmetry structure, the wheel has a central hub seven spokes, the distal region of the wheel spoke has a Y-shape [57]. Apaf-1 has structurally important regions: N-terminal CARD region, central nucleotide-binding and oligomerization region (NOD) and a C-terminal WD40 region [57]. Under normal conditions, Apaf-1 exists in a monomeric form, where the WD40 domain is folded onto the protein, thereby keeping the protein in an autoinhibited state [58]. Under pro-apoptotic conditions cytochrome c binds to the WD40 domain of Apaf-1 and upon hydrolysis of dATP/ATP the CARD region of Apaf-1 is exposed and enables binding to the CARD of procaspase-9 [58, 59]. Each Apaf-1 CARD domain interacts with a procaspase-9 CARD domain (1:1) mediated by homotypic interactions [60] and the conformational changes during Apaf-1 assembly allow procaspase-9 activation [59]. The oligomerization occurs only in the presence of seven Apaf-1 proteins together with seven cytochrome c molecules and sufficient dATP/ATP [56].

Apaf-1 was discovered by Xiaodong Wang *et al.* in 1996, where they showed that dATP induced caspase activation involving three apoptotic protease-activating factors [51, 61]. These three factors (termed Apaf-1-3), were later identified as Apaf-1, cytochrome c (Apaf-2) and caspase-9 (Apaf-3) [62, 63], which are now known to be the core components of the apoptosome. In response to diverse stimuli, this huge multi-subunit caspase-activating scaffold of the apoptosome (ca. 700-1400 kDa) assembles [51, 64]. The stoichiometric ratio of procaspase-9 to Apaf-1 is approximately 1 to 1 in the complex and as soon as caspase-9 is activated it dissociates from the complex and activates downstream effector caspases such as

caspase-3 [56]. Subsequently, the caspase cascade is initiated that is responsible for the final execution of apoptosis [51] (**Figure 1**).

The activation of the intrinsic suicide program is regulated by the family of B cell lymphoma 2 (Bcl-2) proteins, which are master regulators in the maintenance of cellular homeostasis [65]. The Bcl-2 protein family comprises approximately 20 members acting either anti- or pro-apoptotic [66]. The Bcl-2 family members share at least one of four homology regions within their sequence, which are termed Bcl-2 homology (BH) domains (1 - 4) [65]. A comprehensive review about apoptosis regulation at the mitochondria membrane level is given in [65]. Subgroups within the Bcl-2 protein family are classified depending on their structure and subsequent function: (i) BH-3 only proteins are pro-apoptotic and contain only the BH3 domain (such as Bcl-2 interacting mediator of cell death (Bim), BH3 interacting domain death agonist (Bid), p53 upregulated modulator of apoptosis (Puma), phorbol-12-myristate-13-acetate-induced protein 1 (Noxa), Bcl-2 interacting killer (Bik), Harakiri Bcl-2 interacting protein (Hrk), Bcl-2 modifying factor (Bmf) and Bcl-2 associated agonist of cell death protein (Bad)); (ii) The multi-domain effectors are either pro-apoptotic and contain BH domain 1 to 4 (Bcl-2 antagonist killer 1 (Bak), Bcl-2-associated x protein (Bax) and Bcl-2-related ovarian killer (Bok)) or (iii) anti-apoptotic proteins containing also BH domain 1 to 4 (Bcl-2-related gene A1 (A1), Bcl-2, Bcl-2-related gene long isoform (Bcl-$_{XL}$), Bcl-2 like protein 2 (Bcl-$_{W}$) and myeloid cell leukemia 1 (Mcl-1) [67].

Thus, the balanced interaction between members of the Bcl-2 proteins in response to a pro-apoptotic stimulus determine whether MOMP occurs or not. Therefore, MOMP is also considered as ‘point of no return’ since the cell is committed to die as soon as the threshold is reached [65]. There are different models and drivers discussed in the literature regarding MOMP formation as shown schematically in **Figure 2**.

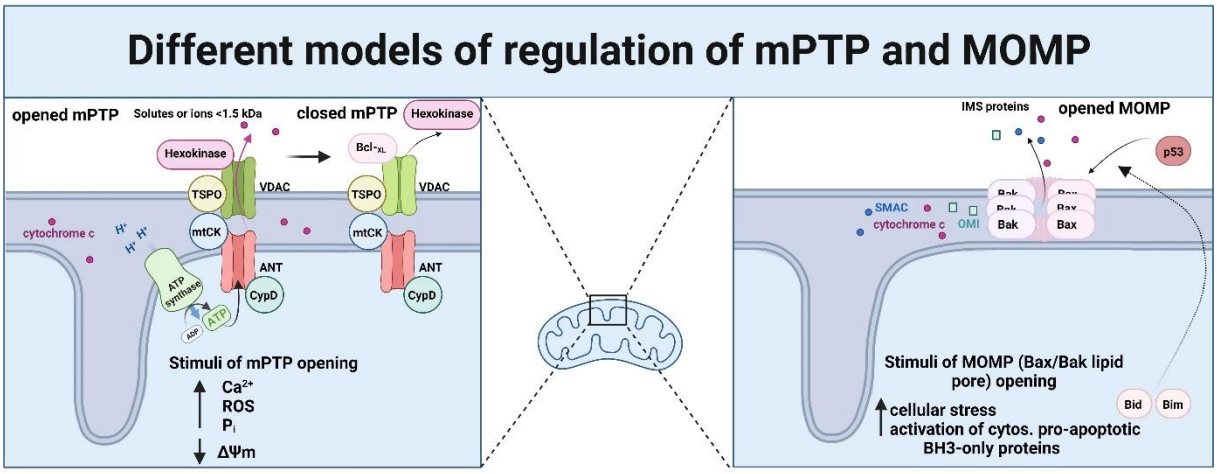

Figure 2 Different models of mPTP and MOMP regulation. On the left, the model for an opened mPTP (mitochondrial permeability transition pore) is shown, with hexokinase bound to the mitochondrial VDAC-ANT-CypD complex coupled to ETC (electron transport chain) complex V (ATP-Synthase) to release solutes and ions. This mPTP gets induced by high calcium (Ca^{2+}) levels, high reactive oxygen species (ROS) or decreased membrane potential ($\Delta\Psi m$) resulting from ETC dysfunction or accumulating phosphate (P_i). These stimuli cause an opening of the mPTP, which allows an influx of

ions and water into the matrix, thereby causing matrix swelling which leads to membrane rupture and the release of IMS proteins like cytochrome c [51, 68-71]. On the right, another model proposes the MOMP opening relies solely on pore-formation by Bax and Bak. Proteins from the Bcl-2 family, including Bax and Bak, that contain BH3 can come together and form pores in the outer mitochondrial membrane (OMM), resulting in the discharge of cytochrome c. BH3-only proteins, such as Bid, are thought to contribute in pore formation by interacting with Bax and Bak. Some other members of the BH3-only family act as detectors of cellular stress and are linked to different cellular membranes or need modification at the transcriptional or post-translational level to become active. The MOMP pores mediate the release of proteins including cytochrome c, SMAC and OMI from the intermembrane space. (This figure was created with Biorender.com according the information and figures shown in [51, 69-75]).

One model postulates that the permeabilization of OMM is mediated by a pore – the mitochondrial permeability transition pore (mPTP) – between OMM and IMM [76]. The supramolecular pore between the contact sites of IMM and OMM is composed of voltage-dependent anion channel (VDAC) in the OMM, adenine nucleotide translocator (ANT) in the IMM, cyclophilin D (a peptidoyl-prolyl-isomerase in the matrix; CypD) and hexokinase (HK) [51, 77, 78]. Cyclosporine A (CsA), an inhibitor of the enzymatic activity of CypD, was found to correlate its CypD inhibition with inhibition of the mPTP-opening (CsA binds matrix CypD) [79-82]. Stimuli inducing opening of the mPTP are oxidative stress, ceramide, low ATP levels or most important high calcium (Ca^{2+}) levels. Opening of the mPTP allows molecules of low molecular weight up to ~ 1.5 kDa to diffuse through the IMM [51] (**Figure 2**)**.** It is known that the IMM is an impermeable barrier and the OMM is permeable to molecules up to 5 kDa [51]. The opening of mPTP induces a depolarization of the mitochondria, swelling of the matrix and causes damage to the OMM and thereby releasing IMS proteins, for instance cytochrome c [51, 77]. Cell-free systems have shown that Bid, Bax and lipids form supramolecular openings in the OMM, which allows the passage of up to 2000 kDa molecules [83], which can be inhibited by Bcl-$_{XL}$ [77].

Another model postulates that pore-forming proteins of the Bcl-2 family (Bax and Bak) are responsible for MOMP formation. Under normal conditions, monomeric Bax is localized in the cytoplasm, while Bax translocates at pro-apoptotic conditions to the mitochondria [84, 85]. Bax undergoes conformational changes, which lead to oligomerization [86] and colocalization at the mitochondrial membrane [77]. Contrary to Bax, Bak resides at the mitochondria under normal conditions and under pro-apoptotic conditions it undergoes a series of conformational changes leading to oligomerization [87] (**Figure 2**). Bax and Bak are the main targets of the regulatory machinery determining the cell's fate since BH3-only proteins and anti-apoptotic Bcl-2 proteins regulate Bax and Bak in a positive and negative way. However, neither activation of BH3-only proteins nor suppression of anti-apoptotic Bcl-2 proteins is sufficient to kill cells in the absence of Bax and Bak [77, 88].

For the mechanism of MOMP formation (via Bax/Bak activation by BH3-only proteins), three models are discussed in the literature [65, 77]. (i) The first model is known as the direct activation model [65, 77, 89]. This model states that Bax and Bak get directly activated by tBid, Bim, Puma or

other BH3-only proteins after the release from their association with anti-apoptotic Bcl-2 proteins [65, 77, 89]. Thus, tBid, Bim or Puma bind with their BH3-domain into the hydrophobic groove of Bax and Bak, thereby inducing a conformational change and their activation [90]. (ii) The second model proposes an indirect activation (indirect activation model or displacement model). Bax and Bak get indirectly activated when anti-apoptotic Bcl-2 proteins are bound by BH3-only proteins [91]. The role of BH3-only proteins to displace Bax and Bak from anti-apoptotic proteins allowing MOMP is supported by live cell studies, demonstrating that Bax is in a dynamic equilibrium between cytosol and mitochondria, constantly removed from OMM by Bcl-$_{XL}$ [65, 92-94]. (iii) The third model is an 'embedding together model', where the insertion of Bax and Bak via their C-terminal transmembrane domain into the OMM was identified as a prerequisite for MOMP [65, 95]. It shows membrane permeabilization by the stepwise activation of Bax via tBid, since tBid and Bax get inserted into the membrane [65, 96]. Besides Bax, Bcl-$_{XL}$ is also capable of inserting into the OMM, but the difference is that Bcl-$_{XL}$ cannot form long-lived pores to induce MOMP, otherwise it can inhibit Bax oligomerization [65, 97, 98]. (iv) A fourth model integrates factors from all models described above and is termed 'integrated model of apoptosis regulation' [65]. The interplay between Bcl-2 proteins, either directly or indirectly activated, dictates the formation of Bax/Bak pores resulting in permeabilization of the OMM [96]. In more detail, Bax and Bak undergo conformational changes and oligomerize. The N-terminus is opened up by these conformational changes and releases an α9 transmembrane helix for insertion into the OMM, with exposure of the BH3 domain [65]. The BH3-into-groove dimer formation between α-helices (α2- α5) initiates pore formation, this is followed by another dimer interface within the membrane (formed by an α9 helix from another Bax molecule) and thereby the pore is formed [65, 99]. Recent studies showed that lipids have been observed at oligomerization interfaces of membrane proteins [100] and were reported to promote stability of the membrane protein oligomers [101]. Another study supports the importance of lipids in the Bax/Bak pore formation and proposes that the interfaces are primarily mediated by lipids, leading to flexibility between the oligomeric components [102]. In summary, mitochondrial lipid composition, mitochondrial dynamics and the membrane environment regulate the apoptosis executive function of Bax and Bak [65].

1.3.1 Mitochondrial dynamics in apoptosis regulation

Mitochondria are highly dynamic structures, building an interconnected tubular network within the cell, which continuously undergoes fusion and fission processes by the action of dynamin-related proteins (DRPs), a group of GTPases whose main function is to shape biological membranes [47, 65] (**Figure 3**). The IMM delimits the matrix (mitochondrial lumen) and can be sub-grouped into two further compartments, the inner boundary membrane (parallel to OMM) and

the cristae (pleomorphic, convoluted invaginations providing an expansion of the surface area required for mitochondrial respiration) [47]. The OMM and IMM are composed of different lipids with an unequal distribution of phospholipids. Cardiolipin (CLN) is the characteristic phospholipid of the IMM, generally of energy-transducing membranes, where it constitutes approximately 15-20% of the total mitochondrial phospholipids [103]. Structurally it differs from all phospholipid species, since it exhibits a dimeric structure with four acyl chains and two phosphatidyl moieties that are connected to a glycerol. This exclusive constitution of CLN yields a conical shape, which enables CLN to promote the curvature of the IMM [103-105]. CLN is involved in several processes and reactions such as mitochondrial respiration and energy production, mitochondrial cristae morphology and stability, mitochondrial quality control and dynamics through fusion and fission and serves as binding partner in the recruitment of apoptotic factors [103, 105-111]. Regarding permeability, the OMM is permeable and only limits diffusion of molecules bigger than ~5 kDa, it represents a platform where signaling pathways interconnect and get transmitted into the mitochondria [47]. The IMM is mostly implicated in mitochondrial energy generation, since the cristae of the IMM are hosting all the electron transport chain (ETC) complexes (mitochondrial respiratory chain and F_1F_0-ATP synthase) that mediate oxidative phosphorylation (OXPHOS) [47, 112, 113]. Also the pro-apoptotic protein cytochrome c is localized mainly in the intracristal compartment, it is also the only soluble OXPHOS member [114, 115]. However, the main function of IMM is to harbor the ETC, thereby converting the free energy stored in reducing equivalents produced in the Krebs cycle into ATP, the energy currency of the cell [47]. Regarding membrane dynamics, the IMM undergoes dramatic structural changes during cell death, which are referred to as cristae remodeling. Cytochrome c needs to be redistributed intramitochondrial from the cristae to the IMS, followed by its release through pores within the OMM into the cytosol where it initiates apoptosome formation [47, 114].

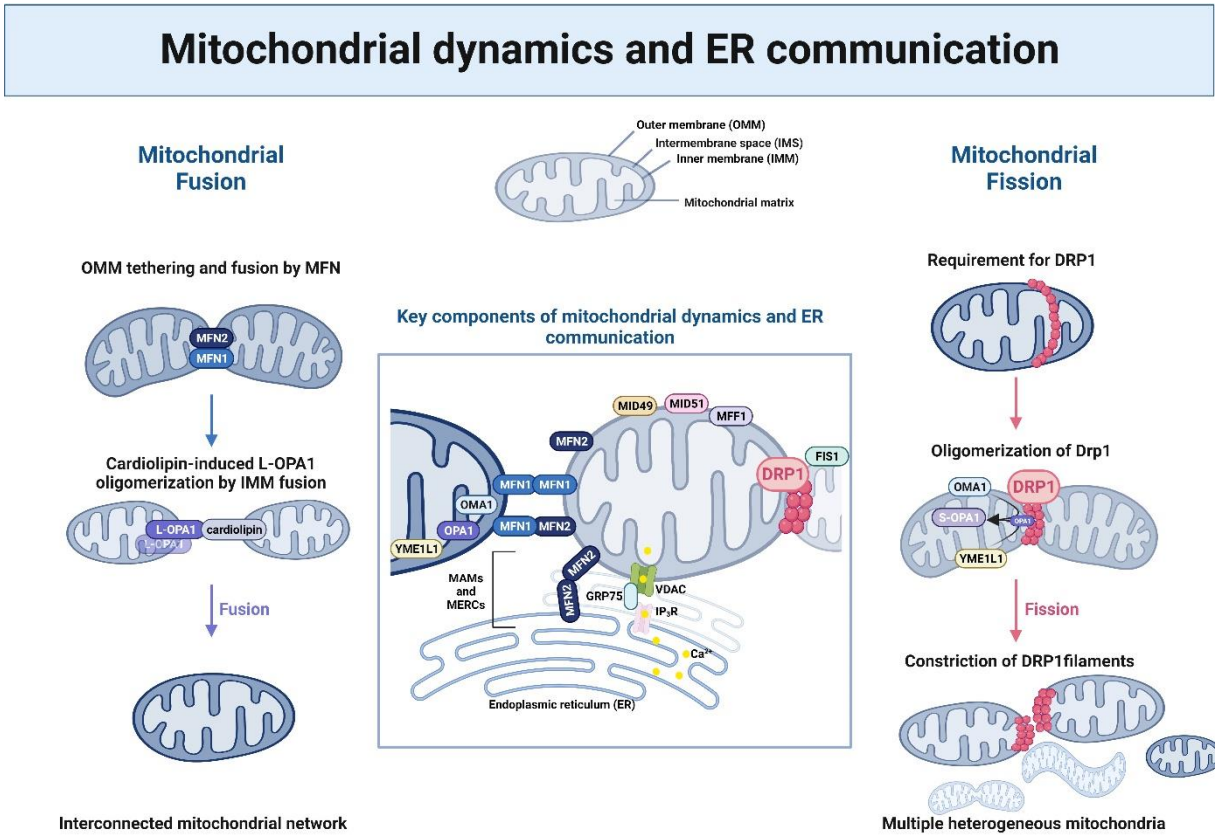

Figure 3 Key components of mitochondrial dynamics and communication between the Endoplasmic Reticulum (ER) and mitochondria. Fusion: Tethering of the OMM is mediated by mitofusin 1 and 2 (MFN1; MFN2). Fusion of the IMM is mediated by cardiolipin and L-OPA1 interactions. Fission: Mitochondrial division is initiated by the DRP1 GTPase, which is recruited to the mitochondria via interactions with receptor proteins such as MFF1, MID49, MID51 and FIS1. The oligomerization of DRP1 leads to a wrapping around the mitochondria and a constriction of DRP1 filaments, with the subsequent OMA1 or YMEL1L1 dependent cleavage of OPA1 as characteristic feature of mitochondrial fragmentation [116-118]. The key components of mitochondrial dynamics and ER communication are main contributors to cellular physiology. As shown, the mitochondria undergo fusion and fission depending on the cellular environment and stress levels. Distinguishing between mild and severe stress, different processes are activated. Under mild stress, the mitochondria form an elongated network to adapt, whereas under severe stress, the mitochondria fragment. These processes mainly involve the membranes. Since mitochondria and ER are in close proximity to each other, they are termed mitochondria associated membranes (MAMs) or mitochondria-ER-contact sites (MERCs). These areas allow exchange of Calcium (Ca^{2+}) via 1,4,5-trisphosphate receptor (IP_3R) and voltage dependent anion cannel (VDAC). MFN2 is located on both organelles, mediating the tethering of both [119]. (The figure was created with Biorender.com according the information and figures in [47, 116-119]).

The bidirectional crosstalk between mitochondrial dynamics and apoptosis signaling is an excellent example to visualize the dual role of mitochondria and especially the OMM as platform of mitochondrial integration within cellular signaling [47]. The two main processes of mitochondrial membrane dynamics are known as fusion and fission of OMM and IMM and delineated in (**Figure 3**).

Fusion is regulated by proteins of the dynamin-related family of large GTPases: Mitofusin 1 and 2 (MFN1 and MFN2), which regulate fusion of the OMM [120], whereas optic atrophy 1 protein (OPA1) mediates fusion of the IMM (dependent on MFN1) [65, 121] (**Figure 3**). For OPA1 it is known, that the protease-cleaved, soluble, OPA1-form (short OPA1; S-OPA1) is present

in the intermembrane space serving as a bridge to the unprocessed, membrane-bound OPA1 (long OPA1; L-OPA1) [47]. However, fusion depends on the balance between S- and L-OPA1 [47]. OPA1 is processed by several enzymes with the YME1 like 1 ATPase (YME1L1) as the key enzyme for generating S-OPA1 [122]. In addition to IMM fusion, OPA1 also regulates the formation, size and maintenance of cristae junctions [47]. An aspect of the mitochondrial morphological shape that changes during apoptosis is OPA1-dependent cristae remodeling, whereby the neck of the cristae enlarges facilitating cytochrome c release [123-125]. Another mechanism how OPA1 gets cleaved, is the hyperactivation of the OMA1 protease via accumulation of reactive oxygen species (ROS) [126, 127].

Fission is regulated also by dynamin-related protein 1 (DRP1) [128], which translocates from the cytosol to the mitochondria, binding to its OMM receptors (mitochondrial dynamics protein of 49 kDa and 51 kDa (MID49 and MID51), mitochondrial fission factor (MFF1) and mitochondrial fission 1 protein (FIS1) [129-131] (**Figure 3**). Resulting from this binding, DRP1 oligomerizes and drives membrane scission [47, 132]. The translocation of DRP1 to the mitochondria is regulated by two mechanisms: (i) Phosphorylation of Ser637 by protein kinase A (PKA), decreasing DRP1 GTPase activity [133, 134] (mediating mitochondrial elongation and fusion), (ii) dephosphorylation of Ser637 by the Ca^{2+}-dependent phosphatase calcineurin (driving DRP1 association to mitochondria and their subsequent fission) [135]. In the process of fission, the IMM peptidase OMA1 processes OPA1, inducing mitochondrial fragmentation and dysfunction [136-138].

Homeostasis of the mitochondrial network is closely interconnected with intrinsic mitochondria dependent apoptosis, since many studies showed the interplay between fusion and fission regulating proteins (MFN1, MFN2 and DRP1) with Bcl-2 family members (Bax, Bak, Bcl-$_{XL}$ and Bcl-2) [65, 139-141]. Such an example is the SUMOylation of DRP1 by the mitochondria-associated SUMO E3 protein ligase (MAPL) [142, 143], which leads to the stabilization of DRP1 on the mitochondrial membrane and a colocalization with MFN2 and Bax (but not other mitochondria-shaping proteins [47]). This colocalization was associated with a block of fusion, which results in apoptotic mitochondrial fragmentation [144]. Bax and Bak promote DRP1 stabilization at fission sites, blocking the translocation between cytosol and mitochondria, thereby ultimately inducing apoptotic fragmentation [145]. During cell death, the modification of DRP1 also stabilizes contact sites between the Endoplasmic Reticulum (ER) and the mitochondria, building a stabilized functional network for cristae remodeling and cytochrome c release [65, 141, 146]. In addition to that, the platform for the transmission of Ca^{2+} signals from ER to mitochondria is stabilized, by subsequent cristae remodeling and an amplification of cytochrome c release und enhanced mitochondrial apoptosis [141, 145] (**Figure 3**). Another example is that under normal conditions, Bax and Bak facilitate MFN2 oligomerization while under pro-apoptotic conditions, Bak dissociates from MFN2 and associates with MFN1. Moreover, under pro-apoptotic condition a

phosphorylation of MFN1 facilitates Bak oligomerization and subsequently cytochrome c release and the execution of intrinsic apoptosis [65, 147]. Besides the regulation of IMM and OMM structures, the mitochondrial cristae remodeling is of importance since it plays a major role in the release of cytochrome c during MOMP [148].

1.3.2 Interactions with other organelles – ER-mitochondria interactions

The ER is an interconnected network composed of the rough endoplasmic reticulum (RER) and the smooth endoplasmic reticulum (SER). The RER has ribosomes attached to its surface and is involved in protein synthesis and folding, whereas the SER is involved in metabolic processes [119]. Protein synthesis takes place at the ribosomes and subsequent folding and modifications take place in the ER [149-151]. The ER is involved in lipid and steroid synthesis, carbohydrate metabolism and functions as central Ca^{2+} storage of the cell [152-155]. The extracellular Ca^{2+} concentration is ~2 mM, the typical cytosolic Ca^{2+} concentration is ~100 nM and in the ER lumen it is 100-800 µM [154, 156]. Mitochondria are able to store Ca^{2+} in mM concentrations but Ca^{2+} homeostasis in mitochondria is distinctly regulated [154]. The interaction between the ER and mitochondria was first discovered when ER membrane patches were biochemically isolated attached to OMM [157]. These interactions between mitochondria-associated ER membranes and the mitochondria themselves are termed mitochondria-ER-contact-sites (MERCs) mediated by connecting protein bridges shown schematically in **Figure 4** [158, 159]. Here, MFN2 acts as a key MERC since it localizes both on the ER membrane and the OMM with an ability to homo-oligomerize [47]. MERCs are also the place where mitochondrial fission occurs. They are in close proximity to the smooth ER, which wraps around mitochondria. These MERCs permit transfer of Ca^{2+} to mitochondria, thereby activating DRP1-independent IMM constriction, subsequent fission [160] and push mitochondrial apoptosis. Besides the regulation of fission, MERCs are involved in the exchange of lipids between the mitochondria and the ER [161]. Interestingly, a disturbance or loss of lipid homeostasis at MERCs was shown to result in damage to mitochondrial network, meaning shortened cristae, mitochondrial hyperfusion and subsequent dysfunctional respiration [162]. Besides ER-mitochondria interactions, also plasma membrane-mitochondria interactions are involved in the regulation of Ca^{2+} influx from the extracellular space and found to be regulated by MFN2 [163].

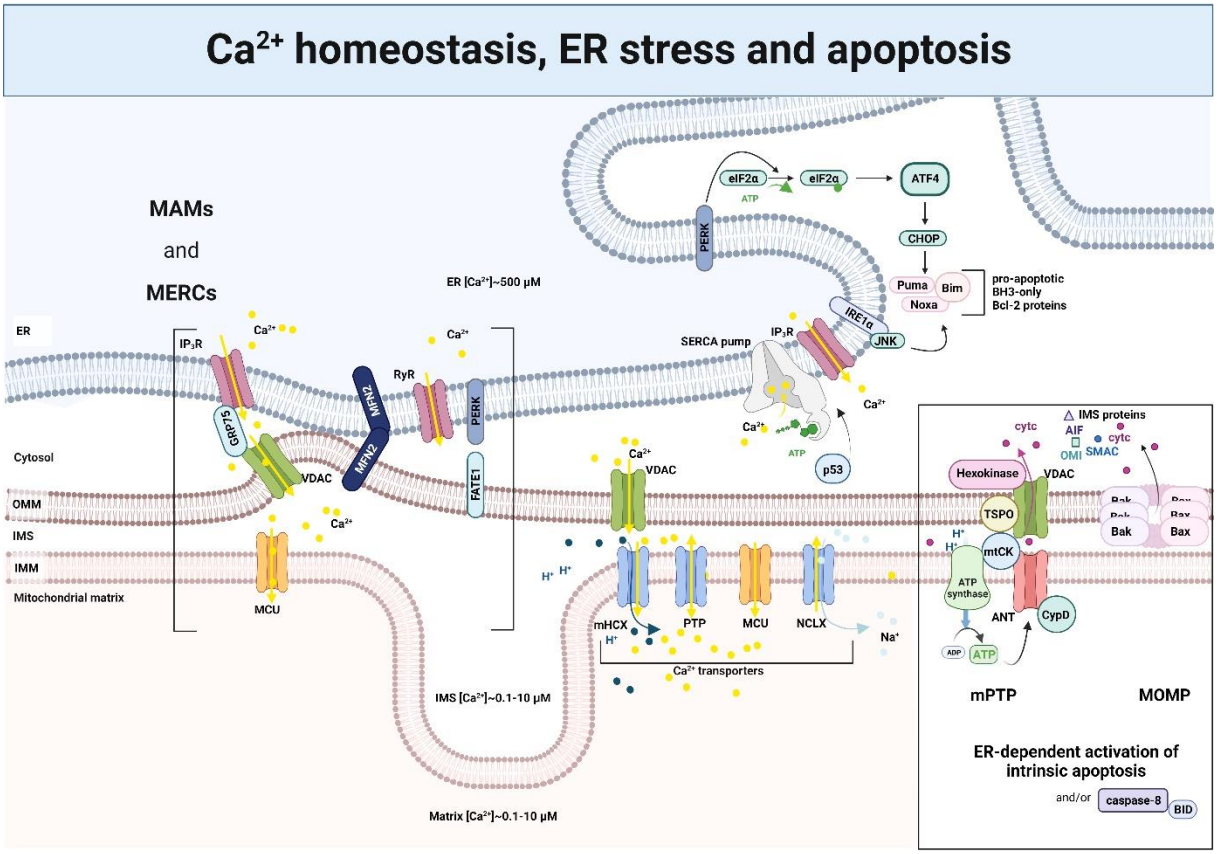

Figure 4 Key aspects of Calcium signaling in the Endoplasmic Reticulum and the mitochondria with links to unfolded protein response (UPR) and apoptosis induction. Membranes of the ER and mitochondria are linked at mitochondria associated membranes (MAMs) and mitochondria and ER contact sites (MERCs) via tethering proteins such as VDAC and inositol 1,4,5-trisphosphate receptor (IP_3R) forming a complex via glucose-regulated protein 75 (GRP75), fetal and adult testis expressed 1 (FATE1), the protein kinase RNA-like ER kinase (PERK) and MFN2. Generally, Ca^{2+} has to cross two membranes to enter the mitochondria. It passes the OMM via the non-selective channel VDAC and the IMM via more Ca^{2+} specific transporters such as H^+/Ca^{2+} exchanger (mHCX), permeability transition pore (PTP), mitochondrial Ca^{2+} uniporter (MCU) or Na^+/Ca^{2+} exchanger (NCLX) [164]. Depicted here are the major UPR pathways initiated from the ER. Under ER stress PERK is activated and phosphorylates the eukaryotic translation initiation factor 2 subunit-α (eIF2α), leading to an overall reduction of mRNA translation. Under ER stress, activating transcription factor 4 (ATF4) gets translated, which promotes the transcription of UPR target genes involved in apoptosis such as Puma, Noxa and Bim. The RNase IRE1α leads to caspase-2 and -8 dependent or Bax/Bak dependent apoptosis through TRAF2–JUN N-terminal kinase (JNK) signaling [165]. Another stress induced ER response acts on SERCA pumps and gets signaled via p53 [166]. (The figure was created with Biorender.com according the information and figures in [164-166]).

Ca^{2+} homeostasis, ER stress and apoptosis

Another possible trigger for MOMP induction is ER stress, which is also shown schematically in the upper right part of **Figure 4**. ER stress can be triggered by ROS, since they increase intracellular Ca^{2+} levels by acting on the activity of inositol triphosphate receptor (IP_3R) of the ER, on Ca^{2+} channels and the sarco- and endoplasmic reticulum Ca^{2+}-ATPase (SERCA pumps) on ER and sarcoplasmic reticulum (SR) [167]. The main contribution of Ca^{2+} to apoptosis is taking place at the interface between ER and mitochondria, where an apoptotic mitochondrial Ca^{2+} overload leads to cristae remodeling that depends on the mPTP [141, 168], also referred to as a Ca^{2+} dependent high-conductance IMM channel, schematically drawn in **Figure**

4 [47, 169]. Cellular Ca^{2+} overload leads to membrane hyperpolarization, increase of intracellular ROS production by inhibition of the respiratory complexes followed by release of cytochrome c [169, 170]. An impaired regulation of Ca^{2+} gradient decreases also the protein folding capacity of the ER, consequentially misfolded proteins accumulate in the ER lumen, a condition called ER stress, then the unfolded protein response (UPR) is induced as depicted in **Figure 4** [154, 171]. The UPR integrates diverse pathways signaled by tumor antigen p53 (p53) apoptosis effector related to PMP-22 (PERP), activating transcription factor 6 (ATF6) and inositol-requiring enzyme 1 (IRE1) – if the stress prolongs or the adaptive response fails, apoptotic cell death will be triggered by these proteins [172]. However, they do not directly cause cell death, they rather initiate the downstream activation of CHOP (known as growth-arrest- and DNA-damage-inducible gene 153 (GADD153)) or c-Jun N-terminal kinase (JNK), which further trigger cell death execution, as shown in **Figure 4** [172]. For JNK, which is activated by IRE1α-TRAF2-ASK1 pathway of the UPR, it is known to regulate Bcl-2 proteins by phosphorylation. Moreover, JNK can target the BH3-only members of the Bcl-2 family, such as Puma, Noxa and Bim, which have been reported to be involved in ER stress [172]. Taken together, JNK gets activated by ER stress and targets Bcl-2 proteins, allowing the activation of Bax/Bak leading to the execution of apoptosis, which is also shown in **Figure 4** [172]. Another mechanism how Ca^{2+}-dependent ER stress induces apoptosis was discovered recently. The regulation of the Ca^{2+} pump on the ER/SR – SERCA2 – modulates the sensitivity to apoptosis; its activity is regulated by the apoptosis modulator p53, which activates SERCA2 to promote Ca^{2+}-dependent apoptosis [166]. Furthermore, it was shown that PERP-SERCA2b interaction mediates apoptosis by mitochondrial Ca^{2+} overload [166], which is supported by the finding that PERP induces apoptosis via increased OMM permeability and cytochrome c release [173].

1.4 Cell cycle

This dissertation was introduced by the circle of life and death with a subsequent review of controlled cell death. In this chapter, other aspects of cellular life, namely proliferation and cell division, will be summarized with the main focus on cell cycle regulation. The cell cycle is a series of events that take place in a cell causing it to divide into two daughter cells. These events include DNA-replication, organelle-replication and the respective portioning of DNA, cytoplasm and organelles into two daughter cells by cell division [174]. The cell cycle consists of four phases, the G_1 phase, S phase and G_2 phase (together called the interphase) and M phase, which consists of mitosis and cytokinesis [175, 176] (**Figure 5**). Cells that temporarily or reversibly stop dividing enter a state of quiescence called G_0 phase. A brief description of each phase can be found in **Table 1**. The most important protein families involved in the cell cycle are (i) Cyclin-dependent kinases (CDKs; kinases that bind Cyclin-like proteins, responsible for

transition between cell cycle stages), (ii) the respective Cyclins, (iii) interconnected complexes containing transcription factors (E2F, B-MYB and Forkhead box protein M1 (FOXM1)), (iv) Aurora kinase family (controls chromatid segregation, formation of mitotic spindle and centrosome separation) and (v) kinases of the anaphase-promoting complex/cyclosome (APC/C; multiprotein E3 ubiquitin ligase complex targeting mitotic proteins for degradation and promoting anaphase) [47, 176]. The expression of cell cycle regulators follows a periodic pattern that consists of two main waves, with maximum expression during transitions between the G_1/S and G_2/M phases (**Figure 5**). They are governed by a series of interconnected complexes containing transcription factors (E2F, B-MYB, FOXM1) and Rb tumor suppressors, which function as transcriptional repressors. These networks regulate each other by forming feedback loops and redundancies, with collectively creating an almost fail-save system for cell cycle progression [176].

Table 1 Description of each cell phase in brief with the respective checkpoints.

State	Phase	Description
Resting	G_0	A phase where the cell has left the cycle and stopped dividing.
Interphase	G_1	Cell growth. G_1 checkpoint ensures that everything is ready for DNA synthesis.
	S	DNA replication.
	G_2	Growth and preparation for mitosis. G_2 checkpoint ensures that everything is ready to enter M phase to divide.
Cell division	M	Cell division occurs. Metaphase checkpoint ensures that cell is ready to complete cell division.

A fundamental aspect of cancer is dysregulated cell cycle control. This control is mainly focused on two events: The replication of genomic DNA and its segregation between daughter cells [175]. As Matthews *et al.* [175] reviewed extensively, cancer cells continue to divide because specific mutations allow the cell cycle to proceed and prevent the cell from exit. In consequence cancer cells depend on continuous cell division and many become increasingly dependent on remaining cell cycle control mechanisms preventing the excessive accumulation and propagation of genomic instability [175]. First high-throughput screenings in 2002 identified genes periodically expressed in the human cell cycle (and expression in tumors). Based on their expression profiles during the cell cycle, these genes were classified as Cyclins [177]. The progression of the cell cycle is propagated by the accumulation of CDK activity during inter- and M phase as drawn schematically in **Figure 5**.

Regulation of the cell cycle involves processes which are crucial to survival, such as detection and repair of genetic damage as well as the prevention of uncontrolled division. Two key classes of regulatory molecules, Cyclins and CDKs determine a cell's progress through the cell cycle [174, 178]. Cyclins are the regulatory subunits and CDKs the catalytic subunits of an activated heterodimer. The Cyclins have no catalytic activity and CDKs are inactive in absence of their Cyclin partner [174]. Briefly, Cyclins accumulate in specific stages of the cell cycle and

this process is regulated by transcription and inhibition of protein degradation. Whereas in turn, this transcription is regulated by CDK activity and this regulatory network establishes an interdependence that guarantees that cell cycle progression follows a sequential and unidirectional pattern [175, 179, 180]. In more detail, in pre-replicative G_1, CDK activity is needed to initiate DNA replication; whereas in the post-replicative G_2, CDK activity is needed to prepare for chromosome segregation (initiation of condensation, permeabilization of nuclear envelope and alignment of replicated chromosomal DNA). The complex responsible for the inactivation of CDKs is the anaphase-promoting complex/cyclosome (APC/C^{CDC20}) [175, 181]. The degradation of Cyclins and a return to interphase occurs when this activity is lost through APC/C in association with the activator protein CDC20 (APC/C^{CDC20}) during mitosis and subsequently with CDH1 (APC/C^{CDH1}) during G_1. To prevent cell cycle exit, accumulation of CDK4/6/Cyclin D is necessary for entry into the cell cycle (**Figure 5**). S phase entry and replication initiation are tightly dependent on the activity of the E2F-transcriptional network and their dimerization partner proteins [182]. The E2F family is composed of transcriptional E2F members (E2F-1, E2F-2, E2F-3A) or members with repression-activity (E2F-3B, -4, -5, -6, -7, -8), which is reviewed extensively in [182]. Upstream, this network is regulated by the MAPK pathway (composed of RAS-RAF-MEK-ERK), which acts together with the transcriptional regulator myc, controlling expression of positive cell cycle regulators. Subsequently, this growth signal and mitogen dependent signaling acts on CDK activity by antagonizing CDK inhibitor activity and thereby mediating E2F-dependent transcription [175, 182]. E2F-dependent transcription leads to the accumulation of Cyclin E and A, creating a decision point to enter S phase (**Figure 5**). CDK2/Cyclin E activity further activates E2F-dependent transcription, resulting in an increase in CDK2/Cyclin E and CDK2/Cyclin A activity through a positive feedback loop. The subsequent increase in CDK2/Cyclin A activity initiates replication and entry into S phase by inactivating APC/C^{CDH1} activity. Post S phase completion, the increase of CDK1/Cyclin A/B activity drives mitotic entry (**Figure 5**), allowing APC/C^{CDC20} activation, which is necessary for mitotic exit and targeted degradation of Cyclins in order to complete a full cycle [175]. After each division, the daughter cell begins a new cycle with the interphase.

However, the CDKs get activated by binding to their Cyclin partner in order to phosphorylate their target proteins, e.g.: RNA polymerase II (RNA pol II) or retinoblastoma protein (Rb) as shown in **Figure 5**. The E2F suppressor Rb has a major role in the cell cycle, especially in the decision to re-enter a new cycle [183, 184] and this role through the cell cycle is summarized in the following. Rb was the first tumor suppressor to be identified and is absent in one-third of all human cancers [185, 186]. This protein exists mainly in two major forms of phosphorylation state, CDK4/6/Cyclin D can monophosphorylate Rb on any of 14 known phosphosites, whereas CDK1 and CDK2 are the main contributors to the multi- or hyperphosphorylation of Rb as shown in **Figure 5** [176, 187].

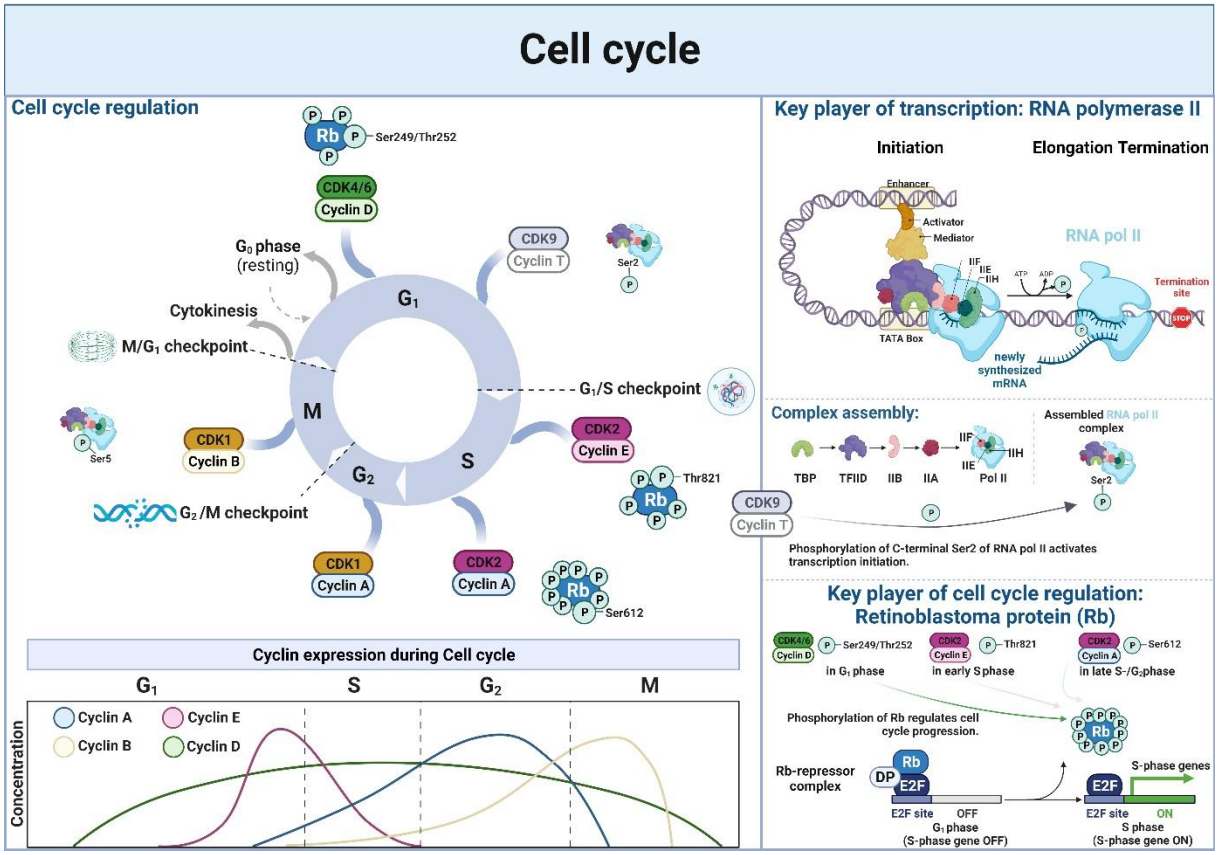

Figure 5 CDK activity and periodic expression of Cyclins are the main regulators of cell cycle progression and act via phosphorylations on key mediators of the cell cycle. The cell cycle is separated in G_1, S, G_2 and M phase, the depicted CDKs in complex with their Cyclin binding partners mediate progression of the cell cycle by phosphorylating their downstream targets. These downstream targets are for example RNA polymerase II (RNA pol II) or retinoblastoma protein (Rb), which get phosphorylated by different CDK/Cyclin complexes: CDK9/Cyclin T phosphorylates RNA pol II at Ser2 in G_1 to initiate transcription, whereas CDK1/Cyclin B phosphorylates RNA pol II at Ser5 in M to inhibit transcription. The Rb protein is the main regulator protein for gene expression, since it suppresses in its hypo- or mono-phosphorylated form in a complex with the transcription factor DP, E2F-dependent gene expression during G_1. This complex dissociates from E2F regulated genes, as soon as Rb gets phosphorylated by CDK4/6/Cyclin D on Ser249/Thr252, further phosphorylations take action on the protein such as CDK2/Cyclin E in early S phase on Thr821 or CDK2/Cyclin A in late S-/G_2 phase on Ser612 and many more, since the Rb protein has in total 14 *in vivo* CDK phosphorylation sites [188]. (This figure was created with Biorender.com according to figures in [175, 189-195]).

G_1-phase

The different phosphorylation states of Rb decipher its activity and role in progression of the cell cycle. Rb is hypophosphorylated during G_0 and early G_1 and this hypophosphorylated form binds and thereby inhibits E2F (**Figure 5**). In pre-replicative G_1, Rb holds E2F-dependent transcription in an inactive state. The phosphorylation of Rb is regulated by CDKs (1, 2 and 4/6), inactivates Rb which leads to the dissociation from E2F genes thereby allowing activated E2F-dependent transcription (**Figure 5**). An important example for an E2F-dependent gene, is Cyclin E, since its expression leads to an increase in overall CDK activity [175]. Increased CDK activity then in turn induces further phosphorylation of Rb, which leads to the complete inactivation of Rb with its E2F inhibitory function and thus to the full expression of E2F-dependent genes. Examples for E2F-dependent genes are the Cyclins, DNA replication factors

such as DNA polymerase, DNA ligase and MCM proteins (involved in DNA synthesis), DNA repair genes like DNA repair protein RAD51 homolog 1 ((RAD51); required for homologous recombination) and apoptosis regulators such as Bax [181]. In G_1 phase, CDK4 and CDK6 are the primary CDKs promoting the transition from G_1 to S phase [175, 181]. In G_1 the cell fulfills its normal functions with some exemplary key events: Protein synthesis for growth, mitochondria and ribosome duplication in order to support growth, cell growth itself by increase in size, nutrient and energy accumulation to support upcoming S phase; and checkpoint control (referred to as restriction checkpoint) to ensure that the conditions are favorable to enter S phase and perform DNA replication and finally cell division [181] (**Figure 5**).

S-phase

The feedback loop created in G_1, allows to enter S phase with the increase of Cyclin E- and A-dependent CDK activity and following initiation of DNA replication [175, 196]. Along with S phase goes the replication of DNA, which depends on CDK2/Cyclin A activity. Here, CDK activity also has the role in ensuring a replication of the genome, especially only one per cell cycle [175]. Thus, the sequential phosphorylation as shown in **Figure 5** inactivating the Rb suppressor activity allows cell cycle progression. At the end of S phase, Cyclin A replaces Cyclin E by forming a new complex with CDK2, then Cyclin E is degraded [191]. The CDK2/Cyclin A complex is responsible for the termination of S phase, driving the transition from S phase to G_2, with subsequent activation of CDK1 by Cyclin A leading the cell to enter the transition to M phase [191].

G_2-phase

During G_2, the cell continues to grow and prepares for division. Moreover, the cell checks successful DNA replication in S phase, synthesizes proteins needed for division, duplicates organelles and grows in preparation for division [181]. CDK1 activity leads to the condensation of chromosomes, the assembly of the mitotic spindle and the breakdown of the nuclear envelope [197].

Mitosis

The decision to enter mitosis is mainly regulated by CDK1 and its activity is linked to Cyclin A or B, which accumulate in S phase (extensively reviewed in [198]). The entry into mitosis takes place once a threshold for CDK1 activity is reached, then mitosis is activated by CDK1-mediated phosphorylation of thousands of substrates (listed in [199-201]). A wave of mitotic phosphorylation (mediated by activation of serine/threonine-protein kinase 1 (PLK1), Aurora A and B) activates structural changes and primes the cell for DNA separation and division [199, 202]. The main CDK regulating mitosis is the CDK1/Cyclin B complex and with decreasing levels of Cyclin B, the CDK activity simultaneously going down, which effectively prepares the cell for pre-replicative G_1 again [175].

The genomic integrity and cell cycle progression is safeguarded by cell cycle checkpoints that monitor and regulate the progress and success of each phase in the cell cycle at several stages [203]. They prevent progression of the cycle at a specific point, allowing verification of necessary phase processes and DNA-damage repair, respectively. There are several checkpoints to ensure that damaged or incomplete DNA is not passed on to daughter cells. Three main checkpoints exist: G_1/S, G_2/M and M checkpoint as depicted in **Figure 5** (another one is G_0 where maturity is checked). During interphase, DNA damage is monitored as well as a loss of replication fork integrity in S phase and in M phase the cell is checked for correct spindle assembly [175]. In the following the cell's response to DNA damage and replication stress will be reviewed, whereas the different types of DNA damage and mechanisms for DNA damage responses are introduced afterwards in detail.

Checkpoints

Regardless of the type of DNA stress that a cell experiences, its response at checkpoints is to decelerate the cell cycle by inhibiting CDKs and the APC/C complex. The DNA damage checkpoint gets activated upon double strand breaks (DSBs) in the DNA, subsequently the checkpoint kinases ataxia telangiectasia mutated (ATM) and checkpoint kinase 2 (CHK2) block propagation of the cycle. The time of error, in the beginning or ending of S phase, determines which of the proteins blocks the cell cycle progression. In the beginning of S phase, p53 and p21 lead to inhibition of CDK/Cyclin E/A blocking replication initiation. At the end of S phase, ATM acts via CHK2 on the phosphatase cell division control 25 (CDC25) acting on CDK1/Cyclin B resulting in block of mitotic entry during S phase and G_2. If damage like single strand breaks (SSBs) occurs during S phase/replication, the replication checkpoint gets activated mediated by ataxia telangiectasia and Rad3-related protein (ATR) and checkpoint kinase 1 (CHK1). These two checkpoint kinases act downstream on CDK1/2/Cyclin A/B activity, blocking mitotic entry [175].

However, the severity of the damage mediates the cells destiny. A threshold of what is too severe is depending on the environment and also on the cell type. In S and G_2 phase, a long-term cell cycle arrest results in an irreversible cell cycle arrest finalized in senescence or apoptosis. In G_1 phase, if the cell does not exit the cell cycle and activates the apoptosis cascade, the cell either enters the reversible cell cycle arrest, called quiescence, or irreversible arrest ending up as senescent cell [175, 204, 205].

1.5 DNA- and RNA-Damage

On a daily basis, we are exposed in our life to endo- and exogenous DNA-damaging stimuli, which, if left unrepaired, cause genomic instability as these errors are perpetuated over

subsequent cellular divisions [206, 207]. Approximately 10^5 spontaneous DNA lesions are generated daily in the mammalian genome [208]. First, exemplary endogenous sources of DNA damage are ROS or NOS (nitric oxygen species) originating from OXPHOS, endogenous alkylating agents, byproducts of lipid peroxidation, metabolites such as estrogen, free cholesterol or reactive carbonyl species, also spontaneous hydrolysis, oxidation and non-enzymatic methylation of DNA [207, 209, 210]. Second, exemplary exogenous sources of DNA damage are ultraviolet (UV) light, ionizing radiation (IR), genotoxic chemicals such as benzo[α]pyrene, Aflatoxin B1, Cisplatin, Etoposide, Mitomycin C (full list in [211]) and more which are used as chemotherapeutics [207, 212].

If the DNA damage remains unrepaired, mutations occur resulting in carcinogenesis, senescence or cell death. More detailed, these mutations can cause transcription- or replication-blocks, they alter the epigenetic landscape of the cell and induce cell cycle dysregulation. Depending on the type of DNA damage, different phenotypes and subsequent different repair mechanisms get activated [207] (drawn schematically in **Figure 7**). The maintenance of genomic stability has highest priority, therefore the cell focuses on activating signaling pathways depending on the type of lesion and repair mechanisms: DSB, SSB, inter-strand crosslinks (ICL), activation of damage-sensing proteins and signaling kinases by phosphorylation, activation and recruitment of repair proteins to lesion areas, cell cycle checkpoints and the activation of either senescence or apoptosis [207, 213].

In the following the DNA damage response (DDR) and DNA repair pathways (DRP) will be summarized. This signaling route consists of proteins that are divided in damage-sensing, response-mediating, and transducing-proteins enabling downstream signaling of effector proteins [207]. IR, chemotherapy and free radicals are known to cause DSBs [214] and they are considered to be the greatest threat to genomic stability of the healthy cell [215]. Two repair pathways exist for DSBs: Homologous recombination (HR), which is less efficient and less error-prone and non-homologous end-joining (NHEJ), which is more efficient but more error-prone [216, 217], both pathways will be introduced in the following.

DSB repair

NHEJ occurs during G_1 phase of the cell cycle and repairs lesions by combining free ends. Activation of NHEJ requires the recruitment of the phosphatidylinositol 3-kinase (PI_3K)-like kinases (PIKKs) like ATM and the DNA-PK to the sites of DSBs, inducing the phosphorylation of the histone variant H2A.X (γh2ax) next to the DSBs, building γh2ax DNA damage foci [207, 218, 219]. The phosphorylation of γh2ax is used in research as a central marker for DDR signaling. Subsequent, the PIKK-dependent phosphorylation of checkpoint kinases, such as checkpoint kinase 1 and/or 2 (CHK1, CHK2) and p53 mediates the overall cellular response, including cell cycle arrest and upregulation of genes associated with repair [220-222], inducing

cellular senescence or apoptosis [223] (**Figure 6**). Following PIKK activation, γh2ax gets polyubiquitinated and p53-binding protein 1 (53BP1) is recruited to the ubiquitin modifications on γh2ax, where 53BP1 then facilitates NHEJ or once it's removed, HR is facilitated [224-226]. A well characterized key mediator of DNA damage is p53, it is known to induce expression of a wide array of death effectors and these p53-inducible genes were shown to contribute to induction of both apoptosis pathways, the extrinsic death-receptor pathway and the intrinsic mitochondria dependent pathway [223] (**Figure 6**). Depending on the phosphorylation state of p53, the decision for either pro-survival or pro-apoptosis, is taken [223].

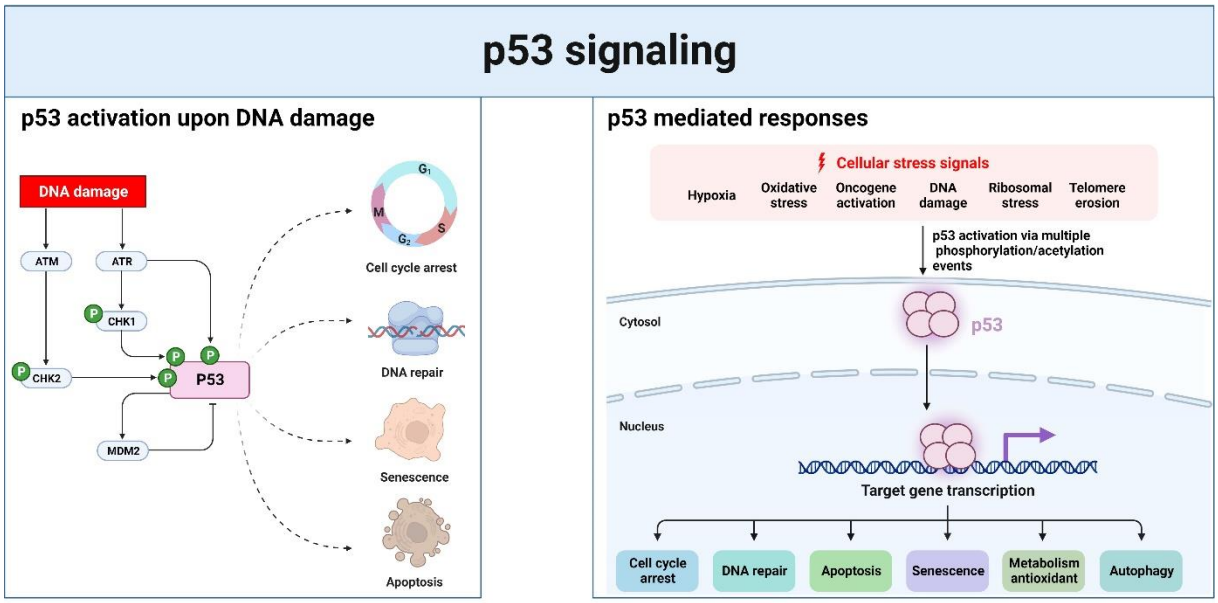

Figure 6 Overview of p53 activation, regulation and transcriptional signaling. Cellular stress signals such as DNA damage, hypoxia, oxidative or ribosomal stress, oncogene activation and telomere erosion lead to the activation of p53. For example, via the sensor proteins ATM and ATR, which then phosphorylate the checkpoint kinases CHK1 or CHK2. These kinases phosphorylate and activate p53, leading to its stabilization and oligomerization. The stability of p53 is regulated by MDM2. The multi-step regulation of p53 activation defines output on target gene transcription and the cells response to diverse stressors [227]. (This figure was created with Biorender.com according to figures in [215, 227]).

Moreover, p53 was shown to activate expression of genes that also inhibit survival signaling and is involved in mitochondrial cytochrome c and SMAC release [228]. Exemplary pathways that are p53-induced are nicely illustrated in [223] and briefly summarized: (i) DR-pathways: DR5 and CD95 (ii) Inhibition of survival signaling occurs via insulin-like growth factor 3 (IGF), binding protein 3 (BP3) and phosphatase and tensin homolog (PTEN) (iii) mitochondrial pathways: Apaf-1, Bax, Noxa, Puma [223].

Another mechanism of DNA damage repair of DSBs is HR (**Figure 7**), which occurs during G_2 and S phase of the cell cycle and a sister chromatid is needed as template for correct alignment and annealing of the DSBs during HR. For the phosphorylation of γh2ax, the PIKK protein ATR is needed and recruits key proteins such as breast cancer type 1 susceptibility protein 1 and 2 (BRCA1 and BRCA2) to the replication fork to perform HR [207, 229]. The various inducers of DNA

damage, with the different types of DNA damage and the subsequent repair mechanisms are shown in **Figure 7**.

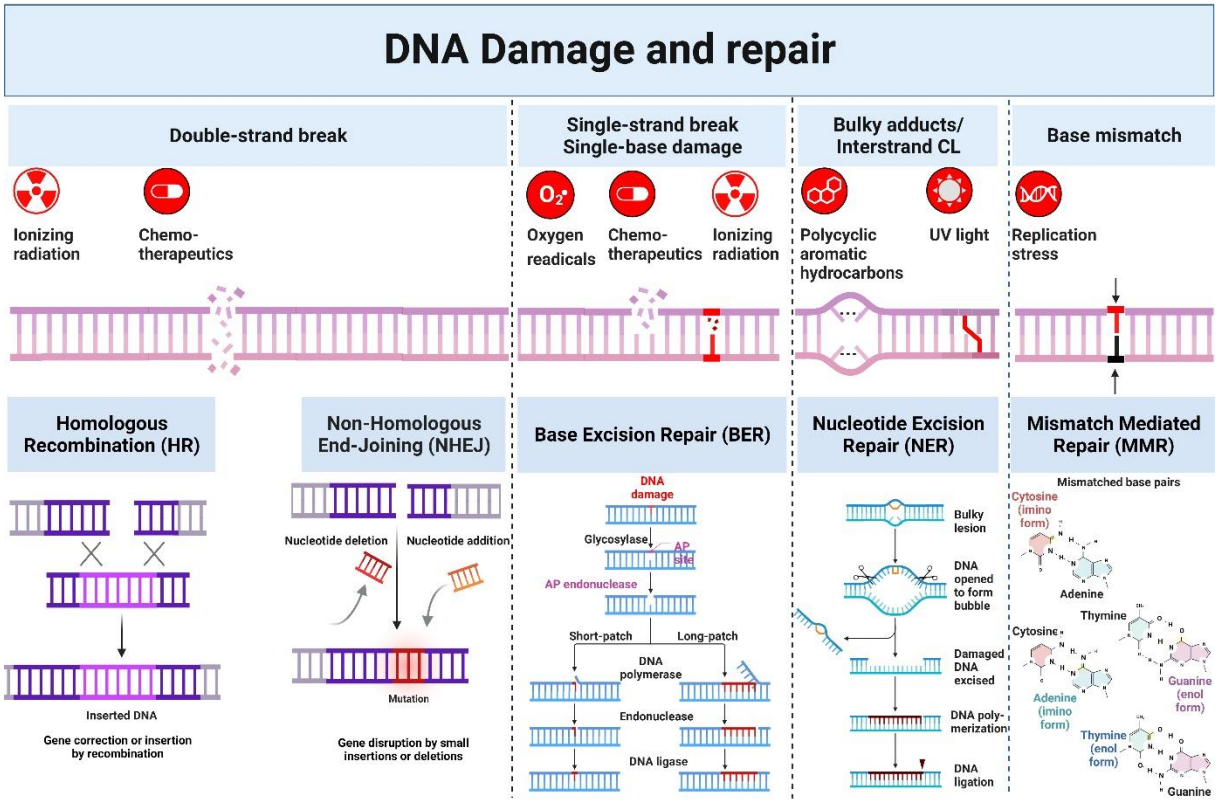

Figure 7 Common causes of DNA damage with the respective DNA repair mechanisms. A variety of cellular stressors such as ionizing radiation, chemotherapeutics, oxygen radicals, polycyclic aromatic hydrocarbons, UV light or replication stress can induce DNA damage in cells, represented by the symbols shown in red. The respective kinds of DNA damage are double-strand breaks (DSBs), single-strand breaks (SSBs)/ single-base damage, bulky adducts or interstrand crosslinks (CL) or base mismatches. The lower panel summarizes the specific DNA repair pathways that are instigated to repair the damages shown above the respective pathway. DSBs are repaired either via homologous recombination (HR), where the gene is corrected or inserted by recombination, or by non-homologous end-joining (NHEJ), where nucleotides are deleted or added into the damaged gene, resulting in a gene disruption and mutation. Base excision repair (BER) repairs SSBs in the DNA backbone. Nucleotide excision repair (NER) removes bulky lesions from the DNA strand. Mismatch mediated repair (MMR) corrects base mismatches or replication errors [214]. (This figure was created with Biorender.com according to figures in [206, 214, 230]).

Nucleotide excision repair and base excision repair

One repair pathway for SSBs is the nucleotide excision repair (NER) pathway (**Figure 7**). NER has broad substrate specificity and takes care of lesions (SSBs) caused by UV light, crosslinks, and oxidized bases or chemical-induced DNA adducts [231]. The NER pathway reacts to distinct types of DNA lesions: (i) The transcription-coupled NER (TC-NER) exclusively repairs lesions on single-stranded DNA templates during transcription and obliges the recruitment of the proteins Cockayne Syndrome A and B to the stalled RNA polymerase II at lesion sites [207, 232-234]. (ii) The general-genome NER (GG-NER) responds to genome-wide DNA damage which is recognized by the protein group of xeroderma pigmentosum C (XP)/ Human Homolog of

Rad23 B (XPC/HHR23B) complex [207, 235]. Another mechanism which recognizes and repairs SSBs is the base excision repair (BER) (**Figure 7**) and it also responds to DNA damage originating from cellular metabolism such as damaged nucleotide bases induced by ROS, methylation, hydroxylation or deamination [207, 236, 237].

Mismatch repair

The mismatch repair (MMR) system removes biosynthetic errors from newly synthesized DNA caused by DNA polymerase, such as wrong base-pairing or in-frame deletions caused by polymerase misincorporation errors between heteroallelic DNAs and chemical damage to nucleotides [238, 239] (**Figure 7**). To ensure correct replication, mismatches are repaired by a protein complex comprising the proliferating cell nuclear antigen (PCNA) ring protein [240], MutS Homolog proteins 2, 3 and/or 6 (MSH2, MSH3 and/or MSH6), MutL Homolog 1 (MLH1), exonuclease 1 (Exo1) and DNA polymerase forming the MMR assembly complex [239, 240].

Interstrand crosslink repair

To perform interstrand crosslink repair (ICR), a multitude of proteins are required, since this repair mechanism connects crosslinks between two strands, leading to roadblocks for replication and transcription, inducing replication and/or transcription-stress [241, 242] (**Figure 7**). Interstrand DNA crosslinks are formed in presence of bifunctional alkylating agents [243-246]. It was shown, that ICR-inducing agents introduce DSBs in S-phase cells associated with DNA replication forks [247-249], which are repaired predominantly by HR and not NHEJ [248, 250]. In summary, many proteins of NER, HR, structure-specific endonucleases, translesion DNA synthesis and factors responsible for Fanconi anemia (FA) are involved in ICR [207].

RNA-damage

Additional to DNA damage there exists a role of RNA in DNA DSB repair and also RNA damage [251]. A growing body of evidence suggests that RNA has a major impact in the repair of DNA damage through up to now unsolved pathways [251-259]. It is believed, that understanding the contribution of RNA to DDR will provide new insights into genome maintenance, since an emerging role of transcription, RNA-interacting and processing proteins and the RNA itself in the repair of DNA is becoming increasingly evident [251, 260-263]. To understand RNA-dependent DNA repair (RDDR) mechanisms could lead to the development of novel treatment strategies in cancer research, considering the recent emergence of RNA therapies such as for triple-negative breast cancer [264], lung cancer [265] and rare metabolic diseases [251, 266-269]. The novel role for RNA in the DNA damage signaling is that RNA pol II is recruited to DSBs, where it synthesizes damage-induced long non-coding RNAs (dilncRNAs) [270, 271]. To promote DDR signaling, these dilncRNAs are processed to generate DNA damage response RNAs (DDRNAs) [254, 261, 270-273]. The different types of RNA and their structure are schematically shown in **Figure 8** with a form of RNA damage, the RNA loop formation.

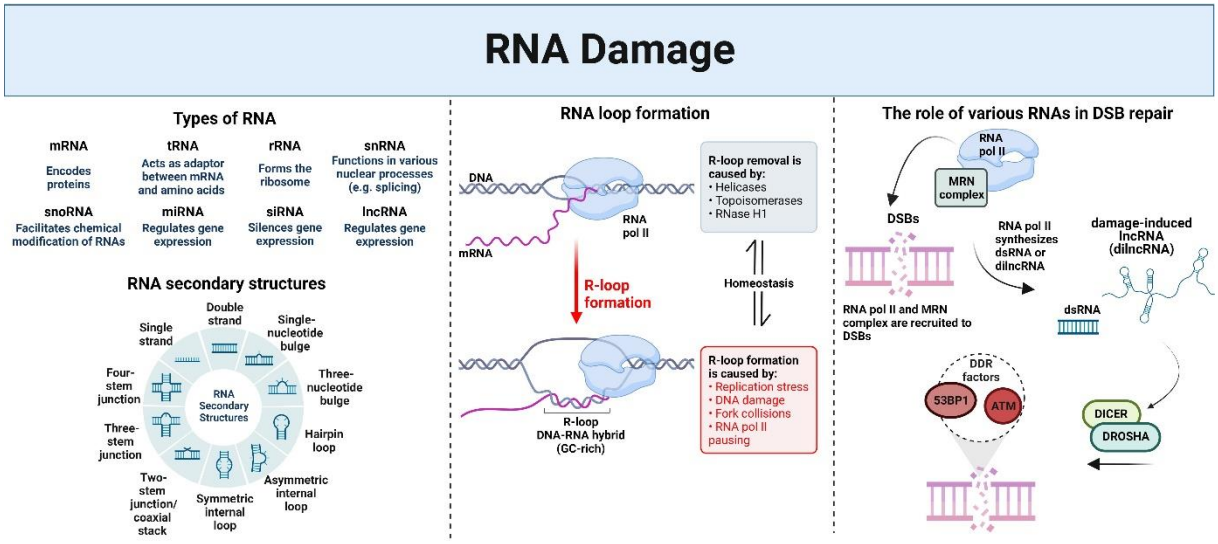

Figure 8 Different types of RNA with their secondary structure and the formation of R-loops. Different types of RNA are produced in a cell with various functions and secondary structure. Similar to DNA, also RNA can be damaged, upon different stimuli, such as replication stress, also during DNA damage, replication fork collapse or dysfunctions of RNA pol II. As response, R-loops are formed, where partially un-annealed double stranded DNA allows complementary single stranded RNA to anneal partially. These loops can be removed by helicases, topoisomerases or RNases. Upon DSBs, RNA pol II and the MRN complex get recruited to the damaged sites, where dsRNA and dilncRNA get synthesized, recruiting DICER and DROSHA which then enhance the recruitment of DDR factors like 53BP1 and ATM. (This figure was created with Biorender.com according to figures in [251, 254, 261, 270, 274]).

It was proposed by several groups, that the endoribonucleases DICER and DROSHA promote DDR activation by generating small non-coding RNAs (sncRNA) with the sequence of the DNA site of the DSB [253-255, 275, 276]. Following the DDR, ATM phosphorylates the KH-type splicing regulatory protein (KSRP) [277], which is a multifunctional RNA-binding protein that interacts with DICER and DROSHA [273, 278, 279]. Next in the DNA damage response, RNA pol II is recruited to DSBs, binds to MRE11-RAD50-NBS1 (MRN) complex and synthesizes dilncRNAs from and towards DNA ends [270]. Thereby the dilncRNAs act as DDRNA precursor and DDRNA recruiter through RNA-RNA pairing [270] (**Figure 8**). The MRN complex plays a major role in sensing and repairing DNA damage. Mutations in any of this complex members lead to hypersensitivity to genotoxic agents and predisposition to malignancy [280]. MRN triggers cell cycle checkpoint response via its interaction with ATM and ATR [281]. The data showed, that dilncRNAs together with DDRNAs drive DDR foci formation and that they associate with 53BP1 [270]. Subsequently, an inhibition of the RNA pol II prevents DDRNA recruitment, DDR activation and DNA damage repair [270].

R-Loops

An RNA:DNA hybrid interactome study showed a strong correlation between RNA-processing proteins and R-loops (composed of RNA:DNA hybrids and a single strand of DNA) [282] and that RNA:DNA hybrids directly connect RNA- and DNA-related processes, such as contribution of RNA species to DNA repair [258, 259, 272] (**Figure 8**). DilncRNAs get transcribed from damaged

DNA ends and thereby contribute to DDR signaling and repair by HR [272]. The dilncRNAs are involved in the recruitment of BRCA1, BRCA2 and RAD51 during HR without affecting DNA-end resection [272]. In detail, during S/G_2-phase the dilncRNAs pair with resected DNA ends and form RNA:DNA hybrids, which get recognized by BRCA1 and BRCA2. These RNA:DNA hybrids mediate the recruitment of RNAse H2 to induce their degradation, ensuring efficient HR-mediated repair [272]. This study also showed, that the production of dilncRNAs is dependent on RNA pol II [261, 271] and that RNA:DNA hybrid accumulation at the damaged site is dependent on RNA pol II [272]. Additionally, lncRNAs can also acts as indirect regulators of DNA repair, a list of lncRNAs and their functions in DNA repair can be found in [283]. However, R-loops do not cause genome instability directly [284] and their involvement in DNA repair is now increasingly investigated to preserve genomic stability [258, 274, 285]. The concept of RNA-dependent DNA repair has the potential to develop novel RNA therapeutic strategies in cancer.

1.6 Cancer metabolism

The processes of regulated cell death, sustained proliferation, cell division and DNA damage/ repair are all dependent on a functional cellular metabolism, since these processes are ATP-dependent. Thus in the following chapter, the cell's pathways of energy production as glycolysis, Krebs cycle and mitochondrial respiration will be reviewed. The utilization of carbohydrates, proteins and fats to synthesize energy is a process of cellular metabolism that occurs in both normal cells and cancer cells [286]. Especially, the alteration of anabolic or biosynthetic pathways is important for cancer metabolism since their manipulation enables cancer cells to produce substrates essential for enhanced division, proliferation and tumor growth. Generally, simple nutrients such as amino acids and glucose are imported into the cell. There, the conversion into usable intermediates via key metabolic pathways such as glycolysis, tricarboxylic acid (TCA) cycle, pentose-phosphate pathway (PPP) and non-essential amino acid synthesis takes place in addition to the formation of macromolecules via ATP-dependent processes [287]. The substrates can be grouped in lipids, proteins and nucleic acids [287]. The following chapter introduces the metabolic processes glycolysis and pyruvate oxidation, metabolization of fatty acids through fatty acid β-oxidation and the function of the electron transport chain, whereas detailed macromolecule synthesis and amino acid processing through oxidative deamination and transamination can be found in other sources [287-289].

1.6.1 Glycolysis

The oldest metabolic pathway that provides the cell with energy in form of ATP is glycolysis. Glycolysis was first investigated by Louis Pasteur around 1800, after decades of research it was fully elucidated with the complete pathway proposed by Embden, Meyerhof and Parnas in the 1940s [290, 291]. In general, there exist three glucose metabolism processes, glycolysis (anaerob), complete oxidation (aerob) and the PPP [292]. Glycolysis takes place in the cytosol without the need for oxygen, where glucose is converted into pyruvate and thereby ATP is produced. In sum, 10 steps catalyzed by 10 enzymes are involved in this process: Hexokinase (HK), glucose-6-phosphate isomerase (PGI), phosphofructokinase-1 (PFK), fructose-biphosphate aldolase (ALDO), triosephosphate isomerase (TPI), glyceraldehyde-3-phosphate dehydrogenase (GAPDH), phosphoglycerate kinase (PGK), phosphoglycerate mutase (PGM), phosphopyruvate hydratase (enolase) (ENO) and pyruvate kinase (PK) [292] (**Figure 9**). In normal cells, two molecules ATP are utilized and four ATP generated. Oxidizing glucose yields around 30-32 ATP molecules theoretically, originating two molecules from glycolysis [293]. Besides ATP, glycolysis produces many relevant molecules for other metabolic processes, for example glucose-6-phosphate (G-6-P) can enter the PPP producing pentose sugars and NADPH for the synthesis of fatty acids and cholesterol [294], pyruvate, which gets transported into the mitochondria for the subsequent incorporation into the TCA cycle [295]. G-6-P serves as starting point for glycogen and also lipid synthesis, since glucose-3-phosphate (G-3-P) produces glycerol used for the production of triglycerides and phospholipids [294]. Finally, the main regulators of glycolysis in cancer are HK, PFK and PK which are reviewed extensively in [292]. How glycolysis dysregulation in cancer can be targeted with therapies can be found in **1.7.4 Deregulating cellular metabolism**. An overview about the main metabolic pathways contributing to ATP production is schematically drawn in **Figure 9** and shows glycolysis, the electron transport chain coupled to oxidative phosphorylation and the Krebs cycle.

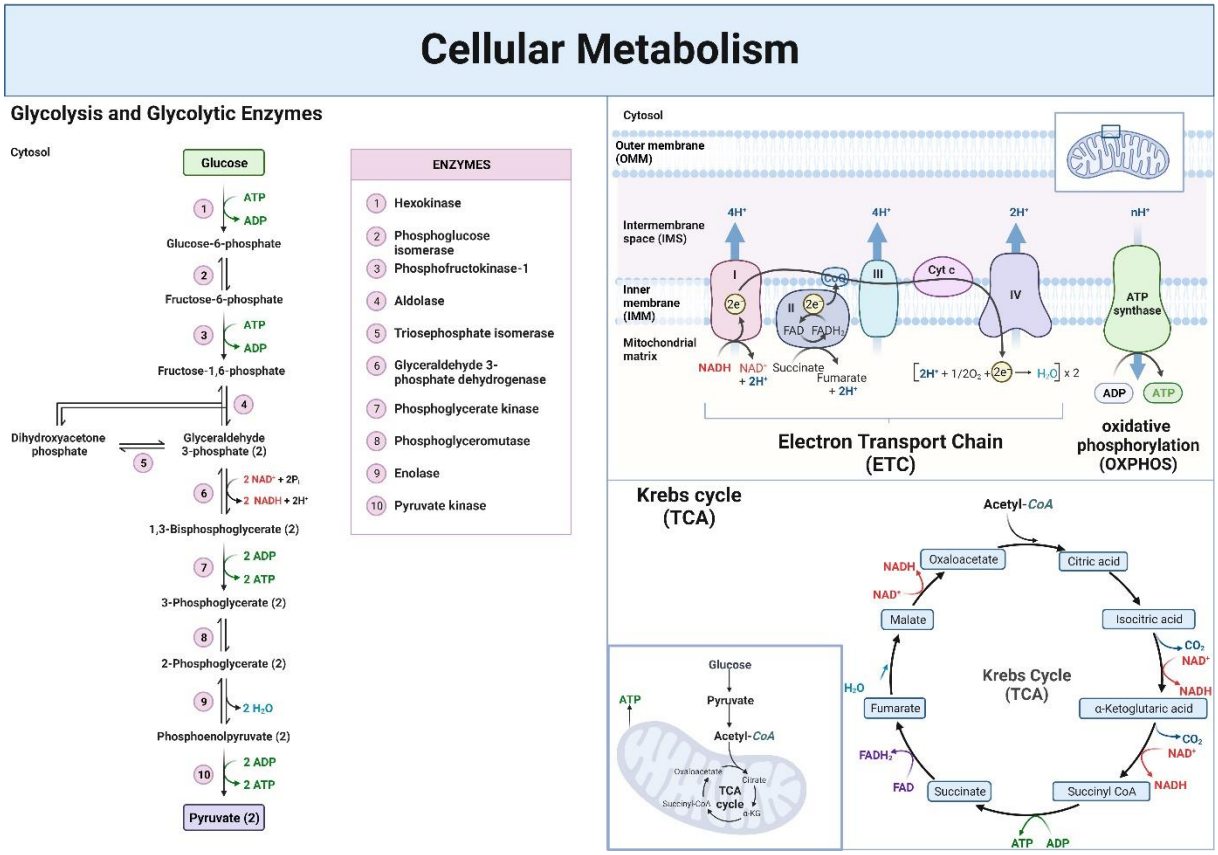

Figure 9 The main metabolic pathways procuring energy in the cell are glycolysis, the electron transport chain (ETC) coupled to oxidative phosphorylation (OXPHOS) and the Krebs cycle (tricarboxylic acid (TCA) cycle). Glycolysis takes place in the cytosol, where glucose is converted into pyruvate and thereby ATP is produced. In sum, 10 steps catalyzed by 10 enzymes are involved in this process: Hexokinase (HK), glucose-6-phosphate isomerase (PGI), phosphofructokinase-1 (PFK), fructose-biphosphate aldolase (ALDO), triosephosphate isomerase (TPI), glyceraldehyde-3-phosphate dehydrogenase (GAPDH), phosphoglycerate kinase (PGK), phosphoglycerate mutase (PGM), phosphopyruvate hydratase (enolase) (ENO) and pyruvate kinase (PK). Glycolysis produces relevant molecules for other metabolic processes, like pyruvate, which gets transported into the mitochondria for the subsequent incorporation as acetyl-CoA into the TCA cycle. The TCA takes place mainly in the mitochondrial matrix and consists of eight enzymes. The only enzyme participating in ETC, which is associated with the IMM is the succinate dehydrogenase. The TCA is supplied with pyruvate from glycolysis and once pyruvate is transported into the mitochondria, it gets converted to acetyl-CoA and CO_2, with each molecule of acetyl-CoA yielding 12 ATP molecules [295]. The electron transport chain (ETC) is located in the IMM with its main function to generate ATP via the transfer of electrons leading to and coupled with an electrochemical proton gradient driving ATP synthesis via oxidative phosphorylation (OXPHOS). The ETC is composed of four protein complexes (I-IV) and two electron carriers (coenzyme Q and cytochrome c), and the ATP synthase is (complex V). (This figure was created with Biorender.com according to information and figures in [286, 287, 296, 297]).

1.6.2 TCA cycle

Closely connected to glycolysis is the tricarboxylic acid (TCA) cycle, which is also known as Krebs cycle or citric acid cycle that takes place in the mitochondria. Hans Adolf Krebs discovered this pathway in 1937 and marked a milestone in biochemistry [298]. The TCA cycle consists of eight enzymes, with all of them being present in the mitochondrial matrix except for succinate dehydrogenase, which is associated with the IMM and participates in the ETC. The TCA is supplied with pyruvate from glycolysis and once pyruvate is transported into the

mitochondria, it gets converted to acetyl-CoA and CO_2, with each molecule of acetyl-CoA yielding 12 ATP molecules [295]. In detail, acetyl-CoA undergoes oxidation to CO_2 in eight steps and the reactions yield NADH+H$^+$, $FADH_2$ and GTP [295] (**Figure 9**). Finally, NADH+H$^+$ and $FADH_2$ are provided for the ETC complex I (NADH dehydrogenase) and complex II (succinate dehydrogenase) [295, 297, 299]. Regulation of the TCA cycle is performed through three enzymatic reactions by citrate synthase, isocitrate dehydrogenase and α-ketoglutarate dehydrogenase, whereas the availability of substrates like NAD$^+$ and FAD also control the cycle [295]. However, a continual interplay between glycolysis, TCA and OXPHOS is crucial to maintain the cells in a stable equilibrium ensuring continuous energy supply.

1.6.3 Electron transport chain and OXPHOS

The mitochondrion was initially branded in 1957 by Peter Siekevitz the 'powerhouse' of the cell [300]. Peter Mitchell stated in the chemi-osmotic theory in 1961 [301] that substrate oxidation and the resulting electrons are linked to ATP synthesis coupled in mitochondrial ETC [302]. Later in 1966, Jensen reported that mitochondria generate ROS as a byproduct of cellular respiration [303]. It is now widely recognized that mitochondria, as highly dynamic organelles, play a significant role in maintaining cellular homeostasis by producing ROS for intracellular signaling and ensuring a continuous supply of ATP [286]. Mitochondrial ATP generation and ROS production are linked through function of the ETC [286].

As already introduced in the first chapter, the ETC is a process that occurs in the IMM in order to generate ATP (**Figure 9**). The ETC is a series of electron transfer reactions in which electrons are passed along a chain of protein complexes and co-factors, ultimately leading to the generation of an electrochemical proton gradient across the membrane. The process of electron transfer is coupled to the pumping of protons from the mitochondrial matrix to the IMS, creating a gradient of protons that is then used to drive ATP synthesis via an ATP synthase. The ETC is composed of four protein complexes (I-IV) and two electron carriers (coenzyme Q and cytochrome c), where the ATP synthase is commonly referred to as complex V. Mitochondrial respiration via the ETC involves the transfer of electrons from NADH and $FADH_2$ to oxygen (O_2), which is the final electron acceptor, byproduct of the ETC and reason for the name 'mitochondrial respiration' [286, 288, 289, 302]. The function and structure of each complex will be introduced in the following.

Complex I

The NADH-ubiquinone oxidoreductase - complex I - transfers electrons from matrix NADH to ubiquinone. Structural analysis showed that complex I has two domains, a matrix arm protruding into the matrix and an inner arm which is embedded in the inner membrane [304]. A series of co-factors, including flavin mononucleotide (FMN) and seven iron-sulfur (FeS)

clusters with varying potential, facilitate the transfer of electrons from NADH (produced in TCA) to ubiquinone (CoQ) in complex I. This transfer process, known as the Q cycle, leads to the reduction of CoQ to ubiquinol (QH_2) while also triggering the movement of protons from the matrix to the IMS via complex I [286, 304-306].

Complex II

The succinate dehydrogenase – complex II – is part of the ETC and also a component of TCA cycle, OXPHOS and metabolism. In the TCA, complex II catalyzes the oxidation of succinate to fumarate [295]. In the ETC, complex II is another entry complex for electrons, transferring them from succinate to coenzyme Q via iron-sulfur clusters. Structurally, complex II consists of two subunits. First is composed of two membrane-integrated proteins serving as anchor to the inner membrane, which additionally contain the coenzyme Q binding site. Second is composed of two subunits located on the matrix of the IMM, containing a succinate binding site, iron-sulfur cluster and a flavoprotein bound to FAD. With receiving electrons from succinate, FAD is reduced to $FADH_2$, which then transfers the electrons to the iron-sulfur clusters. Subsequently coenzyme Q obtains electrons from the FeS cluster and gets reduced to QH_2 [302, 307-310].

Complex III

The coenzyme Q-cytochrome c reductase – complex III – transfers electrons carried by QH_2 to cytochrome c. Structurally, complex III has a dimeric structure with each monomer consisting of 11 subunits [311]. The catalytically active subunits are cytochrome b, cytochrome c, an iron-sulfur cluster enveloped by an iron-sulfur protein [312]. Two coenzyme Q binding sites are embedded in the IMM and located on both ends of cytochrome b. The QH_2 oxidation site (Q_O) is situated at the cytoplasmic side, while the Q-reduction site (Q_i) is located on the matrix side [313]. The electron transport process begins in complex III at QH_2 being oxidized to ubisemiquinone (QH^-) after an electron is transferred to the iron-sulfur cluster with the subsequent release of two protons into the IMS [314]. The iron-sulfur cluster transfers this electron to cytochrome c and the reductive QH^- transfers the second electron to cytochrome b. The reduced cytochrome b then transfers this electron to coenzyme Q. To complete the Q-cycle, the second QH_2 is oxidized while releasing the two other protons. Similarly, one electron is transferred to the iron-sulfur cluster, while the other is transferred to cytochrome b and then QH^- to produce QH_2 [286, 302, 310].

Complex IV

The cytochrome c oxidase – complex IV – transfers electrons from cytochrome c to oxygen as the terminal electron acceptor to generate water H_2O [302]. Complex IV has a very complicated structure and is composed of 13 subunits, each of which contains four redox-reactive metal centers: Cu_A, heme a (Fe_a) and a binuclear center consisting of heme a_3 (Fe_{a3}) and Cu_B [302, 315, 316]. The 13 subunits are composed of 10 nuclear encoded accessory and three

subunits encoded by mitochondrial DNA (mtDNA) which are the key subunits [302, 317, 318]. Subunit I contains two copper centers and two heme groups that are responsible for oxygen binding and oxygen reduction. Heme groups are also attached in subunit II and are involved in electron transfer processes from cytochrome c to subunit I. Subunit III stabilizes the whole complex during electron transfer. Additional to the core subunits (IV, V_a, V_b, VI_a), the accessory subunits are also involved in stabilization and assembly and regulation of the complex. Three main domains arrange the overall structure: The transmembrane, the catalytic and the peripheral domain. The transmembrane domain spans the IMM and consists of subunits I, II and IV, while the catalytic domain is located on the matrix side containing the subunits I, II and III. The peripheral domain is on the intermembrane side of the complex and includes the remaining accessory subunits. Via the transmission over complex IV, from cytochrome c to oxygen, a proton gradient is generated enabling the production of ATP in the inner membrane with the ATP synthase [286, 302, 310].

Complex V

F_1F_0 ATP synthase – complex V – is made up of two functional domains: F_0 and F_1, whereas F_1 is located to the mitochondrial matrix [319, 320] and F_0 is situated in the IMM [319, 321]. Two electrons at a time are transferred to O_2 to generate one H_2O molecule, which is accompanied by the pumping of four protons from the matrix to the IMS through complex I, III and IV [302]. From there, protons pass from the IMS to the matrix through F_0, which transfers the energy created by the electrochemical gradient to F_1, causing a conformational change in F_1F_0 ATP synthase enabling the phosphorylation from adenosine diphosphate (ADP) with inorganic phosphate (P_i) to ATP [321]. The proton gradient generates a proton-motive force composed of an electrical membrane potential ($\Delta\Psi m$) and a pH differential [322]. Recently, another role of ATP synthase beyond oxidative phosphorylation is discussed – its function as a unique regulator of mPTP opening. Several studies suggested that the F_1F_0 ATP synthase houses the channel of mPTP [323-334]. In more detail, it was suggested that the channel is formed by ATP synthase dimers together with subunit e and g [325, 326, 328, 329, 333], since experiments in yeast mutants lacking subunit e and g displayed resistance to channel opening [325, 326, 330].

1.6.4 Mitochondrial fatty acid β-oxidation

As reviewed above, minor ATP synthesis takes place by glycolysis in the cytoplasm, but the majority is produced in mitochondria by close exchange between TCA cycle and respiratory chain. As reviewed above, the oxidation of glucose yields around 30-32 ATP molecules, of which two molecules originate from glycolysis, two from TCA and around 26-28 molecules from ETC (theoretical values) [293]. Another source for ATP synthesis is mitochondrial fatty acid β-oxidation (FAO). FAO is the process, where free fatty acids (FFAs) are translocated into the

mitochondria where they are oxidized to ketone bodies. Palmitate, an exemplary FFA yields 106 ATP molecules [293]. Thus, FAO is defined as the catabolic process through which fatty acids (FAs) are degraded in mitochondria in order to produce acetyl-CoA [47] and schematically shown in **Figure 10**.

Fatty acids are hydrophobic molecules, composed of an aliphatic hydrocarbon chain and a carboxylic acid moiety at the end [335]. Typically, these chains are made up of 16-18 carbons and can either be saturated or unsaturated and contain one or more double bonds [335, 336]. FAs can be grouped depending on their chain length into short, medium or long chain FAs (SCFA- , MCFA- , LCFA-acyl-CoA such as palmitoyl-CoA) [293]. Fatty acids have many biologically important roles and serve as substrates for acyl-CoA synthase. Acyl-CoA synthase activates the FAs by linking them to acyl-CoA molecules, passing them from the cytosol into the IMS [293]. However, these activated FA-CoAs are impermeable to cross lipid membranes, but with the reversible replacement of the CoA moiety by $_{L}$-carnitine via the carnitine palmitoyl transferase 1 (CPT1) [337], the acyl-carnitines are able to pass the IMM via the carnitine/acyl-carnitine translocase into the mitochondrial matrix, the location of the β-oxidation process [293, 338]. During β-oxidation FA molecules are broken down into smaller carbon molecules that subsequently enter the TCA cycle. This results in the production of acetyl-CoA fragments from the FA molecules which are utilized by the TCA to generate ATP [339]. The β-oxidation is composed of four biochemical cyclic reactions. Acyl-CoA undergoes oxidation with flavin-adenine dinucleotide (FAD) as cofactor, reducing ubiquinone to ubiquinol (Acyl-CoA dehydrogenase). The electron transfer from ubiquinol to the ETC generates 1.5 ATP molecules. The Acyl-CoA is oxidized to an alkene at the α, β-position, which is transformed to an alcohol by Enoyl-CoA hydratase in the second step. The third step involves another oxidation to a ketone group (3-Hydroxy acyl CoA dehydrogenase), coupled to NAD^+ reduction to NADH and 2.5 ATP molecules as byproduct. In the fourth and last reaction, the thiol group of the next CoA molecule catalyzes cleavage of 3-ketoacyl-CoA into acyl-CoA and acetyl-CoA (3-Ketoacyl CoA thiolase). This cycle repeats until the FA chain is completely converted into acetyl-CoA, entering the TCA resulting in 10 ATP molecules [335, 340, 341].

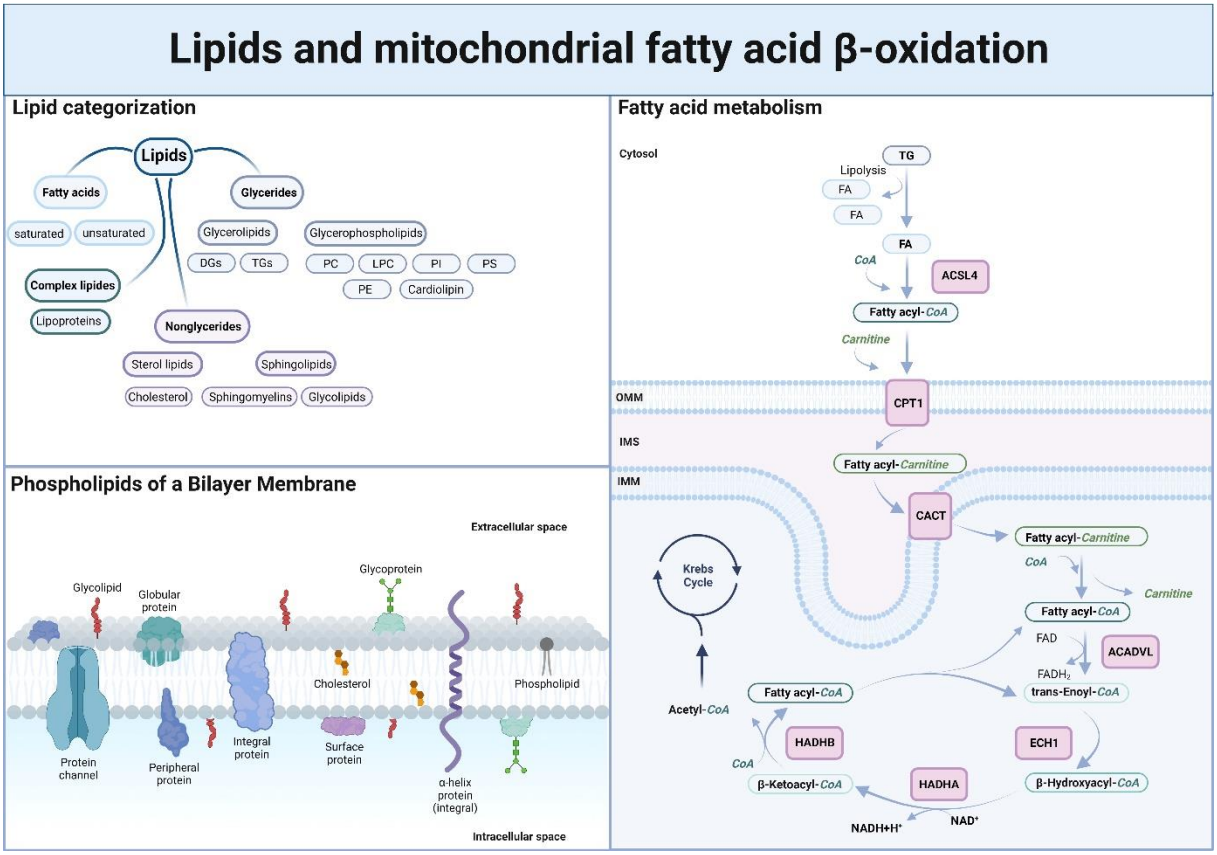

Figure 10 Lipid categorization and mitochondrial fatty acid β-oxidation (FAO). Including lipid categorization and the phospholipids of a bilayer membrane on the left and mitochondrial FAO on the right. Lipids can be categorized in fatty acids (unsaturated or saturated), complex lipids like lipoproteins and glycerides such as glycerolipids (diglycerides (DGs) and triglycerides (TGs)) and glycerophospholipids like phosphatidylcholine (PC), lisophosphatidylcholine (LPC), phosphatidylinositol (PI), phosphatidylserine (PS), phosphatidylethanolamine (PE) and cardiolipin (CLN). An additional category are nonglycerides including sterol lipids as cholesterol and sphingolipids as sphingomyelin or glycolipids. A biological bilayer membrane can be composed of the shown phospholipids differing from membrane to membrane. The fatty acid metabolism is shown as the release of fatty acids (FAs) from triacylglycerol in lipolysis and translocated to the mitochondria, where the FAs get activated by acyl-CoA syntethase long chain 4 (ACSL4) with coenzyme A (CoA). Together with carnitine, the carnitine palmitoyltranslocase (CPT1) transports the FAs across the OMM into the IMS and with the carnitine/acyl-carnitine translocase (CACT) into the mitochondrial matrix, where the process of β-oxidation takes place. This process consists of four main reactions, the oxidation of acyl-CoA with participation of FAD by acyl-CoA dehydrogenase very long chain (ACADVL), here electrons from $FADH_2$ reduce ubiquinone to ubiquinol, transferring them to the ETC leading to ATP generation. The acyl-CoA oxidation introduces a double bond in the FA chain, which gets hydrolyzed in the second step by enoyl-CoA hydratase 1 (ECH1). Next, an oxidation creates a ketone group at the C-3 and reduces NAD^+ to $NADH^+H^+$ (which generates 2.5 ATP molecules) via hydroxyacyl-CoA dehydrogenase trifunctional multi-enzyme complex subunit α (HADHA). In the last step, the thiol group of the next CoA molecule resolves ketoacyl-CoA into acyl-CoA and acetyl-CoA via thiolytic cleavage by hydroxyacyl-CoA dehydrogenase trifunctional multi-enzyme complex subunit β (HADHB). The process of intramitochondrial β-oxidation is repeated until the initial FA chain is converted into acetyl-CoA. This acetyl-CoA is fueled into the Krebs cycle in order to generate 10 ATP [335, 340, 341]. (This figure was created with Biorender.com according to information and figures in [335, 339, 342, 343]).

The process of FAO gained more attention since the knowledge about its involvement in the development of various cancer types increased in the last years [288, 344-356]. However, the mechanisms by which FAO promotes chemotherapy resistance in tumor cells is unknown. Also, it is not known how the increased rate of FAO in chemotherapy resistant cells counteracts

apoptosis [354]. All metabolic pathways are interconnected and intercontrolled within a cell and the breakdown of substrates such as glucose, fatty acids or amino acids ultimately aims to generate ATP. The interplay between glycolysis, Krebs cycle and mitochondrial respiration is extremely vulnerable in cancer cells, therefore new therapies to target chemotherapy resistant cancer cells are needed.

The next chapter reviews the hallmarks of cancer, provides current therapeutic options targeting four selected hallmarks (‘*Resisting cell death’* (apoptosis), *‘genome instability and mutation’* (DNA-damage), *‘sustaining proliferative signaling’* (cell cycle) and *‘deregulating cellular metabolism’*) and reviews known mechanisms by which the cancer cells in turn develop chemotherapy-resistance.

1.7 Targeting the hallmarks of cancer

Cancer is known as one of the main causes of death around the world. It’s still a major threat to human health and the current therapies include surgery, radiationtherapy, chemotherapy, immunotherapy, targeted therapy, hormone therapy, stem cell transplantation, precision medicine and combinatorial treatments of these.

While many anticancer drugs demonstrate impressive effectiveness in initial treatment, a considerable number of cancer patients develop drug resistance during their treatment progresses [357-359]. Cancer cells become resistant to chemotherapy by mechanisms including drug inactivation, apoptosis inhibition, alterations in drug metabolism, changes in the epigenetic landscape, mutations in the drug target, enhanced DNA repair, reduced drug absorption and metabolic optimization for tumor growth and metastasis [360]. For instance 30-55% of patients with non-small cell lung cancer (NSCLC) relapse after treatment [361], 50-70% of ovarian adenocarcinomas recur after surgery and chemotherapy [361, 362] and 20% of pediatric acute lymphoblastic leukemia cases recur [363, 364]. At present (recently updated 2022 by D. Hanahan), the eight hallmarks of cancer denote the attained abilities to ‘*maintain proliferative signaling, avoid growth suppressors, withstand cell death, facilitate replicative immortality, initiate/access vasculature, trigger invasion and metastasis, alter cellular metabolism and evade immune destruction’* [365] (**Figure 11**). Additional to the core hallmarks, emerging hallmarks and enabling characteristics have been added, comprising the *‘unlocking of phenotypic plasticity, nonmutational epigenetic reprogramming, polymorphic microbes and senescent cells’* [365] (**Figure 11**). Finally, several therapeutic strategies have been developed and new ones are continuously needed to overcome radiation- and chemotherapy-resistance. Each one targets another hallmark of cancer, which will be described for four selected hallmarks (marked in red in **Figure 11**): *‘Resisting cell death’* (apoptosis), *‘genome instability*

and mutation' (DNA-damage), *'sustaining proliferative signaling'* (cell cycle) and *'deregulating cellular metabolism'*.

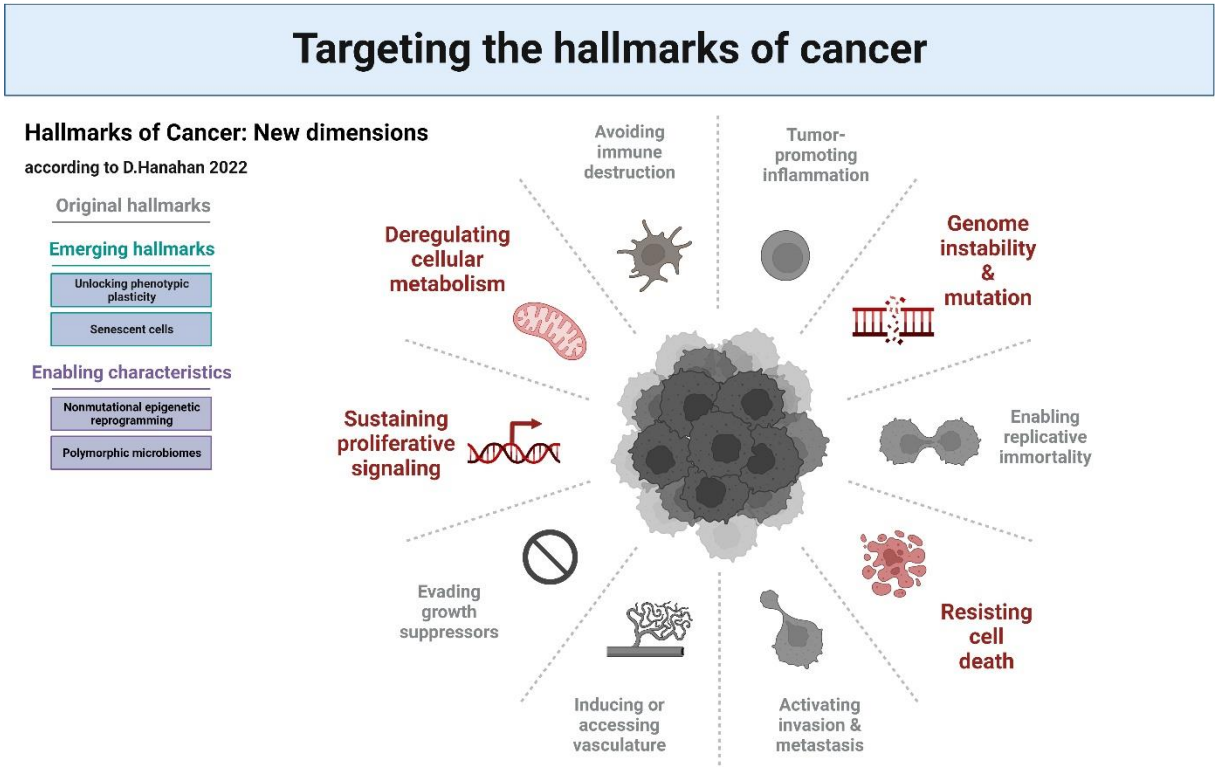

Figure 11 Targeting the hallmarks of cancer. The hallmarks of cancer from 2022 by D. Hanahan consist of ten key hallmarks (in grey), two emerging hallmarks (on the left in green) and two enabling characteristics (on the left in purple) [365]. Here, four hallmarks are highlighted in dark red, since deregulating cellular metabolism, sustaining proliferative signaling, genome instability and mutation and resisting cell death are the four hallmarks that will be addressed in this dissertation, which is explained further in **Aims**. (This figure was created with Biorender.com according to information and figures in [365]).

1.7.1 Resisting cell death

'Resisting cell death' was established as a hallmark of cancer already in 2000 as 'evading apoptosis' [366]. Resistance to apoptosis can be acquired by cancer cells through various strategies, most commonly through the development of mutations leading to the loss of pro-apoptotic regulators such as p53 or mutations in the PI_3K-Akt survival pathway [366]. In summary, increased expression of anti-apoptotic and survival signaling proteins, decreased expression of pro-apoptotic proteins or alteration of the extrinsic death receptor pathway, all cancerous alterations lead to apoptosis-evading mechanisms [367], which can and are targeted by therapies. A list of therapeutic approaches targeting the apoptosis intrinsic pathway (only active clinical trials, updated manually, that were active until 14.03.2023) includes: BH3-mimetics such as dual Bcl-2 and Bcl-x_L inhibitors (Navitoclax), selective Bcl-2 inhibitors (Venetoclax, APG-2575), Bcl-x_L inhibitors (ABBV-155), Mcl-1 inhibitors (AMG 176) and IAP protein inhibitors and SMAC mimetics (Birinapant) [368] (this review summarizes intrinsic, extrinsic apoptosis targeting drugs, as well as other approaches targeting apoptosis in cancer

cells [368]). An example of acquired radiation- and chemoresistance (to paclitaxel) is developed in ovarian cancer cells by the inactivation of p53-mediated apoptosis via the active repression of pro-apoptotic genes such as Puma, ATM and PTEN [369]. One example are human breast cancer cells (MCF7 cells) which overexpress Bcl-2 and thereby acquire chemotherapy resistance to Adriamycin [370]. Generally, an increased Bcl-2 expression correlates with impaired and/or inhibited apoptosis and is involved in the development of multidrug resistance (MDR) [371]. Furthermore, the upregulation of Bcl-2, Akt, Bcl-x_L, Bcl-$_w$, Mcl-1 and other anti-apoptotic genes increases tumor cell resistance to chemotherapy [360, 363, 367].

1.7.2 Genome instability and mutation

'Genome instability and mutation' is a hallmark of cancer which gets addressed by therapies acting on the DNA damage response [372] and was introduced in 2011 as an enabling characteristic in the hallmarks of cancer [367].

The proteins regulating genomic stability and DNA maintenance are often called 'caretakers' of the genome. Various abnormalities that impact different parts of the DNA maintenance machinery include inactivating mutations or epigenetic repressions of proteins involved in (i) identifying DNA damage and initiating repair mechanisms, (ii) directly restoring damaged DNA and (iii) deactivating or intercepting mutagenic molecules before they can harm the DNA [367]. In terms of genomic stability, the role of p53 has to be highlighted, since it is being called the 'guardian of the genome' for healthy cells [373]. Therefore it is not surprising, that somatic p53 mutations occur in almost every type of cancer at rates from 38-50% in ovarian, esophageal, colorectal, head and neck, larynx and lung cancers), to about 5% in primary leukemia, sarcoma, testicular cancer, malignant melanoma and cervical cancer as analyzed in [374]. Generally, p53 is a tumor suppressor gene that plays a crucial role in preventing the development of cancer since it monitors DNA damage and promotes either repair or apoptosis in cells with irreparable damage. Thereby, mutations in the p53 gene that disrupt its function lead to tumorigenesis. Exemplary mutations are functional loss of p53 (loss of its tumor suppressor function), dominant-negative effect (expression of mutant protein which interferes with function of normal p53 protein, leading to reduced tumor suppressor activity) and gain of function (leading to new functions, promoting cell survival, proliferation or invasion, thereby contributing to development and progression of cancer) [375]. Overall, p53 mutations are associated with increased genomic instability, resistance to apoptosis and an altered metabolism, contributing to the hallmark of cancer *'genome instability and mutation'*.

The gold standard for cancer therapy in the last 30 years has been mainly the usage of genotoxic drugs that cause DNA damage and catastrophic levels of genome instability [372]. Exemplary genotoxic drugs damaging the DNA are substances that alkylate bases

(Temozolomide) [376], cleaving the sugar-phosphate backbone of the DNA (Bleomycin) [377] or that covalently crosslink DNA strands (Cisplatin) [378]. DDR modulation is indirectly induced by drugs inhibiting epigenetic proteinogenic regulators (DNA methyltransferase 1; DNMT1), DNA synthesis proteins (DNA polymerase)) and proteins that have an indirect role in DNA replication (topoisomerase) (reviewed in [372]). Drugs addressing genome instability and mutation as hallmark (reviewed in [372]) are under current clinical evaluation: They include compounds targeting protein kinases of the cell cycle DNA checkpoints (CHK1 and WEE1), enzymes involved in BER (apurinic-apyrimidinic endonuclease 1; APEX1), direct repair (6-O-methylguanine-DNA methyltransferase; MGMT), NHEJ; DNA-PK and telomere regulation (telomerase reverse transcriptase; TERT) are under current clinical evaluation addressing *'genome instability and mutation'* as hallmark (reviewed in [372]). Exemplary drugs targeting DNA repair mechanisms are targeting for example: Replication protein A (RPA) inhibitors (TDRL-552, SMI MCI13E), ATR inhibitors (VX-970, AZD6738), DNA-PK inhibitors (NU7026, NU7441, AZD7648), inhibitors of homologous recombination (B02) and inhibitors of translesion synthesis (TLS; responsible for repair of inter-strand cross-links) (JH-RE-06, T2AA) (extensively reviewed in [379]). The efficiency of the drug depends on the inhibition of DNA repair or the induction of high levels of DNA damage, thus the development of mutations or epigenetic silencing of the executive proteins in these regulatory pathways is then responsible for the generation of chemotherapy-resistance. Resistance to these agents occurs by mutations in the DNA repair systems as described above in **1.5 DNA- and RNA-Damage** (NER, HR). An example for chemotherapy resistance is cisplatin-resistance in gastric cancer patients with human epidermal growth factor 2 (HER2) overexpression [380]. Induction of DNA damage in cancer with chemotherapeutics has unfavorable side effects to healthy cells and has to be treated ambivalently [381]. However, the activation or inactivation of DDR genes in various cancers and the development of the respective activator or inhibitors is still of major interest in cancer therapy research [230, 382].

1.7.3 Sustaining proliferative signaling

Another toxic trait of cancer is the hallmark *'sustaining proliferative signaling'*, which was introduced in 2011 [367] including processes like altered differentiation, increased proliferation, dysregulated DNA repair leading to genetic instability, malignancy and tumorigenesis [383]. Cancer cells form tumors by ensuring proliferative signaling and dysregulating the cell cycle. These mechanisms and therapeutic opportunities will be reviewed below.

Genes involved in cell cycle regulation, such as Rb or p53 are often mutated to enable the cancer cell to proliferate uncontrollably, forming a tumor. In the case of Rb, its functional inactivation and consequent deregulation of E2F-dependent gene transcription are main

contributors to tumorigenesis [185]. Thus, it is not surprising that high oncogene-driven E2F activity induces aberrant cell proliferation, since under oncogenic conditions, the cell has prolonged E2F activity in S phase, which enables it to recover from replicative stress thereby regulating its genomic stability [384]. Moreover, cancer cells frequently bypass the DNA damage checkpoint, which permits them to undergo uninterrupted cell division in spite of the buildup of genetic anomalies [175]. Enhanced cell proliferation and metastasis is mostly driven by mutations in proteins of the cell cycle, especially increased CDK activity has been widely reported in various cancer entities [385], rendering CDKs attractive targets for new treatments.

The ongoing research focuses on targeting the CDK-Rb-E2F axis with several highly specific small molecule inhibitors for CDK4/6 (Palbociclib, Ribociclib, Abemaciclib) [386] which lead to Rb hypophosphorylation and a stable cell cycle arrest in G_1 [384] (clinical trials with results can be found in [387-390]). So far only two small molecules have been described that directly target and inhibit E2F activity without the upstream involvement of CDK-Rb regulation: HLM006474 [391, 392] resulting in a downregulated E2F target gene expression with anti-proliferative and anti-apoptotic activity in multiple cancer cell lines [391] (which was additionally observed to prevent tumor initiation [384, 393]). The second molecule is the nucleoside analogue ly101-4B, which was found to decrease E2F activity, reducing viability in cell lines being more efficient in lines with high E2F activity. When comparing these two, HLM006464 was acting independent on cell-specific E2F levels, leading to the assumption that ly101-4B might be more specific despite its unknown mechanism of action [384, 394].

A direct targeting of the CDK-Rb-E2F axis is to target the CDKs directly with CDK inhibitors (CDKi), differentiating between pan-CDKi and specific CDKi. In general, 21 CDKs have been identified [395] (their CDKis are reviewed in Zhang 2021 [396]), with all having different roles in cell cycle, gene transcription, insulin secretion, neuronal functions and glycogen synthesis [397]. As mentioned in chapter **1.4 Cell cycle**, CDK4/6, CDK1 and CDK2 are responsible for the cell cycle, whereas CDK7, 8, 9 and 11 have a regulative transcriptional role [395]. CDK7 initiates transcription by phosphorylating RNA polymerase II at Ser5 and CDK9 promotes elongation of transcription by phosphorylating RNA polymerase II at Ser2. CDK8 is involved in a mediator complex regulating many genes and CDK11 acts on the splicing machinery [396].

Since the 1990s CDKis have been studied and many drugs targeting specific or pan-CDK activity have been developed and analyzed in clinical trials, some of which will be reviewed briefly. Pan-CDK inhibitors such as Flavopiridol or Roscovitine block cell cycle and inhibit proliferation, whereas their flaw is to lack selectivity, with high toxicity and thereby harm normal cells [396] (most of them failed in clinical trials [386, 398, 399]). The second generation CDKis (Dinaciclib, AT7519, TG02, Roniciclib, RGB-286638, P276-00) are efficient in terms of anti-tumor activity in preclinical trials, but the efficacy and safety of these drugs is currently under verification in clinical trials [396]. In sum, pan-CDKis were observed to exhibit serious side effects

and safety concerns besides their promising clinical efficacy ([396] reviews pan-CDKis under development and [400] reviews CDKis in solid tumors in clinical trials).

Since the clinical application of pan-CDKi revealed their low specificity and high side effects on normal cells, this thesis focused on specific CDKi used in cancer therapy. Each cancer type is associated with its own abnormal gene expression levels, thus the selection of appropriate specific CDKi is needed to ensure therapeutic efficacy. The first specific CDK4/6 inhibitors approved by the U.S. Food and Drug Administration for clinical treatments are Palbociclib, Ribociclib or Abemaciclib [401-404]. These types of CDK4/6i induce cell cycle stop between G_1 to S phase by blocking the phosphorylation of Rb [404]. Combinational therapies with CDK4/6i are currently in clinical trials for anticancer therapy and other diseases. CDK7 fulfills a dual role as it acts in cell cycle control and transcriptional control mediation. Many specific inhibitors with anti-tumor activity have been developed (BS-181, ICE0942, LDC4297, QS1189 & THZ1, THZ2, YKL-5-124 [396]). Another polyfunctional CDK as an attractive therapeutic target for cancer treatment is CDK9, which regulates cellular transcriptional elongation and mRNA maturation [405, 406]. A review summarizing the progress in CDK9i showed, that most compounds, targeting non-transcriptional CDKs with less specificity, were more successfully evaluated and also induce apoptosis in various tumor cells (for instance Dinaciclib (CDK1,2,5,9,12) or TG-02, targeting CDK1,2,3,5 [407-409]). However, molecules that are capable of inhibiting the cell cycle and exhibiting transcriptional CDK activity may provide even superior anticancer efficacy [410, 411].

Many CDKi share a structural azaindole framework and azaindole-derivatives were reviewed as preclinical drugs or clinical candidates with high biological activity and promising therapeutically advanced properties [412].

1.7.4 Deregulating cellular metabolism

The formation of tumors and their growth depends on various metabolic processes that are distinctly different from normal tissues. *'Deregulating cellular metabolism'* was newly introduced in 2022 as a hallmark of cancer [365] since tumor cells undergo metabolic reprogramming as a consequence of mutations, resulting in an in- or decreased metabolic flux through conventional metabolic pathways [287]. This altered metabolic activity is used to support anabolic growth during nutrient-replete conditions or catabolism to ensure cell survival in nutrient limited conditions and the protection of redox homeostasis (maintaining NAD^+/NADH redox balance [413]) to counteract negative effects of oncogene activation and tumor suppressor loss [287, 414].

Most tumor cells prefer aerobic glycolysis to mitochondrial OXPHOS, even in the presence of oxygen. This phenomenon is known as Warburg effect and a classic example for

reprogrammed metabolic pathways in cancer metabolism [415]. Glycolysis is usually a physiological response to hypoxic conditions, but during the 1920s Otto Warburg observed abundant lactate levels in tumor slices, regardless of the availability of oxygen [416]. Molecular upregulation of glycolysis is induced by hypoxia-inducible factor 1α (HIF-1α), which enhances transcription of phosphoglycerate kinase 1 (PGK) and lactate dehydrogenase (LDH) [417]. The increase in glycolytic flux is used to fulfill the increased metabolic demand of proliferating cancer cells [413].

A well characterized deregulated pathway in cancer is gain of function of myc (c-myc; MYC henceforth) by gene amplification, chromosomal translocation and single-nucleotide polymorphisms (SNPs) [287]. Myc is a transcription factor, that regulates the expression of genes supporting anabolic growth, such as transporters and proteins involved in fatty acid synthesis, glycolysis, glutaminolysis, serine metabolism and mitochondrial metabolism [287, 418]. Tumor suppressors like p53 (mutated or deleted in 50% of all human cancers [287]) regulates also metabolism since its loss was found to increase glycolytic flux, thereby promoting anabolism and redox balance [419]. As already known, p53 further influences the cell via its tumor-suppressive functions on DNA repair, cell cycle arrest, senescence and apoptosis [287], being a key player mediating crosstalk between the metabolic needs of a cell and pro-apoptotic decisions.

Besides pyruvate from glycolysis, the TCA cycle is also supplied by fatty acids and amino acids. The TCA cycle is fueled through glutaminolysis where the amino acid glutamine is metabolized to glutamate and α-ketoglutarate, which gets incorporated into TCA cycle [420]. Branched chain amino acids (BCAAs), such as isoleucine, leucine and valine can be converted into acetyl-CoA and other substrates that fuel the TCA cycle [421]. Additionally to the TCA, the mitochondrial ETC is supplied with the reducing equivalents $NADH+H^+$, $FADH_2$ together with acetyl-CoA deriving from the mitochondrial breakdown of fatty acids during the mitochondrial β-oxidation of fatty acids [340]. Finally, the type of substrates used by the mitochondria which support tumor growth is probably determined by a combination of the local tumor microenvironment and oncogenic mutations [287]. However, mitochondrial dysfunction and aerobic glycolysis have become widely accepted as hallmarks of cancer [367]. Manifold therapy options have been established over decades of cancer therapy research that target transporters and proteins of the glycolytic pathway, such as the glucose transporter 1 (GLUT1), HK, pyruvate dehydrogenase (PDH) and LDH [422, 423]. Inhibition of GLUT1 by WZB117 inhibited growth of human lung cancer cells *in vitro* and *in vivo* [424, 425]. For HK, the inhibitors 2-deoxyglucose (2-DG) and 3-bromopyruvate (3-BP) both were shown to decrease proliferation rates of several cancer cells *in vitro* [426-428]. Targeting the mitochondrial ETC in cancer therapy is essential for poorly vascularized tumor cores with limited glucose availability. The respiration in these tumors relies on the feature that the ETC functions even at 0.5% low oxygen levels

and thereby ensures the generation of mitochondrial ATP for survival [289, 429, 430]. Therefore, targeting ETC would deplete the tumor of ATP, preventing oxidative TCA cycle from functioning and diminish macromolecule synthesis. A putative complex I inhibitor used in clinical trials as an anticancer agent in combination with standard care is for example the biguanide Metformin [289, 431]. Targeting mitochondrial TCA cycle in cancer therapy was exemplary demonstrated with the inhibitor CPI-613, which is a lipoate analog able to inhibit α-KGDH and PDH [432] demonstrating a significant therapeutic index in pancreatic cancer and acute myeloid leukemia (AML) [433, 434].

For over 50 years, natural products with notable chemical diversity have been extensively studied for their potential as anticancer agents. Over the past decades, significant efforts have been made to identify new bioactive natural products from various organisms such as microbes and plants in order to evaluate their anticancer potential with the subsequent mechanism of action [435]. According to estimates, approximately 25% of all newly approved anticancer drugs between 1981 and 2019 were derived from natural products [436, 437].

In the 1940s the primary success of medications like alkylating agents, Fluorouracil, Methotrexate and Cyclophosphamide introduced the natural product research decade. However, many of these drugs were found to exhibit severe side effects. Ten years later, the research focused more on natural small molecules for anticancer therapy, grouped in alkaloids, flavonoids, non-flavonoid phenolic compounds, quinones and others (exemplary group members are shown in [438]). Summarizing briefly a number of commonly-used anticancer drugs originating from natural sources such as Vincristine, Etoposide, Paclitaxel (Taxol), Camptothecin from plants and Mitomycin C or Bleomycin from bacteria [435]. Additionally, numerous compounds with potential anticancer properties or unique structural features that may be useful in exploring new drug targets or developing new lead structures for further optimization are steadily investigated.

In this thesis, several natural products will be screened for their anticancer activity and the mechanism of action in terms of metabolism and apoptosis induction of selected candidates will be analyzed – with the potential to address some of the hallmarks of cancer (detailed description can be found in the following chapter **2 Aims**).

2 Aims

The primary aim of the present work as a subproject of the Research Training Group 2158 (RTG 2158) was the identification and characterization of natural-products in order to eliminate chemotherapeutic-resistant tumors by natural product-induced cell death. For this objective, molecules isolated from organisms from highly competitive environments were tested for their bioactivity in a multi-step screening procedure. In sum, over 150 substances were tested in the previous funding period by my predecessor Dr. Stuhldreier. These substances were isolated and made available by Prof. Proksch's group (Institute for Pharmaceutical Biology and Biotechnology, Heinrich-Heine University Düsseldorf) who established an extensive library of natural products.

The top hits from the primary screening, were then validated with an initial screening for cytotoxicity in leukemia and lymphoma cells and the toxic substances were then examined for their potential to induce apoptotic cell death in these cells. Next, highly effective compounds with a rapid onset were studied to determine their potential in eliminating chemotherapy-resistant cancer cells in order to overcome therapy resistance. Finally, natural products that demonstrated notably favorable properties were assessed to determine their mechanism of action in terms of cellular metabolism, namely Viriditoxin and Bromoxib (earlier termed P01F08).

Similarly to the study of natural products, also semisynthetic substances were investigated in the present work as potential therapeutics in leukemia and lymphoma cells. Meriolin derivatives, provided by Prof. Müller's group (Institute for Organic Chemistry and Macromolecular Chemistry, Heinrich-Heine University Düsseldorf) were characterized in a comparative analysis in terms of cytotoxicity, apoptosis efficiency and induction of the DNA-damage response as well as targeting of the cell cycle.

Therefore, the mode of action of the mycotoxin Viriditoxin, which has already been identified by my predecessor Dr. Stuhldreier as a strong apoptosis inducer, should be further investigated. Furthermore, collaboration partners within the RTG 2158 should be assisted in testing synthesized compounds, which were designed based on natural product scaffolds, to determine their existing bioactivity and to develop effective apoptosis inducers.

The pursuit of these objectives resulted in the publication of several manuscripts, some of which are highlighted in the following sections.

3 Publications with author contributions

3.1 Publications within the scope of this dissertation

3.1.1 The mycotoxin viriditoxin induces leukemia- and lymphoma-specific apoptosis by targeting mitochondrial metabolism

Stuhldreier F*, **Schmitt L***, Lenz T, Hinxlage I, Zimmermann M, Wollnitzke P, Schliehe-Diecks J, Liu Y, Jäger P, Geyh S, Teusch N, Peter C, Bhatia S, Haas R, Levkau B, Reichert A, Stühler K, Proksch P, Stork B, Wesselborg S. The mycotoxin viriditoxin induces leukemia- and lymphoma-specific apoptosis by targeting mitochondrial metabolism. *Cell Death and Disease*. 2022, *equally contributing first authors, doi: 10.1038/s41419-022-05356-w [1]

Author contribution:

The author of this dissertation contributed in the characterization of the apoptosis pathway (Fig. 1F, 4A, B, D, E; Fig. 5B, C; Suppl. Fig. 1, 3B), designed and carried out the experiments to validate the potential targets of Viriditoxin (Fig. 7C, D; Suppl. Fig. 4A). Additionally, the author performed largely the extensive revision, including the cell specificity screening of the drug (Suppl. Fig 1), performing quantitative analyses of Western blots and graphs including statistics, revised and corrected the manuscript together with Prof. Wesselborg.

3.1.2 40 Years of research on polybrominated diphenyl ethers (PBDEs) – A historical overview and newest data of a promising anticancer drug

Schmitt L, Hinxlage I, A Cea P, Gohlke H, Wesselborg S. 40 Years of research on polybrominated diphenyl ethers (PBDEs) – A historical overview and newest data of a promising anticancer drug. *Molecules*. 2021, doi: 10.3390/molecules26040995 [2]

Author contribution:

The author of this dissertation developed and managed the project, independently planned, designed and carried out the majority of the experiments and performed the whole literature analysis with subsequent data analysis and writing of the manuscript.

3.2 Publications beyond the scope of this dissertation

While pursuing her doctoral degree, the author of this dissertation also made contributions to other publications. However, since these publications were outside the thematic scope of this work, they have not been included.

3.2.1 Sesterterpenes and macrolide derivatives from the endophytic fungus Aplosporella javeedii

Gao Y, Stuhldreier F, **Schmitt L**, Wesselborg S, Wang L, Müller WEG, Kalscheuer R, Guo Z, Zou K, Liu Z, Proksch P. *Fitoterapia*. 2020, doi: 10.1016/j.fitote.2020.104652 [439]

Author contribution:

The author of this dissertation performed the experiments on cytotoxicity and apoptosis in leukemia and lymphoma cell lines together with F. Stuhldreier.

3.2.2 Induction of new lactam derivatives from the endophytic fungus aplosporella javeedii through an OSMAC Approach

Gao Y, Stuhldreier F, **Schmitt L**, Wesselborg S, Guo Z, Zou K, Mándi A, Kurtán T, Liu Z, Proksch P. *Front. Microbiol.* 2020, doi: 10.3389/fmicb.2020.600983 [440]

Author contribution:

The author of this dissertation performed the experiments on cytotoxicity and apoptosis in leukemia and lymphoma cell lines together with F. Stuhldreier.

4 Materials

4.1 Natural products and semisynthetic compounds

All natural products were obtained from the biobank (natural compound library) of the Institute for Pharmaceutical Biology and Biotechnology of the Heinrich-Heine University Düsseldorf. All natural products including Viriditoxin and Bromoxib (4,5,6-tribromo-2-(2',4'-dibromophenoxy) phenol), earlier termed P01F08 [2, 441], were freshly prepared and dissolved in DMSO as 10 mM stock solution. Until used in the assays the compounds were kept at -20 °C.

The semisynthetic Meriolins DD31 or 5f (4-(1*H*-pyrrolo[2,3-*b*]pyridine-3-yl)pyridine-2,6-diamin; hereafter called Meriolin 31) and DD36 or 5k (*N*-benzyl-4-(1*H*-pyrrolo2,3-*b*]pyridine-3-yl)pyridine-2-amine); hereafter called Meriolin 36) were synthesized and provided by Dr. Daniel Drießen [442] and Marco Kruppa in the group of Prof. Dr. T.J.J.Müller from the Institute of Organic Chemistry of Heinrich-Heine University Düsseldorf [443]. Meriolins were dissolved in DMSO at a 10 mM stock solution and stored at -20 °C. The biosynthesis of 31 and 36 was published in [442, 443]. Meriolin 16 (5p or DD219) (4-(4-methoxy-1*H*-pyrrolo2,3-*b*]pyridine-3-yl)pyridine-2,6-diamine) was newly synthesized based on the structure of 31 with an additional methoxy-group, its synthesis is described in [442]. Meriolin DD17 or 5r (3-(2-chlorophyrimidin-4-yl)3*H*-pyrrolo[2,3-*b*]pyridine; hereafter called Meriolin 17) is a biological inactive Meriolin derivative which was synthesized by Dr. Daniel Drießen described in [442].

4.2 Antibodies

All primary antibodies were diluted in 1x TBS-T supplemented with 0.05% NaN_3 (without 5% BSA) according to manufacturer's suggestions. The antibody baths were stored at 4 °C and re-used.

Table 2 List of primary antibodies used for this thesis.

Primary antibodies	Host	Company	Catalog number	Used concentration
Anti-β-Actin	Mouse	Sigma	#A5316	1:20,000
Anti-GAPDH	Mouse	Abcam	#ab8245	1:5000
Anti-Vinculin	Mouse	Sigma	#V9131	1:2000
Anti-Tubulin	Mouse	Sigma	#T5168	1:2000
Anti-PARP1	Mouse	Enzo	#BML-SA250	1:2000
Anti-OPA1	Rabbit	[444]		1:1000

Anti-OXPHOS WB antibody cocktail	Mouse	Abcam	#ab110411	1:500
Anti-CHK1	Mouse	Thermofisher	#MA1-23336	1 µg/mL
Anti-p-CHK1 (Ser345)	Rabbit	Thermofisher	#PA5-34625	2 µg/mL
Anti-CHK2	Mouse	CST	#P3440	1:1000
Anti-p-CHK2 (T68)	Rabbit	Abcam	#ab85743	1 µg/mL
Anti-Claspin	Rabbit	Novus Biologicals	#NB100-248	1:500
Anti-CDK2	Rabbit	Invitrogen	#MA5-32017	1:1000
Anti-Cyclin E	Rabbit	Thermofisher	#MA5-42650	1:1000
Anti-Cyclin A2	Mouse	Thermofisher	#MA1-154	1:1000
Anti-CDK1	Mouse	Thermofisher	#MA5-11472	2 µg/mL
Anti-Cyclin B1	Mouse	Thermofisher	#MA5-13128	2 µg/mL
Anti-CDK9	Rabbit	Thermofisher	#MA5-32397	1:1000
Anti-Cyclin T1	Rabbit	Thermofisher	#PA5-82177	0.4 µg/ml
Anti-RNA polymerase II	Rabbit	Biomol	#A300-653A	1:2000
Anti-p-RNA polymerase II (Ser2)	Rabbit	Biomol	#A300-654A	1:1000
Anti-Retinoblastoma protein (Rb)	Mouse	BD	#554136	2 µg/ml
Anti-p-Rb (Ser612)	Rabbit	Thermofisher	#PA5-64513	1:1000
Anti-p-Rb (Thr821)	Rabbit	Invitrogen	#44-582G	1:1000
Anti-PP2-C	Rabbit	CST	#2259	1:1000
Anti-p27/Kip1	Mouse	CST	#3698	1:1000
Anti-Hexokinase II	Rabbit	Abcam	#ab11352	1:5000
Anti-Mcl-1	Mouse	Enzo	#AAM-241	1:500
Anti-PP1α	Mouse	Invitrogen	#438100	2 µg/mL
Anti-TP53BP1	Rabbit	Novusbio	#NB100-304	1:5000
Anti-p-γh2ax (S139)	Mouse	Millipore	#05636	1:1000
Anti-LRPPRC	Rabbit	Abcam	#ab2599227	1:1000
Anti-GRSF1	Rabbit	Abcam	#ab205531	1:1000
Anti-HADHA	Mouse	Santa Cruz	sc-374497	1:1000
Anti-HADHB	Mouse	Santa Cruz	sc-271495	1:1000
Anti-ACSL4	Mouse	Santa Cruz	sc-365230	1:1000
Anti-ECH1	Mouse	Santa Cruz	sc-515270	1:1000

Anti-ACADVL	Mouse	Santa Cruz	sc-376239	1:1000

IRDye® 680RD-conjugated secondary antibodies were diluted 1:20,000 in 1x TBS-T. IRDye® 800RD-conjugated secondary antibodies were diluted 1:10,000 in 1x TBS-T (**Table 3**).

Table 3 List of secondary antibodies used for this thesis.

Secondary antibodies	Company	Catalog number
IRDye® 680RD Donkey anti-Mouse	LICOR® Bioscience	#926-68072
IRDye® 800CW Donkey anti-Mouse	LICOR® Bioscience	#926-32212
IRDye® 800RD Donkey anti-Rabbit	LICOR® Bioscience	#926-32213
IRDye® 680RCW Donkey anti-Rabbit	LICOR® Bioscience	#926-68073

4.3 Buffers and solutions

Standard lysis buffer

Tris-HCl pH 7.5	20 mM
NaCl	150 mM
Triton X-100	1% (v/v)
EDTA	0.5 mM
1x Protease and Phosphatase Inhibitor	
dH_2O	

6x Lämmli buffer

Tris pH 6.8	375 mM
Glycerol	51.6% (v/v)
SDS	12.3% (w/v)
Bromophenol blue	200 µg/ml
dH_2O	
β-Mercaptoethanol	6% (v/v) add only to aliquots in use

Stacking gel buffer

Tris-HCl pH 6.8	1 M
SDS	0.74%
dH_2O	

Separation gel buffer

Tris-HCl pH 8.8	1.5 M
SDS	0.386%
dH_2O	

10x SDS-PAGE running buffer

Tris	250 mM
Glycine	1.9 M
SDS	1%
dH_2O	

10x Wet transfer buffer

Tris	436 mM
Glycine	390 mM
dH_2O	

10x TBS-T pH 7.6

Tris	100 mM
NaCl	1.5 M
Tween-20	0.5%
dH_2O	

Blocking solution

Milk powder	5% (w/v)
1x TBS-T	

Tris/HCl

0.5-1.5 M Tris; adjusted pH to 6.8-8.8 with HCl

4.4 Cell culture

Table 4 List of media and antibiotics used for cell culture.

Name	Manufacturer	Catalog number
DMEM high glucose (4.5 g/l)	Gibco® by Life Technologies	#41965-039
RPMI 1640	Gibco® by Life Technologies	#21875-091
Modified IMEM	Gibco® by Life Technologies	#A10489-01
DPBS 1x	Gibco® by Life Technologies	#14190-094
Trypsin/EDTA solution 1x	Gibco® by Life Technologies	#25300-054
HEPES (1M)	Gibco® by Life Technologies	#51630-080
Penicillin/Streptomycin	Gibco® by Life Technologies	#15140-122
Fetal Bovine Serum (FBS)	Sigma-Aldrich®	#F9665 LOT:0001655439

4.5 Compounds

Table 5 Compounds with the respective manufacturer and catalog number used in this thesis.

Name	Manufacturer	Catalog number
Staurosporine	LC Laboratories	#9300
Q-VD-OPH	Selleckchem	#S7311
Etoposide	BioVision	#1043-100
Ionomycin	Sigma	#10635
Thapsigargin	Sigma	#T9033
CCCP	Sigma	#2759
Rotenone	Sigma	#45656
TTFA	Sigma	#88300
Antimycin A	Sigma	#8674
Sodium Azide	Sigma	#S2002
Paclitaxel	Sigma	#T7402
Vinblastine	Sigma	#V1377
N-acetylcysteine	Sigma	#A7250
Nocodazole	Sigma	#M1404
R547	Selleckchem	#S2688
SUPERKILLER TRAIL® Protein (soluble) human	Enzo Life Sciences	#ALX-201-115-C010
3-Bromopyruvat	Merck	#3786817
Lonidamine	Sigma	#L4900
Clotrimazol	Sigma	#C6019
Tigecycline	Merck	#220620-09-7
Cyclohexamide	Roth	#8682.1
Chloramphenicol	Sigma	#C0378

4.6 Additional material

Table 6 List of additional material and solutions used for this thesis.

Name	Manufacturer	Catalog number
6x DNA loading dye	Thermo Scientific	R0611

Ac-DEVD-AMC	Biomol	#ABD-13402
Albumin Fraktion V (BSA)	Roth®	#8076.4
APS	Merck	#7727-54-0
Blotting pads	VWR	#732-0594
Cell culture equipment	Falcon™, Sarstedt	
Cuvettes	Sarstedt	#67.742
Milk powder	Roth®	#T145.3
PageRuler Prestained Protein Ladder	Thermo Scientific	#26616
PhosSTOP	Roche	#04906837001
Protease Inhibitor	Roche	#58698000
Rotiphorese® Gel 30	Roth	#3029.1
TEMED	Roth	#2367.1
Trichloroacetic acid (TCA)	Sigma-Aldrich	#T6399-100G

4.7 Kits

Table 7 List of kits used for this thesis.

Type and name	Manufacturer	Catalog number
MitoCheck® complex I	Cayman Chemical	#700930
MitoCheck® complex II	Cayman Chemical	#900740
MitoCheck® complex II/III	Cayman Chemical	#700950
MitoCheck® complex IV	Cayman Chemical	#700990
MitoCheck® complex V	Cayman Chemical	#701000
CDK1/Cyclin B1	BPS Bioscience	#79597
CDK2/Cyclin A2	BPS Bioscience	#79599
CDK4/Cyclin D3	BPS Bioscience	#79674
CDK9/Cyclin T	BPS Bioscience	#79628
Tubulin polymerization kit	Cytoskeleton	#BK006P
Hexokinase II assay kit	Abcam	#ab211114
ATP Assay	Promega	#G8000
EdU-Click 488	Baseclick GmbH	#BCK-TCell-FC488

Click-iT RNA Imaging Kit	Invitrogen	#C10329, C10330

4.8 Technical equipment

Table 8 List of all devices used for this thesis.

Type and name	Manufacturer	Application
Axiovert 25	Zeiss	Microscope
BioPhotometer	Eppendorf	Measurement of protein concentration
Forma 900 Series	Thermo Scientific™	-80 °C refrigerator
HERAcell VIOS 250i CO2	Thermo Scientific™	Cell culture incubator
Heraeus™ Fresco™ 17	Thermo Scientific™	Centrifuge
Heraeus™ Megafuge 40R TX-750	Thermo Scientific™	Centrifuge
Horizontal shaker (Modell 3006)	GFL Technology	Membrane shaker
Luna™	Biozym	Automated cell counter
Metal Block Thermostat	Kleinfeld	Heater
Mini-PROTEAN Tetra	Bio-Rad	Electrophoresis chamber for mini gels
Nanodrop 1000	Thermo Scientific™	Measurement of DNA concentration
Odyssey® CLx	LI-COR® Biosciences	Infrared imaging system
PowerPac™ HC	Bio-Rad	Power supply
Roller Mixer	Stuart™	Tube roller
SAFE 2020	Thermo Scientific™	Sterile cell culture bench
Thermomixer comfort	Eppendorf	Heater
Trans-Blot® Cell	Bio-Rad	Blotting tank
Vacusafe™ Comfort	Integra Biosciences™	Aspiration pump
LSRFortessa™ Cell Analyzer	BD Biosciences	Flow-cytometry

4.9 Software

Table 9 List of all used programs and software used for this thesis.

Name	Company
CorelDRAW X8	Corel Corporation
ChemDraw 19.1	PerkinElmer Informatics

FlowJo _V10	BD Biosciences
GraphPad Prism 7.01	Dotmatics
Li-COR® Image Studio Lite 5.2	Li-COR® Biotechnology
Microsoft Office 2016	Microsoft Corporation
Zen 3.2 (blue edition)	Carl Zeiss Microscopy GmbH

4.10 Internet resources and databases

Table 10 List of used internet resources and databases for this thesis.

Link
https://www.proteinatlas.org/
https://www.uniprot.org/
https://www.ncbi.nlm.nih.gov/
https://www.atcc.org/
https://www.tebu-bio.com/
https://en.wikipedia.org/wiki/Main_Page
https://string-db.org
Manufacturers homepages and guidelines

5 Methods

5.1 Methods in Cell Biology

5.1.1 Cell lines and their culture conditions

Ramos (human B cell Burkitt lymphoma) cells were kindly provided by Michael Engelke (Institute of Cellular and Molecular Immunology, University Hospital Göttingen, Germany). Stable transfectants of Jurkat cells (human T cell acute lymphoblastic leukemia) with Bcl-2 overexpression and corresponding empty vector control cells were kindly provided by Claus Belka [445] (Department of Radiation Oncology, University Hospital, LMU Munich, Germany). Jurkat cells deficient for Caspase-8 and the parental cell line A3 were kindly provided by John Blenis (Sandra and Edward Meyer Cancer Center, New York, NY, USA). Jurkat cells deficient for Caspase-9 were kindly provided by Klaus Schulze-Osthoff (Interfaculty Institute for Biochemistry, University of Tübingen, Tübingen, Germany) and retrovirally transduced with either empty pMSCVpuro vector (Clontech, Heidelberg, Germany) or pMSCVpuro containing cDNAs coding for untagged human wild-type caspase-9 as previously described [446]. DG75 (human B cell Burkitt lymphoma; #ACC-83), MCF7 (human breast carcinoma; #ACC-115), RT112 (human urinary bladder carcinoma; #ACC-418), HL60 (human acute myeloid leukemia; #ACC-3), HPBALL (human T cell acute lymphoblastic leukemia; #ACC-483), MOLT4 (human T cell acute lymphoblastic leukemia; #ACC-362), K562 (human chronic myeloid leukemia; #ACC-10) and SUPB15 (human B cell acute lymphoblastic leukemia; #ACC-389) were obtained from DSMZ. KOPTK1 (human T cell acuty lymphoblatic leukemia; CVCL-4965) were kindly provided by Oskar Haas (Children's Cancer Research Institute, St. Anna Children's Hospital, Vienna, Austria). HeLa cells stably expressing mito-DsRed were kindly provided by Aviva M. Tolkovsky (Department of Clinical Neurosciences, University of Cambridge, England, UK) and have been described previously [447]. MEF (mouse embryonic fibroblast) cells deficient for OMA1 and/or YME1L as well as the corresponding wild-type cells were generated by Ruchika Anand and kindly provided by Thomas Langer (Institute for Genetics, University of Cologne, Germany) [448]. The glioblastoma cell line LN-229 (#CRL-2611) was obtained from ATCC). The glioblastoma cell lines LN308 andTP365MG were kindly gifted by Prof. Guido Reifenberger, University Hospital Düsseldorf. The glioblastoma cell line SJ-GBM2 was obtained from Children's Oncology Group (COG) and YKG-1 from tebu-bio (ref JCRB0746). Apaf-1-deficient SK-Mel-94 (human melanoma cells) were kindly provided by Maria S. Soengas (University of Michigan, Ann Arbor, MI, USA) [449].

All cell lines were maintained at 5% CO_2, 37 °C, and stable humidity in the following cell culture media. The suspension cells and MCF7 cells were maintained in media with 10% FCS, 100 U/mL penicillin and 100 µg/mL streptomycin. MEF cells, RT112, HeLa, YKG-1, TP365MG, Sk-Mel-94, LN-229 and LN308 cells were cultured in high-glucose Dulbecco's Modified Eagle's medium (DMEM) supplemented with 10% FCS, 100 U/mL penicillin and 100 µg/mL streptomycin. SJGBM2 was maintained in IMEM medium supplemented with 10% FCS, 100 U/mL penicillin and 100 µg/mL streptomycin.

5.1.2 Cryoconservation of cells and thawing

For long-term storage, mammalian cells were washed with 1x DPBS, trypsinized and centrifuged at 1200 rpm for 5 min at RT. Cell pellets were resuspended in freezing media (90% FCS and 10% DMSO) and transferred into cryotubes. Cells were slowly cooled down at a rate of -1 °C per minute using Mr. Frosty (Nalgene, 5100-0001) or CoolCell (Biocision, BCS-405) freezing containers. Mr.Frosty and the cryotubes were first stored at -80 °C and after one-two days the cryotubes were transferred to liquid nitrogen for long-term storage. For thawing of cells, the cryotubes were warmed in 37 °C water bath, immediately resuspended in full growth medium, centrifuged at 600 x g for 5 min at RT, resuspended in full growth medium again, and transferred to flasks and the incubator for cultivation.

5.2 Biochemical methods

5.2.1 Cell lysis

For the preparation of cleared cellular lysates (CCLs), suspension cells (mostly 12-well plate) were directly harvested and adherent cells were harvested at 80-90% confluence (mostly 6-well plate) by scraping. Cells were centrifuged at 3000 rpm x 5 min at 4 °C and the supernatant was discarded, the pellets were quick frozen in liquid nitrogen. After three freeze-thaw cycles in liquid nitrogen, the cell pellets were resuspended in the respective lysis buffer (40 µL) and lysed for 30 min on ice, including vortexing in between. Then, lysates were centrifuged at maximum speed (13.300 rpm) for 15 min at 4 °C. The supernatants were transferred into new tubes.

5.2.2 Determination of protein concentration using the Bradford-Assay

In order to load equal protein amounts during SDS-PAGE, the protein concentration of the CCLs was determined by the Bradford method. The colorimetric assay depends on the color

change of Coomassie Brilliant Blue G-250 (CBB), since under acidic conditions CCB is in an unstable protonated state. When CCB binds to proteins, the dye's absorption maximum shifts from 470 nm to 595 nm, resulting in a visible color change from red-brown to blue. The amount of blue dye is proportional to the protein concentration [450].

For determination of protein concentration of CCLs, 1 ml of reagent solution from Bio-Rad (previously diluted 1:5 in dH_2O) was mixed with 2 µl CCL in a cuvette. The optical density (OD) was measured at 600 nm with a spectrophotometer. An OD_{600} of 1.5 corresponded to a protein concentration of 25 µg/µl. Based on this, the protein concentration of each CCL was calculated with the following formula:

$$concentration\ [\mu g/\mu l] = \frac{\frac{OD600}{1.5} \times 25}{2}$$

5.2.3 Discontinuous SDS-PAGE

Discontinuous SDS-PAGE (short for sodium dodecylsulfate polyacrylamide gel electrophoresis) is an analytical biochemical method used for the separation of protein mixtures according to their molecular weight under denaturing conditions [451, 452]. Samples for SDS-PAGE were prepared by mixing CCLs with 6x Lämmli buffer containing SDS. SDS, as the detergent, binds and denatures the proteins, conferring a negative net charge to all proteins. To reinforce the denaturation and also to avoid the formation of protein aggregates, Lämmli buffer contains β-Mercaptoethanol as reducing agent. SDS-PAGE samples underwent a boiling step at 95 °C for 5 min.

The polyacrylamide gel consists of two parts: The lower separation gel and the upper stacking gel. 25 µg protein of every sample was loaded into the stacking gel pockets and a constant current of 45 mA per gel was applied for 1 - 2 h depending on the acrylamide percentage and the molecular weight of the protein of interest. Due to the negative charge of SDS, all proteins migrate to the same electric pole, enabling a separation exclusively according to size. Proteins are firstly concentrated in the stacking gel. The separation gel works as a molecular separator: Smaller proteins move faster through the gel pores and bigger proteins migrate much slower, depending on the percentage of the gel. A size marker (PageRuler Prestained Protein Ladder or PageRuler Plus) was loaded along with the samples to assign the approximate protein sizes.

5.2.4 Immunoblot analysis

The separated proteins were transferred electrophoretically from the polyacrylamide gel onto a positively charged polyvinylidene fluoride (PVDF) membrane without changing the

electrophoretic separation pattern. The membrane was first activated in methanol and equilibrated with the gel, Whatman papers and sponges in 1x transfer buffer. The wet transfer system was built following the manufacturer's instructions. For detection of protein sizes between 10 – 180 kDa the blotting step was performed at 110 V for 1 h at 4 °. For the detection of larger proteins the blotting duration was elongated to 1.5 h. To prevent unspecific antibody binding the membrane was incubated with blocking buffer for 1 h at RT to and washed three times with 1x TBS-T for 5 min. Membranes were cut and incubated in a respective primary antibody solution overnight at 4 °C on a roller mixer. Primary antibodies were removed by washing three times with 1x TBS-T for 5 min at RT. Membrane pieces were incubated in respective secondary antibodies for 1 h at RT in the dark. Secondary antibodies were conjugated to an IRDye® 680 or 800 and diluted 1:20,000 or 1:10,000, respectively. Membranes were washed three times with 1x TBS-T for 5 min, dried between Whatman papers and scanned with the Odyssey® CLx Infrared Imaging System from Li-COR® Biosciences.

5.2.5 Statistical analysis of Western blots

Protein band signal intensity was quantified using Image Studio lite 5.2 (Li-COR Biosciences). The density of each protein band was divided by the density of the corresponding loading control. Each negative control was normalized to the average value of all negative controls (treated with DMSO 0.1% v/v). Each treatment line was normalized to the average value of all negative controls. The results are shown as mean width standard deviation. Statistical analysis was performed as 1-way ANOVA, corrected by Dunnett's multiple comparisons test. **** = $p \leq 0.0001$. All statistical data were calculated with GraphPad Prism v7.01 (GraphPad Software, La Jolla, CA, USA).

5.2.6 Cytotoxicity measurements

AlamarBlue® assay was performed to determine the cytotoxicity and is described in [443]. Suspension cells were seeded at a density of 1 x 10^6 cells/mL and adherent cells were seeded at a density of 0.2 x 10^6/ml. Suspension cells were treated immediately and adherent cells were treated the next day with increasing compound concentration. According to the specified incubation time Resazurin (Sigma, #R7017) was added (final concentration = 40 µM) and incubated for 120 min. Resorufin fluorescence (excitation (Ex): 535 nm, emission (EM); 590 nm) was measured with a microplate spectrophotometer (Synergy Mix platereader). Viability of cells after indicated treatments was normalized to controls (treatment with 0.1% v/v DMSO) and the dose-response curves were fitted with PRISM v7.01 (GraphPad Software, La Jolla, CA, USA).

5.2.7 Fluorometric caspase-3 activity assay

Cells were seeded at a density of 1 x 10^6 cells/mL in a 96-well plate, treated with the compound for the depicted time (kinetics 0-8 h) and harvested by centrifugation at 600 g. The supernatant was removed and the cells were lysed with 50 µL of ice-cold lysis buffer (20 mM HEPES, 84 mM KCl, 10 mM $MgCl_2$, 200 µM EDTA, 200 µM EGTA, 0.5% NP40, 1 µg/mL leupeptin, 1 µg/mL pepstatin, 5 µg/mL aprotinin) on ice for 10 min. Lysates were transferred to a flat-bottom microplate. There, the lysates are mixed with 150 µL ice-cold reaction buffer (50 mM HEPES, 100 mM NaCl, 10% sucrose, 0.1% CHAPS, 2 mM $CaCl_2$, 13.35 mM DTT) which contains 70 µM of the profluorescent caspase substrate Ac-DEVD-AMC (Biomol GmbH, Hamburg, Germany, #ABD-13420). The AMC fluorescence intensity (Ex: 360 nm; Em: 450 nm) was measured as kinetics of AMC release at 37 °C every 2 min over total of 120 min, using a Synergy Mix microplate reader. Caspase-3 activity was determined by considering the slope of the fluorescence curves' linear range (Δrfu/min). The slopes of the individual treatments were normalized to that of DMSO (set to 100%) of the respective time points.

5.2.8 Analysis of apoptotic cell death and cell cycle

DNA content during cell cycles and fragmented DNA leaking from apoptotic nuclei were measured by the method of Nicoletti et al. [453]. Nuclei were prepared by lysing cells in a hypotonic lysis buffer (1% sodium citrate, 0.1% Triton X-100, and 50 µg/mL propidium iodide) and then analyzed by flow-cytometry. Prepared nuclei were measured on linear mode to clearly differentiate G_1-, S-, G_2-Phase, and hypodiploid nuclei. Hypodiploid nuclei were measured in logarithmic mode. Flow-cytometry analysis was performed on a LSRFortessa™ (Becton, Dickinson, Heidelberg, Germany) and data analysis was performed using FlowJo_V10 (BD Biosciences). Statistical analysis of hypodiploid nuclei was performed comparing DMSO treatments (0.1% v/v) by 1-way ANOVA with Dunnett's multiple comparison's test (**** $p \leq 0.0001$).

5.2.9 Apoptosis Array

The apoptosis assay (R&D Systems, #ARY009) was used to detect the relative expression of 35 apoptosis-related proteins in a single sample and was performed according to manufacturer's instructions. Selected capture antibodies were applied to nitrocellulose membranes in duplicates. For apoptosis induction the cells were seeded (ρ = 1 x 10^6 cells/ml) and incubated with 10 µM of Meriolin 16 or 2.5 µM Staurosporine (as positive control) for 8 hours. The cells were lysed, whole cell extracts are diluted and incubated with the array for 24 hours. Membranes were washed to remove unbound proteins, incubated with biotinylated

detection antibodies and Streptavidin-HRP and chemiluminescent detection reagents were applied detected for (fluorescence detection). Signal intensity correlates with protein amount at the spot. Data analysis was performed according to manufacturer's instructions. The average pixel density of each duplicate spot represents each apoptosis-related protein quantity. Averaged background signal was subtracted from each spot and the apoptosis-related protein pixel density was normalized to the corresponding reference spot. Red indicates protein quantities and green indicates low protein quantities.

5.2.10 Live cell imaging

Mito-DsRed HeLa cells [447] were seeded on IBIDI-slides (µ-slide 8-well) (IBIDI #80826) for live cell imaging, incubated with the respective treatments under culture conditions in the incubator. The cells were immediately analyzed with the Axiovert 25 microscope. The images were processed with ZEN 3.2 blue edition. Only the most representative images are shown.

5.2.11 Immunofluorescence

Detection of changes in intracellular protein localization, immunofluorescence analysis was performed in HeLa cells. 0.5 x 10^6 cells/ml were seeded on autoclaved coverslips (12 mm) in a 24-well plate in duplicates and incubated overnight. The medium was removed, and the cells were subjected to the specified compounds for the designated duration. Medium was removed, the cells were washed with 1x PBS and fixated with 4% PFA at RT for 10 min. The cells were washed three times with 1x PBS, permeabilized with 0.2% Triton X-100 at RT for 10 min and washed three times with 1x PBS. Unspecific bindings were blocked with 5% BSA in 1x PBS at RT for 1 h. The cells were incubated with primary antibodies (1:500 in PBS with 5% BSA, unless otherwise noted) at 4 °C overnight. Cells were washed three times with 1x PBS, incubated with the secondary antibody (Invitrogen, Alexa Fluor) at RT for 1 h and washed two times with 1x PBS. DAPI (Roth #6335, 1:1000 in 1x PBS) was added, the suspension was incubated at RT for 10 min and washed with 1x PBS. 7 µL ProLong Glass were placed on object slides (Antifade Mountant; Invitrogen #P36984), and the coverslips with cells were placed inverted on top. The object slides were analyzed the next day with an Axiovert 25 microscope (Carl Zeiss). Images were processed with ZEN 3.2 blue edition. Only the most representative images are shown.

5.2.12 Microscopy-based analysis of EdU-incorporation

The EdU-assay (EdU-click 488 kit from Baseclick GmbH, #BCK-TCell-FC488) measures the incorporation no 5-ethynyl-2'-deoxyuridine (EdU) into the DNA and serves as a measurement

for cell proliferation. Proliferation is characterized by *de novo* DNA synthesis during S phase of the cell cycle. The cells grow in the presence of 5-EdU and incorporate the compound at thymidine bases during S phase. A fluorophore-labeled azide reacts with the incorporated EdU allowing the detection by microscopy (sigmaaldrich.com). The cells are seeded and grow to the desired density, they get treated as needed, and subsequently EdU is added into the media. Next, they are fixed, permeabilized and the EdU detection, together with DAPI-stained nuclei, is performed by fluorescent microscopy.

5.2.13 Microscopy-based analysis of EU-incorporation

The Click-iT® RNA imaging kit of Invitrogen (#C10329) was used to detect newly synthesized RNA via the incorporation of 5-Ethynyl-uridine (EU). The EU-assay serves as a measurement of global RNA synthesis. Briefly, the cells were plated the day before, treated with the respective substances for the depicted time and then pulsed with EU for 1 h and EU incorporation was monitored according to manufacturer's instructions. Next, the cells are fixed, permeabilized and the EU detection, together with DAPI-stained nuclei, is performed by fluorescent microscopy.

5.2.14 Live measurement of mitochondrial membrane potential

In order to observe any alterations in the mitochondrial membrane potential (ΔΨm), Ramos cells were exposed to the cell-permeable, positively charged dye, tetramethylrhodamine ethyl ester (TMRE). Mitochondria possess a negative net charge, whereas the dye is not retained by depolarized mitochondria. The cells were suspended in fresh medium, which included 10 mM HEPES and supplemented with 100 nM TMRE (AAT Bioquest, Sunnyvale, CA, USA; #22220), and then incubated at 37 °C for 15 minutes. The cells were washed two times with 10 mM HEPES in RPMI and incubated for additional 15 min. TMRE fluorescence was measured by flow-cytometry (Ex: 488, Em: 575) at LSRFortessa^{TM}. First, for each sample the basal fluorescence level was measured for 2 min, then the test compound was added to the sample tube, mixed and measured continuously for the indicated time. The pre-substance basal fluorescence level was set to 100%. Carbonyl cyanide m-chlorophenyl hydrazone treatment (CCCP, 10 µM) as protonophore was used as positive control for the complete breakdown of the mitochondrial membrane potential.

5.2.15 Live measurement of total and intracellular Calcium mobilization

Changes in Ca^{2+} homeostasis were measured live using a flow-cytometer (LSRFortessa^{TM}). Ramos cells (1 x 10^6) were incubated in growth medium containing 1 µM Fluo-4-AM (Life

Technologies; #F14201), 0.005% w/v Pluronic F-127 (Sigma, #540025), 10 mM HEPES and 5% v/v FCS at 30 °C for 25 min. An equal amount of full growth medium was added and the samples were incubated at 37 °C for 10 min. The cells were pelletized at 3000 rpm for 3 min and resuspended in Krebs-Ringer buffer (10 mM HEPES pH 7.0, 140 mM NaCl, 4 mM KCl, 1 mM $MgCl_2$, 10 mM glucose) in 1 mM $CaCl_2$. The cells were stored at RT in the dark until measurement and were washed and resuspended in pure Krebs-Ringer buffer for total Ca^{2+} mobilization. For the measurement of intracellular Ca^{2+} mobilization cells were washed with Krebs-Ringer buffer supplemented with 0.5 mM EGTA. Fluo-4-AM fluorescence was measured live using flow-cytometer LSRFortessa™ recording fluorescence in the FITC channel (Ex: 488, Em: 530±30 nm). For each sample, after at least 30 s of baseline measurement, the stimulus was added and measurement was continued for the depicted time.

5.2.16 Measurement of cellular ROS level by DCF-DA

During the assay Ramos cells were cultivated in RPMI medium without phenol red. Cells were loaded with 20 µM 2',7'-dichlorodihydrofluorescein diacetate (H_2DCF-DA, Sigma, #D6883), incubated in the dark for 1 h at 37 °C. The suspension was centrifuged (600 g x 5 min), washed with medium (without phenol red), and treated with the noted compounds at 37 °C for the noted time. Cells were centrifuged (600 g x 5 min), washed with PBS and transferred to FACS tubes. DCF fluorescence correlates to the cellular ROS level and was measured by flow-cytometry. DCF was excited with λ_{Ex} = 488 nm and fluorescence was measured at λ_{Ex} = 530 nm (FITC channel) at LSRFortessa™.

5.2.17 Measurement of cellular ATP-levels

Changes in cellular ATP-levels, were detected by the mitochondrial ToxGlo™ assay (Promega, Mannheim, Germany; #G8000) and was performed according to the manufacturer's instructions. In order to enhance the sensitivity in detecting mitotoxins, cells were cultured in medium that had either glucose or galactose as the sole available sugar source. The ATP-assay was measured with a microplate spectrophotometer (Synergy Mix platereader). Statistical analysis was performed using 2-way ANOVA and Sidak's multiple comparisons test. **** $p \leq 0.0001$.

5.2.18 Measurement of electron transport chain complex (I-V) activity

Activities of complex I-V in the electron transport chain (ETC), were measured by using the MitoCheck® complex I-V activity assay kits (Cayman Chemical, Ann Arbor, MI, USA; #700930/700940/700950/700990/701000), according to manufacturer's instructions. Complex

activity was measured with a microplate spectrophotometer (Synergy Mix platereader). Each complex had an appropriate positive control for its inhibition (I: Rotenone; II: Thenoyltrifluoroacetone (TTFA); III: Antimycin A; IV: Potassium cyanide (KCN); V: Oligomycin). The activity of the negative control (DMSO 0.1% v/v) was set to 100%. All treatments were normalized to DMSO. Statistical analysis was performed using unpaired t-test comparing treatment to DMSO (0.1% v/v). **** $p \leq 0.0001$.

5.2.19 Mito Stress Test – Seahorse analysis

Mito Stress Test Kit (Agilent Technologies, Santa Clara, CA, USA) was used according to the manufacturer's instructions with the Seahorse XFe96 Extracellular Flux Analyzer (Agilent Technologies, Santa Clara, CA, USA). Injection compounds were used in concentrations of 1 µM (Oligomycin), 1 µM (FCCP) and 0.5 µM (Rotenone/Antimycin A) per well. 10,000 HeLa cells were seeded 24 h prior to Seahorse analysis. Bromoxib (10 µM in DMSO) or DMSO (0.1% v/v) solvent control was injected via acute injection, oxygen consumption rate (OCR) was measured at three time points every 6 minutes and Oligomycin was injected. For Bromoxib, different concentrations (0.5 – 10 µM) were injected and four time points every 3 minutes were measured.

Mitochondrial respiration parameters were defined as following:

Non-mitochondrial respiration is defined as the lowest measured OCR after blocking respiration with Rotenone/Antimycin A.

Basal Respiration is defined as the mean of the first three OCR values prior to acute injection – (non-mitochondrial respiration).

Maximal Respiration was defined as the maximal OCR after FCCP injection = (maximal OCR) – (non-mitochondrial respiration).

Spare respiratory capacity (SRC) is defined as (maximal respiration) – (basal respiration) and serves as parameter to determine the cell's ability to react to higher energy demands. *Respiration after treatment* was defined as the OCR prior to Oligomycin injection after injection of Bromoxib or DMSO vehicle – (non-mitochondrial respiration). Proton leak = lowest OCR value after Oligomycin injection – (non-mitochondrial respiration). Acute response = (respiration after treatment) – (basal respiration).

5.2.20 Hexokinase II inhibitor assay

Potential inhibition of Hexokinase II (HK II) was analyzed with the Hexokinase II inhibitor assay kit (#ab211114) and was performed according to manufacturer's instructions. This assay is

based on the key function of HK II to convert glucose into glucose-6-phosphate. Glucose-6-phosphate dehydrogenase catalyzes the oxidation of Glucose-6-phosphate to form NADH from NAD^+. NAD^+ reduces a probe and the OD is measured at OD 450 nm. 3-Bromopyruvate (Bromopyruvic acid), is a known inhibitor of HK II was used as positive control and thereby decreases the rate of HK II dependent absorbance of the probe at OD 450 nm. The HK II assay was measured with a microplate spectrophotometer (Synergy Mix platereader).

5.2.21 Tubulin polymerization assay

Changes in tubulin polymerization were detected with the tubulin polymerization assay kit (Cytoskeleton, Inc., Denver, CO, USA; #BK006P) in porcine mitochondria and was performed according to manufacturer's instructions. Monomeric tubulin polymerization is accompanied by an increase in absorption (340 nm), therefore the reaction can be measured photometrical. The velocity of polymerization has been calculated using the formulas provided by the manufacturer. Respective controls for tubulin stabilization and increased polymerization rate was Paclitaxel, and Nocodazole was used as control for reduced polymerization rates.

5.2.22 Thermal proteome profiling (TPP) for Viriditoxin

Except for MS analysis and data analysis for protein identification and quantification, TPP was conducted following the method described by Franken *et al.* [454]. The TPP was performed by Thomas Lenz, BMFZ, RG Stühler from the Molecular Proteomics Laboratory (MPL), Heinrich-Heine Düsseldorf. Exact detailed methodological procedure are noted in the supplemental material of publication [1].

5.2.23 Thermal proteome profiling (TPP) for Bromoxib

3.5×10^8 Ramos cells, were diluted in medium (~1.5×10^6 cells/ml) and incubated with 40 µM, 10 µM, 2.5 µM, 625 nM, 159 nM, 39 nM, 9.8 nM, 2.4 nM 0.6 nM Bromoxib or 0.4% v/v DMSO (solvent control according to the highest used concentration) at 37 °C with 5% CO_2 for 30 min. The cells were centrifuged at 1200 rpm for 5 min at 4 °C. Supernatants were removed, pellets were resuspended in 39 mL ice-cold 1x DPBS and centrifuged. All supernatants were removed, the pellets were resuspended in ice-cold 1x DPBS and transferred to pre-weighed 2 mL Eppendorf tubes. Suspensions were centrifuged (5000 rpm, 4 °C, 5 min and supernatants were discarded. Wet pellets were weighed and further work was conducted under the supervision of Thomas Lenz, BMFZ, RG Stühler from the Molecular Proteomics Laboratory (MPL), Heinrich-Heine Düsseldorf according to Franken *et al.* [454] with modifications to the TMT labeling sets and statistical data analysis performed by Thomas Lenz.

5.2.24 Lipidomics and measurement of fatty acid oxidation

Methods described below were performed by Dr. Xabier Buqué from RG Aspichueta (Lipids and Liver group from the Department of Physiology, Faculty of Medicine and Nursing at Universidad del País Vasco in Spain).

Quantification of lipids

For lipid quantification in Ramos cells 1.5 x 10^6 cells per milliliter (treated and untreated by the author of this thesis), were directly resuspended in 0.3 mL of distilled H_2O. Lipids were extracted from 0.15-0.35 mg of protein [455], separated by thin layer chromatography (TLC) and quantified as described in [456]. For total quantification of lisophosphaticylcholine (LPC), phosphatidylcholine (PC), phosphatidylserine (PS), phosphatodylinositol (PI), phosphatidylethanolamine (PE), cardiolipin (CLN), free cholesterol (FC), diacylglycerides (DG), triacylglycerides (TG) and cholesteryl ester (CE), TLC plates were stained with a solution of 10% $CuSO_4$ (w/v) in 8% H_3PO_4 (v/v) and an image of the plate was digitalized with ChemiDoc*TM* PM imaging system (Bio-Rad Laboratories, USA). Quantification was performed with Image Lab software (Bio-Rad Laboratories, USA). Free fatty acids were measured with a commercial kit (WAKO Fujifilm; Japan) directly from the cell suspension following manufacturer´s protocol. Lipid levels were expressed relative to the cell protein.

Fatty acid oxidation in cells

The rate of fatty acid oxidation in Ramos cells was determined by measuring the amount of [^{14}C]-CO_2 (complete oxidation) and the amount of [^{14}C]-acid-soluble metabolites (ASM) (incomplete oxidation) released from [1-^{14}C]-palmitate (Perkin Elmer, USA) oxidation, as described by others with minor modifications [457, 458]. Briefly, 1.5 million cells per milliliter were starved overnight with assay medium (low glucose MEM supplemented with 0.3 g/L of glutamine, 6 g/L HEPES, 5% penicillin/streptomycin mix (v/v) and 0.5% fatty acid free BSA (w/v)), then pretreated for 30 minutes with Bromoxib or the vehicle alone (DMSO 0.1% (v/v)) (Sigma-Aldrich, USA) in assay medium and finally, were incubated for 4 hours with medium supplemented with fatty acid free BSA complexed with 0.2 mM palmitate containing 0.5 µCi/ml [1-^{14}C]-palmitate. After that, medium was collected in a tube containing Whatman filter paper soaked with 0.1 M NaOH in the cap and 500 µl of 3 M perchloric acid were added in the media to release the CO_2, which was captured in the filter paper. The acidified medium was centrifuged at 21,000 x g for 10 min to remove particulate matter. The radioactivity of CO_2 captured by the filter papers and of ASM (the supernatants of the culture media) was measured by a Tricarb 2810 TR scintillation counter (Perkin Elmer, USA) and expressed relative to the cell protein.

5.2.25 CDK activity assays

The activity of selected CDKs and their Cyclins was measured by the usage of CDK kits from BPS Bioscience (CDK1/Cyclin B1 #79597; CDK2/Cyclin A2 #79599; CDK4/Cyclin D3 #79674; CDK9/Cyclin T #79628) and the assays were performed according to manufacturer's instructions. In brief, the CDK/Cyclin complexes themselves are active as purified recombinant enzymes that react with the CDK substrate peptide in the presence of ATP and kinase buffer. Reactions are initiated by addition of diluted CDK/Cyclin enzyme and incubation at 30 °C for 45 min and Kinase-Glo-Max® reagent was added. Luciferase luminescence from the reagent is inversely proportional to kinase activity. Luminescent CDK/Cyclin assays enable quantification of remaining ATP after a kinase reaction. Luminescence was measured with a Synergy Mix microplatereader as endpoint measurement. Data analyses were performed according to the manufacturer's instructions. Statistical analysis was performed by 1-way ANOVA, corrected by Bonferroni's multiple comparison test; ****= $p \leq 0.0001$.

5.2.26 Kinome Screening with Reaction Biology

The Kinome Screening was performed by Reaction Biology Europe GmbH (http://reactionbiology.com; Freiburg i. Br., Germany). In case of CDKs with their corresponding Cyclins, treatment with Meriolin 16 (tested concentrations: 0.03 µM and 0.3 µM), Meriolin 36 (tested concentrations: 0.3 µM and 3 µM) and an inactive structurally related Meriolin derivative (17, tested concentrations: 0.3 µM and 3 µM), the company measured the activity of 335 wild-type protein kinases as recombinant purified active proteins. Meriolin 17 as inactive derivative was chosen to rule out false positive results. A kinase inhibition profile of the three Meriolins was determined by measuring residual activity at two concentrations each in single values in 335 wild-type protein kinase assays.

The residual activity was calculated as:

$$Res.Activity\ (\%) = 100\ x\ (\frac{(Signal\ of\ compound - low\ control)}{high\ control - low\ control})$$

The selectivity score was calculated as:

$$Selectivity\ Score = \frac{(Count\ of\ data\ points < 50\%)}{(Total\ number\ of\ data\ points)}$$

5.2.27 Replicates and statistical analysis

Experiments were replicated at least three times and only representative data are shown. Error bars indicate standard deviation (SD). All statistical analyses were performed using Prism v7.01 (GraphPad Software, La Jolla, CA, USA).

6 Results

B cell acute lymphoblastic leukemia (B ALL) is the prevalent cancer type found in children. The 5-year event free survival rate has been increased to over 80% with multidrug high-dose chemotherapy. Despite this result the prognosis for refractory/relapsed B ALL remains bleak and chemotherapy resistance is a major challenge in therapy [459]. In parallel chemoresistance in refractory/relapsed T cell acute lymphoblastic leukemia (T ALL) is quite common and the treatment of refractory T and B ALL remains challenging [460].

New bioactive molecules with anticancer properties in order to treat malignancies as single treatment or to increase the effectiveness of established drugs in combinational therapies is a hot topic in cancer research. The exceptional chemical diversity in nature provides natural products as a valuable source of bioactive compounds with therapeutic potential. This work focuses on the validation of cytotoxic natural products and semisynthetic substances as potential anticancer drugs in leukemia and lymphoma. Elucidating the molecular mechanism of anticancer drugs is important for understanding structure-activity relationships. Therefore the substances, Viriditoxin, Bromoxib and Meriolin derivatives, have been investigated in terms of apoptosis induction, effects on metabolism, DNA-damage or cell cycle.

6.1 Validation of natural product-induced cytotoxicity and analysis of their apoptosis induction capacity in leukemia and lymphoma cells

It was first aimed to validate the natural compounds with high cytotoxicity determined by my predecessor Dr. Stuhldreier and colleagues [441]. Most experiments used Burkitt B cell lymphoma (Ramos) and acute T cell leukemia (Jurkat) cells as dual cellular model system. Cytotoxicity screenings of ten selected natural products were conducted in Ramos and Jurkat cells for 24 and 72 hours. Cell viability was determined with the AlamarBlue® viability assay (**Figure 12 A**). IC_{50} values (half maximal inhibitory concentration) display a measure for the potency of the molecules in diminishing cell viability, displaying its cytotoxicity in leukemia and lymphoma cells (**Figure 12 B**). The lowest IC_{50} values for Helenalin, P01F08 (Bromoxib), Enniatin B, Aranorosin, 5-epi-Nakijiquinone, Viriditoxin, Pyrenocine A and Coniellin were reviewed in literature and summarized in (**Figure 12 B**). Based on the high cytotoxicity in normal cells, number of publications and availability of an already fully published molecular mechanism the following natural products were excluded for further studies within this thesis: 5-epi-Nakijiquinone, Pyrenocine A and Coniellin. Further experiments were performed with Helenalin, P01F08 (Bromoxib), Enniatin B, Aranorosin and Viriditoxin.

A

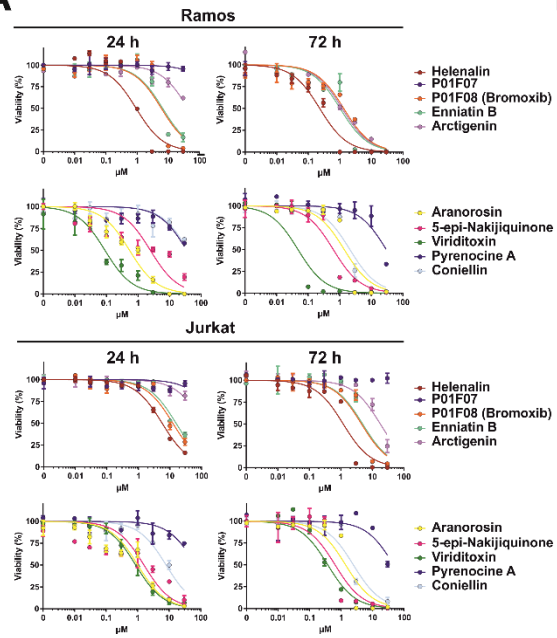

B

Natural product		IC_{50} (μM)			
		Ramos		Jurkat	
		24 h	72 h	24 h	72 h
	Helenalin	0.93	0.23	5.67	1.19
	P01F07	n.d.	n.d.	n.d.	n.d.
	P01F08 (Bromoxib)	6.0	1.33	12.34	4.53
	Enniatin B	6.62	1.02	15.6	4.94
	Arctigenin	n.d.	1.18	n.d.	17.9
	Aranorosin	0.54	1.39	2.04	1.39
	5-epi-Nakijiquinone	5.68	0.63	8.22	0.65
	Viriditoxin	0.09	0.05	0.94	0.38
	Pyrenocine A	5.14	30.0	n.d.	n.d.
	Coniellin	4.07	2.1	8.0	2.55

Figure 12 Cytotoxicity screening of ten natural products in Burkitt B cell lymphoma (Ramos) and acute T cell leukemia (Jurkat). (A) Cytotoxicity in Ramos or Jurkat cells was determined after the indicated incubation periods of 24 and 72 h using AlamarBlue® viability assay. Shown in each graph is the mean ± SD of one representative experiment performed in triplicates. **(B)** Overview of the resulting IC_{50} values in the individual cell lines at the respective incubation times. This initial screening experiment was performed with three technical replicates; the values were normalized to DMSO (0.1% v/v; negative control). n.d.= not detected in the depicted concentration range.

In order to identify natural compounds that are able to induce cell death in the dual cellular model system, Ramos cells were treated with sublethal (1 μM) and high (10 μM) concentrations of Helenalin, P01F08 (Bromoxib), Enniatin B or Aranorosin for 24 h (**Figure 13**). To measure caspase activity, PARP1 cleavage was analyzed via immunoblotting. Due to its recognition sequence (aspartic acid, glutamic acid, valine, aspartic acid (DEVD)), PARP1 is a substrate for effector caspases and gets cleaved into 89 kDa and 24 kDa fragments, inactivating and inhibiting its function in DNA repair [15]. To differentiate the caspase-dependency of PARP1 cleavage, the cells were pre- and co-treated with the broad-range caspase inhibitor Q-VD-OPh (QVD), shown in (**Figure 13 A**). Immunoblotting revealed PARP1 cleavage by P01F08 (Bromoxib) and Enniatin B at a concentration of 10 μM, whereas Aranorosin cleaved PARP1 at 1 and 10 μM concentration. Helenalin did not show any PARP1 cleavage and was therefore excluded for further analysis. Apoptosis-inducing Staurosporine (STS), originally isolated in 1977 from the bacterium *Streptomyces staurosporeus* [461], was used as positive control. STS induces apoptosis by the canonical intrinsic apoptosis pathway, including cytochrome c, apoptosome formation and caspase-9 activation or alternatively via an intrinsic pathway. Latter is independent of Bcl-2 and does not rely on Apaf-1 and apoptosome formation [446]. Caspase-3 activity (DEVDase activity) was determined in Ramos (upper graphs) and Jurkat cells (lower graphs) (**Figure 13 B**) to exploit the apoptosis induction capacity of P01F08 (Bromoxib), Enniatin B and Aranorosin. Generally, caspase-3 is ubiquitously expressed in normal tissues, but cancer cells exhibit variable levels of the executioner caspase-3 [462]. In our

experiments, Ramos cells appear, to be more susceptible against cytotoxic agents and exhibit higher levels of caspase-3 activity compared to Jurkat cells in the AlamarBlue® or DEVDase activity assay. Here, P01F08 (Bromoxib), Enniatin B and Aranorosin were observed to induce potent caspase-3 activity in Ramos and Jurkat cells at higher concentrations (10 µM) (**Figure 13 B**). Caspase-3 activity measurement itself does not serve as a sufficient method to differentiate the pathway of cell death induction. Therefore, the direct impact on mitochondria was investigated. If the mitochondria are targeted directly, the mitochondrial membrane potential (ΔΨm) should decrease (**Figure 13 C**). In consequence, ΔΨm-driven ATP synthesis and protein transport processes are inhibited and pro-apoptotic factors are released into the cytosol. P01F08 (Bromoxib) induced a rapid breakdown of mitochondrial membrane potential within 2 minutes, similar to the positive control CCCP (carbonyl cyanide m-chlorophenyl hydrazone) (**Figure 13 C**). CCCP is described as an uncoupler of mitochondrial oxidative phosphorylation (OXPHOS) and as a protonophoric ATP synthesis disruptor [463-465]. Therefore, Bromoxib seems to impact directly the mitochondrial metabolism.

As a second readout for an effect on the mitochondria, the cellular ATP-levels were measured under only glucose-condition or only galactose-condition, which enables to distinguish effects on glycolysis or OXPHOs as ATP-producing metabolic pathways (**Figure 13 D**). Here, Enniatin B and Aranorosin were observed to reduce ATP-levels under galactose-conditions, whereas P01F08 (Bromoxib) reduced ATP-levels under both conditions (**Figure 13 D**).

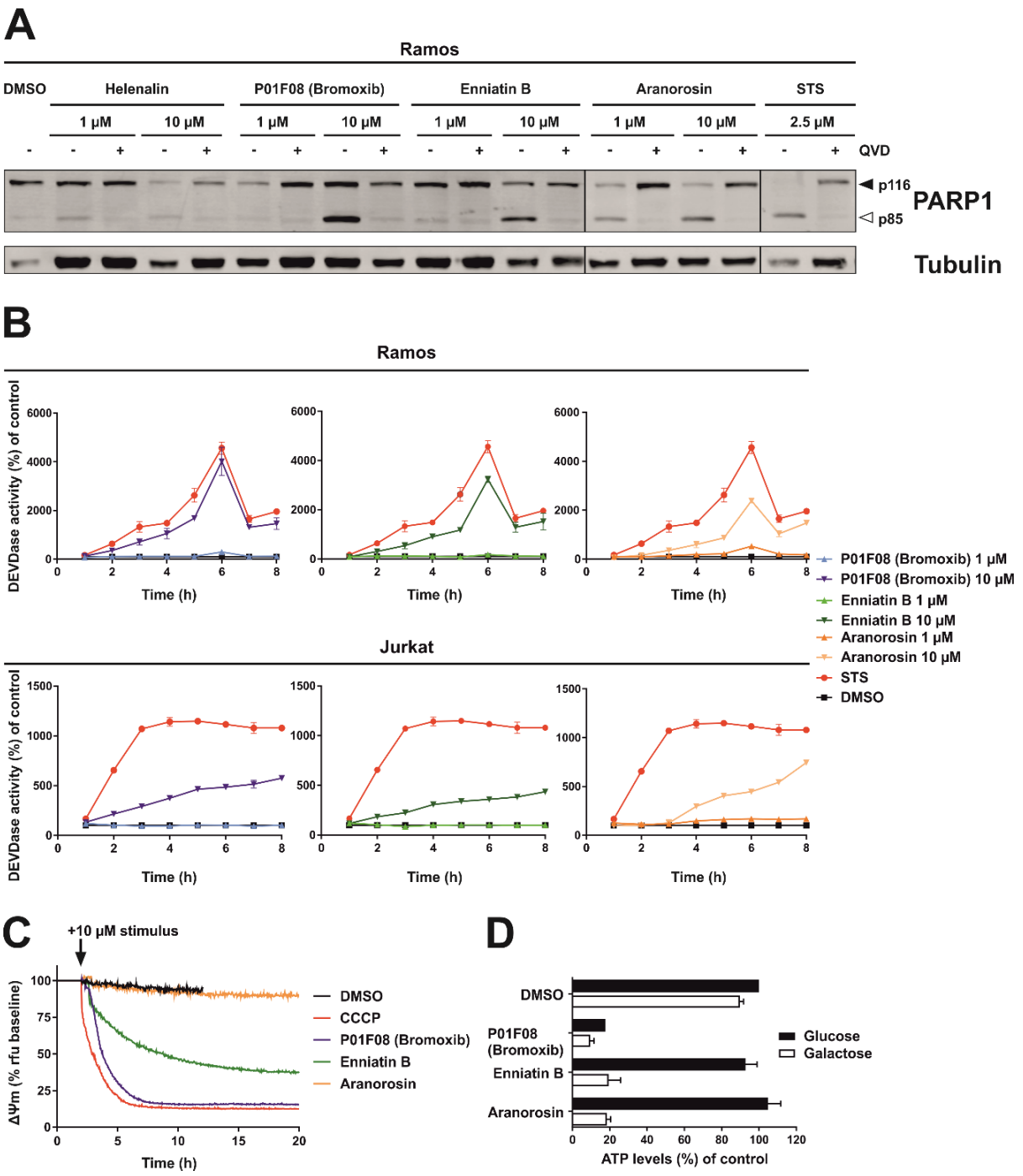

Figure 13 Initial cell death screening of selected natural products in Burkitt B cell lymphoma (Ramos) and acute T cell leukemia (Jurkat). (A) Ramos cells were pre-and co-treated with QVD (10 µM) and subsequently treated with 1 or 10 µM natural product. PARP1 cleavage was determined after 24 h via immunoblotting. Staurosporine (STS; 2.5 µM) was used as positive control for the induction of apoptosis. Tubulin served as loading control. **(B)** Ramos and Jurkat cells were treated with 1 or 10 µM P01F08, Enniatin B or Aranorosin and Staurosporine (STS; 2.5 µM) as positive control for caspase-3-activity for up to 8 h. Subsequently, DEVDase activity was used as marker for caspase-3 activity. DEVDase activity was determined via measurement of the pro-fluorescent caspase-3 substrate DEVD-AMC in a micro-spectrophotometer. DEVDase activity was assessed by the slope of the linear range of fluorescence increase. The values obtained for the DMSO control were considered 100%, and the normalized relative fold induction was calculated as per the description given in the Materials and Methods section. Shown in each graph is the mean ± SD of one representative experiment performed in duplicates. **(C)** Measurement of the mitochondrial membrane potential (ΔΨm) in Ramos cells after the addition of 10 µM CCCP (mitochondrial uncoupler; positive control), P01F08 (Bromoxib), Enniatin B, Aranorosin or DMSO (0.1% v/v; negative control) by flow-cytometric measurement of TMRE fluorescence. Shown is a representative graph. **(D)** Measurement of the ATP-levels in full growth

medium containing either glucose or galactose as the only available sugar. Ramos cells were treated with 10 µM P01F08 (Bromoxib), Enniatin B or Aranorosin. With only galactose, the cell is forced to rely entirely on OXPHOS for ATP synthesis. The ATP-levels were measured using the mitochondrial ToxGlo™ assay from Promega which is luminescence based. The depicted values were normalized to DMSO (0.1% v/v) treated cells in glucose containing media which were set 100%. Error bars = mean ± SD values of technical triplicates of one experiment are shown.

6.2 The mycotoxin viriditoxin induces leukemia- and lymphoma-specific apoptosis by targeting mitochondrial metabolism

Viriditoxin was validated as a top candidate in the primary screening of natural products shown in **Figure 12** and excluded from the experiments in **Figure 13** since it was primarily investigated and characterized by my predecessor Dr. Stuhldreier as one research topic in the scope of his dissertation [466].

The Viriditoxin (VDT) project, was published by Dr. Fabian Stuhldreier and the author of this thesis as equally contributing first authors in 2022, entitled: 'Mycotoxin viriditoxin induces leukemia- and lymphoma-specific apoptosis by targeting mitochondrial metabolism' [1]. In the following, the key findings of this publication [1] about VDT will be summarized below.

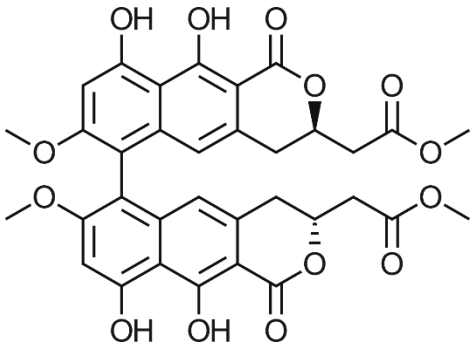

Figure 14 Structure of Viriditoxin (VDT) [1]

The natural compound Viriditoxin (VDT) (**Figure 14**) derives from the endophytic fungus *Cladosporium cladosporioides* and was identified as a promising therapeutic for leukemia and lymphoma treatment [1, 466]. VDT exhibited a high level of cytotoxicity and caused quick activation of caspases in both Jurkat leukemia and Ramos lymphoma cells. However, its impact on solid tumor cells was significantly less [1]. An intriguing observation was that human hematopoietic stem and progenitor cells, as well as peripheral blood mononuclear cells derived from healthy donors, were highly resistant to VDT-induced cytotoxicity. Additionally, the colony-forming capacity was impacted only at very high concentrations, suggesting a promising therapeutic window for treatment strategies [1]. Even in the presence of anti-apoptotic Bcl-2, VDT activates the intrinsic mitochondrial apoptosis pathway in leukemia cells. In addition, VDT's mitochondrial toxicity was verified by its ability to inhibit mitochondrial respiration, generate ROS, diminish the mitochondrial membrane potential (ΔΨm), discharge cytochrome c from

mitochondria, activate dynamin-like GTPase OPA1, and result in mitochondrial fragmentation. In the VDT project reviewed above, I contributed in the characterization of the apoptosis pathway ([1] Fig. 4B, D, E; Fig. 5B, C; Suppl. Fig. 3B), the validation of potential VDT targets ([1] Fig. 7; Suppl. Fig. 4A) and performed largely the extensive revision, including the cell specificity screening of the drug ([1] Suppl. Fig 1), performing quantitative analyses of Western blots and graphs including statistics, revised and corrected the manuscript together with my supervisor Prof. Wesselborg.

In the scope of this thesis I included data about the validation of potential VDT targets (**Figure 15**, taken from the publication [1]) and further investigations about molecular mechanisms of two selected target proteins (**Figure 16**).

With confirmation of the mitochondrial toxicity, the next aim was to identify the molecular target of VDT. An unbiased proteomic approach using thermal proteome profiling (TPP) was performed by Thomas Lenz (working group of Prof. Kai Stühler, Molecular Proteomics Laboratory, Biological-Medical-Research Center (BMFZ), University of Düsseldorf). By identifying proteins whose thermal stabilities are impacted by drug-binding, this approach facilitates the detection of drug-protein interactions within living cells. For successful identification of respective drug targets, affected proteins' thermal profiles can be analyzed by mass spectrometry [454, 467]. Utilization of the TPP-approach after VDT treatment identified 43 proteins in Ramos cells. All proteins with decreased thermal stability are shown on the left side of the graph (**Figure 15 A**). A functional protein association network (STRING) analysis of the top 43 proteins is shown in **Figure 15 B** [1] and 29 proteins originated from mitochondria. VDT treatment has a significant effect on several enzymes that participate in the TCA cycle, including two subunits of the pyruvate dehydrogenase complex (PDHA1, PDHB), two succinate-CoA ligase subunits (SUCLG1, SUCGL2), and isocitrate dehydrogenase 2 (IDH2) (**Figure 15 A**, **B**) [1]. These enzymes require NAD^+ and produce $NADH+H^+$. Thus, the NAD^+/NADH ratio was evaluated, but VDT treatment did not affect this ratio. As a result, TCA enzymes were concluded to be not affected by VDT treatment [1].

It is noteworthy that among the 20 identified candidates, there were mitochondrial ribosomal (mitoribosomal) proteins (MRPs), which are either part of the large 39S-subunit (12 proteins) or small 28S-subunit (8 proteins) (**Figure 15 A**, **B**) [1]. Three controls were used: Cycloheximide (CHX) as an inhibitor of cytosolic protein translation, Chloramphenicol (CAP) as an inhibitor of mitochondrial translation [468] and Tigecycline (TIG) as mitochondrial translation inhibitor, which also inhibits the ETC complexes I and IV and selectively kills leukemia stem and progenitor cells [1, 468, 469]. Hence it was possible that VDT, like TIG might target the mitochondrial translation [1, 468]. In order to investigate whether VDT affects the function of mitoribosomes, the protein expression levels of cytochrome c oxidase 2 and 4 (Cox-2, Cox-4) were analyzed, which are subunits of the mitochondrial respiration complex IV in the ETC and are translated

by mitochondrial or cytosolic ribosomes, respectively (as depicted in **Figure 15 C**) [1]. Cox-2 is translated by mitochondrial ribosomes, whereas Cox-4 is translated by cytosolic ribosomes [470]. To this end, Ramos cells were exposed to increasing concentrations of VDT for 36 hours, and the levels of Cox-2 and Cox-4 proteins were evaluated through immunoblotting (**Figure 15 C**). To rule out the possibility that caspase-mediated proteolysis affected the protein levels, QVD was applied. The results shown in **Figure 15 C** demonstrate that VDT and TIG did not significantly reduce the mitochondrial Cox-2 expression after 36 h treatment. A minor reduction in Cox-2 expression was observed for CAP after 36 h. Therefore, it was concluded that the protein expression of Cox-2 in Ramos cells remained rather stable after 36 h without substantial impact of VDT or TIG treatment (**Figure 15 C**). Given the stable expression of Cox-2, the possibility of VDT inducing apoptosis primarily through the inhibition of mitochondrial protein translation was excluded. Furthermore, CAP, which is known to inhibit mitochondrial translation, did not cause cytotoxicity in Ramos cells even after 48 hours of treatment. In contrast VDT induced cytotoxicity at distinctly lower concentrations (IC_{50} (36 h) = 0.024 µM), more substantial than TIG (IC_{50} 36 h: 5.32 µM) (**Figure 15 D**).

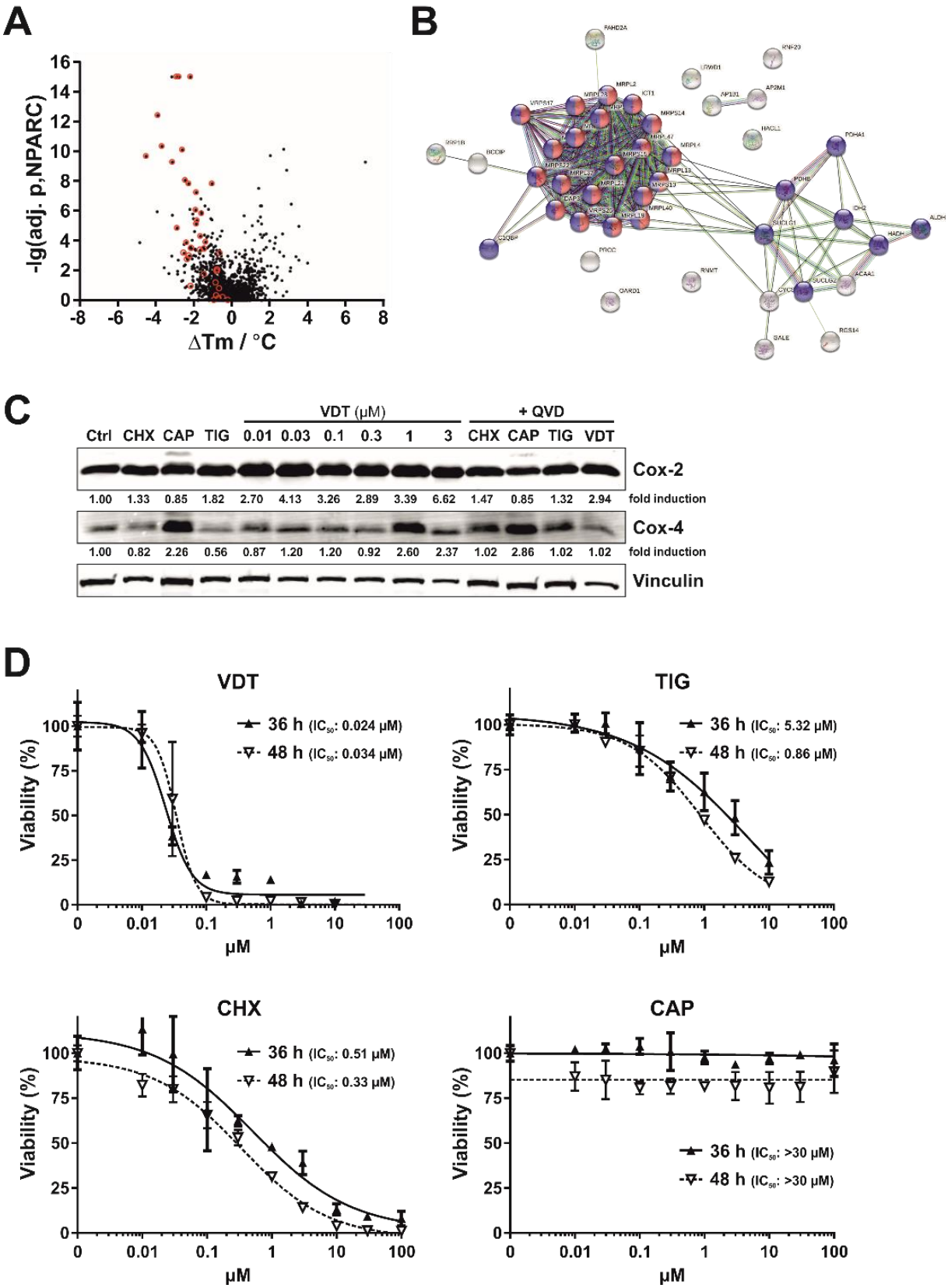

Figure 15 Thermal proteome profiling of potential VDT target proteins and effect of the inhibition of mitochondrial and cytosolic translation on protein expression and viability. (A) For mass spectrometry based thermal proteome profiling (TPP), Ramos cells were treated with 10 µM viriditoxin (VDT) or diluent control for 30 min. The statistical significance for the VDT-induced difference in protein melting behavior (expressed as the negative decadic logarithm of the adjusted NPARC p-value, -lg(adj. p, NPARC)) is plotted against the melting point difference (difference of the means of the melting points, ΔTm). Mitoribosomal proteins are shown in red within the plot. **(B)** Shown is the functional protein

association network (based on the STRING database) of the top 43 proteins destabilized by VDT, selected by p-value and melting point difference. Mitochondrial proteins are labeled in blue, mitoribosomal proteins in blue/red and non-mitochondrial proteins in grey. **(C)** Ramos cells were treated with increasing concentrations of VDT. Cycloheximide (CHX; 1 µM) was used as inhibitor of cytosolic protein translation and chloramphenicol (CAP; 150 µM) and tigecycline (TIG; 10 µM) as inhibitors of mitochondrial translation. In order to prevent caspase-mediated protein degradation the pan-caspase inhibitor QVD (10 µM) was added prior to application of CHX, CAP, TIG, or VDT (3 µM; right lane). After 36 h immunoblotting against cytochrome c oxidase 2 and 4 (Cox-2 and Cox-4) was performed. Cox-2 is translated within the mitochondria whereas Cox-4 is translated in the cytosol. Immunoblotting for vinculin was used as loading control. Numbers under Cox-2 and Cox-4 immunoblots indicate densitometric analyses of the fold induction of Cox-2/-4 relative to loading control. **(D)** Ramos cells were treated with increasing concentrations of VDT, CHX, CAP, or TIG for 36 h and 48 h, respectively. Subsequently, cell viability was monitored by AlamarBlue® assay. Mean ± SD values of triplicates are shown. Respective IC_{50} values are given in parentheses. (Figure and legend taken from [1] without changes).

A direct effect of VDT on mitochondrial protein translation as the primary mechanism for apoptosis was excluded in the published manuscript [1]. Since the exact molecular target of VDT is still unknown, it was aimed to address this point via a detailed further investigation of the other, the stabilized candidates, as shown in **Table 11.** The TPP identifies proteins with a destabilized melting behavior which were shown and analyzed in the publication [1], but it also reveals proteins with a stabilized melting behavior, which are significantly stabilized upon VDT treatment **Table 11** and **Figure 16**.

Table 11 List of proteins stabilized by VDT. The proteins were identified by thermal proteome profiling which was performed as described in Methods. Proteins with -lg(adj. p, NPARC) > 3.85 and ΔTm > 0 were regarded as significantly stabilized.

Gene name	Protein name(s)	-lg(adj. p, NPARC)	ΔTm
AACS	Acetoacetyl-CoA synthetase; ACSF1, FLJ12389, SUR-5	8,73	2,88
AARS2	Alanine-tRNA ligase; AARSL, bA444E17.1, KIAA127	5,57	1,49
ALDH18A1	Delta-1-pyrroline-5-carboxylate synthase; GSAS, P5CS, PYCS, SPG9	7,53	1,39
CDC37L1	Hsp90 co-chaperone CDC37-like 1; CDC37B, FLJ20639, HARC	4,46	1,8
COG3	Conserved oligomeric Golgi complex subunit 3	4	2
COX6B1	Cytochrome c oxidase subunit 6B1; COX6B, COXG	4,45	2,67
DECR1	2,4-dienoyl-CoA reductase; DECR, SDR18C1	4,42	1,51
GRSF1	G-rich sequence factor 1	6,33	1,57
HARS1	Histidine-tRNA ligase, USH3B	5,02	1,07
IK	Protein Red; RED, RER	5,32	1,38
INPP5D	Phosphatidylinositol 3,4,5-trisphosphate 5-phosphatase 1; hp51CN, SHIP, SHIP1	9,25	7,03
LRPPRC	Leucine-rich PPR motif-containing protein; GP130, LRP130, LSFC	9,71	2,01
POLE4	DNA polymerase epsilon subunit 4; p12	4,97	3,54

Gene name	Protein name(s)	-lg(adj. p, NPARC)	ΔTm
PPP2R1B	Serine/threonine-protein phosphatase 2A 65 kDa regulatory subunit A beta; PP2A-A beta, PR65B	4,04	1,18
PPP6R1	Serine/threonine-protein phosphatase 6 reg. subunit 1; KIAA1115, SAP190, SAPS1	5,1	1,56
PTRHD1	Putative peptidyl-tRNA hydrolase; C2orf79, LOC391356	6,33	1,49
STRBP	Spermatid perinuclear RNA-binding protein; FLJ11307, ILF3L, SPN	6,47	3,13
SUMO2	Small ubiquitin-related modifier 2; SMT3B, SMT3H2	4,24	2,3
TATDN1	Putative deoxyribonuclease TATDN1	10,14	2,74
TPD52	Tumor protein D52; D52, hD52, N8L	4,24	1,59
WIBG	Partner of Y14 and mago	4,39	1,69
YWHAG	14-3-3 protein gamma; PPP1R170	4,57	0,71
YWHAH	14-3-3 protein eta; YWHA1	5,66	0,64

An extensive literature research was performed on the stabilized candidates of **Table 11** in terms of their subcellular localization and biological function. The most interesting candidates were analyzed in three different cell lines: Ramos, SUPB-15 (B cell acute lymphoblastic leukemia; B ALL) and HeLa cells on their protein expression levels and in HeLa cells on their subcellular localization after VDT treatment in order to validate them as targets. Ramos and SUPB-15 were selected to be compared since the cell specificity screening showed, that SUPB-15 with an IC_{50} of 0.4 µM (24 h) was almost as sensitive to VDT treatment as Ramos with an IC_{50} of 0.06 µM (24 h) [1]. In the development of acute leukemia, the bone marrow's resources and capacity are utilized to create immature B lymphocyte progenitors that are characteristic for the disease. In B cell ALL, these blast cells are immature B lymphocyte progenitors. This type of leukemia is most prevalent in children with an incidence rate of 46 cases per 100,000 individuals worldwide [471, 472]. However, Ramos are human B cell lymphoma and SUPB-15 are lymphoblastic leukemia cells and they share a common cellular origin according to the hematopoiesis of blood cells [472, 473]. Thus, it was aimed to investigate whether a common mechanism regarding the two stabilized proteins is responsible for the comparable susceptibility regarding cytotoxicity, respectively.

Two candidate proteins were selected for further analysis: **1.) LRPPRC** (Leucine-rich PPR motif-containing protein) is localized in the mitochondria and involved in mRNA transport, transcription and regulation of transcription. This protein is of interest since it plays a role in maintaining the stability of the mitochondrial encoded cytochrome c oxidase (COX) subunits according to the human protein atlas [474]. Another study shows the downregulation of LRPPRC expression in relation to apoptosis induction through the mitochondria-mediated pathway in prostate cancer cells. These experimental data suggest that LRPPRC plays a critical role in

the development of prostate cancer and thus its inhibition presents a potential approach for prostate cancer treatment [475]. Moreover, the overexpression of LRPPRC is associated with poor prognosis, whereas the downregulation of LRPPRC inhibits growth and invasion, resulting in apoptosis induction [476]. An interaction between LRPPRC and VDT could lead to an inhibition of mitochondrial-mRNA transport to the mitoribosomes, giving an explanation for the destabilization of the mitoribosomal protein-cluster [477]. **2.) GRSF1** (G-rich sequence factor 1) is localized in the mitochondria and regulates post-transcriptional mitochondrial gene expression, which is required for the assembly of the mitochondrial ribosome and the recruitment of mRNA and lncRNA (human protein atlas [474]). It was named together with LRPPRC and SLIRP (SRA stem-loop interacting RNA binding protein) in a group of proteins involved in mitochondrial RNA metabolism and coordination of translation of mitochondrial mRNAs [478]. An interaction between VDT and GRSF1, disturbs possibly the assembly of mitoribosomal proteins. Consequentially it is a possible hypothesis, since GRSF1 is required for mitochondrial ribosome assembly and the MRPs were the most prominent destabilized protein cluster (**Figure 15**) [1]. To characterize cell specificity, concentration and time dependency, the direct effect of VDT, was tested on these two candidates (**Figure 16**). **Figure 16 A** shows the volcano plot, visualizing -lg(adj.p,NPARC with a cutoff > 3.85 and ΔTm > 0. **Figure 16 B** shows the respective STRING analysis of these 23 candidates. To analyze rapid effects on the selected candidate target proteins LRPPRC and GRSF 1, Ramos, SUPB-15 and HeLa cells were treated with a sublethal (1 µM) and a lethal VDT-concentration (10 µM) for either 30 min or 4 h (**Figure 16 C**). Leukemic cell lines Ramos and SUPB-15 have shown no rapid effect after 30 min and 4 h on both proteins. HeLa cells have shown a concentration dependent effect. LRPPRC and GRSF1 protein levels decreased after treatment with 10 µM VDT after 4 h. In contrast, GRSF1 protein levels increased with a sublethal dose of 1 µM VDT (**Figure 16 C**).

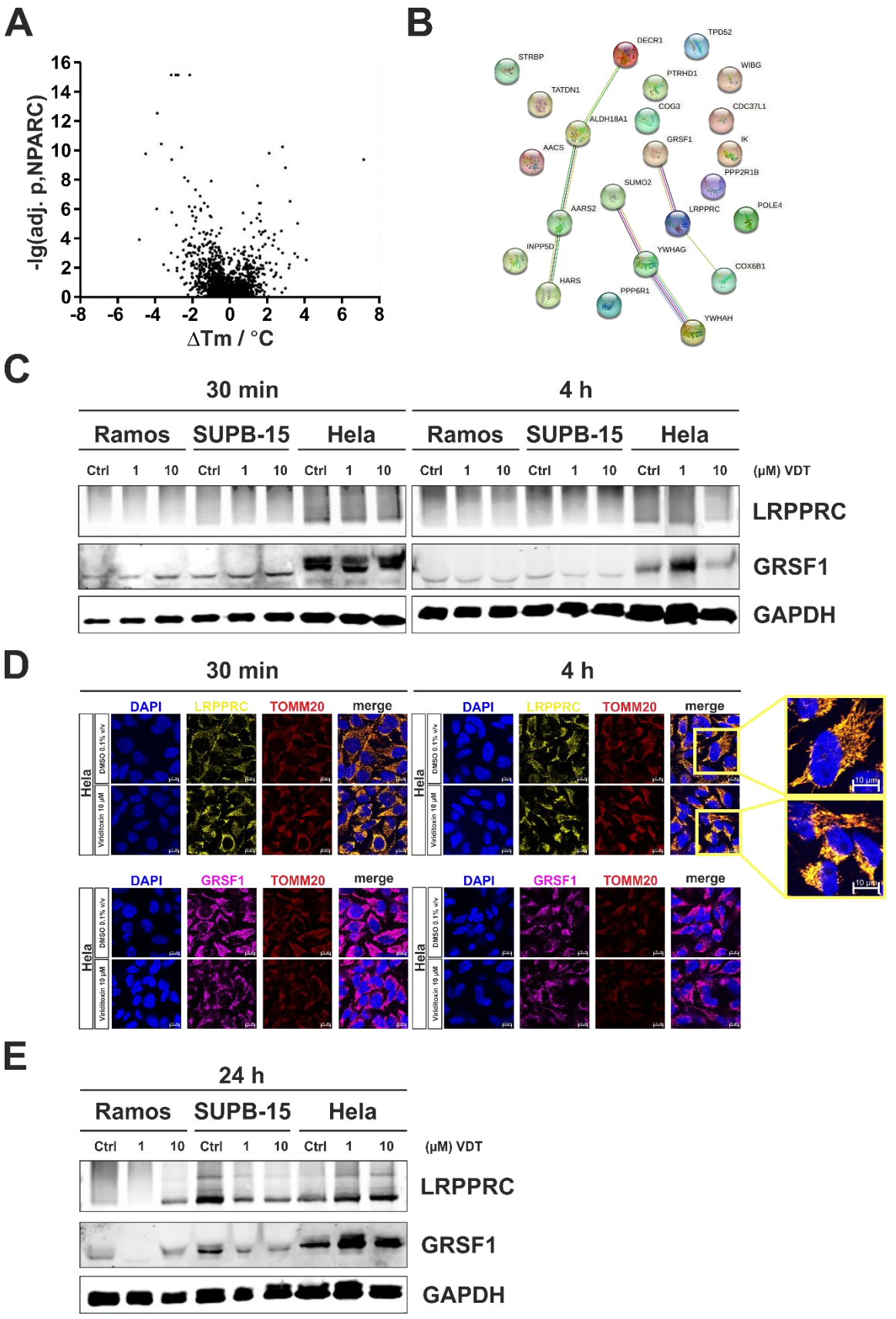

Figure 16 Thermal proteome profiling of stabilized VDT target proteins with the effect of VDT on two selected candidate proteins: LRPPRC and GRSF1.(A) For mass spectrometry-based thermal proteome profiling (TPP), Ramos cells were treated with 10 μM VDT or diluent control for 30 min. The statistical significance for the VDT-induced difference in protein melting behavior (expressed as the negative decadic logarithm of the adjusted NPARC p-value, -lg(adj. p, NPARC)) is plotted against the melting point difference (difference of the means of the melting points, ΔTm). **(B)** Shown is the functional

protein association network (based on the STRING database) of the top 23 proteins stabilized by VDT, selected by p-value and melting point difference. **(C)** and **(E)** Ramos, SUPB-15 and HeLa cells were treated with 0.1% (v/v) DMSO (negative control), 1 or 10 µM of VDT for 30 min and 4 hours **(C)** and 24 h **(E).** The protein levels of LRPPRC and GRSF1 were determined via immunoblotting. GAPDH served as loading control. **(D)** HeLa cells were treated with DMSO (0.1% (v/v); negative control) or 10 µM of VDT for 30 min and 4 hours. By immunofluorescence the protein localization of LRPPRC in yellow and GRSF1 in purple was determined. TOMM20 in red was used as marker for the outer mitochondrial membrane and DAPI in blue served as marker for the nucleus. Representative images of three independent biological replicates are shown.

To monitor the subcellular localization of LRPPRC after 30 min and 4 h, HeLa cells were incubated with either DMSO (0.1% v/v) or 10 µM VDT (**Figure 16 D**). GRSF1 colocalizes with, TOMM20 (Translocase of the outer mitochondrial membrane complex subunit 20), a common marker of the OMM. No change in subcellular localization was observed (**Figure 16 D**). In steady state LRPPRC colocalizes also with TOMM20 at the mitochondrial membrane. Upon 4 h VDT incubation the mitochondrial staining reveals increased punctae formation, indicating increased fission of the tubular mitochondrial structures (**Figure 16 D**). Punctae are morphological indicative for mitochondrial fragmentation, which we previously observed as one effect of VDT treatment [1]. Since the targets of VDT are not fully evaluated, this project will be further investigated within the collaborative research program RTG 2158, together with Dr. Bhatia (Department of Pediatric Oncology, Hematology and Clinical Immunology, University Hospital Düsseldorf).

6.3 40 Years of research on polybrominated diphenyl ethers (PBDEs) – A historical overview and newest data of a promising anticancer drug

The next chapter links to the initial cell death screening of selected natural products in Burkitt B cell lymphoma (Ramos) and acute T cell leukemia (Jurkat) cells (**Figure 12** and **Figure 13**) highlights P01F08 (Bromoxib) (**Figure 17**) as an interesting natural product worth of further investigation.

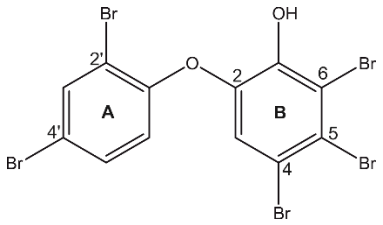

Figure 17 Structure of P01F08 (Bromoxib) (4,5,6-tribromo-2-(2',4'-dibromophenoxy) phenol) [2]

Natural products of marine origin often serve as structural prototypes for new classes of anticancer drugs that target cancer cells specifically at their vulnerabilities [479]. The natural compound P01F08 (Bromoxib) was identified in a screening of 300 natural compounds from the biobank of Prof. Proksch (Institute for Pharmaceutical Biology and Biotechnology, Heinrich-Heine University Düsseldorf), which aimed to identify natural products in order to overcome therapy resistance in chemotherapeutic-resistant tumors and microorganisms [441]. Bromoxib was previously termed P01F08, according to its plate coding identity or 4,5,6-tribromo-2-(2',4'-dibromophenoxy) phenol. It has shown extensive antineoplastic activity in T cell leukemia and Burkitt B cell lymphoma cell lines as model system [441]. Bromoxib affected primary AML cells 3.2-fold stronger than their healthy counterparts (peripheral blood mononuclear cells; PBMNC) and was therefore postulated as a natural product of therapeutic relevance for patients with AML [441]. These results rendered Bromoxib as an interesting candidate for further investigation of its molecular mechanism of cell death induction. In order to elucidate the mechanistic pathway of apoptosis, the author of this dissertation and colleagues published in 2021 the cytotoxicity and apoptosis induction capacity of P01F08 (Bromoxib) in Ramos and Jurkat cells in 2021, entitled '40 Years of research on polybrominated diphenyl ethers (PBDEs) – A historical overview and newest data of a promising anticancer drug' [2].

The article provides an overview of the primary research areas concerning the compound class known as polybrominated diphenyl ethers (PBDEs). Specifically, the research focuses on two distinct aspects: (i) the chemistry of naturally occurring PBDEs found in marine environments, and (ii) the toxicology of synthetic flame-retardant PBDEs found in the environment. By examining the structural similarities and differences between these two groups, the article

evaluates their varying bioactivity patterns with providing a first structure-activity relationship analysis comparing both PBDE groups [2].

As reviewed in the introduction, the anticancer field was pioneered first by natural products beginning in the 1940s. Bromoxib was first isolated by Carté and Faulkner in 1981 [480] from a marine sponge from *Dysidea* species. First ^{13}C NMR data were initially published in 1996 [481]. Fu and Schmitz initially started to investigate the anticancer properties of Bromoxib in 1995 and determined an IC_{50} values of 7.4 µM for 15-lipoxygenase. Another PBDE (compound 14 in [482]) was determined with an EC_{50} of 4.4 µM for inosine monophosphate dehydrogenase. The compound also exhibited 71% inhibition of guanosine monophosphate synthetase at 50 µM, but did not inhibit protein tyrosine kinases or matrix metalloproteases [482]. A recent publication isolated Bromoxib from *Dysidea granulosa* collections and evaluated its cytotoxicity against a monkey kidney cell line (Bsc-1) and a human colorectal tumor cell line (HCT-116). Interestingly, Bromoxib acts cytotoxic against Bsc-1 cells with an IC_{50} of 15 µg/mL and inhibits certain bacteria growth, including *S. aureus* ATCC 29213, *S. aureus* ATCC 43300, *E. faecium* ATCC 29212, and *E. faecium* ATCC 51299 at minimum inhibitory concentrations ranging from 3.7 to 0.4 µg/mL [483] (reviewed in our publication [2]).

Although there is accumulated evidence that P01F08 (Bromoxib) might display a therapeutic benefit in leukemia and lymphoma, the exact mechanism of action still needs to be unraveled. Therefore, the cell specificity was investigated and cytotoxicity measurements were performed for Ramos and Jurkat cells, with Ramos cells displaying a higher cytotoxicity to P01F08 (Bromoxib; IC_{50} of 5.39 µM) (**Figure 18**).

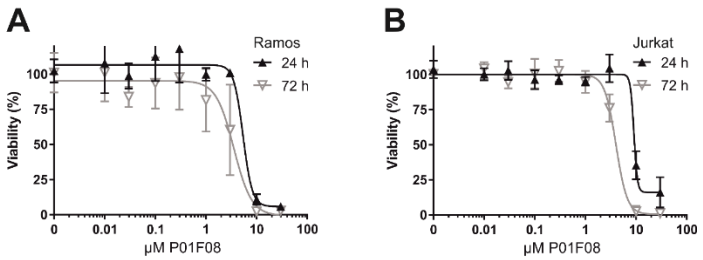

C

IC_{50}	24 h	72 h
Ramos	5.39 µM	3.55 µM
Jurkat	9.08 µM	4.0 µM

Figure 18 P01F08 acts highly cytotoxic in acute T cell leukemia (Jurkat) and Burkitt B cell lymphoma (Ramos) cells. Cytotoxicity in Ramos **(A)** or Jurkat **(B)** cells was determined after the indicated incubation periods using AlamarBlue® viability assay. **(C)** Overview of the resulting IC_{50} values in the individual cell lines at the respective incubation times. All experiments were performed in triplicates; the values were normalized to DMSO (0.1% v/v; negative control). Error bars = SD of three independent experiments performed in triplicates. (Figure and legend taken from [2] without changes).

P01F08 (Bromoxib) was tested on its capability to induce apoptosis in Ramos and Jurkat cells (**Figure 19**). Both cell lines were treated with 1 or 10 µM P01F08 (Bromoxib) and the caspase-3 activity was monitored over 8 h (**Figure 19 A** and **B**). However, treatment with 1 µM

P01F08 (Bromoxib) did not result in significant caspase-3 activity in both cell lines. Ramos cells showed detectable caspase-3 activity after 2 to 3 hours and that peaked at 6 hours. Jurkat cells showed a steady increase of caspase-3 activity. The results indicate that Ramos cells may be slightly more sensitive to P01F08 (Bromoxib) treatment than Jurkat cells, demonstrated by lower IC_{50} values and higher caspase-3 activity [2]. To investigate the ability of P01F08 (Bromoxib) for apoptosis induction, both cell lines were treated with 10 µM of P01F08 (Bromoxib). Caspase-3 activity was monitored by PARP1 cleavage over 8 h (**Figure 19**). In Ramos cells (**Figure 19 C**), PARP1 cleavage was observed within the first 2 hours of P01F08 (Bromoxib) incubation. PARP1 cleavage in Jurkat cells (**Figure 19 D**) was delayed and only observed after 4 hours incubation time. To confirm the P01F08 induced caspase activation, cells were pre-treated with QVD-OPH as pan-caspase inhibitor to prevent PARP1 cleavage in both cell lines. This suggests that the cell death induced by P01F08 (Bromoxib) is dependent on caspase activation. To determine the amount of apoptotic hypodiploid nuclei, propidium iodide (PI) staining was used to detect DNA fragmentation according to the method of Nicoletti *et al.* [453]. The results in **Figure 19** show that P01F08 (Bromoxib) caused a concentration-dependent increase in hypodiploid nuclei in both cell lines. Ramos cells (**Figure 19 E**) are again more susceptible than Jurkat cells (**Figure 19 F**) [2].

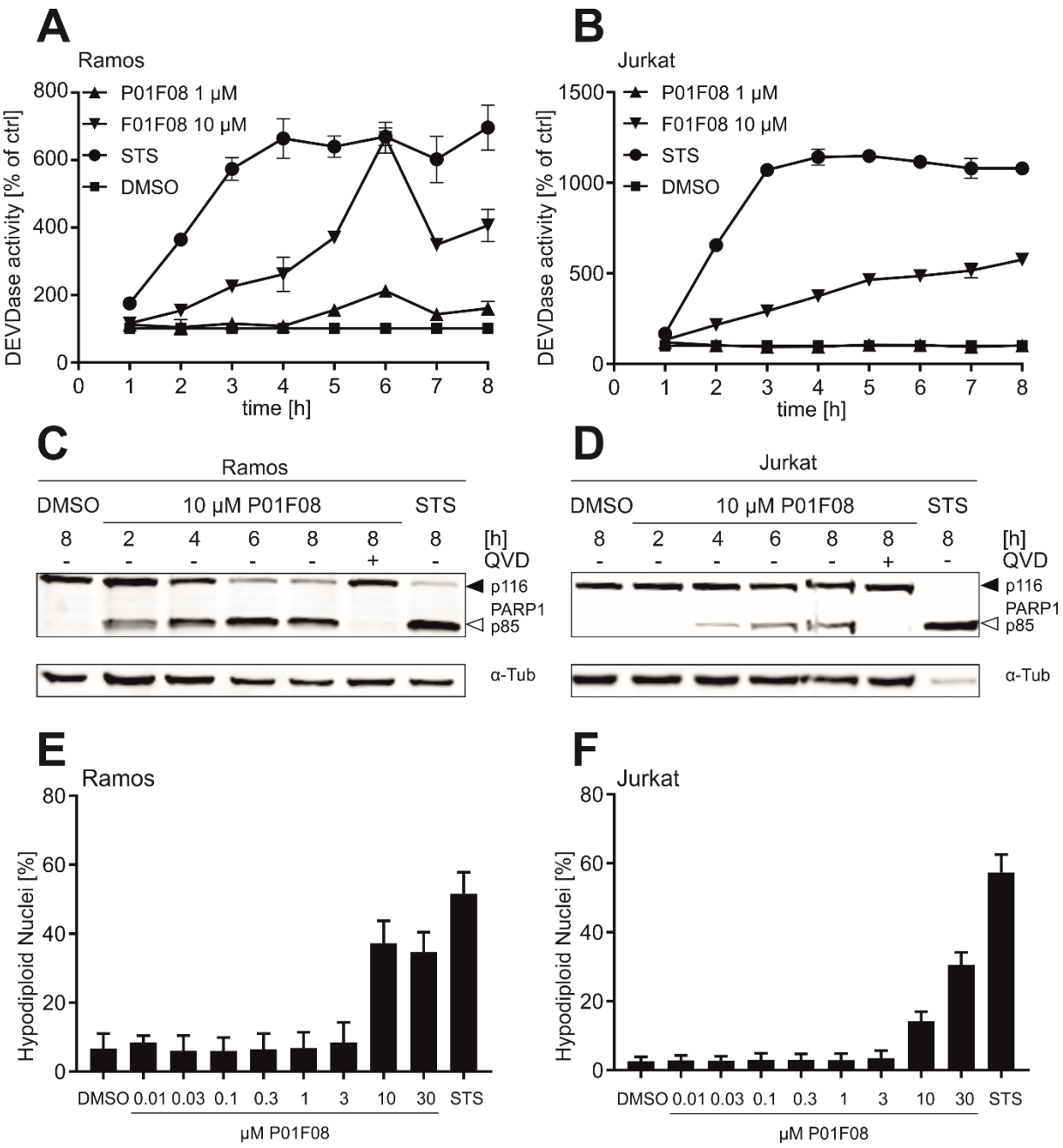

Figure 19 P01F08 is a potent inducer of apoptosis in leukemia and lymphoma cells with short latency and rapid kinetics especially in Ramos (lymphoma) cells. Ramos **(A)** and Jurkat **(B)** cells were treated with a high concentration of P01F08 (10 µM) or Staurosporine (STS; 2.5 µM; positive control) for the induction of apoptosis for 8 h. Subsequently, DEVDase activity as a surrogate marker for caspase-3 activity was determined via measurement of the fluorescence of the profluorescent caspase-3 substrate DEVD-AMC in a micro-spectrophotometer. The slope of the linear range of fluorescence increase served as a measure for DEVDase activity. The DMSO control values were set to 100% and the normalized relative fold induction was calculated as described in Materials and Methods. **(A)** and **(B)** are representative for three independent experiments, mean and SD of technical triplicates are depicted. **(C)** and **(D)** show representative immunoblots of three independent experiments of cleavage of the caspase-3 substrate poly(ADP-ribose) polymerase 1 (PARP1; full-length 116 kDa, cleaved form 85 kDa) as an indicator for apoptotic cell death in Ramos cells **(C)** and Jurkat cells **(D).** Cells were treated with P01F08 (10 µM), DMSO (0.1% v/v), and STS (2.5 µM) for the indicated incubation times alone or with pre-treatment (30 min) of the pan-caspase inhibitor QVD (10 µM). alpha-tubulin (α-Tub) served as a loading control. **(E)** and **(F)** Apoptosis-related DNA degradation was detected after 24 h incubation via flow-cytometric measurement of propidium iodide stained hypodiploid nuclei in **(E)** Ramos and **(F)** Jurkat cells. Mean and SD of three independent experiments performed in triplicates are depicted. (Figure and legend taken from [2] without changes).

Shown above, P01F08 (Bromoxib) induces caspase-mediated apoptosis in both cell lines, but to different degrees. Further investigations focused on the activation of the intrinsic apoptotic mitochondrial pathway. Considering the broad bioactivity pattern of polybrominated diphenyl ether derivatives, also targeting many bacterial species, it is very likely that P01F08 (Bromoxib) also affects mitochondria. Therefore, it was investigated whether the induction of apoptosis by P01F08 (Bromoxib) is mediated via the mitochondrial death pathway. To achieve this, Jurkat cells that overexpressed anti-apoptotic Bcl-2 or the corresponding empty vector control were treated with P01F08 (Bromoxib) and apoptotic hypodiploid nuclei were quantified after 24 hours by the Nicoletti assay (**Figure 20 A**). Cells were also treated with Staurosporine (STS; 2.5 µM) and Etoposide (Eto; 50 µM) as respective controls (**Figure 20 A** and **B**) [2]. As mentioned previously, STS is a potent apoptotic stimulus, commonly used to activate the mitochondrial death pathway, similar to DNA-damaging anticancer drugs and without external death receptor signaling. Additionally, STS can induce apoptosis through an alternative route that is independent of the mitochondrial apoptosis pathway [446]. Therefore, overexpression of Bcl-2 does not block apoptosis induction via STS due to the activation of an alternative pathway. Etoposide is an anticancer drug that inhibits topoisomerase II, causing DNA damage and inducing the intrinsic apoptosis cascade [484]. In contrast, intrinsic apoptosis induced by Etoposide is inhibited upon Bcl-2 overexpression, as confirmed by Nicoletti and Western blot analysis. With regards to P01F08 (Bromoxib), the substance generally induced lower levels of apoptosis in Jurkat cells, but interestingly apoptosis was completely blocked by Bcl-2 overexpression. This finding clearly indicates that apoptosis induction by P01F08 (Bromoxib) activates the intrinsic mitochondrial pathway of apoptosis (**Figure 20 A** and **B**) [2].

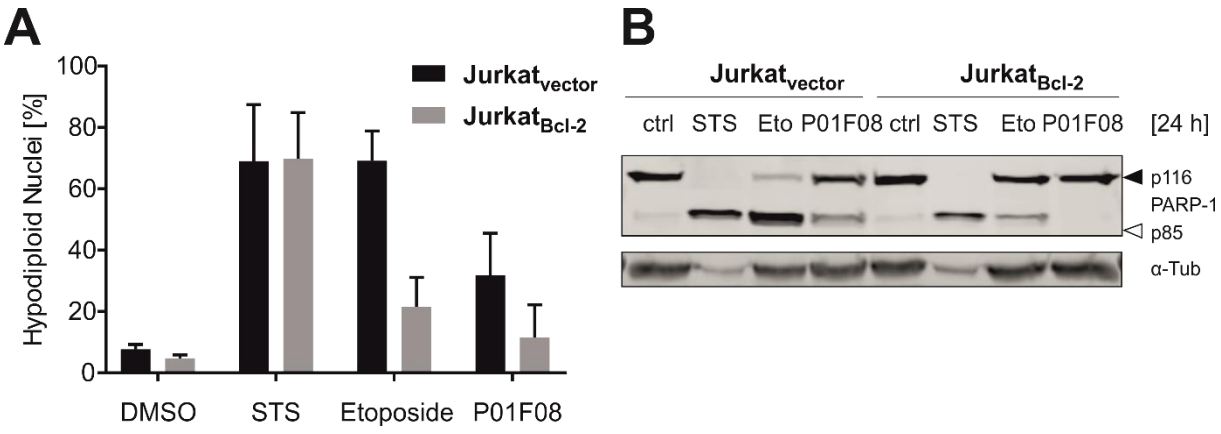

Figure 20 P01F08 induces Bcl-2 dependent apoptosis. Jurkat cells overexpressing Bcl-2 and corresponding vector control cells were treated with 2.5 µM Staurosporine (STS), 50 µM Etoposide and 10 µM P01F08 for 24 h. **(A)** Apoptosis-related DNA degradation was detected via flow-cytometric measurement of propidium iodide stained hypodiploid nuclei. Mean and SD of three independent experiments performed in triplicates are depicted. **(B)** Representative immunoblot of three independent experiments of cleavage of the caspase-3 substrate poly(ADP-ribose) polymerase 1 (PARP1; full-length 116 kDa, cleaved form 85 kDa) as an indicator for apoptotic cell death. alpha-tubulin (α-Tub) served as a loading control. (Figure and legend taken from [2] without changes).

6.3.1 Bromoxib – small molecule with extraordinary features targeting deregulated metabolism in cancer

Further investigations aimed on identifying various effects of P01F08 (Bromoxib) in cancer cells. From now on, P01F08 (Bromoxib) will be termed only 'Bromoxib'. We named the compound after its molecular mechanism as soon as we unraveled it. The nomination of 'Bromoxib' will be solved in the discussion (**7.2 Bromoxib**).

To perform the experiments in the correct cellular system the cancer specificity of Bromoxib was investigated. Therefore, 18 cell lines including blood cancer cell lines (**Figure 21 A**) as well as solid tumor cell lines (**Figure 21 B**) were incubated with increasing concentrations of Bromoxib for 24 h. First results showed prevalent cytotoxicity in acute lymphoblastic leukemia (SUPB-15) (IC_{50} 6.5 µM) and Burkitt B cell lymphoma (Ramos) cells (IC_{50} 2.38 µM) (**Figure 21**). Since we were interested in revealing the Bromoxib induced apoptosis pathway, it was differentiated between extrinsic death receptor mediated apoptosis and intrinsic mitochondria dependent apoptosis. To address this, caspase-8 deficient Jurkat cells and the caspase-8 proficient parental cell line A3 were treated with Bromoxib, STS or Etoposide as inducer of caspase-8 independent apoptosis, TRAIL as positive control for caspase-8 dependent apoptosis (**Figure 21 C**) or DMSO as solvent control. Subsequently the percentage of apoptosis in terms of hypodiploid nuclei was determined via flow-cytometry, according to the method of Nicoletti *et al*. It can be concluded from the data, that Bromoxib induces apoptosis in Jurkat cells to a low rate, but independent of caspase-8 and the extrinsic death receptor pathway (**Figure 21 C**). For the intrinsic pathway, Jurkat cells proficient and deficient for caspase-9 (as the central initiator caspase of the intrinsic mitochondrial apoptosis pathway) were treated in the same experimental setup for 24 h with DMSO as solvent control, Bromoxib, STS as inducer of partially caspase-9 independent apoptosis and Etoposide as positive control for the induction of fully caspase-9 dependent apoptosis (**Figure 21 D**). To underline this result, Bcl-2 overexpressing cells and the corresponding empty vector control cells were treated with Bromoxib (**Figure 21 E**). Bromoxib induces concentration dependent apoptosis, which is dependent on the presence of Bcl-2, supporting the intrinsic apoptosis as primary signaling pathway (**Figure 21 E**). In analogy to **Figure 21 C** and **D**, DMSO was used as solvent control, STS as Bcl-2 independent apoptosis inducer, Etoposide as inducer for partially Bcl-2 independent apoptosis and TRAIL as inducer of extrinsic and partially Bcl-2 dependent apoptosis (bar graph on the right; **Figure 21 E**). In summary, Bromoxib does not induce apoptosis through extrinsic death receptor pathway in leukemia and lymphoma cells, but rather via the intrinsic mitochondria-dependent pathway that relies on Bcl-2 and caspase-9.

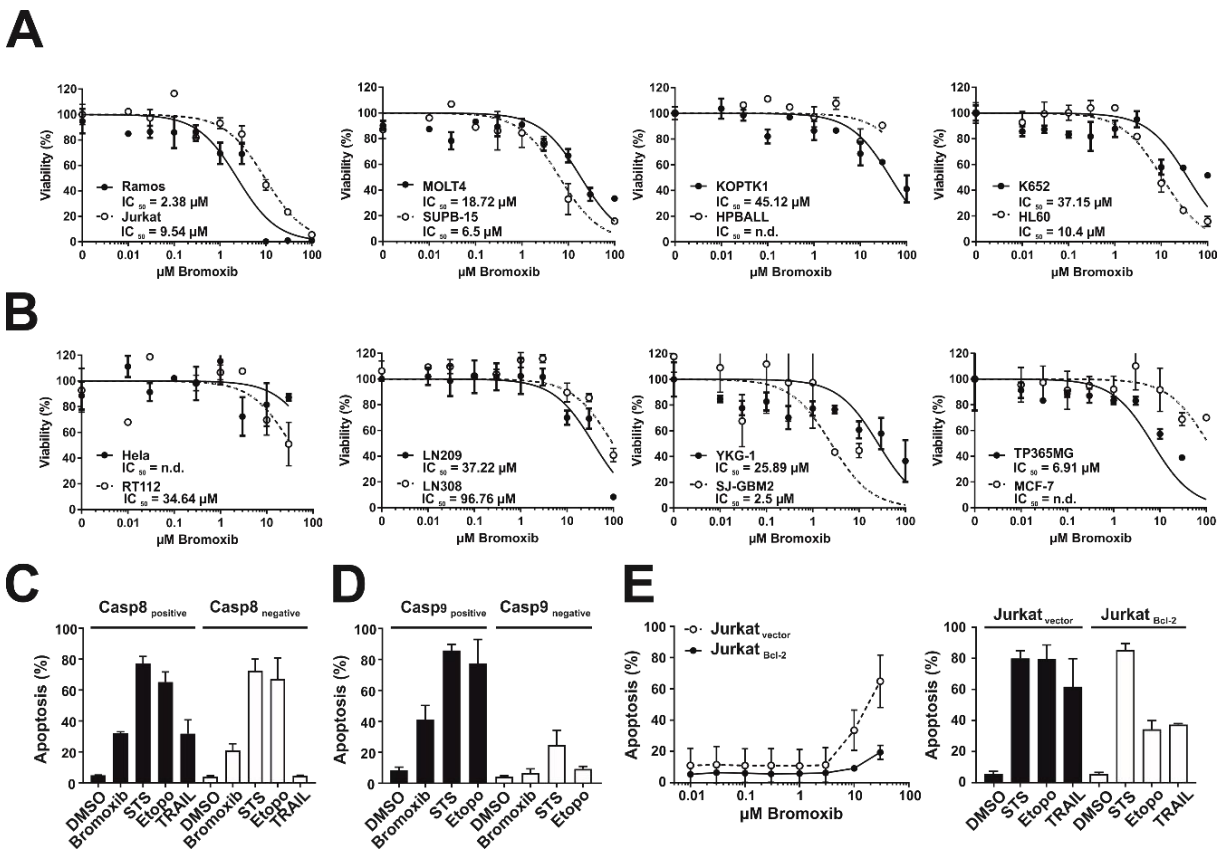

Figure 21 Bromoxib is cytotoxic in different cancer cell lines and induces intrinsic mitochondria dependent apoptosis. Cytotoxicity was determined after 24 h with increasing concentrations of Bromoxib in various cancer cell lines: **(A)** Leukemic cell lines: Ramos (Burkitt B cell lymphoma), Jurkat (acute T cell leukemia), MOLT4 (human T-ALL), SUPB-15 (human B cell acute lymphoblastic leukemia; B-ALL), KOPTK (human T-ALL), HPBALL (human T cell acute lymphoblastic leukemia; T-ALL), K652 (human chronic myeloid leukemia; CML), HL60 (human acute myeloid leukemia; AML), and **(B)** non-blood-cancer cell lines: HeLa (cervical cancer), RT112 (bladder cancer), MCF7 (breast cancer), LN209, LN308, YKG-1, SJ-GBM2, TP365MG (different glioblastoma cell lines). Cell viability was assessed by AlamarBlue® viability assay, shown in each graph is the mean ± SD of one representative experiment performed in triplicates. The respective IC_{50} values are given in the graphs. n.d.=not detected in the depicted concentration range. **(C)** Bromoxib induces caspase-8 independent and **(D)** caspase-9 dependent apoptosis. Apoptosis-related DNA degradation was detected after 24 h of incubation via flow-cytometry measurement of propidium iodide-stained apoptotic nuclei in **(C)** caspase-8-positive and caspase-8-negative Jurkat cells and **(D)** caspase-9-positive and caspase-9-negative Jurkat cells. Cells were stimulated with Bromoxib (10 µM), Staurosporine (STS; 2.5 µM), Etoposide (Etopo; 50 µM), TRAIL (Tumor Necrosis Factor Related Apoptosis Inducing Ligand; 40 ng/ml) and DMSO (0.1% v/v). Error bars = mean ± SD of three independent experiments performed in triplicates. **(E)** Bromoxib induces apoptosis upon overexpression of anti-apoptotic Bcl-2. Apoptosis induction was analyzed in Jurkat cells stably transfected with vectors encoding Bcl-2 or empty vector. After 24 h apoptosis induction was assessed by propidium iodide staining of apoptotic nuclei and flow-cytometry. Cells were stimulated with different concentrations of Bromoxib (left panel) and STS (2.5 µM), Etopo (50 µM), TRAIL (40 ng/ml), and DMSO (0.1% v/v) (right panel). Error bars = mean ± SD of three independent experiments performed in triplicates.

The next step was to identify the intracellular target(s), including the targeted organelles and characterization of the Bromoxib mediated effects. Since Ramos cells are most susceptible to Bromoxib, the following experiments were mainly performed in Ramos cells. Initially, a measurement of the mitochondrial membrane potential ($\Delta\Psi m$) was performed in Ramos cells, since changes in the potential of the mitochondrial membrane are closely associated with the

activation of the intrinsic apoptosis pathway. As reviewed above, the loss of mitochondrial membrane potential is an early event leading to the release of pro-apoptotic factors, activating the intrinsic apoptosis pathway. The mitochondrial membrane potential (ΔΨm) was measured in Ramos cells first as a baseline for 2 minutes and then, the stimulus (either Bromoxib or CCCP as positive control) was added (**Figure 22 A**). Bromoxib induces a rapid breakdown of ΔΨm within minutes, similar to the protonophore CCCP (**Figure 22 A**). To investigate the mitochondrial membrane potential breakdown in association with morphological changes of the mitochondria, the morphology of the mitochondria was monitored via live cell imaging of stably mitoDSRed expressing HeLa cells (**Figure 22 B**). Generally, the mitochondria have a tubular interconnected network and undergo continuous fusion and fission as maintenance of mitochondrial quality control. This tubular network can be seen for DMSO as solvent control (**Figure 22 B**). Similar to CCCP (**Figure 22 B**), Bromoxib incubation (30 and 120 min) leads to the formation of punctate structured mitochondria (**Figure 22 B**). CCCP induces mitochondrial fragmentation/fission through the activation of the mitochondrial fission machinery, which is mediated via the dynamin-related protein 1 (DRP1), a key regulator of mitochondrial fission [132, 485] . Activated DRP1 translocates from the cytosol to mitochondria and ER interaction sites (MERCs) [486]. At the MERCs, DRP1 di- and oligomerizes into helical structures, which then via GTP hydrolysis and constriction of DRP1 lead to scission of the mitochondria [486]. In summary, CCCP induces mitochondrial fragmentation through fission activation and fusion inhibition. Similar to CCCP, Bromoxib also seems to alter mitochondrial morphology and induces mitochondrial fission already after 30 min (**Figure 22 B**). Thus, Bromoxib activates another hallmark of the mitochondrial apoptosis pathway, inducing fragmentation (fission) of the mitochondria. An additional method to measure the induction of mitochondrial fragmentation is the detection of long unprocessed, membrane-bound OPA1 form (L-OPA1) and the soluble OPA1 form (S-OPA1) via immunoblotting (**Figure 22 C**). The short and long form have different effects on mitochondrial fission. L-OPA1 is required for normal fusion and the maintenance of mitochondrial cristae structure, whereas S-OPA1 promotes mitochondrial fission [448, 487]. The stress-induced cleavage of OPA1 and the loss of the long isoforms (L-OPA1) shifts the balance to increased fission of the mitochondria and simultaneously an increased sensitivity to pro-apoptotic stimuli [488, 489]. To address whether Bromoxib alters the S- and L-OPA1 levels, Ramos cells were treated for 5, 15, 30 or 120 min with Bromoxib, for 120 min with DMSO as solvent control and for 120 min with CCCP as positive control for the induction of OPA1 cleavage (upper Western blot; **Figure 22 C**). L-OPA1 disappears already after 5 min incubation (upper Western blot; **Figure 22 C**). The recovery of long OPA1 forms assesses the activity of the regulatory fusion and fission machinery with the balance between both events, fusion and fission, respectively. To measure L-OPA1 recovery, Ramos cells were treated with Bromoxib or CCCP as positive control for 30 min and the substances were then removed via

centrifugation. Subsequently, the recovery of L-OPA1 was detected over time for 2, 4 and 6 h (lower Western blot; **Figure 22 C**). Bromoxib induces, similar to CCCP, the depletion of L-OPA1 when incubated continuously, whereas the removal of Bromoxib and CCCP enables the recovery of the long OPA1 forms (lower Western blot; **Figure 22 C**). According to these Western blot data the effect on the mitochondrial fission is reversible. Furthermore, S-OPA1 is generated through proteolytic cleavage of L-OPA1 by proteases such as OMA1 or YME1L1 [122, 126]. This raised the question, which protease, OMA1 or YME1L1, is catalyzing the cleavage of L-OPA1 into S-OPA1 forms? Treatment of mouse embryonic fibroblasts (MEFs) with knockout of either OMA1 or YME1L1 or dual knockout of OMA1 and YME1L1 (**Figure 22 D**) addressed this issue. The cells were treated with Bromoxib or CCCP and the OPA1 short- and long forms were determined via immunoblotting (**Figure 22 D**). OMA1 is required to cleave L-OPA1 into S-OPA1, since no cleavage could be detected in the OMA1 knockouts. YME1L1 knockout does not prevent the cleavage of OPA1 (**Figure 22 D**). Thus, OMA1 seems to be the responsible protease for Bromoxib (and CCCP) induced OPA1 cleavage, but the exact mechanism inducing mitochondrial fragmentation remained elusive.

Mitochondrial dysfunction is also associated with a decreased mitochondrial calcium (Ca^{2+}) buffer capacity and increased sensitivity to mitochondrial permeability transition opening [490, 491]. As previously mentioned, mitochondria and Endoplasmic Reticulum contact sites (MERCS), regulate the Ca^{2+} transfer and lipid exchange to mitochondria. Mitochondrial fission occurs prevalently at these sites. Ca^{2+} transfer to mitochondria via MERCs triggers DRP1-independent IMM constriction and subsequent fission can be activated [160]. Therefore the ER was investigated as potential target for Bromoxib, possibly inducing total Ca^{2+} mobilization and were compared to Ionomycin. Ionomycin is an ionophore known to raise intracellular Ca^{2+} level and induces the mPTP [492, 493]. Since large-scale Ca^{2+} efflux from the mitochondria can result from persistent opening of the mPTP [492], the observation that Bromoxib caused an even higher Ca^{2+} mobilization than Ionomycin primed the hypothesis that Bromoxib exhibits protonophoric features (**Figure 22 E**). For the measurement of intracellular Ca^{2+} mobilization, cells were washed with Krebs-Ringer buffer, supplemented with EGTA as a chelating agent. Even when the extracellular Ca^{2+} was chelated via EGTA, Bromoxib still induced an increase in cytosolic Ca^{2+}, as shown in **Figure 22 F** (left graph). Thapsigargin was used as positive control to fully deplete the ER-Ca^{2+} stores. Next, it was tried to determine the origin of the released Ca^{2+}. First, Thapsigargin was added to the cells to release all Ca^{2+} stored in the ER. Subsequently, Bromoxib was added and could still mediate a residual release of intracellular Ca^{2+} (**Figure 22 F;** right graph). Thus, it was demonstrated that the Ca^{2+} mobilized by Bromoxib originates from the ER as well as from the mitochondria **Figure 22 F**.

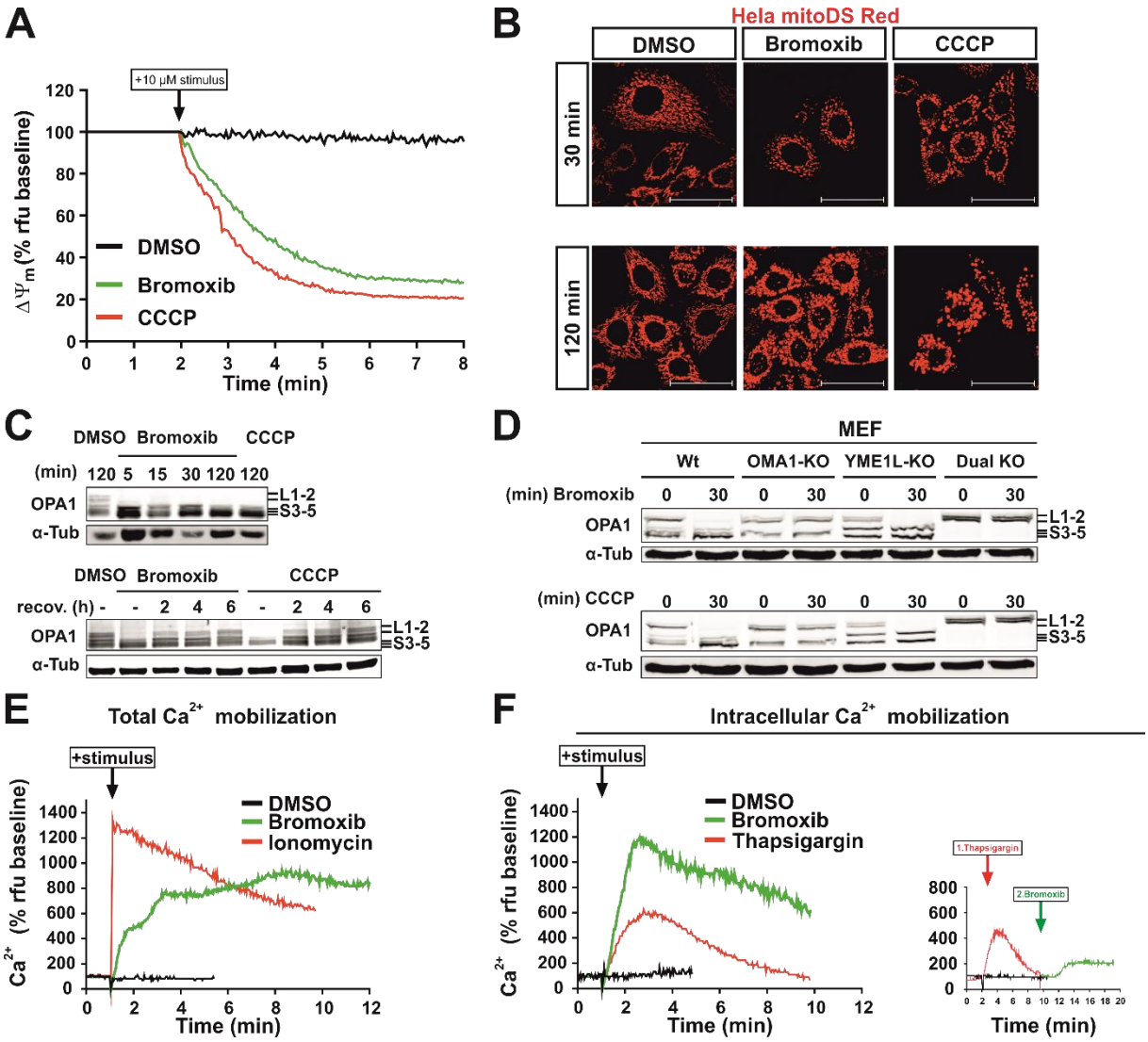

Figure 22 The mitochondrial morphology is altered by Bromoxib – they undergo fission regulated by OPA1 and OMA1. (A) The mitochondrial membrane potential (ΔΨm) breaks down within minutes after treatment with Bromoxib. ΔΨm was monitored in Ramos cells after the addition of DMSO (0.1% v/v), Bromoxib (10 µM), or CCCP (mitochondrial uncoupler; 10 µM) by flow-cytometric measurement of TMRE fluorescence. Shown is one representative graph of three independent biological replicates. **(B)** Mitochondrial fission was observed in HeLa cells stably expressing mito-DsRed targeted to the outer mitochondrial membrane after 30 to 120 minutes of treatment with DMSO (0.1% v/v), Bromoxib (10 µM), or CCCP (10 µM). Representative images of three independent biological replicates are shown. **(C)** Upper panel: The kinetics of Bromoxib-induced OPA1 cleavage were determined by immunoblotting in Ramos cells treated with 10 µM Bromoxib or CCCP. Lower panel: Ramos cells were treated with 10 µM Bromoxib or CCCP for 30 minutes, followed by substance removal and a recovery time of up to 6 h, to monitor the recovery of long forms of OPA1. **(D)** The effect of Bromoxib (10 µM; upper panel) and CCCP (10 µM; lower panel) on OPA1 processing in cells deficient for the OPA1 proteases OMA1 and/or YME1L1 was determined. **(E)** Live measurement of the effect of Bromoxib (10 µM) on total Ca^{2+} mobilization in Ramos cells, where DMSO (0.1% v/v) was used as solvent control and Ionomycin (2 µM) was used as positive control. Shown is one representative graph of three independent biological replicates. **(F)** Left graph: Live measurement of the effect of Bromoxib (10 µM) on intracellular Ca^{2+} mobilization in Ramos cells, where DMSO (0.1% v/v) was used as vehicle control and Thapsigargin (10 µM) was used as positive control. Right graph: Live measurement of the effect of Thapsigargin (10 µM) followed by Bromoxib (10 µM) on intracellular Ca^{2+} mobilization in Ramos cells. Shown is one representative graph of three independent biological replicates.

Interestingly, mitochondrial synthetic uncouplers like CCCP are known to lead to a rapid increase in intracellular/cytosolic Ca^{2+} concentration due to mitochondrial uncoupling [490].

Moreover, ER stress is linked to ROS as a possible trigger for MOMP induction and subsequent apoptosis. The effects resulting from an intracellular Ca^{2+} overload are membrane hyperpolarization, leading to ROS generation and the inhibition of mitochondrial respiration followed by release of cytochrome c [169, 170]. Since severe mitochondrial damage as shown before and oxidative stress are often mutually dependent, the effect of Bromoxib on the mitochondrial metabolism was investigated (**Figure 23**). First, it was studied whether Bromoxib treatment results in the generation of cellular ROS. Measurements with the fluorescent dye H_2-DCF-DA in Ramos cells showed that Bromoxib did not induce any measurable levels of ROS after 5 or 30 min of incubation at low concentrations of 1 µM (**Figure 23 A**). In contrary, a loss of H_2-DCF-DA fluorescence was observed after 5 and 30 min for 10 µM Bromoxib (**Figure 23 A**). This loss of fluorescence can be seen in more detail in the graph in **Figure 23 B.**

To investigate whether later ROS-mediated events are responsible for the cytotoxicity of Bromoxib, Ramos cells were pre- and co-treated with NAC (N-acetyl cysteine; a ROS scavenging compound with antioxidant activity) and increasing Bromoxib concentrations (**Figure 23 C**). Subsequently, the cell viability was determined and showed that the treatment with NAC did not reduce the cytotoxicity of Bromoxib. Thus, oxidative stress is not responsible for Bromoxib-mediated cytotoxicity (**Figure 23 C**). Furthermore, it was tested whether Bromoxib might directly inhibit one of the five electron transport chain (ETC) complexes (**Figure 23 D**). Therefore, the activity of each complex was determined in purified mitochondria upon Bromoxib treatment. Bromoxib showed significant inhibitory activity selectively for ETC complexes II, III, and the ATP-Synthase (complex V) (**Figure 23 D**). However, Bromoxib had no effect on the protein level of any ETC complex in the given time (**Figure 23 E**).

Since the major function of mitochondria is to generate ATP, it was questioned to what extent Bromoxib affects the cellular ATP level if it already inhibits complex II, III and also the ATP-Synthase, as shown in **Figure 23 D**. To distinguish between effects on glycolysis and OXPHOS, the cells were provided with either glucose or galactose as the only sugar supply within the medium. The glycolytic degradation of galactose does not lead to a net ATP gain. Thus, the cell is forced to rely only on OXPHOS for ATP generation which makes it particularly sensitive to inhibitors of the ETC [494]. Bromoxib was able to cause a drastic reduction of ATP levels under both conditions (with glucose or with galactose), which is a unique feature compared to all other tested ETC inhibitors as demonstrated in **Figure 23 F**. To fully prove Bromoxib as mitochondrial respiration inhibitor, the mito stress test from Agilent was performed with HeLa cells (**Figure 23 G**) in collaboration with A. Wolsing from RG Reichert (Institute for Biochemistry and Molecular Biology I, Heinrich-Heine University Düsseldorf). Cells were treated with Bromoxib for 100 minutes and the mitochondrial respiration, represented by the oxygen consumption rate (OCR), was measured. According to the seahorse mito stress test usermanual from Agilent, the compound of interest, Bromoxib or the solvent control (DMSO)

were injected after basal respiration measurement. To inhibit ATP-synthase (complex V) and decrease the electron flow through the ETC, Oligomycin is injected, resulting in reduction of mitochondrial respiration or OCR. Decrease in OCR is linked to cellular ATP production. Subsequently, an uncoupling agent – here FCCP (Carbonyl cyanide-4 (trifluoromethoxy) phenylhydrazone; a CCCP analog) – is injected and the proton gradient collapses and disrupts the mitochondrial membrane potential. As a result, electron flow through the ETC is unlimited, and oxygen consumption by complex IV reaches the maximum, leading to a plateau effect in the DMSO line between 60 to 80 min (**Figure 23 G**). The FCCP-stimulated OCR can then be used to calculate spare respiratory capacity (SRC), defined as the difference between maximal respiration and basal respiration (calculations depicted in **Figure 23 H**). SRC is a measure of the ability of the cell to respond to increased energy demand or under stress. The next injection is a mixture of Rotenone (complex I inhibitor) and Antimycin A (complex III inhibitor). This combination shuts down mitochondrial respiration and enables the calculation of non mitochondrial respiration, driven by processes outside the mitochondria (Agilent usermanual). As soon as Bromoxib was injected with a final concentration of 10 µM, the mitochondrial respiration broke down immediately and OCR was reduced to almost zero (**Figure 23 G**). Basal respiration, ATP production, proton leak, maximal respiration, spare respiratory capacity, and non mitochondrial respiration were calculated from the OCR (**Figure 23 H**). These calculations show an acute response to Bromoxib treatment. An effect on the OCR is clearly detectable and the respiration after treatment is drastically reduced: There is almost no maximal respiration detectable (**Figure 23 H**). In accordance to measured cellular ATP levels in **Figure 23 E**, the ATP synthesis is reduced to low levels. Additionally, Bromoxib treatment induces a proton leak. This result supports the hypothesis of Bromoxib as protonophore targeting mitochondrial morphology and respiratory metabolism, in analogy to CCCP (results supporting this hypothesis are shown later in **Figure 25**).

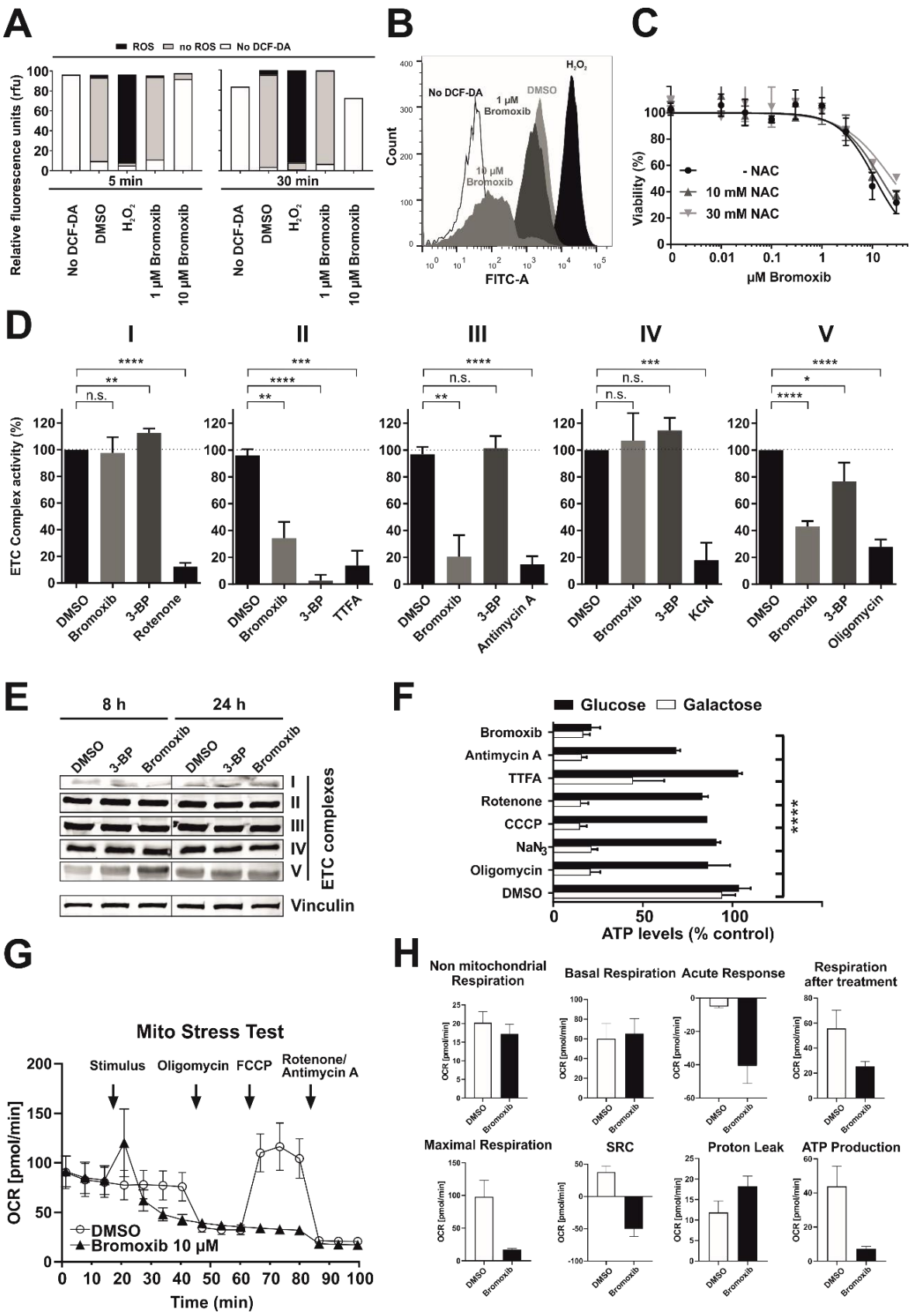

Figure 23 The mitochondrial metabolism is targeted by Bromoxib – oxidative phosphorylation as well as glycolysis are inhibited. The detection of oxidative stress was determined by the DCF-DA assay via flow-cytometric measurement. Ramos cells were treated for 5 and 30 minutes with DMSO (0.1% v/v) as solvent control, 10 mM H_2O_2 as positive control, and 1 or 10 µM Bromoxib. 1 µM Bromoxib induced little ROS after 5 or 30 min, whereas treatment with 10 µM Bromoxib for 5 min induced a loss

of DCF-DA signal. Shown is one representative graph of three independent biological replicates. **(B)** Representative graph for the DCF-DA signal in FITC-A for the different DCF-DA signals after 30 min treatment. **(C)** Ramos cells were treated with increasing concentrations of Bromoxib or pre-and co-treatment with the antioxidant N-acetylcysteine (NAC). Cell viability was assessed by AlamarBlue® viability assay. Shown in each graph is the mean ± SD of one representative experiment performed in triplicates. Oxidative stress is not causative for cytotoxicity of Bromoxib. **(D)** Bromoxib inhibits electron transport chain (ETC) complexes II, III, and ATP-Synthase (complex V). The activities of the individual complexes of the respiratory chain were measured after treatment with Bromoxib (10 µM) or the respective complex inhibitors (complex I: 10 µM Rotenone; complex II: 10 mM Thenoyltrifluoroacetone (TTFA) or 10 µM 3-Bromopyruvate (3-BP); complex III: 10 µM Antimycin A; complex IV: 1 mM Potassium cyanide (KCN); complex V: 10 µM Oligomycin) for 15 minutes using the corresponding MitoCheck® kit (Cayman Chemical; utilizing mitochondria isolated from bovine heart). Depicted activities were normalized to cells treated with DMSO (0.1% v/v). Statistical analysis: Unpaired t test; two-tailed (**** = $p \leq 0.0001$). **(E)** The protein levels of the ETC complexes (in Ramos cells) remain unaltered upon 8 or 24 h treatment with Bromoxib (10 µM) or 3-BP (10 µM). **(F)** Measurement of the effect of Bromoxib (10 µM) and a selection of known mitotoxins on the ATP levels of Ramos cells. Ramos cells were treated with the indicated agents in full growth medium containing either glucose or galactose as the only available sugar. Galactose alone forces the cells to rely entirely on non-mitochondrial ATP production (glycolysis) for ATP synthesis. The following complex-specific inhibitors of the ETC were used (complex I: 10 µM Rotenone; complex II: 10 µM TTFA; complex III: 10 µM Antimycin A; complex IV: 1 mM Sodium azide (NaN_3); complex V: 10 µM Oligomycin; mitochondrial uncoupler and protonophore: 1 µM CCCP and 10 µM Bromoxib as well as DMSO (0.1% v/v) as vehicle control). ATP-levels were measured using the luminescence-based mitochondrial ToxGlo™ assay (Promega). The depicted values were normalized to cells treated with DMSO in glucose containing growth medium (set to 100%). Error bars = mean ± SD of three independent experiments performed in triplicates; p-values were calculated by two-way ANOVA with the Holm-Sidak post-test; (**** = $p \leq 0.0001$). **(G)** The effect of Bromoxib on the mitochondrial oxygen consumption rate (OCR) [pmol O_2/min] was determined in a Seahorse XFe96 Extracellular Flux Analyzer with the Mito Stress Test Kit. HeLa cells were treated via acute injection with Bromoxib (10 µM) or DMSO (0.1% v/v) as solvent control and the oxygen consumption rate was measured over a time of 100 minutes. Error bars = mean ± SD of three independent experiments. **(H)** Different mitochondrial respiration parameters obtained from the Mito Stress Test in HeLa cells with Bromoxib (10 µM) or DMSO (0,1% v/v) treatment. Error bars = mean ± SD of three independent experiments.

Next, literature research was performed to find small molecules displaying a comparable bioactivity pattern to Bromoxib in terms of targeting the mitochondrial morphology and metabolism with the underlying mechanism of inhibiting mitochondrial respiration and ATP synthesis along with an effect on glycolysis. This literature research guided to investigate 3-Bromopyruvate (3-BP), which is a commonly used inhibitor of complex II of the ETC and an inhibitor of the key enzymes of glycolysis [495]. Structurally 3-BP is a halogenated analog of pyruvate with strong alkylating properties that are responsible for its inhibitory activity towards several key glycolytic enzymes (HK II, GAPDH, G-6-P-DH, 3-PGK) with an ability to induce apoptosis via the inhibition of the binding between HK II to VDACs on the OMM. HK II thereby dissociates and the translocation of pro-apoptotic Bax to the OMM takes place [496] (reviewed in [495]). Furthermore, the efficacy of 3-BP was demonstrated for myeloma (since HK II is specifically overexpressed in this cancer entity [497]), in triple negative breast cancer with a prevalent Warburg phenotype of upregulated glycolysis [498] and also in leukemic cells [499]. It is known that an increased metabolic flux towards the Warburg phenotype promotes cancer survival, proliferation and induces chemotherapy resistance, also in leukemic cells. Especially the HK II is predominantly expressed in cancer cells promoting the Warburg phenotype protecting these entities from drug-induced apoptosis such as in leukemic K562 and THP1

cells [499]. The underlying mechanisms of 3-BP mediated antitumor activity are reviewed extensively in [495]. Therefore, 3-BP was examined, since it inhibits aerobic glycolysis as well as mitochondrial oxidative phosphorylation [495] similar to Bromoxib (**Figure 24**). HK II was first localized on subcellular level via immunofluorescence (**Figure 24 A**), using DMSO (solvent control), three known HK II inhibitors to monitor potential protonophoric effects (3-BP, Clotrimazol (CTZ), Lonidamine (Loni) and CCCP) and Bromoxib. Bromoxib and 3-BP showed an increased signal intensity and distribution of HK II after 5 h of incubation (**Figure 24 A**). This signal intensity, was assumed to result from increased permeability during immunofluorescence, due to the physicochemical properties of both compounds. Immunofluorescence was correlated with the cytotoxic potency of the HK II inhibitors in HeLa cells and shows that only Bromoxib and CCCP are cytotoxic in higher concentrations (**Figure 24 B**). Moreover, the HK II inhibition potency of Bromoxib relative to 3-BP was tested in a Hexokinase II specific *in vitro* kinase assay (**Figure 24 C**), correlating the different concentrations of either Bromoxib or 3-BP to the respective kinase activity. However, Bromoxib did not inhibit the HK II kinase activity. Furthermore, the HK II protein levels were analyzed via immunoblotting after 4 and 8 h, comparing the inhibitors 3-BP, Loni, CTZ, to the protonophore CCCP and the apoptosis inducer Staurosporine (STS) (**Figure 24 D**). In summary, Bromoxib does not inhibit HK II activity and does not decrease protein levels in the time window of apoptosis induction, therefore a 3-BP-like mechanism was excluded.

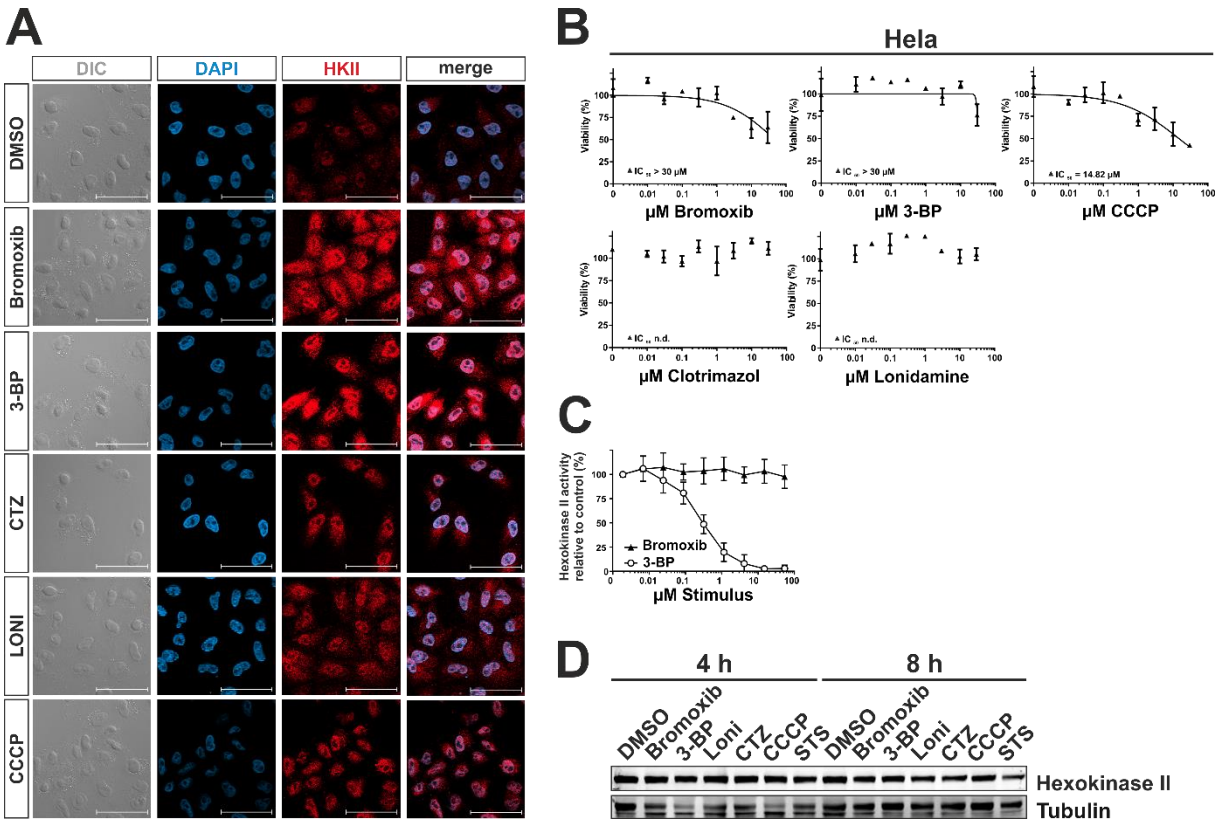

Figure 24 Bromoxib does not inhibit Hexokinase II activity, which is the rate limiting entry-enzyme into the glycolysis pathway. (A) HeLa cells were treated with DMSO (0.1% v/v) as solvent control, 10 µM Bromoxib, 10 µM 3-BP, 10 µM Lonidamine (Loni), 10 µM Clotrimazol (CTZ), 10 µM CCCP or 2.5 µM STS for a duration of 5 h. Immunofluorescence was performed, the differential interference contrast (DIC) shows the total cells, nuclei are shown in blue (DAPI) and the protein localization of Hexokinase II is shown in red. Scale bar equals 20 µm. Representative images of three independent biological replicates are shown. **(B)** Cell viability in HeLa cells was assessed with AlamarBlue® assay with treating the cells with increasing concentrations of Bromoxib, 3-BP, CCCP, Clotrimazol or Lonidamine for 24 h. Shown in each graph is the mean ± SD of one representative experiment performed in triplicates. **(C)** Hexokinase II (HKII) activity was determined after treatment with increasing concentrations of Bromoxib or 3-BP; 3-BP being a selective HKII inhibitor, with the Hexokinase II inhibitor screening kit (abcam211114). Error bars = mean ± SD values of three independent experiments are shown. **(D)** Ramos cells were treated with DMSO (0.1% v/v) as solvent control, 10 µM Bromoxib, 10 µM 3-BP, 10 µM Lonidamine (Loni), 10 µM Clotrimazol (CTZ), 10 µM CCCP or 2.5 µM STS for 4 and 8 h. The protein level of Hexokinase II was determined via immunoblotting, Tubulin served as loading control.

According to the described bioactivity pattern, the molecular mechanism for intrinsic mitochondria dependent apoptosis by Bromoxib remains unanswered and it was still a topic of discussion whether it acts as a protonophore. Generally, a protonophore can be defined as proton translocator or ionophore, which moves protons across membranes. Protonophores are compounds with an aromatic structure and a negative charge which is distributed over atoms by π-orbitals, once a proton attaches to the molecule and the proton's charge gets delocalized. This is the chemical reason for the term protonophore, since positive charged protons with hydrophilic properties are normally unable to cross the membrane without a channel or transporter or in the form of a protonophore by passive diffusion [500-502]. Exemplary protonophores are compounds like CCCP, 2,4-Dinitrophenol or Triphenylphosphonium, that can induce apoptosis in cancer cells. They work by disrupting the normal proton gradient

across the IMM, necessary for ETC and OXPHOS respectively. In terms of CCCP, it interferes with the proton gradient, thereby uncouples OXPHOS, reduces ATP production and causes cell death in a variety of cancer cell types (breast cancer, lung cancer and neuroblastoma [503], glioblastoma cells [504, 505]). Since Bromoxib causes several intracellular effects which primed the assumption that it might act as a protonophore, it was aimed to answer whether the protonophoric activity determines the cytotoxicity, kinetics of caspase-3 activation and the rate of hypodiploid nuclei (apoptosis). As a key characteristic of protonophores the concentration-dependency of the mitochondrial uncoupling was analyzed in collaboration with A. Wolsing from RG Reichert (Institute for Biochemistry and Molecular Biology I, Heinrich-Heine University Düsseldorf) via the mito stress test (**Figure 25 A)**. FCCP mimics a concentration-dependent physiological energy demand by stimulating the respiratory chain to operate at maximum capacity. To counteract this metabolic change, rapid oxidation of substrates (sugars, fats and amino acids) takes place [506]. Comparing the concentration-dependent plateau-like increase of OCR in Bromoxib-treated cells (colored triangles) with the OCR plateau increase of FCCP treated cells, the same cellular response can be observed. Bromoxib may uncouple the mitochondrial respiration by interfering with the proton gradient, similar to FCCP. Thereby the whole respiration is almost shut down to zero (**Figure 25 A**). Bromoxib exhibits the same concentration-dependent protonophoric features in the cells. The parameters of cytotoxicity, caspase-3 activity and apoptosis rate are also comparable (**Figure 25 B, C** and **E**). Interestingly, Bromoxib and CCCP possess similar cytotoxic IC_{50} ranges in Ramos cells: IC_{50} (Bromoxib) = 4.98 µM and IC_{50} (CCCP) = 4.96 µM (**Figure 25 B**). Both compounds were also compared to 3-BP, since it was a point of interest whether a decrease in glycolytic rate via the inhibition of glycolytic enzymes by 3-BP is sufficient in Ramos cells to reduce cell viability and also activate caspase-3 (**Figure 25 B** and **C**). 3-BP requires distinct higher concentrations to reduce cell viability (**Figure 25 B**) and no caspase-3 activation (**Figure 25 C**) was observed. Therefore, a solely 3-BP induced glycolysis inhibition is not sufficient to activate cell death. Conversely, the protonophores Bromoxib and CCCP activate caspase-3 with the same kinetics within 8 h and show a similar activation range (**Figure 25 C**). Comparing the apoptosis level via the detection of apoptotic hypodiploid nuclei, supports this result (**Figure 25 D**). It has to be noted that Bromoxib induced a slightly higher apoptosis rate than CCCP (**Figure 25 D**). However, it could be demonstrated that Bromoxib acts as a mitochondrial uncoupler, exhibiting apoptosis inducing effects in a similar range as the protonophore CCCP in Ramos cells.

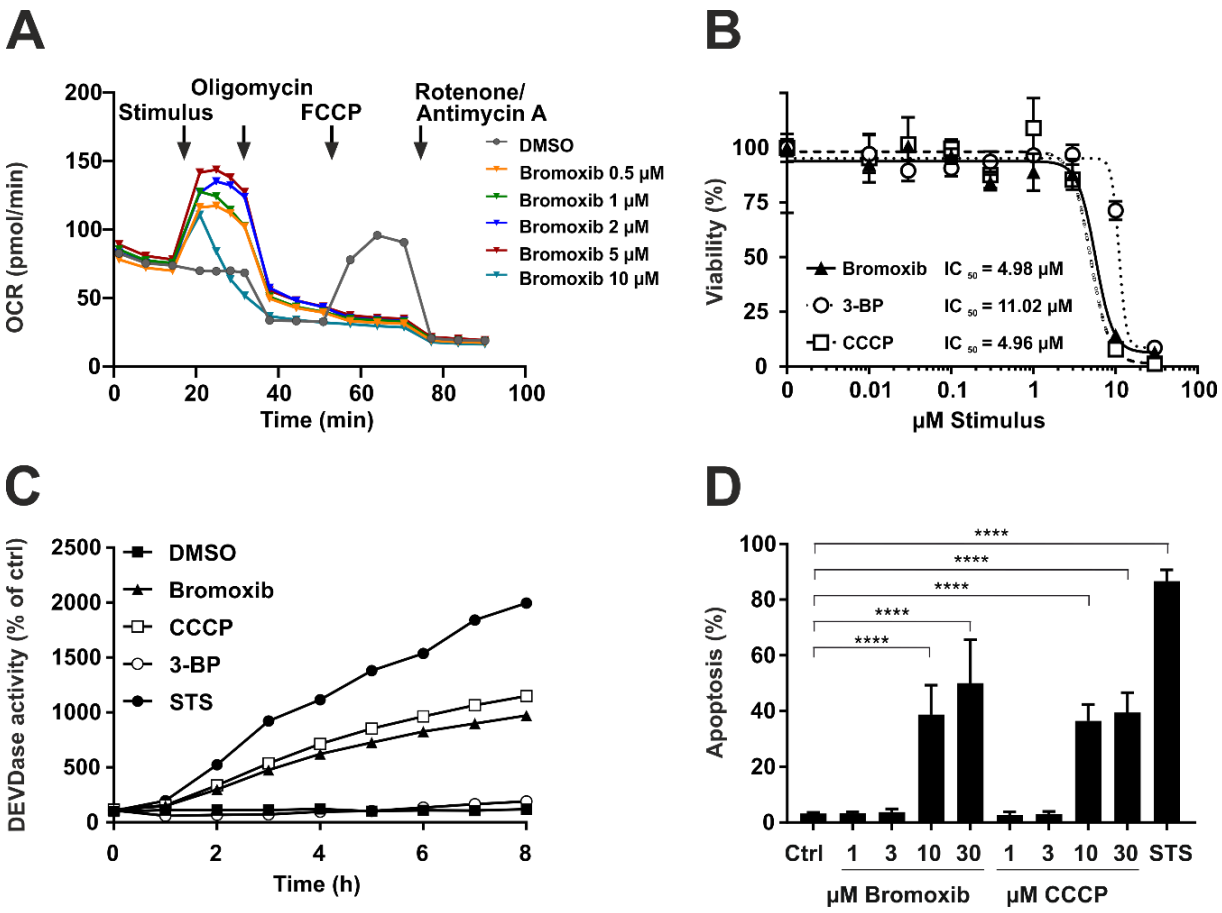

Figure 25 Bromoxib acts as a mitochondrial uncoupler, similar to CCCP. **(A)** Scheme of the Mito Stress Test with injections. HeLa cells were treated via acute injection with different concentrations of Bromoxib (0.5-10 µM) or with DMSO (0.1% v/v) as solvent control. The oxygen consumption rate (OCR) was measured over a time of 90 minutes **(B)** Cytotoxicity of Bromoxib, CCCP and 3-BP was determined after 24 h using the AlamarBlue® viability assay in Ramos cells. Shown in each graph is the mean ± SD of one representative experiment performed in triplicates. Respective IC_{50} values are shown. **(C)** Ramos cells were treated with DMSO (0.1% v/v) as solvent control, Bromoxib (10 µM), CCCP (10 µM), 3-BP (10 µM), or STS (2.5 µM) for up to 8 h. As marker for caspase-3 activation DEVDase activity was determined in a spectrofluorometer. The increase of fluorescence was determined over the course of 2 h for each of the indicated timepoints. The slope of the linear range of fluorescence increase is a parameter for measurement of DEVDase activity. The DMSO control values were set to 100 and the normalized relative fold induction was calculated. Shown in each graph is the mean only of one representative experiment performed in duplicates. **(D)** Ramos cells were treated with increasing concentrations of Bromoxib or CCCP (DMSO 0.1% v/v as solvent control and STS 2.5 µM as positive control) for 24 h. The detection of apoptosis as apoptotic nuclei was determined via flow-cytometry measurement. Error bars = mean ± SD of three independent experiments performed in triplicates. Statistical analysis: 1-way ANOVA with Dunnett's multiple comparisons test; (**** = $p \leq 0.0001$).

The manifold biological effects induced by Bromoxib are now well characterized. Nevertheless, the question for the direct target still remains. Thermal proteome profiling (TPP) identified and validated potential targets of Viriditoxin (**3.1.1**). Therefore, a similar approach was performed for Bromoxib according to the method described by and performed together with T. Lenz as described in (**5.2.23**). Ramos cells were treated with 40 µM Bromoxib or diluent control (DMSO, 0.4% v/v) for 30 minutes and prepared as described (**5.2.23**). Statistical analysis and separation of thermal stabilized proteins are shown in **Figure 26** and **Table 12 A.**

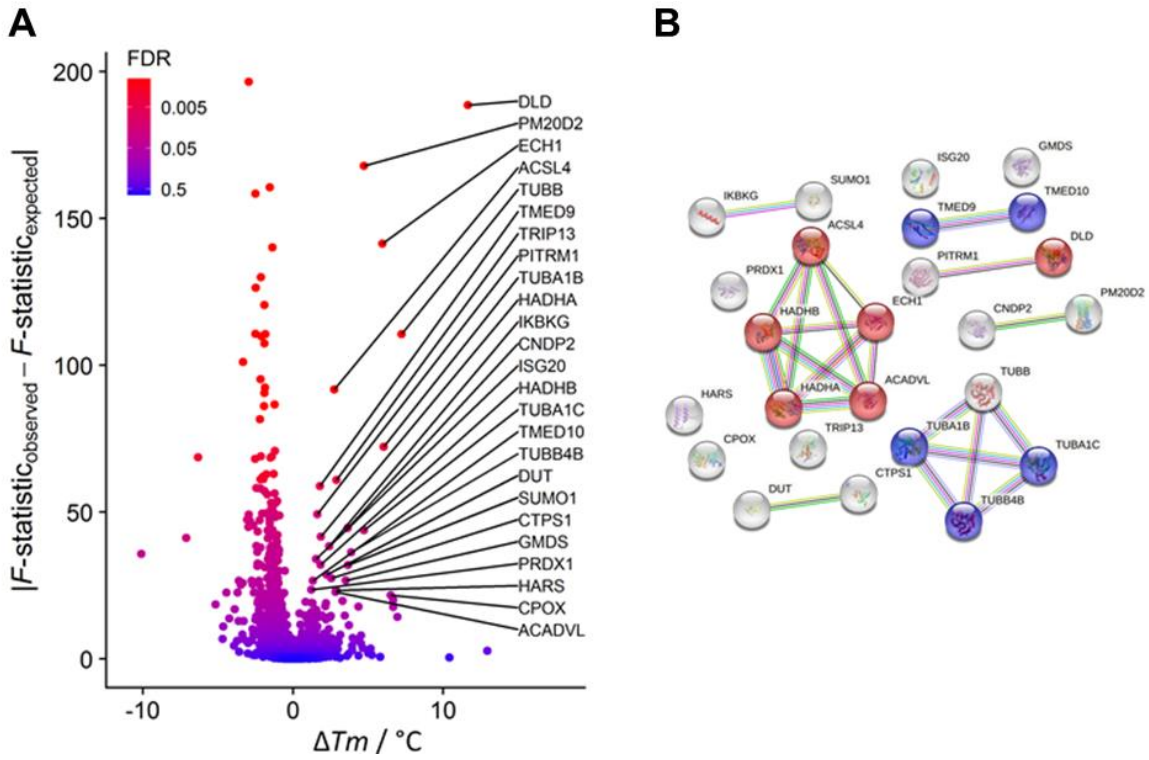

Figure 26 Bromoxib induced stabilization of several proteins, which was shown by thermal proteome profiling (TPP). Bromoxib induced thermal protein (de-)stabilization analyzed by mass spectrometry based thermal proteome profiling (TPP) (stabilized proteins on the right). Ramos cells were treated with 40 µM Bromoxib or diluent control (DMSO, 0.4% v/v) for 30 minutes. **(A)** Volcano-like plot of the statistical significance versus the Bromoxib mediated melting point shift (ΔTm) for each protein. Statistical significance was determined by comparing the observed ANOVA F-statistics (null vs. alternative model, NPARC method [507]) to the expected *F*-statistics without a compound effect, calculated from sample permutations as in the SAM method [508]. FDR denotes the corrected permutation based false discovery rate and the cutoff of 0.054 for selecting proteins was derived from a plot against the SAM-Δ-value (preferably low FDR at preferably low Δ). **(B)** A functional protein association network (based on a STRING database enrichment analysis, https://string-db.org, v11.5) of the selected 25 stabilized proteins. Proteins related to "Fatty acid metabolic process" (GO:0006631) are shown in red and to "COPI-mediated anterograde transport" (HSA-6807878) in blue.

These 25 proteins were analyzed for their intracellular localization, protein function and the biological processes they are involved in with the data bases of Uniprot [509] and Human Protein Atlas [510] (**Table 12**).

Protein analysis focused on COPI-mediated anterograde transport, which is named further as the tubulin-protein-cluster and proteins related to the fatty acid metabolic process (**Figure 26**). The tubulin-protein-cluster is composed of TUBB, TUBA1B, TUBB4B and TUBA1C. Tubulins are heterodimers of α- and β- chains and associate head-to-tail to form protofilaments, running lengthwise along the microtubule wall. Two α-tubulins were stabilized upon Bromoxib treatment: TUBA1B and TUBA1C, besides the two β-tubulins TUBB and TUBB4B. Interestingly, tubulin-binding drugs were investigated since the 1960s: Colchicine, isolated from the plant *Colchicum autumnale*, interferes directly with the tubulin system. However, it did not find any use in cancer treatment due to its high toxicity. The first clinically approved drugs were Vinca alkaloids: Vinblastine, isolated from the plant *Catharanthus roseus*, inhibits tubulin

polymerization [511]. Microtubule dynamics are required for proper mitotic functions. Inhibition or suppression leads to a block in cell cycle progression, resulting in apoptosis [512]. For example, Taxanes interfere with tubulins, stabilizing tubulin polymerization and inhibiting degradation. This class of diterpenes were originally isolated from plants of the genus *Taxus* and are widely used in chemotherapy since the 1990s for metastatic breast cancer. A prominent derivative in clinical treatment is Paclitaxel [513]. Another example is the anti-mitotic agent Nocodazole, which binds to β-Tubulin and disrupts microtubule assembly/disassembly dynamics. Disruption of these dynamics leads to cell cycle arrest and apoptosis [511, 514].

The TPP shows stabilization of the tubulin-protein-cluster upon Bromoxib treatment. The effect on the cell cycle was investigated after 30 min. Treatment with Paclitaxel and Vinblastine for 24 h were used as positive controls for the induction of cell cycle blockade. DMSO was used as solvent control (**Figure 27**).

Table 12 List of proteins stabilized by Bromoxib as identified by TPP which was performed as described in Methods. Proteins with statistical significance determined by comparing the observed ANOVA F-statistics (null vs. alternative model, NPARC method [507]) to the expected F-statistics without a compound effect, calculated from sample permutations as in the SAM method [508]. FDR denotes the corrected permutation based false discovery rate and the cutoff of 0.054 for selecting proteins was derived from a plot against the SAM-Δ-value (preferably low FDR at preferably low Δ). $F\text{-statistic}_{observed} - F\text{-statistic}_{expected} > 0.054$ and ΔTm / °C were regarded as significantly stabilized. Shown in the table below are the proteins stabilized with their gene and protein name, intracellular localization, protein function and highlighted biological process and the analytical data composed of $F\text{-statistic}_{observed} - F\text{-statistic}_{expected} > 0.054$ and ΔTm / °C.

Gene name	Protein name(s)	Localization	Protein function and biological process (human protein atlas) [510]	Δ*Tm*	*F*-statistic observed	*F*-statistic expected
DLD	Dihydrolipoamide dehydrogenase	Mitochondria, Nucleoplasm	Lipoamide dehydrogenase is a component of the glycine cleavage system as well as an E3 component of three alpha-ketoacid dehydrogenase complexes.	11.6	239.4	50.8
PM20D2	Peptidase M20 domain containing 2	Nucleoplasm	Catalyzes the peptide bond hydrolysis in dipeptides having basic amino acids lysine, ornithine or arginine at C-terminus. Postulated to function in a metabolite repair mechanism by eliminating alternate dipeptide by-products formed during carnosine synthesis.	4.7	214.3	46.4
ECH1	Enoyl-CoA hydratase 1	Mitochondria	Isomerization of 3-trans,5-cis-dienoyl-CoA to 2-trans,4-trans-dienoyl-CoA. **Fatty acid metabolism, Lipid metabolism**	5.9	179.3	37.9
ACSL4	Acyl-CoA synthetase long chain family member 4	Mitochondria, Golgi apparatus	Catalyzes the conversion of long-chain fatty acids to their active form acyl-CoA for both synthesis of cellular lipids, and degradation via beta-oxidation. **Fatty acid metabolism, Lipid metabolism**	2.7	118.6	26.9
TUBB	Tubulin beta class I	Microtubules, Cytokinetic bridge, Mitotic spindle	Tubulin is the major constituent of microtubules. It binds two moles of GTP, one at an exchangeable site on the beta chain and one at a non-exchangeable site on the alpha chain.	7.2	141.6	31.1
TMED9	Transmembrane p24 trafficking protein 9	ER, Golgi apparatus	Involved in vesicular protein trafficking, mainly in the early secretory pathway.	1.8	78.8	20.0
TRIP13	Thyroid hormone receptor interactor 13	Nucleoplasm	Promotes early steps of the DNA double-strand breaks (DSBs) repair process upstream of the assembly of RAD51 complexes. Required for depletion of HORMAD1 and HORMAD2 from synapsed chromosomes (By similarity). Plays a role in mitotic spindle assembly checkpoint (SAC) activation.	2.9	81.2	20.2
PITRM1	Pitrilysin metallopeptidase 1	Mitochondria	Metalloendopeptidase of the mitochondrial matrix that functions in peptide cleavage and degradation, it degrades the transit peptides of mitochondrial proteins after their cleavage.	1.6	66.7	17.4
TUBA1B	Tubulin alpha 1 b	Microtubules	See TUBB.	6.0	96.4	24.1
HADHA	Hydroxyacyl-CoA dehydrogenase trifunctional multienzyme complex subunit alpha	Mitochondria	Mitochondrial trifunctional enzyme catalyzes the last three of the four reactions of the mitochondrial beta-oxidation pathway. HADH is a heterotetrameric complex composed of two proteins, the trifunctional	1.9	56.6	15.0

Gene name	Protein name(s)	Localization	Protein function and biological process (human protein atlas) [510]	Δ*Tm*	*F*-statistic observed	*F*-statistic expected
			enzyme subunit alpha/HADHA carries the 2,3-enoyl-CoA hydratase and the 3-hydroxyacyl-CoA dehydrogenase activities. **Fatty acid metabolism, Lipid metabolism**			
IKBKG	Inhibitor of nuclear factor kappa B kinase regulatory subunit gamma	Cytosol, intracellular	Regulatory subunit of the IKK core complex which phosphorylates inhibitors of NF-kappa-B thus leading to the dissociation of the inhibitor/NF-kappa-B complex and ultimately the degradation of the inhibitor.	2.4	52.7	14.4
CNDP2	Carnosine dipeptidase 2	Cytosol, Nucleoplasm	Catalyzes the peptide bond hydrolysis in dipeptides.	3.6	60.4	15.8
ISG20	Interferon stimulated exonuclease gene 20	intracellular	Interferon-induced antiviral exoribonuclease that acts on single-stranded RNA and also has minor activity towards single-stranded DNA. May also play additional roles in the maturation of snRNAs and rRNAs, and in ribosome biogenesis.	1.5	47.3	13.3
HADHB	Hydroxyacyl-CoA dehydrogenase trifunctional multienzyme complex subunit beta	Mitochondria	See HADHA. HADH is a heterotetrameric complex composed of two proteins, the trifunctional enzyme subunit beta/HADHB bears the 3-ketoacyl-CoA thiolase activity. **Fatty acid metabolism, Lipid metabolism**	1.8	44.9	12.8
TUBA1C	Tubulin alpha 1 c	Microtubules	See TUBB and TUBA1B	4.7	59.4	15.6
TMED10	Transmembrane p24 trafficking protein 10	Golgi apparatus	Cargo receptor involved in protein vesicular trafficking and quality control in the endoplasmic reticulum (ER) and Golgi.	1.3	38.1	11.5
TUBB4B	Tubulin beta 4B class Ivb	Microtubules, Cytokinetic bridge, Mitotic spindle	See TUBB, TUBA1B, TUBA1C	3.9	50.1	13.7
DUT	Deoxyuridine Triphosphatase	Nucleoplasm	Catalyzes the cleavage of 2'-deoxyuridine 5'-triphosphate (dUTP) into 2'-deoxyuridine 5'-monophosphate (dUMP) and inorganic pyrophosphate and through its action efficiently prevents uracil misincorporation into DNA and at the same time provides dUMP, the substrate for *de novo* thymidylate biosynthesis.	2.2	40.7	12.0
SUMO1	Small ubiquitin like modifier 1	Nucleoplasm, Nuclear membrane, Nucleoli, Nuclear bodies	Ubiquitin-like protein that can be covalently attached to proteins as a monomer or a lysine-linked polymer. This post-translational modification on lysine residues of proteins plays a crucial role in a number of cellular processes such as nuclear transport, DNA replication and repair, mitosis and signal transduction. Involved for instance in targeting RANGAP1 to the nuclear pore complex protein RANBP2.	3.7	44.7	12.7
CTPS1	CTP Synthase 1	Cytosol, in actin filaments	This enzyme is involved in the *de novo* synthesis of CTP, a precursor of DNA, RNA and phospholipids.	2.6	39.1	11.7

Gene name	Protein name(s)	Localization	Protein function and biological process (human protein atlas) [510]	Δ*Tm*	*F*-statistic observed	*F*-statistic expected
GMDS	GDP-mannose 4,6 dehydratase	Intracellular	Catalyzes the conversion of GDP-D-mannose to GDP-4-dehydro-6-deoxy-D-mannose.	3.5	38.3	11.6
PRDX1	Peroxiredoxin 1	Mitochondria	Thiol-specific peroxidase that catalyzes the reduction of hydrogen peroxide and organic hydroperoxides to water and alcohols, respectively. Plays a role in cell protection against oxidative stress by detoxifying peroxides and as sensor of hydrogen peroxide-mediated signaling events.	1.2	34.2	10.6
HARS	Histidyl-tRNA synthetase 2, mitochondrial	Mitochondria	Mitochondrial aminoacyl-tRNA synthetase that catalyzes the ATP-dependent ligation of histidine to the 3'-end of its cognate tRNA, via the formation of an aminoacyl-adenylate intermediate (His-AMP).	2.9	33.9	10.5
CPOX	Coproporphyrinogen oxidase	Mitochondria	Catalyzes the aerobic oxidative decarboxylation of propionate groups of rings A and B of coproporphyrinogen-III to yield the vinyl groups in protoporphyrinogen-IX and participates to the sixth step in the heme biosynthetic pathway.	6.5	31.6	9.9
ACADVL	Acyl-CoA dehydrogenase very long chain	Nucleoplasm, Nucleoli, Mitochondria	Very long-chain specific acyl-CoA dehydrogenase is one of the acyl-CoA dehydrogenases that catalyze the first step of mitochondrial fatty acid beta-oxidation, an aerobic process breaking down fatty acids into acetyl-CoA and allowing the production of energy from fats. The first step of fatty acid beta-oxidation consists in the removal of one hydrogen from C-2 and C-3 of the straight-chain fatty acyl-CoA thioester, resulting in the formation of trans-2-enoyl-CoA. **Fatty acid metabolism, Lipid metabolism**	2.8	33.2	10.4

Paclitaxel or Vinblastine are tubulin-binding drugs and kill cancerous cells by inhibiting the microtubule dynamics, which are required for DNA segregation and cell division. An alternative mechanism is observed with Nocodazole. Nocodazole disrupts the cell cycle and causes mitotic arrest by direct interaction with microtubules. Cell cycle analysis by flow-cytometry showed no cell cycle disruption by Bromoxib (**Figure 27 A**). Additionally, the tubulin polymerization rate was measured with a tubulin polymerization assay, using DMSO as solvent control, Nocodazole as tubulin polymerization rate decreasing/inhibiting (negative) control and Paclitaxel as tubulin polymerization rate enhancing (positive) control (**Figure 27 B**). Even at higher Bromoxib concentrations (40 µM), there was no effect on the tubulin polymerization rate observable (**Figure 27 B**). Thus, Bromoxib does not seem to induce apoptosis by a tubulin-dependent mechanism.

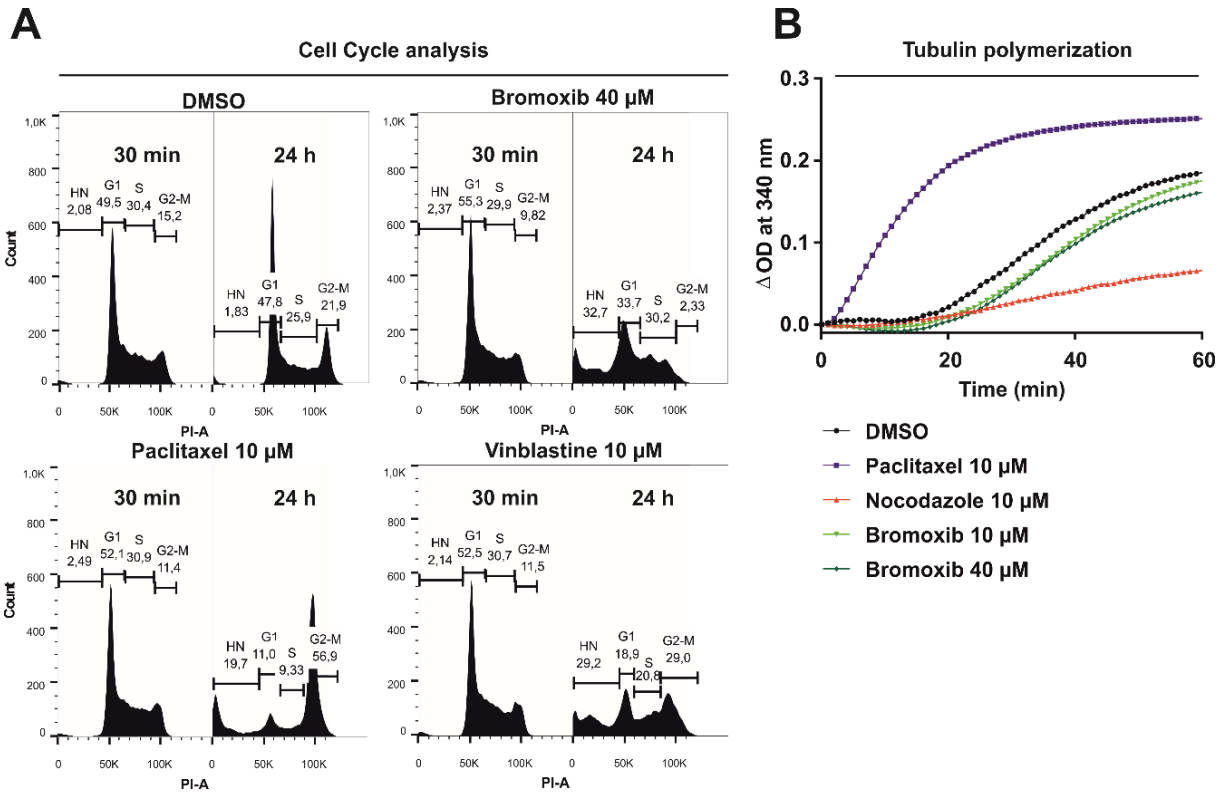

Figure 27 Bromoxib exerts no effect on cell cycle distribution or tubulin polymerization at cytotoxic concentrations. (A) Ramos cells were treated for 30 minutes or 24 h with DMSO (0.1% v/v) as solvent control, Bromoxib (40 µM) and Paclitaxel (10 µM) or Vinblastine (10 µM) as positive controls for cell cycle disruption. Cell cycle analysis was performed by propidium iodide staining and flow-cytometric measurement in a linear mode. The different cell cycle phases are shown as representative images of three independent experiments. Bromoxib did not alter the cell cycle distribution. **(B)** Bromoxib has no effect on the tubulin polymerization rate. The tubulin polymerization rate of porcine neuronal tubulin was determined upon treatment with either DMSO (0.1% v/v), Paclitaxel (10 µM), Nocodazole (10 µM), or Bromoxib (10 or 40 µM). Polymerization was started by incubation at 37 °C and followed by monitoring of the absorption at 340 nm for 60 minutes. The absorption is proportional to the concentration of the microtubule polymer. The graph shows the mean values of three independent experiments.

The TPP showed also protein-clusters from the fatty acid and lipid metabolism, including ACSL4, HADHA, HADHB, ECH1 and ACADVL (**Figure 26**). Since Bromoxib targets mainly the mitochondria, it was not surprising that proteins of mitochondrial localization were stabilized top-candidates of the TPP-list.

As introduced above (**1.6.4 Mitochondrial fatty acid β-oxidation**), the FA β-oxidation is a major metabolic pathway and is responsible for the mitochondrial breakdown of long-chain acyl-CoA to acetyl-CoA. Long chain FAs are activated by thio esterification (CoA binding) by Acyl-CoA synthetase (ACSL4), transported from the cytosol by carnitine-acylcarnitine translocase (CACT) across the mitochondrial membrane and released in the inner mitochondrial area as acyl-CoA [335]. To unravel the mechanism of Bromoxib, it is noteworthy to consider that all five proteins are responsible for the conduction of the total FAO. These are stabilized after only 30 minutes of treatment with Bromoxib. Their functions in FAO are summarized in the following: Acyl-CoA dehydrogenase (ACADVL) mediates the oxidation, Enoyl-CoA hydratase (ECH1) catalyzes the hydration, 3-Hydroxy acyl CoA dehydrogenase mediates another oxidation step (HADHA), and 3-Ketoacyl CoA thiolase (HADHB) is responsible for the thiolysis, subsequently releasing acetyl-CoA into the Krebs cycle [335].

Thus, the subsequent hypothesis is, that the damaged cell tries to make energy available in form of ATP from fatty acid degradation. The question arises how this is achieved? By stabilizing the protein cluster catalyzing exactly this pathway and why? This will be discussed later in the discussion (**7.2.3 Bromoxib targets the mitochondrial β-oxidation (FAO)**). To validate this hypothesis, Ramos cells were treated with two concentrations of Bromoxib for 30 min and 24 h. The protein levels of ACSL4, HADHB, ECH1, HADHA and ACADVL were analyzed via immunoblotting (**Figure 28**). The quantification of the protein levels showed increased protein levels of ACSL4 and HADHB after 30 min, a significant decrease for ACADVL and a continuous level of ECH1 (**Figure 28 A**). The protein level analysis after 24 h revealed different results: ACSL4 and HADHB protein levels were significantly decreased. ACADVL levels remained unaffected and ECH1 level increased significantly (**Figure 28 B**). Short treatment activates a rapid mechanism, distinguishing from a late response after 24 h. This observation will be discussed below (**7.2.3 Bromoxib targets the mitochondrial β-oxidation (FAO)**).

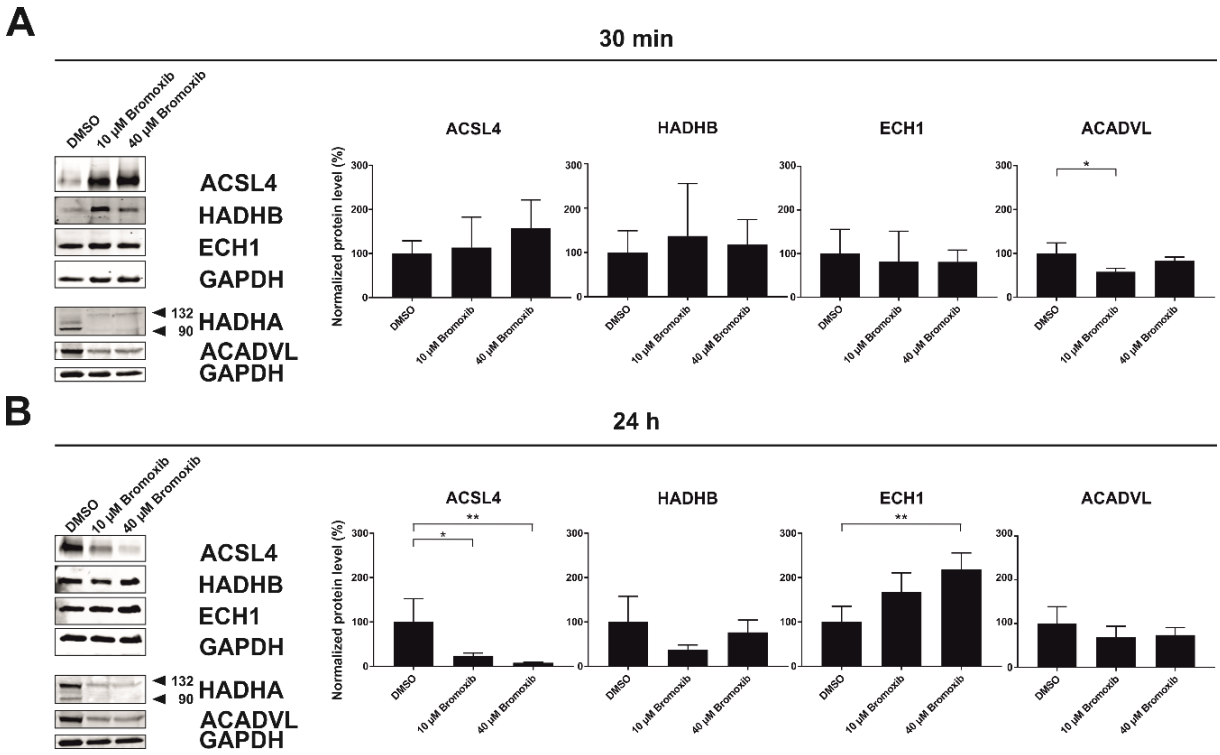

Figure 28 Bromoxib selectively targets proteins of the mitochondrial fatty acid β-oxidation pathway. Ramos cells were treated for **(A)** 30 min and **(B)** 24 h with DMSO (0.1% v/v; negative control), 10 µM and 40 µM Bromoxib. The protein levels of the five stabilized proteins of the mitochondrial fatty acid β-oxidation protein cluster: Acyl-CoA synthetase long chain family member 4 (ACSL4), Hydroxyacyl-CoA dehydrogenase complex subunits A and B (HADHA and HADHB), Enoyl-CoA hydratase (ECH1) and Acyl-CoA dehydrogenase very long chain (ACADVL) were determined via immunoblotting and GAPDH served as a loading control. **(A)** and **(B)** On the left side the representative immunoblots of four independent biological replicates are shown, on the right side the respective quantification of the immunoblots as described in Materials and Methods. Error bars = mean ± SD of three independent experiments. Statistical analysis: 1-way ANOVA with Dunnett's multiple comparison test; (**** = $p \leq 0.0001$).

Further validations of the FA-protein-cluster as targets of Bromoxib included the need for a measurement of the metabolites within the FA β-oxidation according to the method described in **5.2.24 Lipidomics and measurement of fatty acid oxidation**. Therefore, I searched for and established a collaboration with the group of Patricia Aspichueta (Lipids and Liver group from the Department of Physiology, Faculty of Medicine and Nursing at Universidad del País Vasco, Spain), who are experts on the field of lipidomics. The collaboration included the measurements of lipidomics by Dr. Xabier Buqué, with samples generated by the author of this thesis. Moreover, RG Aspichueta performed measurements of total palmitate oxidation and partial palmitate oxidation in Ramos cells via the detection of [^{14}C]-CO_2 (total palmitate oxidation) and [^{14}C]-Acid soluble metabolites (partial palmitate oxidation). Methods are described in chapter **5.2.24 Lipidomics and measurement of fatty acid oxidation**.

Ramos cells were treated with Bromoxib and DMSO (0.1% v/v as solvent control) and were send to the collaborators (six biological replicates in total). Lipidomic analyses (analysis of the

totality of lipids in a cell) were performed (**Figure 29 A** and **B**) and the whole FA β-oxidation was measured *in vitro* by special radioactivity assays (**Figure 29 C**).

FAs are the building blocks of lipid species, as introduced in chapter **1.6.4 Mitochondrial fatty acid β-oxidation.** They are composed of a carboxylic acid group with a hydrocarbon chain of varying carbon length and degrees of saturation [515]. By directing FAs into different metabolic pathways, it is possible to produce more intricate lipid species like diacylglycerides (DGs) and triacylglycerides (TGs). Alternatively, they are transformed into phosphoglycerides, e.g. phosphatic acid (PA), phosphatidylethanolamine (PE), phosphatidylinositol (PI), phosphatidylcholine (PC), lisophosphatidylcholine (LPC) or phosphatidylserine (PS) [152]. In addition, FAs can be employed to create triacylglycerols (TGs) and cholesterylesters (CEs) as energy storage in the form of lipid droplets. When necessary, these droplets are used as fuel for cellular bioenergetics by FAO [516, 517]. CEs are ester derivatives of cholesterol, containing an ester bond between the 5-hydroxy group of cholesterol and the FA carboxylate group. Free FAs undergo esterification in the glycerol phosphate pathway, receiving amphiphilic properties as phospholipids and sphingolipids. Cholesterol, phospho- and sphingolipids are the fundamental building blocks of biological membranes [516, 518].

A large part of lipids is synthesized from FAs. Recent research supports that many human cancers display aberrant activation of *de novo* FA synthesis. Modification and degradation of lipids enables the cells to proliferate, grow and spread effectively [516]. Cell proliferation in cancer cells requires new assembly of lipid membranes. To protect the cancer cells from lipotoxicity, a proper equilibrium between saturated and unsaturated FAs has to be maintained. Changes in membrane fluidity due to cell migration and drug resistance must also be considered [516]. Here it will be focused on the high energy demands of cancer cells mediated through FAO. FAs provide twice as much ATP as carbohydrates. Therefore, the FAO is the most energy-efficient way to generate ATP, among the metabolic pathways [516].

Considering the selective targeting of FAO proteins (ACSL4, ACADVL, ECH1, HADHA, HADHB), several metabolites of FA metabolism were analyzed. These include glycerophospholipids (lysophosphatidylcholine (LPC), phosphatidylcholine (PC), phosphatidylethanolamine (PE), cardiolipin (CLN), phosphatidylserine (PS), phosphatidylinositol (PI) and sterol lipids: Free cholesterol (FC) (**Figure 29 A**), glycerolipids: Diacylglycerides (DG), triacylglycerides (TG), cholesterylester (CE) and free fatty acids (FFAs). Bromoxib treatment significantly increases LPC, PC, PE and free cholesterol levels (**Figure 29 A**). Additionally, it significantly decreases the level of CLN (**Figure 29 A**). In terms of diacylglycerides, only a significant effect on the FFAs is observed.

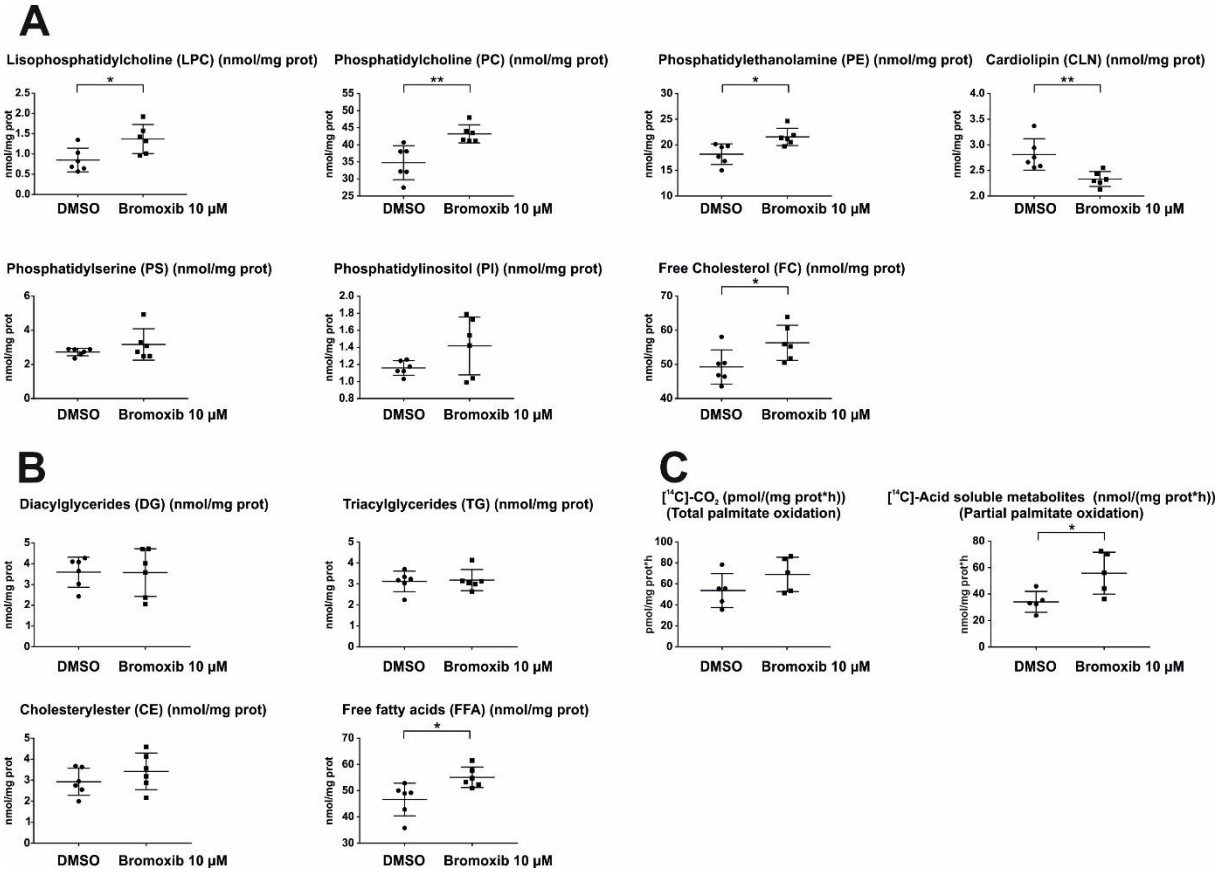

Figure 29 Bromoxib treatment alters the whole lipid composition of Ramos cells and influences palmitate oxidation. Ramos cells were treated for 30 min with 10 µM Bromoxib and DMSO (0.1% v/v; solvent control) and the lysates (six biological replicates) were sent to RG Aspichueta (University of Basque Country UPC/EHU), where Dr. Xabier Buqué performed the lipidomics on: **(A)** Lisophosphatidylcholine (LPC), phosphatidylcholine (PC), phosphatidylethanolamine (PE), cardiolipin (CLN), phosphatidylserine (PS), phosphatidylinositol (PI) and free cholesterol (FC). The lysate was also analyzed for the different fatty acids **(B)** such as diacylglycerides (DGs), triacylglycerides (TGs), cholesterylester (CE) and free fatty acids (FFA). Error bars = mean ± SD of six independent experiments. In **(C)** the total palmitate and partial palmitate oxidation were analyzed by Dr. Xabier Buqué in Ramos cells with DMSO (0.1% v/v) and 10 µM Bromoxib (five biological replicates). [^{14}C]-CO_2 as well as [^{14}C]-Acid soluble metabolites were detected after metabolization as measures for the total palmitate oxidation and partial palmitate oxidation. Error bars = mean ± SD of five independent experiments. Statistical analysis: unpaired two-tailed t-test; (**** = $p \leq 0.0001$).

With regard to the measurement of total and partial palmitate oxidation shown in **Figure 29 C**, a significant accumulation of [^{14}C]-Acid soluble metabolites was detected upon Bromoxib treatment. Therefore, the partial palmitate oxidation is impaired.

In summary, Bromoxib is a selectively cytotoxic natural product to lymphoma and leukemia cells. It induces caspase-3 activity with subsequent PARP1 cleavage and does active the intrinsic mitochondria dependent pathway of apoptosis. Bromoxib-induced apoptosis cannot be executed in the presence of Bcl-2 overexpression. This natural compound targets mainly the mitochondria in terms of metabolism, respiration and induces fragmentation. Furthermore, the compound exhibits protonophoric activity, which is responsible for its manifold biological activity within the cell. Due to its protonophoric activity in combination with its mitotoxic activity, Bromoxib triggers an increased energy demand in the cancer cell. The cell tries to cope this rapid energy demand with the stabilization of a protein cluster catalyzing the mitochondrial β-

oxidation in order to degrade FFAs rapidly in order to generate ATP. Finally, Bromoxib alters thereby the total lipidomics in lymphoma cells and alters FFAs oxidation.

6.4 Meriolin derivatives as unique Swiss Army knife targeting the hallmarks of cancer

Natural products often inspire the development of synthetic or semi-synthetic derivatives. An attractive example are Meriolin derivatives. Meriolins are a class of semisynthetic compounds, derived from combining Meridianins, a family of 3-((2-amino)pyrimidin-4-yl)indoles with Variolins (**Figure 30**) containing a central pyrido[3',2':4,5]pyrrolo[1,2-c]pyridine core substituted with a 2-aminopyrimidine ring. Meridianins were first isolated from *Aplidium meridianum*, an ascidian from the South Atlantic [519-521] and share structural analogies with Variolins, which were isolated from the Antarctic sponge *Kirkpatrickia variolosa* [521-523] as shown in **Figure 30**. The substance class combining these two natural classes was termed Meriolins [519, 524]. A comprehensive review about the synthesis of Variolins, Meridianins and Meriolins can be found in [525]. The structure of the natural products as well as the synthetic derivatives of four selected Meriolins (16, 31, 36 and 17) together with a selective kinase inhibitor named R547 (which is used as control in further experiments) are shown in **Figure 30**. The Meriolins 16, 31, 36 and 17 were synthesized by Dr. D. Drießen (RG Müller, Institute for Organic Chemistry and Macromolecular Chemistry, Düsseldorf) in his dissertation [442]. The Meriolin derivatives 31 (3f) and 36 (3k) were already identified and characterized in a recent publication of our group together with other Meriolin derivatives [443].

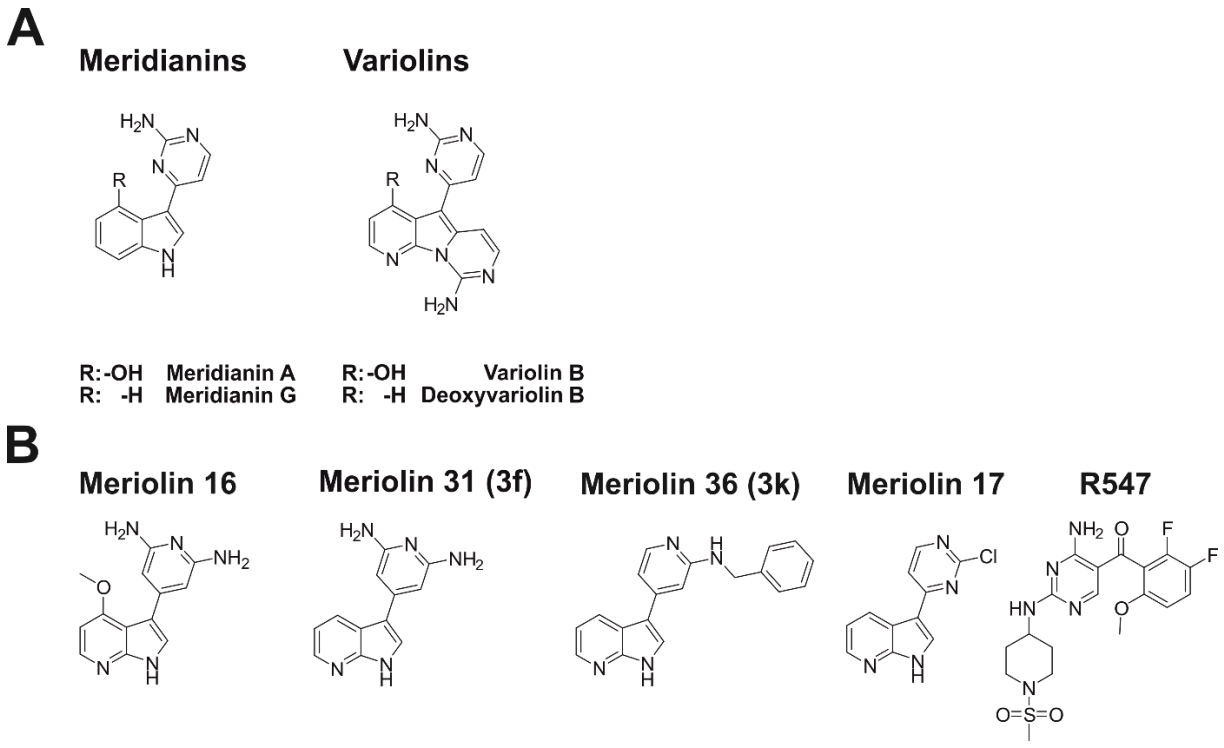

Figure 30 Structures of Meridianins and Variolins – the parental compounds of Meriolins. (A) Meriolin derivatives (lower panel) are inspired from Meridianins and Variolins, a class of marine-derived natural products (upper panel). **(B)** Structure of the Meriolin derivatives 16, 31, 36 and 17. Biological

activity is compared with the selective CDK inhibitor R547 below. (Structures were drawn in ChemDraw according to structures in [442, 443, 519]).

Marine-derived Variolins and Meridianins possess biological activity against CDKs in the micromolar to nanomolar range, representing the first-generation inhibitors of CMGC Kinase-enzymes. The CMGC family is composed of CDKs, MAPKs (mitogen-activated protein kinases), GSKs (glycogen synthase kinases) and CLKs (CDC-like kinases) [411, 443]. To date, the biological activity in terms of cytotoxicity, kinase inhibition and tumor growth inhibition of many Meriolin derivatives was described [410, 411, 443, 519, 524, 526-529]. Chemical derivatization led to higher selectivity, better anti-proliferative and pro-apoptotic properties, compared to their parent molecules [412]. Other drugs inspired by natural products include biologically active 7-azaindole clinical candidates such as Vemurafenib [530], Pexidartinib [531] or AZD6738, which is shown to inhibit growth of ATM deficient xenografts via an ATR inhibition mechanism [412, 532]. 3,5-disubstituted-7-azaindoles have shown anti-tumor activity via the inhibition of CDK2 and CDK9 activity [411].

In this thesis, the molecular mechanism of Meriolin derivatives will be characterized in terms of cytotoxicity, apoptosis induction and disruption of the cell cycle with subsequent crosstalk between checkpoint activation, the DNA-damage response and the activation of apoptosis – aiming to potentially address three hallmarks of cancer: '*Resisting cell death, sustained proliferative signaling* and *genome instability and mutation*'.

Recently the cytotoxicity, caspase-3 activity and PARP1 cleavage of some Meriolin derivatives has been characterized by our group [443]. According to these data, Meriolin 31 and 36 exhibited low IC_{50} values, induced rapid caspase-3 activation with subsequent PARP1 cleavage and have been chosen for further analysis. Meriolin 31 is the parental compound of Meriolin 16 and to date the biological activity of Meriolin 16 has not been characterized. The only difference between them is an additional methoxy group ($-OCH_3$) at the aromatic pyridine ring. This group was added to further increase the cytotoxicity of the parental compound. To verify this hypothesis, Meriolin 16 had to be characterized in terms of cytotoxicity, caspase-3 activity and apoptosis induction (**Figure 31**). As noted above, Burkitt B cell lymphoma (Ramos cells) and acute T cell leukemia (Jurkat cells) were used as model system to allow correct comparison with the parental compound and other derivatives (**Figure 31**). Meriolin 16 treatment for 24 and 72 h resulted in Ramos and Jurkat cells in IC_{50} values of 0.04 µM and 0.03 µM respectively (**Figure 31 A**). Its parental compound Meriolin 31 (3f) showed an IC_{50} of 0.11 $\mu M^{24\ h}$, 0.07 $\mu M^{72\ h}$ in Ramos cells and an IC_{50} of 0.11 $\mu M^{24\ h}$, 0.06 $\mu M^{72\ h}$ in Jurkat cells [443]. Thus, the increase of cytotoxicity due to the additional methoxy group was verified, because Meriolin 16 showed a higher cytotoxicity than Meriolin 31 in the same setup. Meriolin 16 showed rapid kinetics of caspase-3 activation for both cell lines and a slightly higher amplitude in Jurkat cells (**Figure 31 B**). In the apoptosis assays, such as caspase-3 activation, detection of hypodiploid

nuclei and PARP1 cleavage via immunoblotting, the broad-spectrum kinase inhibitor Staurosporine (STS), was used as positive control and DMSO (solvent control) was used as negative control. Meriolin 16 treatment (from 0.1 up to 30 µM) for 24 h exhibited an apoptosis rate of ca. 40-50% in both cell lines (**Figure 31 C**). Pre- and co-treatment with QVD at the highest concentration (30 µM Meriolin 16) inhibited apoptosis, proving a caspase-dependent apoptosis mechanism (**Figure 31 C**). PARP1 cleavage was determined via immunoblotting after treatment for 8 h (**Figure 31 D**). Ramos cells showed PARP1 cleavage after 2 h, whereas Jurkat cells indicated cleavage after 4 h. In analogy to Nicoletti assays, PARP1 cleavage was blocked with the pre-and co-treatment of QVD (**Figure 31 D**). The reversibility of the cytotoxicity was investigated for Meriolin 16, 31 and 36 in (**Figure 31 E**). To investigate the reversibility of cytotoxicity, Ramos cells were incubated with either Meriolin 16, 31 or 36 for 5 min, washed and further incubated without Meriolins for 24 h. For comparison, Ramos cells were treated with Meriolin 16, 31 or 36 for 24 h. The Meriolins 16, 31 and 36 induce irreversible cell death within 5 min incubation (**Figure 31 E**). This result was further supported by the analysis of PARP1 cleavage in Ramos cells via immunoblotting (**Figure 31 F**). Concluding, Meriolin 16, 31 and 36 induce irreversible apoptosis in Ramos cells within 5 min.

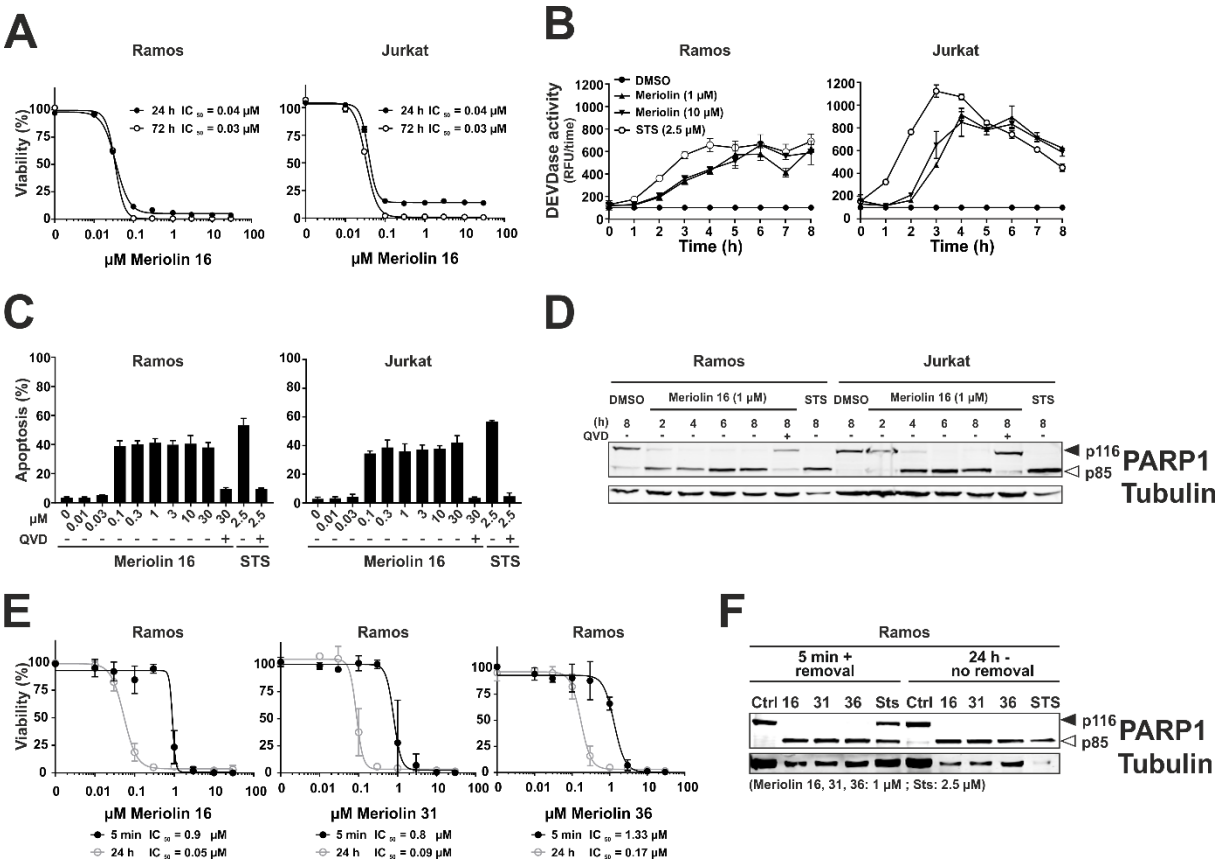

Figure 31 Meriolin 16 is a new derivative and was characterized in terms of cytotoxicity (A), the kinetics of caspase-3 activation (B), apoptosis induction rate (C), and cleavage of PARP1 as substrate of caspases (D). The Meriolins were compared in terms of irreversibility of (E) cytotoxicity and (F) PARP1 cleavage. (A) The cytotoxicity of Meriolin 16 was first determined in Ramos and Jurkat cells with increasing concentrations of Meriolin 16 after 24 and 72 h of treatment, the respective IC_{50} values are given in the parenthesis. Shown in each graph is the mean ± SD of one

representative experiment performed in triplicates. **(B)** Activation of caspase-3 was measured by adding the pro-fluorescent caspase-3 substrate Ac-DEVD-AMC and subsequent measurement of the increase in fluorescence of AMC, which reflects caspase-3 activity in Ramos and Jurkat cells. Shown in each graph is the mean ± SD of one representative experiment performed in duplicates. **(C)** The apoptosis induction efficiency was determined in Ramos and Jurkat cells after 24 h treatment with increasing concentrations of Meriolin 16 by measurement of apoptotic nuclei via flow-cytometry. The highest concentration (30 µM) of Meriolin treatment was pre-and co-treated with QVD. Staurosporine (STS; 2.5 µM) was used as positive control for the induction of apoptosis. Error bars = mean ± SD of three independent experiments performed in triplicates. **(D)** Ramos or Jurkat cells were treated with 1 µM of Meriolin 16 for up to 8 h and the last time point was pre-and co-treated with QVD in order to confirm caspase dependency of PARP cleavage. DMSO (0.1% v/v) was used as solvent control and STS (2.5 µM) as positive control. **(E)** Meriolins prime the cells irreversibly to death within 5 min. Ramos cells were pre-incubated for 5 minutes with Meriolin 16, Meriolin 31 or Meriolin 36 and then the compounds were removed by washing (black graphs). The cells were further incubated for 24 h and subsequently cytotoxicity was determined with AlamarBlue® assay. This was compared to the treatment for 24 h without removal of the compounds (gray graphs). Shown in each graph is the mean ± SD of one representative experiment performed in triplicates. The respective IC_{50} values are given in the legend. **(F)** Meriolin derivatives 16, 31 and 36 prime cells to death within 5 min. Ramos cells were treated with 1 µM Meriolin 16, 31 and 36 for 5 minutes and the stimulus was removed after treatment. Staurosporine (STS; 2.5 µM) was used as positive control for cell death induction and DMSO (0.1% v/v; Ctrl) served as solvent control. The cleavage of PARP1 was determined after 24 h treatment via immunoblotting and Tubulin served as loading control.

So far, the class of Meriolins (31 and 36) was shown to be highly cytotoxic and functions as rapid activators of apoptosis as demonstrated in [443], but the exact molecular mechanism of apoptosis induction remained elusive. To investigate the extrinsic death receptor pathway as possible mechanism, caspase-8 proficient or deficient Jurkat cells were treated with Meriolin 16, 31 or 36. Etoposide and Staurosporine were used as controls for caspase-8 independent apoptosis and TRAIL as control for caspase-8 dependent apoptosis (**Figure 32 A**). The apoptosis rate was determined after 24 h. All three Meriolins do not induce the extrinsic pathway. To investigate the activation of the intrinsic mitochondrial pathway, Bcl-2 overexpressing Jurkat cells were treated with all three derivatives, compared to the respective empty vector control cells. Staurosporine was used as control for Bcl-2 independent intrinsic apoptosis and Etoposide for the induction of Bcl-2 dependent intrinsic apoptosis (**Figure 32 B**). Similar to Staurosporine, Meriolins induced apoptosis independently of Bcl-2 overexpression. Bcl-2 acts anti-apoptotic and is able to inhibit pro-apoptotic Bax and Bak, which are needed to form the apoptotic pore in the mitochondrial membrane. Therefore, it was tested whether Meriolins are able to induce caspase-3 activation in DG75 cells, which are negative for Bax and Bak (**Figure 32 C**). All Meriolins, induced a very low level of caspase-3 activation in Bax and Bak deficient DG75 cells, suggesting Bax and Bak are not required for the activation of the intrinsic apoptosis cascade activated by Meriolins. Following the signaling pathway of intrinsic apoptosis, it was next investigated whether the Meriolins induce cell death depending of caspase-9 by using Jurkat cells that are either negative or positive for caspase-9. The detection of apoptotic hypodiploid nuclei revealed, that Meriolin 16 and 31 induce a high apoptosis rate in caspase-9 positive cells and Meriolin 36 at a low rate. All three derivatives are unable to induce apoptosis in caspase-9 negative cells. The used controls are Etoposide, which induces fully caspase-9 dependent apoptosis and Staurosporine, which induces partially

caspase-9 dependent apoptosis (**Figure 32 D**). Staurosporine triggers also an alternative pathway, which is potentially caspase-9 independent [446]. In summary, the induction of apoptosis by Meriolins is dependent on caspase-9. Since the mitochondrial apoptosis pathway depends on Apaf-1 and apoptosome formation, it was investigated whether Meriolins are proficient to induce caspase activation in Apaf-1 deficient SK-Mel-94 cells. Meriolins induce very low, almost no caspase-3 activation in Apaf-1 negative cells, concluding that Apaf-1 is crucial for the activation of caspase-3 (**Figure 32 E**). Intrinsic apoptosis is dependent on the mitochondria as the main target organelle, where apoptotic signal transduction interconnects and gets integrated into the mitochondria with subsequent release of pro-apoptotic factors. Therefore, the morphology of HeLa cells stably expressing MitoDSRed, a red fluorescent dye tagged to the outer mitochondrial membrane, was assessed (**Figure 32 F**). The cells were treated with Meriolins or CCCP for up to 8 h. CCCP, a known protonophore causing the breakdown of mitochondrial membrane potential, acted as positive control. Meriolin 16 changed the tubular structure to a more punctate morphology starting from 6 h, similar to Meriolin 36. In contrast, Meriolin 31 induced delayed fragmentation starting from 8 h incubation (**Figure 32 F**). The induction of mitochondrial fragmentation is one characteristic of intrinsic apoptosis; hence it has to be noted, that not all Meriolins induced this morphological change in every cell equally. The level of fragmentation changed between cells.

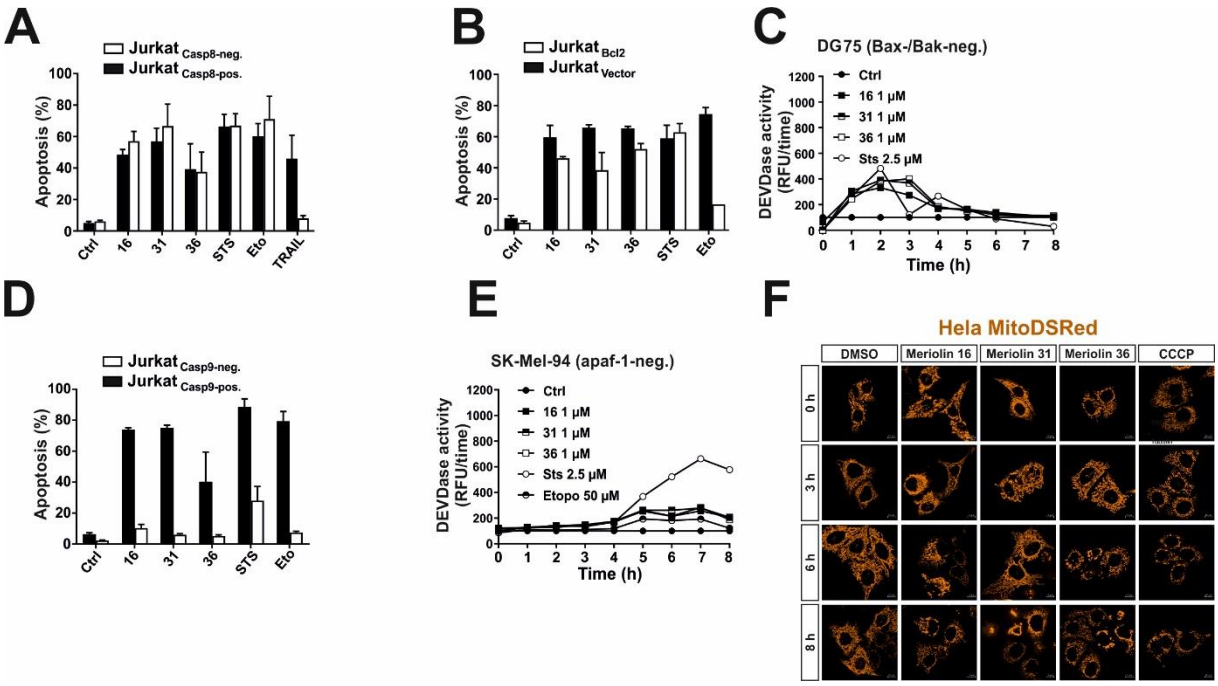

Figure 32 The three Meriolin derivatives 16, 31 and 36 induce apoptosis independent of the extrinsic caspase-8 dependent death receptor pathway. **(A)** Meriolins do not activate the DR pathway. **(B)** They trigger the intrinsic mitochondria dependent apoptosis pathway, partially dependent on Bcl-2, **(C)** not dependent on Bax and Bak, **(D)** dependent on caspase-9 and **(E)** dependent on Apaf-1. **(A)** Meriolin derivatives do not trigger the extrinsic apoptosis pathway. Jurkat cells deficient or proficient for caspase-8 were treated with DMSO (0.1% v/v; Ctrl) as solvent control, the three Meriolin derivatives (1 µM), STS (2.5 µM) and Etoposide (Eto; 50 µM) as positive controls for induction of intrinsic pathway and TRAIL (Tumor Necrosis Factor Related Apoptosis Inducing Ligand; 40 ng/ml) as positive control for induction of extrinsic pathway. The apoptosis rate (%) was determined via flow-cytometry

after 24 h treatment with the Nicoletti assay. Error bars = mean ± SD of three independent experiments performed in triplicates. **(B)** Apoptosis induction (%) by the three Meriolins is reduced in the presence of anti-apoptotic Bcl-2. Analysis was performed in Jurkat cells stably transfected with a vector encoding Bcl-2 or an empty vector. After 24 h apoptosis induction was assessed by propidium iodide staining of apoptotic nuclei and flow-cytometry. Cells were stimulated with DMSO (0.1% v/v; Ctrl), 1 µM of Meriolin derivatives, Staurosporine (STS; 2.5 µM) as positive control for Bcl-2 independent apoptosis, Etoposide (Eto; 50 µM) as positive control for Bcl-2 dependent apoptosis. Error bars = mean ± SD of three independent experiments performed in triplicates. **(C)** The Meriolin derivatives do not trigger caspase-3 activation in Bax-/Bak-negative Jurkat cells. The cells were treated with DMSO (0.1% v/v) as solvent control, 1 µM of Meriolin 16, 31, or 36, and Staurosporine (2.5 µM) as control for Apaf-1 independent caspase-3 activation for up to 8 h. The activation of caspase-3 was determined through fluorometric analysis of DEVDase activity. Shown in each graph is the mean ± SD of one representative experiment performed in duplicates. **(D)** The three Meriolin derivatives induce apoptosis dependent of caspase-9. Apoptosis induction was assessed in caspase-9 deficient and caspase-9 proficient cells after 24 h by staining of apoptotic nuclei with propidium iodide and the detection via flow-cytometry. Cells were stimulated with DMSO (0.1% v/v), 1 µM for Meriolin derivatives, Staurosporine (STS; 2.5 µM) as control for partially caspase-9 independent apoptosis, Etoposide (Eto; 50 µM) as control for caspase-9 dependent apoptosis. Error bars = Mean ± SD of three independent experiments performed in triplicates. **(E)** The Meriolin derivatives do not trigger caspase-3 activation in Apaf-1 negative SK-Mel-94 cells. SK-Mel-94 cells were treated with DMSO (0.1% v/v) as solvent control, 1 µM of Meriolin 16, 31, or 36, and Staurosporine (2.5 µM) as positive control for Apaf-1 independent apoptosis and Etoposide (50 µM) as control for Apaf-1 dependent caspase-3 activation for up to 8 h. The activation of caspase-3 was determined through fluorometric analysis of DEVDase activity. Shown in each graph is the mean ± SD of one representative experiment performed in duplicates. **(F)** Treatment with the Meriolin derivatives leads to a range of changes in the mitochondrial network. HeLa cells stably expressing mito-DsRed targeted to the outer mitochondrial membrane were treated with either DMSO (0.1% v/v) as solvent control, 10 µM Meriolin derivative (16, 31 or 36), or 10 µM CCCP as positive control for up to 8 h; mitochondrial fragmentation could be observed upon Meriolin treatment via live cell imaging. Representative images of three independent biological replicates are shown.

Figure 32 demonstrates that Meriolins are able to activate the mitochondrial cytochrome c/Apaf-1 apoptosis pathway in a direct way – even in the presence of anti-apoptotic Bcl-2. Mitochondrial morphology alters after different time points and further apoptosis induction depends on caspase-9 together with Apaf-1.

Meriolins show, together with their parental compounds Meridianins and Variolins, extensive kinase inhibitory activities [411, 412, 519, 524]. The question if other pathways, additional to the apoptosis signaling, are targeted, remained unanswered. To address this issue, an apoptosis array was performed with Merioline 16 and 36. Ramos cells were treated with high concentrations of Meriolin 16, Meriolin 36 and Staurosporine (control) for 8 h. A broad spectrum of proteins was identified and the signals analyzed according to **5.2.9 Apoptosis Array.** A heatmap represents the results and is shown in **Figure 33 A** supporting previous data, that Meriolin 16 and 36 activate apoptosis and lead to an increase in several apoptosis protein levels. In this experiment it was also focused on proteins which are not only involved in the apoptosis signaling cascade, but also in other pathways. Both Meriolins showed a higher signal intensity for Claspin, a protein for checkpoint mediated cell cycle arrest in response to inhibition of DNA replication or DNA damage [533]. Meriolins have a prevalence to inhibit kinases from the CMGC family and some of them are involved in cell cycle regulation [519, 524]. To investigate the cell cycle as possible targeted signaling pathway by Meriolin 16, 31 or 36, the cell cycle was analyzed with and without the pre-and co-treatment of QVD as caspase-inhibitor. QVD was

pre-and co-incubated to uncouple the effect of apoptosis induction from the cell cycle effect. Therefore, the Nicoletti assay was performed. The exact method can be found in **5.2.8 Analysis of apoptotic cell death and cell cycle**. In order to determine the cell cycle phase, the DNA content of the cell nuclei was determined by FACS in linear mode. For example, the DNA content doubles during S phase and thereby, a higher fluorescence intensity is observed compared to G_1. **Figure 33** shows the signal of PerCP-Cy5-5-A positive nuclei as bar graph, distinguishing the different cell cycle phases, S/G_2, G_1, and the fragmented hypodiploid nuclei (HN).

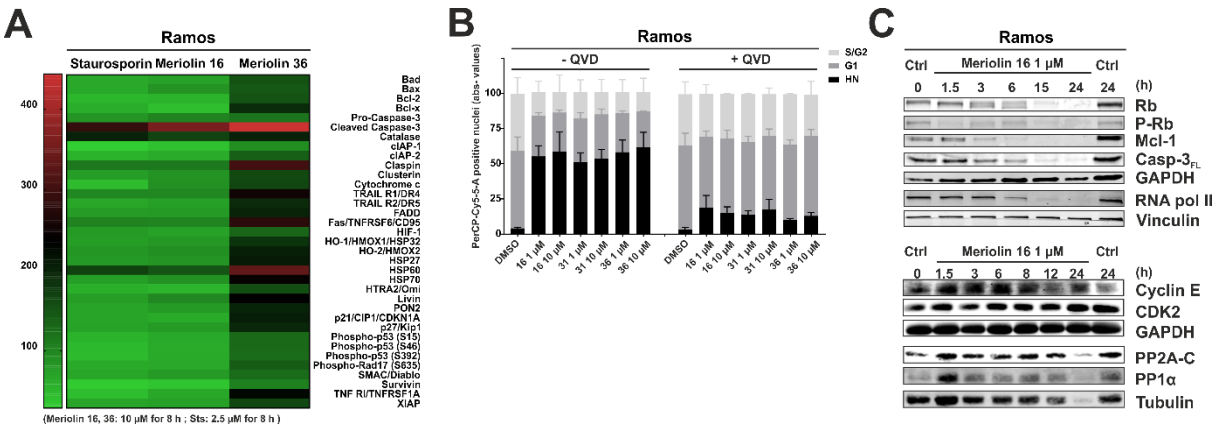

Figure 33 Meriolin derivatives disrupt the cell cycle. (A) Apoptosis array in Ramos cells after 8 h of 10 µM Meriolin 16 and 36 treatment showing increase of DNA-damage response and cell cycle regulating proteins (STS; 2.5 µM as apoptosis inducing control). **(B)** Cell cycle analysis in Ramos cells was determined after 24 h treatment with and without pre-and co-treatment of QVD followed by 1 or 10 µM Meriolin 16, 31 or 36 (DMSO 0.1% v/v; solvent control) via Nicoletti assay by flow-cytometry in the linear mode. Error bars = mean ± SD of three independent experiments performed in triplicates. **(C)** Ramos cells were treated for up to 24 h with 1 µM Meriolin 16 and the influence of Meriolin treatment on cell cycle regulating proteins (Rb, RNA pol II, CDK2/Cyclin E, PP2A-C, PP1α) as well as apoptosis proteins (caspase-3, Mcl-1) was analyzed via immunoblotting. Either GAPDH, Vinculin or Tubulin served as loading control.

The cell cycle analysis without QVD revealed a higher apoptosis rate for the Meriolin treated cells, in agreement with previous analyses (**Figure 33 B**). The condition with QVD pre- and co-treated cells showed a reduction of apoptotic hypodiploid nuclei, because the apoptosis cascade was blocked by caspase-inhibition. Additionally, an increase of the S/G_2-population was observed under this condition. This observation was investigated further via immunoblotting of proteins involved in cell cycle regulation (**Figure 33 C**). Since we were interested in the molecular mechanism of apoptosis and other affected pathways, further experiments were performed without the pre-and co-treatment of QVD. The inhibition of caspases is thought to change the signaling outcome of these surely interconnected pathways in a way that would be too artificial in terms of investigating the real therapeutic potential of this compound class. To address this issue, Ramos cells were treated in a kinetic experiment with Meriolin 16 over a period of 24 h. Proteins of the cell cycle, including Rb, phospho-Ser612-Rb, RNA pol II, CDK2 and Cyclin E were analyzed by immunoblotting (**Figure 33 C**). The serine/threonine phosphatases PP2A-C – a regulator for dephosphorylation of Akt, p53 and c-

myc [534] – and PP1α were analyzed. Both enzymes are involved in the control of mitotic progression [535]. Additionally, two apoptosis proteins, as the full-length form of caspase-3 and the anti-apoptotic protein Mcl-1, were also analyzed (**Figure 33 C**). In summary, anti-apoptotic Mcl-1 and full-length caspase-3 protein levels decrease after 3 hours treatment (**Figure 33 C**). These observations are in agreement with the kinetics of caspase-3 activation, as well as with the PARP1 cleavage shown above. Cell cycle related proteins show decreased protein levels, including RNA pol II and Rb. Under native conditions, Rb gets phosphorylated by CDK2 at its phosphosite (Ser612) [536]. Here, Rb and RNA pol II protein level decrease from 3 to 6 hours and the phosphosite Ser612 (Rb) decreases from 1.5 hours treatment. CDK2 levels seem stable during the time of incubation. Cyclin E shows slight increases between 1.5 to 8 h, due to its periodic protein expression, as explained in the introduction. The phosphatases (PP2A-C and PP1α) show a slight increase after 1.5 hours, but decrease slowly during longer treatment (**Figure 33 C**). In summary, cell cycle regulating proteins are also impaired by Meriolin 16 treatment.

Since the first Meriolin derivatives were synthesized in 2007, it was known, that these compounds are ATP-competitive due to their structural similarities to ATP and bind in the ATP-binding pocket of kinases, preferably CDKs [519, 524]. Consequentially, our Meriolin derivatives (16, 31 and 36) that are structurally different to those published by the Echaliér *et al*. 2008 [524] and Bettayeb *et al.* 2007 [519], were tested in luminescence-based kinase activity assays specific for CDK1/Cyclin B1, CDK2/Cyclin A2, CDK4/Cyclin D3 and CDK9/Cyclin T as shown in **Figure 34**. I selected specifically these four CDKs, since they are the main cell cycle regulating CDKs as reviewed in the introduction **1.4 Cell cycle**. The CDK assays are luminescence-based assays, where the level of relative luminescence correlates with the inhibitory capacity of the treatment and concentration respectively. Here, DMSO was used as negative (solvent) control and the CDK specific inhibitor R547 as positive control for the inhibition of CDK1/Cyclin B, CDK2/Cyclin E and CDK4/Cyclin D1 according to the manufacturer's information (Selleckchem.com [537]). Meriolin 16 and Meriolin 36 equally inhibited CDK1/Cyclin B1 with higher potency than R547 (**Figure 34 A**), but with a weaker inhibition for CDK2/Cyclin A2 at higher concentrations (0.1 and 1 µM), comparable to R547 (**Figure 34 B**). Both Meriolins, as well as R547, did not inhibit CDK4/Cyclin D3 significantly (**Figure 34 C**). CDK9/Cyclin T, the only transcriptionally active CDK tested here, was inhibited in a concentration-dependent manner by both Meriolins and also R547. Latter observation is surprising, since the manufacturer's homepage (Selleckchem.com [537]) stated inactivity against CDK9/Cyclin T. Anyway, it can be concluded from these kinase assays that Meriolin 16 and 36 (also 31 but to a lesser content – data not shown) are able to inhibit CDK1, CDK2 and CDK9 in different levels and in a concentration-dependent manner.

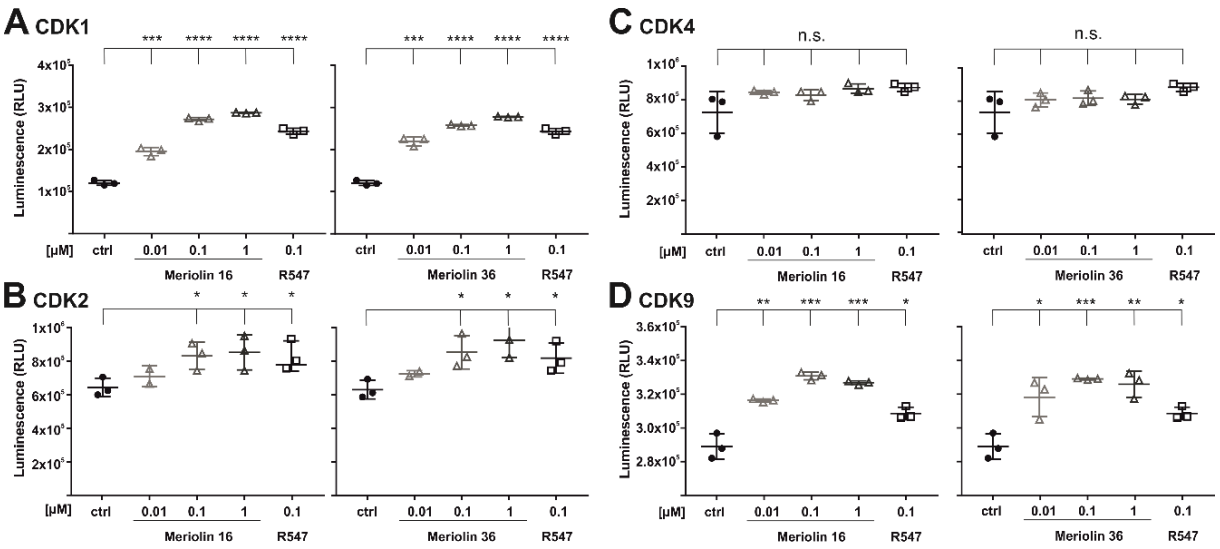

Figure 34 Meriolin 16 and 36 inhibit CDK1, 2, and 9 and have different inhibition specificities depending on the concentration towards each CDK. The CDK inhibition activity of Meriolin 16 and 36 was tested on selected CDKs and their corresponding Cyclins with the usage of CDK Kits from BPS Bioscience (CDK1/Cyclin B1 #79597; CDK2/Cyclin A2 #79599; CDK4/Cyclin D3 #79674; CDK9/Cyclin T #79628), DMSO (0.1% v/v) was used as solvent control and R547 as CDK inhibitor (Selleckchem.com [537]: inhibitor of CDK1/2 and 4). Error bars = mean ± SD values of independent biological experiments are shown. Statistical analysis: 1-way ANOVA, Bonferroni's multiple comparison test; (**** = $p \leq 0.0001$).

Since these CDKs were only selected on a literature base, it was aimed to cover a broader spectrum of kinases. Therefore, I acquired a collaboration with Reaction Biology (reactionbiology.com), who perform kinase drug discovery services offering the largest portfolio of kinase assays in industry. Meriolin 16 and Meriolin 36 were tested each in two concentrations according to their IC_{50} values of our dual cell system, Meriolin 16 for 0.03 and 0.3 µM, Meriolin 36 for 0.3 and 3 µM. Structurally related, but biologically inactive Meriolin 17 (structure shown in **Figure 30**) was used as negative control (0.3 and 3 µM) (data for Meriolin 17 are not shown here). This kinase panel screening tested the inhibitory activity of the Meriolins in two concentrations in singlicates against a panel of kinases (wild type kinase panel composed of 345 kinases in total, the profiler is named ^{33}PanQinase^{TM}). The results are shown as a kinome tree (**Figure 35 A**) and as table with residual activity in (%) (**Table 13**). The diameter of dots reflects the percental kinase inhibition. It can be seen in **Figure 35 A** that the lower concentration of Meriolin 16, which equals the IC_{50} value in Ramos and Jurkat cells shows a specificity for the yellowish arm of the kinome tree, which represents the CMGC family. With increasing concentration to 0.3 µM, a more unspecific inhibition pattern can be seen with increasing diameter of the dots at the CMGC family correlating with an increased inhibition. For Meriolin 36, the concentration of 0.3 µM shows a comparable pattern of dots to 0.3 µM of Meriolin 16, also with a prevalence to the CMGC family but also greenish specificity for the AGC family consisting of 63 evolutionarily related serine/threonine protein kinases (listed in [538]). When looking at the concentration of 3 µM it can be said, that Meriolin 36 appears to inhibit almost all kinases tested, at least to a low amount. In **Figure 35 B** the totality of all

tested CDKs in the kinome screen with their inhibition by Meriolin 16 and 36 are shown as a heatmap, with blue equaling no inhibition of the kinase and white equaling maximum inhibition of the respective kinase. The results generated in the luminescence-based kinase assays from CDK1, 2, 4 and 9 were supported by the results of the kinome screen, since here (**Figure 35 B**) CDK1 was inhibited in complex with either Cyclin A2, Cyclin B1 or Cyclin E1 for Meriolin 16 and 36. Also, CDK2 was inhibited in complex with either Cyclin A2, Cyclin D1 (to a lesser extent) or CyclinE1. For CDK4 and also for CDK6 a very low inhibition for either Meriolin 16 in both concentrations, or Meriolin 36 in 0.3 µM concentration can be seen, also supporting the previous data. CDK9 in complex with Cyclin K or Cyclin T1 are completely inhibited to almost zero residual kinase activity (**Figure 35 B**). The closer look at the heatmap revealed, that Meriolins 16 and 36 inhibit very efficiently and selectively distinct CDKs of the CMGC family in a concentration-dependent manner.

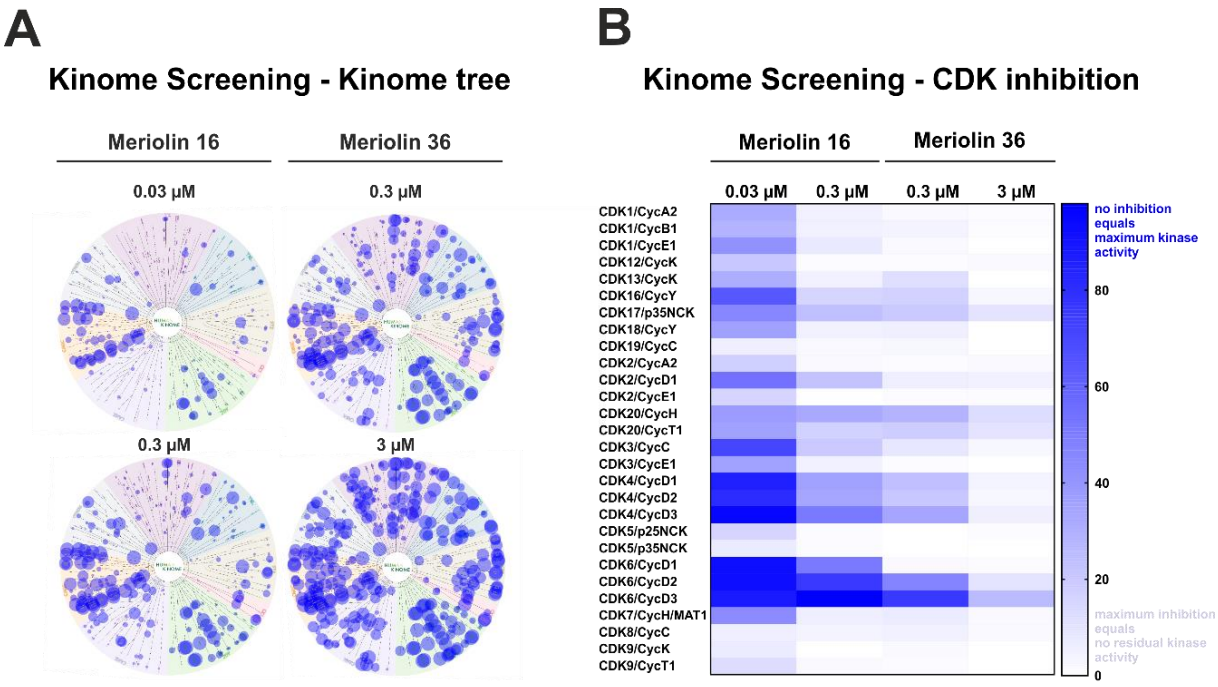

Figure 35 Meriolin 16 and 36 are active against kinases with a prevalence to the CMGC family. Meriolin 16 and 36 were each tested against 335 wild-type protein kinases in kinase *in vitro* assays by Reaction Biology in Freiburg. (A) Meriolin 16 in concentration of 0.03 µM and 0.3 µM, Meriolin 36 in 0.3 µM and 3 µM, as biological inactive control, the structurally related Meriolin 17 was tested in the higher concentrations of 0.3 µM and 3 µM (data not shown here). Depicted are all protein kinases tested in the kinome tree, the diameter of dots reflects % inhibition of 331 kinases (atypical kinases DNAPK, EEF2K mTOR and PKMzeta were excluded), the scale is 0 to ≥ 100% inhibition. **(B)** Heatmap of the CDK/Cyclin family with the inhibition specificity of Meriolin 16 in 0.03 µM and 0.3 µM compared to Meriolin 36 in 0.3 µM and 3 µM concentrations. This heat map shows in dark blue the maximum activity of the kinase at 100% to white which is the minimum activity of the kinase at 0%.

In more detail, **Table 13** shows the percentage of the residual activity of each Meriolin 17, 36 and 16 against the tested kinases. Also the selectivity scores of each Meriolin was calculated as described in **5.2.26** (< 50% residual activity): Meriolin 17 (0.3 µM): 0.009, Meriolin 17 (3 µM): 0.069, Meriolin 36 (0.3 µM): 0.397, Meriolin 36 (3 µM): 0.752, Meriolin 16 (0.03 µM): 0.140,

and Meriolin 16 (0.3 µM): 0.284. Hence, the lower the selectivity score, the higher the specificity. Lower residual activity equals higher inhibition at the respective concentration. Thus, Meriolin 17 was only partially able to inhibit a few kinases (mostly a residual activity of ~80-90%), whereas Meriolin 16 has the highest selectivity at 0.03 µM with a score of 0.140. The detailed percentages of residual kinase activity can be taken from **Table 13**.

Table 13 Kinome profiling (^{33}PanQinase^{TM}) of Meriolin 17 at 0.3 and 3 µM, Meriolin 36 at 0.3 and 3 µM and Meriolin 16 at 0.03 and 0.3 µM each against 335 wild-type protein kinases in singlicates measurement. Shown is the residual kinase activity (% of control) for each treatment. (# = kinase number, * the classification of protein kinase families was performed according to [539]: AGC (containing PKA, PKG and PKC families); CAMK (containing Calcium/Calmodulin-dependent protein kinases); CK1 (Casein kinase 1-like); CMGC (containing CDK, MAPK, GSK3 and CLK families); TK (Tyrosine Kinases); TKL (Tyrosine Kinase-like) and STE (Homologs of Yeast Sterile 7, Sterile 11 and Sterile 20 Kinases). Selectivity Scores (< 50% residual activity): Meriolin 17 (0.3 µM) 0.009, Meriolin 17 (3 µM) 0.069, Meriolin 36 (0.3 µM) 0.397, Meriolin 36 (3 µM) 0.752, Meriolin 16 (0.03 µM) 0.140, Meriolin 16 (0.3 µM) 0.284. (How residual activity and selectivity score were calculated is described in **5.2.26**)

#	Kinase Name	Kinase Family*	17 0.3 µM	17 3 µM	36 0.3 µM	36 3 µM	16 0.03 µM	16 0.3 µM
1	**ABL1**	**TK**	106	106	80	26	103	99
2	**ABL2**	**TK**	89	85	56	18	95	91
3	**ACK1**	**TK**	86	82	59	15	83	72
4	**ACVR1**	**TKL**	86	84	24	1	89	72
5	**ACVR1B**	**TKL**	62	70	43	10	75	69
6	**ACVR2A**	**TKL**	107	86	94	47	103	103
7	**ACVR2B**	**TKL**	74	68	22	5	81	74
8	**ACVRL1**	**TKL**	91	79	43	9	101	89
9	**AKT1**	**AGC**	78	84	89	41	96	70
10	**AKT2**	**AGC**	94	99	102	75	98	79
11	**AKT3**	**AGC**	110	90	93	42	108	82
12	**ALK**	**TK**	92	89	60	14	104	77
13	**AMPKα1**	**CAMK**	109	97	57	9	108	78
14	**ARK5**	**CAMK**	105	90	90	40	92	88
15	**ASK1**	**STE**	89	86	50	15	97	85
16	**AuroraA**	**OTHER**	107	82	81	35	109	107
17	**AuroraB**	**OTHER**	82	55	67	26	85	61
18	**AuroraC**	**OTHER**	81	84	76	41	104	95
19	**AXL**	**TK**	101	86	75	28	101	75
20	**BLK**	**TK**	118	101	88	13	126	95
21	**BMPR1A**	**TKL**	111	97	105	61	94	94
22	**BMPR1B**	**TKL**	86	72	75	45	91	91
23	**BMX**	**TK**	108	112	109	49	118	103
24	**BRAF**	**TKL**	97	95	66	50	94	105
25	**BRK**	**TK**	92	87	66	18	91	85
26	**BRSK1**	**CAMK**	94	82	89	73	91	97
27	**BRSK2**	**CAMK**	112	96	112	61	111	92
28	**BTK**	**TK**	97	81	103	77	114	96
29	**BUB1B**	**OTHER**	94	86	89	73	88	81
30	**CAMK1D**	**CAMK**	98	70	70	38	102	81
31	**CAMK2A**	**CAMK**	107	93	26	2	103	81
32	**CAMK2B**	**CAMK**	116	89	83	31	103	74
33	**CAMK2D**	**CAMK**	102	87	16	1	99	64

#	Kinase Name	Kinase Family*	17 0.3 µM	17 3 µM	36 0.3 µM	36 3 µM	16 0.03 µM	16 0.3 µM
34	**CAMK2G**	**CAMK**	93	82	34	6	94	82
35	**CAMK4**	**CAMK**	90	82	92	73	96	92
36	**CAMKK1**	**OTHER**	86	90	51	18	97	95
37	**CAMKK2**	**OTHER**	87	96	9	1	92	55
38	**CDC42BPA**	**AGC**	100	76	1	1	53	7
39	**CDC42BPB**	**AGC**	116	83	0	0	37	2
40	**CDC7/DBF4**	**OTHER**	105	72	10	2	63	12
41	**CDK1/CycA2**	**CMGC**	78	68	2	1	32	5
42	**CDK1/CycB1**	**CMGC**	98	78	4	1	29	5
43	**CDK1/CycE1**	**CMGC**	84	70	2	0	42	8
44	**CDK12/CycK**	**CMGC**	84	65	1	2	21	1
45	**CDK13/CycK**	**CMGC**	109	92	12	-10	31	5
46	**CDK16/CycY**	**CMGC**	101	88	17	3	64	16
47	**CDK17/p35NCK**	**CMGC**	86	64	20	10	46	24
48	**CDK18/CycY**	**CMGC**	97	81	6	0	36	5
49	**CDK19/CycC**	**CMGC**	41	18	3	0	6	2
50	**CDK2/CycA2**	**CMGC**	83	66	1	2	18	2
51	**CDK2/CycD1**	**CMGC**	82	92	6	5	54	23
52	**CDK2/CycE1**	**CMGC**	90	57	1	1	16	0
53	**CDK20/CycH**	**CMGC**	88	50	29	13	38	33
54	**CDK20/CycT1**	**CMGC**	84	55	19	10	36	17
55	**CDK3/CycC**	**CMGC**	98	85	9	3	71	20
56	**CDK3/CycE1**	**CMGC**	99	65	1	-1	36	5
57	**CDK4/CycD1**	**CMGC**	93	79	24	4	86	36
58	**CDK4/CycD2**	**CMGC**	90	85	21	3	81	34
59	**CDK4/CycD3**	**CMGC**	85	86	34	6	95	51
60	**CDK5/p25NCK**	**CMGC**	93	91	0	1	16	1
61	**CDK5/p35NCK**	**CMGC**	99	73	0	0	7	1
62	**CDK6/CycD1**	**CMGC**	94	86	2	1	93	51
63	**CDK6/CycD2**	**CMGC**	92	84	47	10	93	76
64	**CDK6/CycD3**	**CMGC**	80	84	76	26	88	98
65	**CDK7/CycH/MAT1**	**CMGC**	98	80	7	2	44	6
66	**CDK8/CycC**	**CMGC**	41	13	5	2	6	4
67	**CDK9/CycK**	**CMGC**	73	35	2	0	7	0
68	**CDK9/CycT1**	**CMGC**	87	52	1	0	13	2
69	**CHK1**	**CAMK**	87	68	76	40	96	87
70	**CHK2**	**CAMK**	97	91	81	41	90	82
71	**CK1α1**	**CK1**	136	122	110	51	129	93
72	**CK1Δ**	**CK1**	109	86	43	9	77	17
73	**CK1ε**	**CK1**	124	103	86	23	112	41
74	**CK1γ1**	**CK1**	107	96	23	3	87	38
75	**CK1γ2**	**CK1**	98	97	19	3	86	30
76	**CK1γ3**	**CK1**	105	95	49	9	77	22
77	**CK2α1**	**OTHER**	105	106	99	53	106	104
78	**CK2α2**	**OTHER**	105	99	91	43	110	105
79	**CLK1**	**CMGC**	73	35	4	2	11	3
80	**CLK2**	**CMGC**	102	45	1	2	8	1
81	**CLK3**	**CMGC**	130	108	13	1	94	36
82	**CLK4**	**CMGC**	56	11	1	1	3	0
83	**COT**	**STE**	90	103	85	92	104	86

#	Kinase Name	Kinase Family*	17 0.3 µM	17 3 µM	36 0.3 µM	36 3 µM	16 0.03 µM	16 0.3 µM
84	**CSF1R**	**TK**	97	78	33	14	90	88
85	**CSK**	**TK**	106	103	116	71	114	106
86	**DAPK1**	**CAMK**	154	127	119	64	112	72
87	**DAPK2**	**CAMK**	128	107	118	67	106	78
88	**DAPK3**	**CAMK**	110	91	80	25	98	51
89	**DCAMKL2**	**CAMK**	88	86	91	81	92	85
90	**DDR2**	**TK**	103	92	59	17	105	93
91	**DMPK**	**AGC**	104	92	3	-2	86	63
92	**DNAPK**	**ATYPICAL**	96	88	71	25	100	97
93	**DYRK1A**	**CMGC**	93	57	7	0	11	2
94	**DYRK1B**	**CMGC**	83	36	7	0	8	0
95	**DYRK2**	**CMGC**	93	56	31	4	6	1
96	**DYRK3**	**CMGC**	93	82	59	14	27	2
97	**DYRK4**	**CMGC**	95	82	66	22	39	7
98	**EEF2K**	**ATYPICAL**	86	90	84	97	96	89
99	**EGFR**	**TK**	118	101	107	53	109	90
100	**EIF2AK2**	**OTHER**	76	76	79	63	83	95
101	**EIF2AK3**	**OTHER**	84	82	81	74	87	90
102	**EPHA1**	**TK**	120	114	127	126	128	116
103	**EPHA2**	**TK**	103	92	101	72	109	101
104	**EPHA3**	**TK**	105	100	111	103	102	94
105	**EPHA4**	**TK**	111	80	93	72	105	85
106	**EPHA5**	**TK**	100	102	146	84	115	102
107	**EPHA6**	**TK**	130	85	101	65	98	105
108	**EPHA7**	**TK**	128	107	131	93	122	107
109	**EPHA8**	**TK**	111	96	113	94	119	107
110	**EPHB1**	**TK**	116	107	124	79	98	97
111	**EPHB2**	**TK**	92	89	85	47	97	95
112	**EPHB3**	**TK**	98	98	91	67	101	99
113	**EPHB4**	**TK**	110	98	110	85	97	90
114	**ERBB2**	**TK**	92	84	90	44	102	102
115	**ERBB4**	**TK**	111	90	101	56	108	90
116	**ERK1**	**CMGC**	94	96	72	37	111	96
117	**ERK2**	**CMGC**	104	94	79	30	103	87
118	**ERK5**	**CMGC**	84	43	13	8	28	22
119	**ERK7**	**CMGC**	98	63	7	-3	86	59
120	**FAK**	**TK**	112	96	85	60	102	89
121	**FER**	**TK**	81	81	66	22	63	58
122	**FES**	**TK**	95	72	83	50	93	87
123	**FGFR1**	**TK**	93	82	56	16	103	91
124	**FGFR2**	**TK**	91	84	52	9	94	85
125	**FGFR3**	**TK**	96	93	64	20	93	84
126	**FGFR4**	**TK**	106	100	98	58	91	87
127	**FGR**	**TK**	107	95	40	6	111	105
128	**FLT3**	**TK**	101	78	9	2	49	21
129	**FRK**	**TK**	100	99	54	16	103	99
130	**FYN**	**TK**	98	84	22	3	93	69
131	**GRK2**	**AGC**	102	88	99	51	96	106
132	**GRK3**	**AGC**	117	105	98	74	111	107
133	**GRK4**	**AGC**	118	109	108	95	101	90

#	Kinase Name	Kinase Family*	17 0.3 µM	17 3 µM	36 0.3 µM	36 3 µM	16 0.03 µM	16 0.3 µM
134	**GRK5**	**AGC**	118	110	119	74	118	91
135	**GRK6**	**AGC**	104	96	96	54	98	93
136	**GRK7**	**AGC**	114	98	94	48	105	78
137	**GSG2**	**OTHER**	35	5	2	0	2	0
138	**GSK3α**	**CMGC**	127	80	41	7	99	93
139	**GSK3β**	**CMGC**	81	62	18	2	80	66
140	**HCK**	**TK**	105	81	75	25	106	81
141	**HIPK1**	**CMGC**	113	90	47	10	49	10
142	**HIPK2**	**CMGC**	81	58	22	3	36	4
143	**HIPK3**	**CMGC**	95	82	45	11	53	7
144	**HIPK4**	**CMGC**	95	85	27	2	74	24
145	**HRI**	**OTHER**	106	89	93	71	98	90
146	**IGF1R**	**TK**	130	115	128	83	116	99
147	**IKKα**	**OTHER**	100	39	37	13	27	16
148	**IKKβ**	**OTHER**	96	60	80	36	85	64
149	**IKKε**	**OTHER**	99	90	40	6	94	61
150	**INSR**	**TK**	97	89	82	36	96	91
151	**INSRR**	**TK**	87	89	85	39	97	96
152	**IRAK1**	**TKL**	110	86	49	9	95	76
153	**IRAK4**	**TKL**	85	66	14	2	83	50
154	**ITK**	**TK**	97	93	77	16	105	88
155	**JAK1**	**TK**	88	77	58	25	78	86
156	**JAK2**	**TK**	98	83	40	8	102	80
157	**JAK3**	**TK**	87	66	5	-1	58	15
158	**JNK1**	**CMGC**	106	81	74	23	102	95
159	**JNK2**	**CMGC**	80	73	63	29	78	85
160	**JNK3**	**CMGC**	93	83	54	13	73	68
161	**KIT**	**TK**	96	82	89	46	70	96
162	**LCK**	**TK**	98	90	61	18	87	91
163	**LIMK1**	**TKL**	85	39	9	1	10	3
164	**LIMK2**	**TKL**	105	89	70	27	106	101
165	**LRRK2**	**TKL**	85	58	1	1	50	8
166	**LTK**	**TK**	100	88	46	11	110	98
167	**LYN**	**TK**	103	95	73	25	105	81
168	**MAP3K1**	**STE**	90	89	94	93	105	106
169	**MAP3K10**	**STE**	94	89	50	9	99	76
170	**MAP3K11**	**STE**	104	85	45	4	100	74
171	**MAP3K7/MAP3K7IP1**	**STE**	81	61	15	5	54	17
172	**MAP3K9**	**STE**	93	86	57	12	95	80
173	**MAP4K2**	**STE**	83	50	3	0	22	4
174	**MAP4K4**	**STE**	83	35	6	2	76	29
175	**MAP4K5**	**STE**	98	78	3	0	87	52
176	**MAPKAPK2**	**CAMK**	143	118	130	87	114	95
177	**MAPKAPK3**	**CAMK**	107	96	102	90	99	87
178	**MAPKAPK5**	**CAMK**	106	89	106	69	104	85
179	**MARK1**	**CAMK**	93	99	90	43	121	101
180	**MARK2**	**CAMK**	109	96	98	63	91	88
181	**MARK3**	**CAMK**	111	98	89	48	99	86
182	**MARK4**	**CAMK**	102	93	90	54	99	91
183	**MASTL**	**AGC**	85	84	64	26	87	56

#	Kinase Name	Kinase Family*	17 0.3 µM	17 3 µM	36 0.3 µM	36 3 µM	16 0.03 µM	16 0.3 µM
184	**MATK**	**TK**	122	117	134	94	107	90
185	**MEK1**	**STE**	113	89	35	6	108	102
186	**MEK2**	**STE**	88	61	13	3	66	48
187	**MEK5**	**STE**	88	52	30	12	35	31
188	**MEKK2**	**STE**	105	100	66	18	95	91
189	**MEKK3**	**STE**	104	97	66	26	106	90
190	**MELK**	**CAMK**	91	29	36	9	74	14
191	**MERTK**	**TK**	109	95	69	36	97	86
192	**MET**	**TK**	103	99	99	48	110	106
193	**MINK1**	**STE**	78	25	2	0	75	20
194	**MKK4**	**STE**	86	81	45	9	86	66
195	**MKK6 SDTD**	**STE**	77	75	63	30	77	87
196	**MKK7**	**STE**	94	83	81	48	96	88
197	**MKNK1**	**CAMK**	86	68	48	16	97	70
198	**MKNK2**	**CAMK**	91	65	16	3	93	62
199	**MLK4**	**TKL**	103	101	73	40	105	75
200	**MST1**	**STE**	97	87	4	1	88	49
201	**MST2**	**STE**	104	87	19	4	100	77
202	**MST3**	**STE**	88	87	71	32	101	91
203	**MST4**	**STE**	81	72	52	12	78	81
204	**MTOR**	**ATYPICAL**	104	87	78	24	91	105
205	**MUSK**	**TK**	83	73	28	5	88	70
206	**MYLK**	**CAMK**	107	66	62	25	103	71
207	**MYLK2**	**CAMK**	78	58	61	26	65	32
208	**MYLK3**	**CAMK**	116	68	71	21	119	77
209	**NEK1**	**OTHER**	82	79	84	55	86	67
210	**NEK11**	**OTHER**	92	85	105	85	97	87
211	**NEK2**	**OTHER**	103	94	95	72	103	96
212	**NEK3**	**OTHER**	101	87	94	79	96	78
213	**NEK4**	**OTHER**	104	90	84	37	89	47
214	**NEK6**	**OTHER**	100	109	112	108	107	104
215	**NEK7**	**OTHER**	111	104	103	107	111	96
216	**NEK9**	**OTHER**	86	86	88	67	89	87
217	**NIK**	**STE**	89	84	59	33	94	79
218	**NLK**	**CMGC**	101	87	78	29	96	81
219	**p38α**	**CMGC**	85	79	78	80	94	74
220	**p38β**	**CMGC**	81	76	77	84	79	88
221	**p38Δ**	**CMGC**	101	85	59	14	79	24
222	**p38γ**	**CMGC**	94	84	64	19	56	8
223	**PAK1**	**STE**	88	88	85	76	106	98
224	**PAK2**	**STE**	108	103	71	17	92	93
225	**PAK3**	**STE**	100	92	85	40	85	84
226	**PAK4**	**STE**	101	86	56	16	86	74
227	**PAK6**	**STE**	94	83	54	14	88	76
228	**PAK7**	**STE**	94	77	42	9	89	81
229	**PASK**	**CAMK**	100	47	3	0	82	39
230	**PBK**	**OTHER**	110	67	69	80	95	90
231	**PDGFRα**	**TK**	85	73	25	8	89	60
232	**PDGFRβ**	**TK**	97	81	24	4	93	75
233	**PDK1**	**AGC**	91	75	160	39	98	83

#	Kinase Name	Kinase Family*	17 0.3 µM	17 3 µM	36 0.3 µM	36 3 µM	16 0.03 µM	16 0.3 µM
234	**PHKG1**	**CAMK**	105	88	16	2	85	39
235	**PHKG2**	**CAMK**	66	62	52	23	74	52
236	**PIM1**	**CAMK**	84	57	55	14	77	40
237	**PIM2**	**CAMK**	108	98	119	90	115	83
238	**PIM3**	**CAMK**	89	54	85	46	118	68
239	**PKA**	**AGC**	85	81	12	2	75	43
240	**PKCα**	**AGC**	105	82	49	11	95	80
241	**PKCβ1**	**AGC**	110	92	53	9	103	50
242	**PKCβ2**	**AGC**	106	85	51	11	106	71
243	**PKCΔ**	**AGC**	109	72	4	0	47	6
244	**PKCε**	**AGC**	81	77	5	1	25	4
245	**PKCη**	**AGC**	93	56	2	2	8	2
246	**PKCγ**	**AGC**	100	77	33	5	99	54
247	**PKCι**	**AGC**	91	86	75	32	105	94
248	**PKCμ**	**AGC**	93	74	63	23	77	24
249	**PKCv**	**AGC**	78	65	62	17	89	32
250	**PKCΘ**	**AGC**	97	70	2	1	40	7
251	**PKCζ**	**AGC**	115	106	85	29	97	78
252	**PKMYT1**	**OTHER**	79	53	39	13	32	23
253	**PKMzeta**	**AGC**	102	89	89	68	97	90
254	**PKN3**	**AGC**	84	84	27	3	83	74
255	**PLK1**	**OTHER**	96	92	100	66	95	90
256	**PLK3**	**OTHER**	111	94	97	87	95	92
257	**PRK1**	**AGC**	94	87	17	3	84	35
258	**PRK2**	**AGC**	78	69	8	0	90	42
259	**PRKD2**	**CAMK**	91	80	68	25	87	37
260	**PRKG1**	**AGC**	84	53	6	1	75	30
261	**PRKG2**	**AGC**	77	20	14	2	48	7
262	**PRKX**	**AGC**	123	85	15	-1	54	3
263	**PYK2**	**TK**	93	98	73	24	117	102
264	**RAF1 YDYD**	**TKL**	75	82	67	67	77	96
265	**RET**	**TK**	120	96	61	12	106	100
266	**RIPK2**	**TKL**	75	64	61	33	95	78
267	**RIPK4**	**TKL**	92	86	88	45	94	75
268	**RIPK5**	**TKL**	90	76	58	16	101	86
269	**ROCK1**	**AGC**	85	39	1	1	24	2
270	**ROCK2**	**AGC**	77	39	1	0	12	1
271	**RON**	**TK**	106	91	98	76	92	90
272	**ROS**	**TK**	93	72	26	5	92	81
273	**RPS6KA1**	**AGC**	97	54	20	10	46	22
274	**RPS6KA2**	**AGC**	90	63	6	0	87	34
275	**RPS6KA3**	**AGC**	86	56	7	1	85	39
276	**RPS6KA4**	**AGC**	91	88	71	29	90	89
277	**RPS6KA5**	**AGC**	87	73	46	15	89	82
278	**RPS6KA6**	**AGC**	78	40	13	3	84	48
279	**S6K**	**AGC**	99	73	82	37	99	84
280	**S6Kbeta**	**AGC**	117	100	87	67	89	103
281	**SAK**	**OTHER**	67	62	53	24	97	84
282	**SGK1**	**AGC**	75	41	30	10	92	76
283	**SGK2**	**AGC**	99	78	88	32	97	74

#	Kinase Name	Kinase Family*	17 0.3 µM	17 3 µM	36 0.3 µM	36 3 µM	16 0.03 µM	16 0.3 µM
284	**SGK3**	**AGC**	91	82	81	27	94	84
285	**SIK1**	**CAMK**	89	81	87	48	102	98
286	**SIK2**	**CAMK**	103	81	86	27	96	102
287	**SIK3**	**CAMK**	94	83	72	32	106	88
288	**SLK**	**STE**	74	83	4	1	83	77
289	**SNARK**	**CAMK**	93	79	30	5	99	64
290	**SNK**	**OTHER**	97	95	94	43	96	98
291	**SRC**	**TK**	104	91	88	24	95	86
292	**SRMS**	**TK**	104	91	93	73	101	93
293	**SRPK1**	**CMGC**	109	110	110	70	108	99
294	**SRPK2**	**CMGC**	99	98	87	55	93	91
295	**STK17A**	**CAMK**	87	36	23	4	83	23
296	**STK23**	**CAMK**	94	96	95	88	109	78
297	**STK25**	**STE**	99	91	33	6	99	81
298	**STK33**	**CAMK**	90	76	41	14	73	43
299	**STK39**	**STE**	98	77	40	19	77	66
300	**SYK**	**TK**	98	97	90	64	93	84
301	**TAOK2**	**STE**	125	102	60	19	107	89
302	**TAOK3**	**STE**	100	100	44	6	111	91
303	**TBK1**	**OTHER**	111	90	48	10	114	99
304	**TEC**	**TK**	114	101	114	96	110	101
305	**TGFBR1**	**TKL**	68	58	18	0	65	67
306	**TGFBR2**	**TKL**	67	67	72	24	109	85
307	**TIE2**	**TK**	102	108	113	65	132	105
308	**TLK1**	**AGC**	121	105	119	106	98	89
309	**TLK2**	**AGC**	152	125	149	88	111	91
310	**TNK1**	**TK**	93	86	29	9	82	39
311	**TRKA**	**TK**	101	81	9	1	83	40
312	**TRKB**	**TK**	98	72	10	2	68	29
313	**TRKC**	**TK**	103	91	18	2	72	36
314	**TSF1**	**OTHER**	85	52	57	8	109	104
315	**TSK2**	**CAMK**	102	93	103	94	107	92
316	**TSSK1**	**CAMK**	117	90	50	15	109	83
317	**TTBK1**	**CK1**	104	110	101	77	116	108
318	**TTBK2**	**CK1**	100	94	93	56	96	91
319	**TTK**	**OTHER**	109	85	55	17	49	8
320	**TXK**	**TK**	97	95	84	35	100	90
321	**TYK2**	**TK**	108	84	6	1	105	68
322	**TYRO3**	**TK**	85	87	94	64	104	89
323	**ULK2**	**OTHER**	90	83	82	45	96	54
324	**VEGFR1**	**TK**	98	83	83	43	110	89
325	**VEGFR2**	**TK**	102	82	60	19	102	98
326	**VEGFR3**	**TK**	100	84	64	23	90	77
327	**VRK1**	**CK1**	94	96	104	61	114	108
328	**VRK2**	**CK1**	115	106	93	45	103	92
329	**WEE1**	**OTHER**	98	419	72	37	80	99
330	**WNK1**	**OTHER**	106	97	107	98	101	100
331	**WNK2**	**OTHER**	89	71	86	74	99	86
332	**WNK3**	**OTHER**	106	93	106	104	85	85
333	**YES**	**TK**	108	96	65	19	100	90

#	Kinase Name	Kinase Family*	17 0.3 µM	17 3 µM	36 0.3 µM	36 3 µM	16 0.03 µM	16 0.3 µM
334	**ZAK**	**TKL**	91	91	57	14	96	83
335	**ZAP70**	**TK**	101	89	110	85	95	83

It was aimed in this thesis to identify the molecular mechanism underlying the efficient elimination of lymphoma and leukemia cells within a short time. Summarizing, it was shown, that Meriolin 16 and 36 disrupt the cell cycle and impair cell cycle regulated proteins. Additionally, they inhibit selectively CDKs and other kinases. CDK inhibition might also lead to a disturbance of the cell cycle. For verification, the downstream signaling of cell cycle regulation was analyzed in detail by the author of this thesis and the master student Julia Hoppe as part of her master thesis, which was supervised by the author of this dissertation. Ramos cells were treated with Meriolin 16 and 36 at respective concentrations (0.1 and 1 µM). DMSO (0.01% v/v) and 1 µM R547 were used as control (**Figure 36**, **Figure 37**, **Figure 38**). The incubation was performed in a kinetic range starting from 4 over 8, 12, 16 h and ended at 24 h. Selected proteins of the cell cycle shown in **Figure 5** in the introductory chapter **1.4 Cell cycle** were analyzed by immunoblotting in three independent biological replicates of which one representative immunoblot after 24 h is shown in **(A)** of **Figure 36**, **Figure 37** and **Figure 38**. The respective quantifications of immunoblots after 4, 8, 12, 16, 24 h of a biological replicate are shown in **(B)** of **Figure 36**, **Figure 37** and **Figure 38**. The immunoblots and graphs were divided in three figures structured as explained above, since **Figure 36** addresses the analysis of proteins of the CDK1, CyclinB1 and p-CHK2-signaling. **Figure 37** deals with proteins of the CDK2, Cyclin A2, p-CHK1 and p-Rb-Ser612-signaling. Additionally, in **Figure 38** the transcriptional CDK, CDK9, Cyclin T1 and p-RNA pol II-Ser2-signaling is analyzed.

Figure 36 shows protein levels of the CDK1, Cyclin B1 and p-CHK2-signaling. CDK1/Cyclin B1 is active in the M phase of the cell cycle (**1.4 Cell cycle**, **Figure 5**). Generally, after DNA damage (DSBs), CHK2 arrests the cell cycle at G_1/S and G_2/M [540]. CHK2 monomers are phosphorylated by ATM on T68 and dimerize. As a result, it becomes active upon autophosphorylation and the active monomers dissociate [540]. The molecular mechanism of CHK2-dependent arrest in G_1/S and G_2/M are similar. Briefly CHK2 phosphorylates CDC25, resulting in translocation of CDC25 into the cytoplasm where it can no longer dephosphorylate and activate the CDK1/Cyclin B1 complex, which is crucial for G_2/M transition [540]. Additionally, CHK2 phosphorylates p53, promoting p21 accumulation in order to sustain G_2/M arrest [541]. Our analysis revealed that CDK1 levels remain relatively stable for both concentrations of Meriolin 16 and 36. With Meriolin 16 treatment, the Cyclin B1 levels decrease over time, whereas they remain stable for Meriolin 36 (**Figure 36**). In terms of the phosphorylation of CHK2, the antibody detects the phosphorylation of CHK2 at T68 by ATM. Both Meriolins induce an increase of p-CHK2 protein

levels. For Meriolin 16, the levels increase by 15-fold and for Meriolin 36 by 25-fold. Here, p-CHK2 gets phosphorylated at T68 between 12 and 24 h treatment (**Figure 36**).

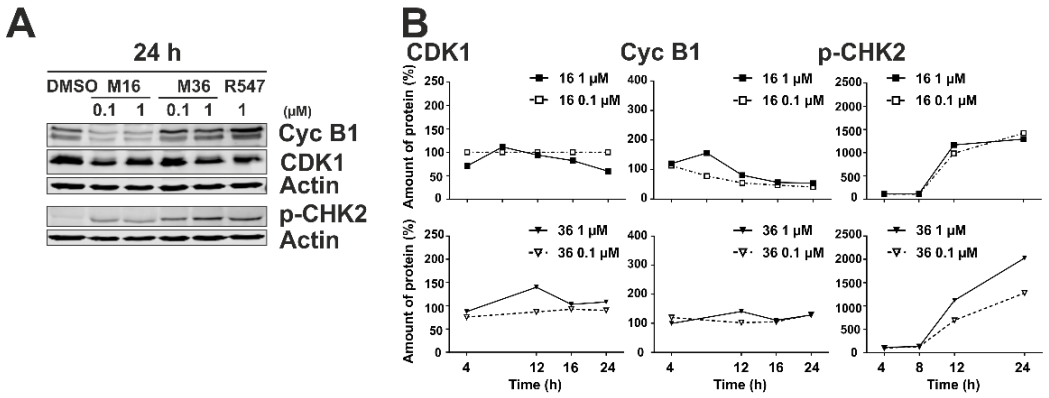

Figure 36 Meriolin 16 and 36 do not alter CDK1/Cyclin B1 protein levels but do increase p-CHK2 protein level over time. Ramos cells were treated with two different concentrations (0.1 and 1 µM) of each Meriolin 16 or 36, DMSO (0.1% v/v) as solvent control and R547 as another selective CDK inhibitor, for up to 24 h, the respective proteins of interest were analyzed via immunoblotting. For each time point the respective protein levels were analyzed via immunoblotting and subsequently quantified. Shown is one representative immunoblot after 24 h and the graphs originate from the quantification of each immunoblot for each time point. In **(A)** the CDK1/CyclinB1 pathway, as well as cell cycle arrest via the phosphorylation of CHK2 are depicted. In **(B)** the respective quantification of the protein levels of CDK1, Cyclin B1 and p-CHK2 over time is shown as amount of protein (%) over 4, 8, 12, 16 and 24 h.

To investigate the influence on the signaling in S phase of the cell cycle, CDK2, Cyclin A2, p-CHK1 and p-Rb-Ser612-pathway were analyzed via immunoblotting (**Figure 37**). Once, damage like SSBs occurs during S phase or replication, ATR as replication checkpoint kinase gets activated and phosphorylates CHK1, both act on CDK2/Cyclin A or CDK1/Cyclin A or B preventing entry into mitosis [175]. However, CHK1 gets phosphorylated on S345 by ATR (also on S317 and autophosphorylated on S296) and it is indispensable for S- and G_2/M checkpoints [542]. The immunoblotting kinetics with quantification (**Figure 37 A** and **B**) revealed that CDK2 and Cyclin A2 protein levels remain relatively stable under Meriolin 16 treatment, whereas greater fluctuations are observed for both concentrations of Meriolin 36. Referring to the phosphorylation of S345 at CHK1, the protein level remains stable under both Meriolin treatments (**Figure 37**). Additionally, the phosphorylation of Ser612 at the Rb protein was monitored. This phosphorylation is mediated by CDK2/Cyclin A and enhances cell cycle progression in S phase [536]. The phosphorylation of Rb results in the release of E2F family members and crucial E2F-responsive genes for S phase can be transcribed [543]. Interestingly, the protein level of p-Ser612 Rb differs between the treatment with either Meriolin 16 concentrations or Meriolin 36 concentration (**Figure 37**). For Meriolin 16 the phosphosite specific protein level of p-Ser612 Rb decreases over time, whereas it increases for both concentrations of Meriolin 36 (**Figure 37**). This was surprising, it was expected that the phosphorylation decreases due to the inhibition of CDK2/Cyclin A2 suggesting that the cells might not continue to progress in the cell cycle. However, this point will be discussed later in the discussion (**7.3 Meriolins**). In summary, it can be concluded from **Figure 37** that similar to

Figure 36 the protein levels of CDK (1 or 2) in complex with a Cyclin (A2 or B1) remain stable upon Meriolin 16 and 36 treatment comparing 4 and 24 h. Here, p-CHK1 seems not to get phosphorylated over time upon Meriolin treatment. The CDK2/Cyclin A specific phosphorylation of Rb at Ser612 revealed distinct results for both Meriolins – i.e. for Meriolin 16 a total decrease of the protein signal and for Meriolin 36 a 4-fold increase was observed (**Figure 37**).

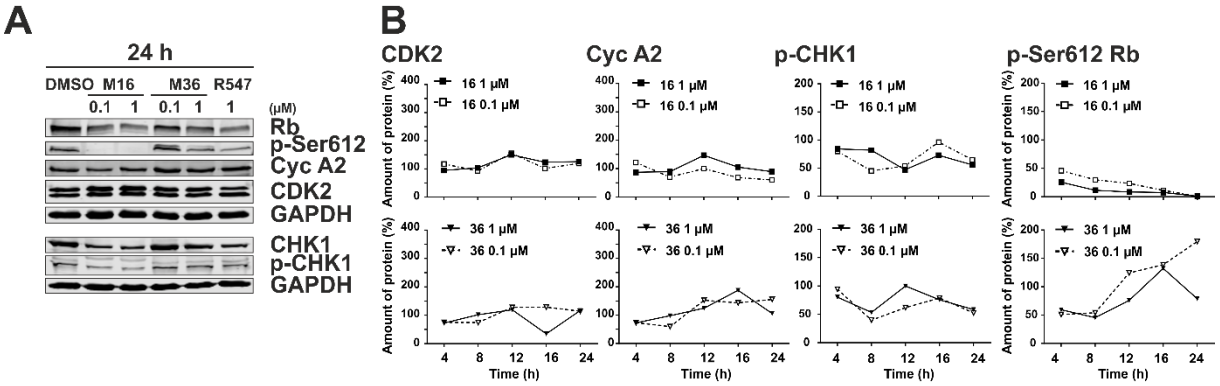

Figure 37 Meriolin 16 and 36 do not alter CDK2/Cyclin A2 protein levels and do not increase p-CHK1 protein level over time. The Meriolins act different on p-Ser612 Rb, Meriolin 16 induce a decrease and Meriolin 36 an increase of the phosphosite-specific protein level. Ramos cells were treated with two different concentrations (0.1 and 1 µM) of each Meriolin 16 or 36, DMSO (0.1% v/v) as solvent control and R547 as another selective CDK inhibitor, for up to 24 h. For each time point, the respective proteins of interest were analyzed via immunoblotting and subsequently quantified. Shown is one representative immunoblot after 24 h and the graphs originate from the quantification of each immunoblot for each time point. In **(A)** the immunoblotting after 24 h Meriolin treatment for the CDK2/Cyclin A2 pathway, CHK1 and the phosphorylation of p-CHK1 (S345) and the phosphorylation of the Rb protein (p-Ser612) are shown. In **(B)** the respective quantification of the protein levels of CDK2, Cyclin A2, p-CHK1 and p-Ser612 Rb (which gets phosphorylated by CDK2) over time is shown as amount of protein (%) over 4, 8, 12, 16 and 24 h.

In this analysis, CDK9 is especially interesting, since it was inhibited in the kinome screen to very low residual activities (**Table 13**): 13% (0.03 µM Meriolin 16), 2% (0.3 µM Meriolin 16), 1% (0.3 µM Meriolin 36) and 0% (3 µM Meriolin 36). The relevance of transcriptional CDKs has been verified just recently, since many cancers extensively exploit CDKs such as CDK9 as essential regulators of transcription, allowing them to continuously generate short-lived gene products that sustain their survival [544]. CDK9/Cyclin T regulates transcriptional elongation and termination (**1.4 Cell cycle**). During transcription, the regulation of gene expression takes place, involving many factors to the C-terminal domain (CTD) of RNA pol II, thereby guiding RNA pol II to gain access to transcription sites with subsequent initiation and elongation of transcription [544]. The CTD comprises of 52 tandem heptapeptide repeats of the sequence $Y_1S_2P_3T_4S_5P_6S_7$ [545, 546]. One of these factors is the transcription factor P-TEFb, since this kinase activity mediating subunit of CDK9/Cyclin T phosphorylates the CTD of RNA pol II at Ser2 [544, 547-549]. P-TEFb stands for positive transcription elongation factor and it mediates the transition from transcription initiation to productive elongation of pre-mRNA transcripts by the phosphorylation at RNA pol II Ser2. Also noteworthy is that the expression and kinase activity of CDK9/Cyclin

T1 does not change in a cell cycle-dependent manner unlike other cell cycle CDKs [544, 550, 551]. In **Figure 38**, the protein levels of CDK9/Cyclin T1, RNA pol II and the phosphosite specific protein level of p-Ser2 RNA pol II were analyzed over time and quantified via immunoblotting. Meriolin 16 induces the decrease of CDK9 and Cyclin T1 protein levels over 4, 8, 12, 16 and 24 h in low (0.1 µM) and high (1 µM) concentrations. In contrast, these protein levels are relatively stable for Meriolin 36 (**Figure 38**). Within 4 hours incubation with both Meriolin 16 concentrations, the phosphorylation at Ser2 is completely gone (p-Ser2 RNA pol II), similar to the protein level of RNA pol II. In contrast, Meriolin 36 induces time- and concentration-dependent changes of the phosphorylation signal (**Figure 38**). Comparing both Meriolins, Meriolin 16 treatment has a higher impact on this signaling than Meriolin 36. Possible explanations for this observation will be discussed in the discussion (**7.3 Meriolins**).

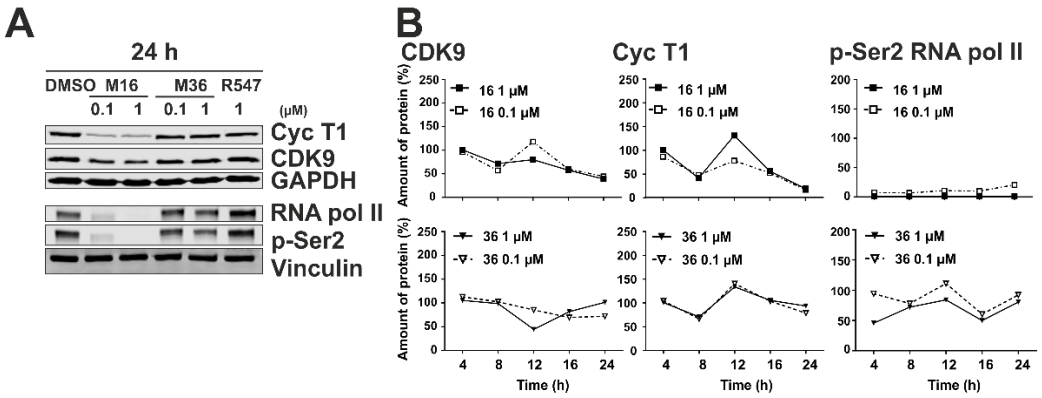

Figure 38 Meriolin 16 and 36 do alter CDK9/Cyclin T1 protein levels concentration depended. Meriolin 16 prevents the phosphorylation of Ser2 immediately, whereas Meriolin 36 affects this phosphorylation to a lesser extent. Ramos cells were treated with two different concentrations (0.1 and 1 µM) of each Meriolin 16 or 36, DMSO (0.1% v/v) as solvent control and R547 as another selective CDK inhibitor, for up to 24 h, the respective proteins of interest were analyzed via immunoblotting. For each time point the respective protein levels were analyzed via immunoblotting and subsequently quantified. Shown is one representative immunoblot after 24 h and the graphs originate from the quantification of each immunoblot for each time point. In **(A)** the immunoblotting after 24 h Meriolin treatment for the CDK9 /Cyclin T1 pathway and the protein level for RNA pol II with phosphorylation at Ser2 of RNA pol II is shown. In **(B)** the respective quantification of the protein levels of CDK9, Cyclin T1, RNA pol II and p-Ser2 RNA pol II (which gets phosphorylated by CDK9/Cyclin T1) over time is shown as amount of protein (%) over 4, 8, 12, 16 and 24 h.

Analyzing all three figures (**Figure 36**, **Figure 37 Figure 38**) leads to six conclusions: (i) Meriolin 16 and Meriolin 36 are not equally effective in targeting the cell cycle proteins, (ii) the effects of both derivatives are concentration-dependent, (iii) CDK and Cyclin protein level are not altered upon Meriolin treatment (except CDK9/Cyclin T1), (iv) p-CHK2 levels increase, (v) p-CHK1 levels decrease slightly and (vi) downstream phosphorylation targets of CDKs, as Rb and RNA pol II are dephosphorylated at specific phosphosites by Meriolin 16.

This comprehensive study enabled us to gain a deeper understanding of the downstream effects mediated by Meriolin treatment and subsequent CDK inhibition. Additionally, the differences between Meriolin 16 and 36 in terms of selectivity, specificity and concentration-

dependency, as well as time-dependent variations of the underlying molecular mechanisms became more obvious. The assumed causal relations will be discussed further below.

Meriolin 16 and Meriolin 36, disrupt the cell cycle, induce apoptosis and impair the downstream signaling of targets throughout the whole cell cycle. However, whether DNA damage is induced was not explored until then. Therefore, the two Meriolins were compared with the DNA damage inducing agents Camptothecin and Daunorubicin and with the apoptosis inducing substances Staurosporine and Etoposide. A comparison with the CDKi R547 is also shown in **Figure 39**. To determine their IC_{50} values Ramos cells were treated with increasing concentrations of either Camptothecin, Daunorubicin or R547 for 24 h (**Figure 39 A**). Camptothecin is a DNA topoisomerase inhibitor which prevents DNA re-ligation via its binding and stabilization of a complex composed of Camptothecin, topoisomerase I and the DNA complex, which ultimately causes DNA damage resulting in apoptosis [552]. Daunorubicin is an anthracycline antibiotic that is commonly used to treat acute lymphoblastic leukemia (ALL). It is proposed to inhibit macromolecule synthesis through intercalation into DNA strands [553, 554], produces ROS by interaction with molecular oxygen and inhibits topoisomerase II with the subsequent formation of DNA adducts and DSBs [555] (reviewed in [556]). Evaluated IC_{50} values reveal Camptothecin as the most cytotoxic compound (0.8 µM) (**Figure 39 A**). Meriolin 16 with (IC_{50} = 0.03 µM) and Meriolin 36 (IC_{50} = 3 µM) [443], show comparable cytotoxicity ranges with Camptothecin or R547 (IC_{50} = 2.3 µM). Next, the caspase-3 activation was determined with the highest DEVDase activity for Daunorubicin and Camptothecin. Meriolin 16 and Meriolin 36 are equally active, Etoposide and Staurosporine are less active and R547 displayed the lowest activity (**Figure 39 B**). As apoptosis readout for the activity of effector caspases, the PARP1 cleavage was determined via immunoblotting. After 24 h treatment, PARP1 was probed together with the DNA damage signaling proteins p27 and γh2ax (**Figure 39 C**). γh2ax is a biomarker for DSBs and is phosphorylated by ATM or ATR as first step in the recruiting and directing of DNA repair proteins [557]. The regulatory protein p27 is a negative regulator of CDKs and plays a crucial role in control of cell cycle and DNA damage response. p27 inhibits the activity of CDK2 and CDK4/6 complexes, preventing the phosphorylation of their target proteins and thereby blocking the G_1/S transition. Thus, p27 acts as a tumor suppressor by preventing uncontrolled cell growth and proliferation. In response to DNA damage, p27 can be induced by several stress signals, such as DSBs or oxidative stress. Once induced, p27 inhibits CDK activity, leading to cell cycle arrest and DNA repair. p27 also participates in the activation of the p53 tumor suppressor pathway, which is another key regulator of the DNA damage response as reviewed in the introduction [558, 559]. PARP1 was fully cleaved by Meriolin 16, 36 and Camptothecin after 24 h treatment. Incomplete cleavage was observed for R547 and Daunorubicin (**Figure 39 C**). Interestingly, Meriolin 36 showed an increase of γh2ax protein level after 24 h treatment, comparable with Daunorubicin. R547 and Camptothecin showed the

strongest increase in γh2ax protein levels. Meriolin 16 induces the phosphorylation of γh2ax between 3 to 12 hours (**Figure 39 D**). Subsequent analysis of the 53BP1 levels only showed an increase in signal intensity after 24 h, similar to the untreated control. Therefore, Meriolin treatment does not increase protein levels of 53BP1 as main mediator of DDR. Next, the formation of γh2ax and 53BP1 DNA repair foci was investigated. HeLa cells were treated with Meriolin 16 (IC_{25} = 0.04 µM (**Figure 39 E**). Experiments were performed during a laboratory rotation together with L. Schumacher at the Institute of Toxicology at Heinrich-Heine University Düsseldorf, RG Fritz). The IC_{25} value was chosen, since the cells HeLa cells detached from the microscopy slides during fixation, permeabilization and washing steps in previous experiments. This was probably due to the high rate of dying cells, which detach from the slide at too high concentrations (1 µM) and too long incubation times (24 h) as used in the previous experiments. Due to these issues, the IC_{25} value was used for these experiments. The colocalization of γh2ax and 53BP1 is used as a marker for DSBs induced phosphorylation of γh2ax (at Ser139) with subsequent recruitment of the damage sensor protein 53BP1 to the lesion [560]. The cells were treated with either DMSO as (solvent) negative control or Meriolin 16 for 24 h. Ionizing radiation (IR) with 10 Gy for 1 h served as positive control for the induction of γh2ax-53BP1 colocalizing foci, since IR is a well-known inducer of DSBs and the subsequent initiation of DNA damage response (**Figure 39 E**). After 24 h almost no γh2ax foci and a couple of 53BP1 foci were observed for the treatment with Meriolin 16 (**Figure 39 E**). In the positive control with 10 Gy IR, many γh2ax positive nuclei can be seen and only very few 53BP1 foci.

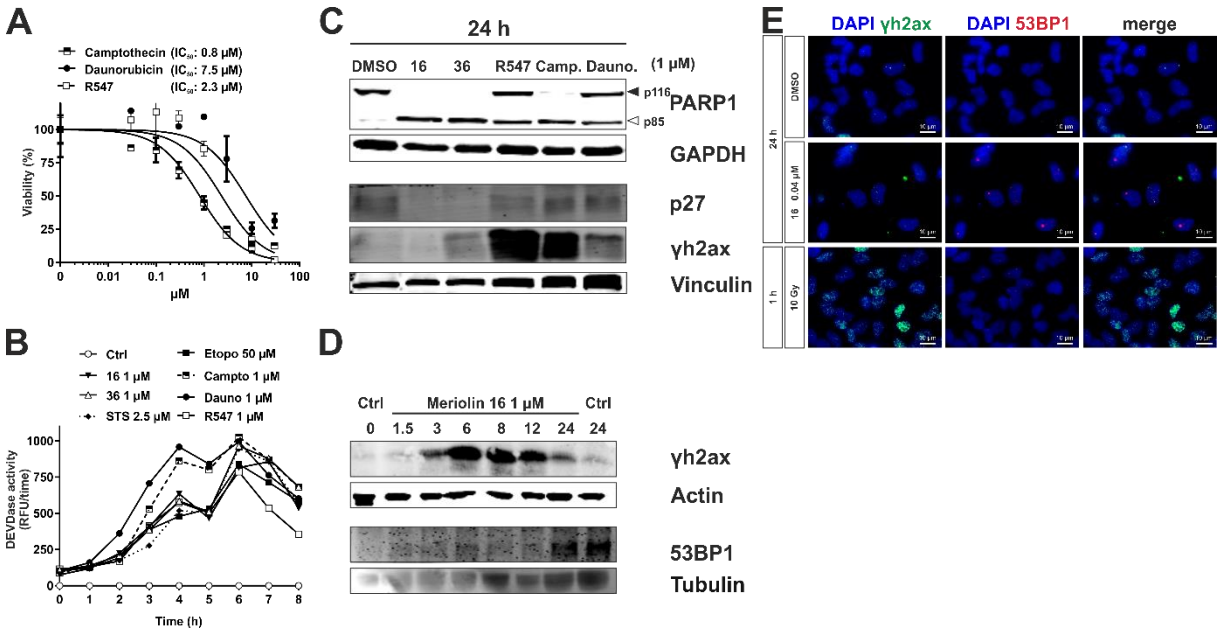

Figure 39 Comparison of Meriolins to DNA damaging substances with subsequent analysis of DNA damage induction. **(A)** Ramos cells were treated with increasing concentrations of R547, Camptothecin and Daunorubicin for 24 h, respectively. Subsequently, cell viability was monitored by AlamarBlue® assay. Shown in each graph is the mean ± SD of one representative experiment performed in triplicates. **(B)** Ramos cells were treated with 1 µM Meriolin 16, 36, Camptothecin (Campto), Daunorubicin (Dauno), R547, 2.5 µM STS, or 50 µM Etoposide (Etopo) over 8 h. The activation of caspase-3 was determined through fluorometric analysis of DEVDase activity. Shown in

each graph is the mean ± SD of one representative experiment performed in duplicates. **(C)** Ramos cells were treated with 1 µM Meriolin 16, 36, R547, Camptothecin, or Daunorubicin for 24 h. Via immunoblotting, the protein levels of PARP1 cleavage, p27 and γh2ax were determined. GAPDH and Vinculin served as loading control. **(D)** Ramos cells were treated with 1 µM Meriolin 16 over 24 h and the protein levels of γh2ax and 53BP1 were analyzed via immunoblotting; Actin and Tubulin served as loading control. **(E)** HeLa cells were treated with 0.04 µM Meriolin 16, DMSO as solvent control for 24 h, or with 10 Gy for 1 h as positive control to induce **γ**h2ax and 53BP1 colocalizing foci. With microscopy **γ**h2ax and 53BP1 colocalization was analyzed and representative images of two independent biological replicates are shown. (DAPI in blue, γh2ax in green, 53BP1 in red).

Evaluating these data, the question whether the Meriolins induce DNA-damage still remained not fully answered, since the analysis of γh2ax via immunoblotting revealed unambiguous results, as well as the γh2ax-53BP1 colocalization study. To address this, further analyses were performed measuring 5-ethynyl-2'-deoxyuridine (EdU) and 5-ethynyl-eridin (EU) incorporation (experiments were performed at the Institute of Toxicology, Heinrich-Heine University Düsseldorf, during a laboratory rotation in collaboration with L. Schumacher). In the EdU assay, the incorporation of EdU (thymidine nucleoside analog) into the DNA was measured and serves as a parameter of proliferation as shown in **Figure 40 A**. After 24 h incubation with the IC_{25} of Meriolin 16 or Meriolin 36, the cell proliferation as measured by EdU incorporation is reduced to residual 10% (**Figure 40 A**). A measurement for *de novo* RNA-synthesis is EU incorporation, which was measured for the same treatment conditions as in **A** (**Figure 40 B**). EU is a nucleoside analog of uracil, which is used to directly image spatially and temporally nascent global RNA transcription. Once incorporated into the RNA, EU can react with an azide-containing detection reagent, forming a stable triazole ring coupled to a fluorescent dye (thermofisher.com). EU was detected via microscopy, showing reduced EU incorporation down to ~60% for Meriolin 16. Meriolin 36 showed reduced values down to ~50%. In sum, both Meriolin derivatives impair DNA-synthesis as well as RNA-synthesis by treatment with nonlethal concentrations.

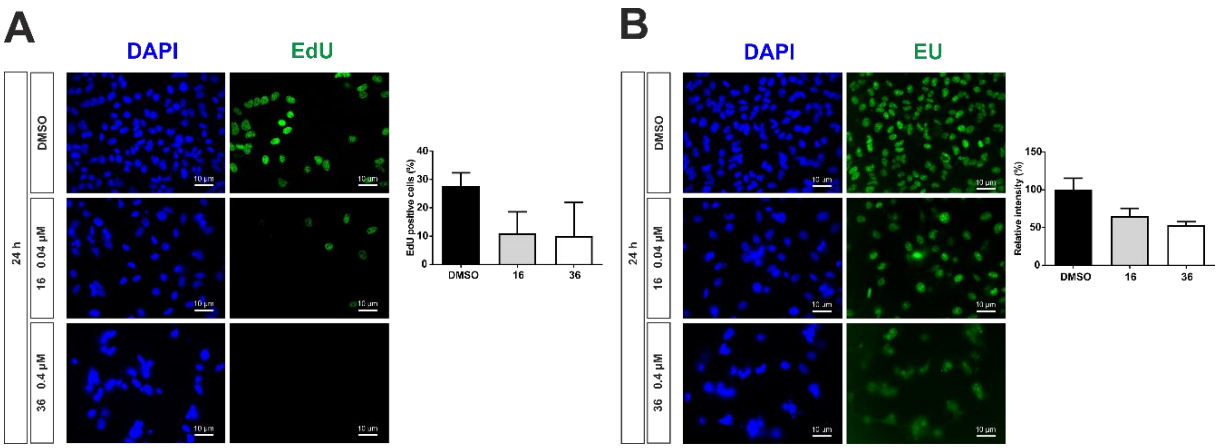

Figure 40 Impact of Meriolin 16 and 36 on *de novo* DNA and RNA synthesis. Analysis of Meriolin 16 and 36 treatment on DNA-synthesis measured by EdU incorporation **(A)** and RNA-synthesis measured by EU incorporation **(B)**. **(A)** HeLa cells were treated for 24 h with 0.04 µM Meriolin 16 and 0.4 µM Meriolin 36 which equals the IC_{25} for HeLa cells, respectively and DMSO served as solvent control. By immunofluorescence, the EdU-incorporation (green) was analyzed and is shown exemplary with microscopy images (DAPI in blue stains the nuclei). From different microscopy images, the EdU-positive

cells were counted and are shown as a bar graph as EdU-positive relative intensity in %. (Biological replicates n = 1-2; 10 cells were counted for DMSO, 30 for Meriolin 16, 22 for Meriolin 36). **(B)** HeLa cells were treated with the same concentrations as in (A) with Meriolin 16 (0.04 µM) and 36 (0.4 µM) and DMSO for 24 h. By microscopy, EU-incorporation (green) was determined and is shown exemplary with microscopy images (DAPI in blue stains the nuclei). From different microscopy images (biological replicates n = 2; 30 cells were counted for DMSO, 30 for Meriolin 16, 30 for Meriolin 36) DMSO-treated cells and their EU-incorporation was set to 100%, shown is the EU-positive relative intensity in %.

Finally, Meriolin 16 was shown to be more cytotoxic than its parental compound. Meriolin 16 and 36 are structurally different and both induce apoptosis and disrupt the cell cycle. They impair signaling pathways to different extents. Moreover, they are able to reduce DNA- and RNA-synthesis.

In summary, the new derivative Meriolin 16 was proven to be more cytotoxic in lower concentrations than previous derivatives. The broad bioactivity of Meriolin derivatives (16, 31 and 36) was characterized, ranging from the irreversible induction of intrinsic apoptosis, to the disruption of cell cycle and the dysregulation of cell cycle propagation. Finally, the effects of Meriolins on one target kinase family, the CMGC family (focus on CDKs), was characterized. Meriolin 16 and 36 are structurally different and exhibit distinct kinase inhibition selectivity resulting in differences in the bioactivity. The affected downstream pathways were characterized, i.e. the effect on regulator proteins of each cell cycle phase. Moreover, the crosstalk between cell cycle inhibition and DNA- and RNA-damage was demonstrated. The upcoming chapter will highlight the outcomes achieved for each individual project.

6.5 Key findings

6.5.1 Viriditoxin

i. The destabilization of mitochondrial ribosomes by VDT was shown in the thermal proteome profiling (TPP). However, this destabilization of mitochondrial ribosomes was shown not to be the primary reason underlying the efficacy of VDT in eliminating lymphoma cells.

ii. Analysis of the stabilized proteins, LRPPRC and GRSF1, revealed that both get stabilized in lymphoma cells (Ramos) with high concentrations of VDT. These proteins were shown to behave differently in three cell types upon different VDT concentrations. Moreover, both proteins colocalize with the outer mitochondrial membrane.

6.5.2 Bromoxib

i. Bromoxib is cytotoxic in lymphoma (Ramos) and leukemia (Jurkat) cells, it induces caspase-3 activity with subsequent PARP1 cleavage and apoptosis.

ii. Bromoxib targets selectively lymphomas in a lower concentration range than other cell types.

iii. Bromoxib does not induce the extrinsic death receptor pathway of apoptosis.

iv. Bromoxib does activate the intrinsic mitochondria dependent pathway of apoptosis.

   a. Bromoxib-induced apoptosis is inhibited in Bcl-2 overexpressing Jurkat cells.

   b. Bromoxib-induced apoptosis is dependent on caspase-9.

v. Bromoxib targets mainly the mitochondria:

   a. It induces rapid (within 5 min) and total breakdown of the mitochondrial membrane potential.

   b. It induces rapid fission/fragmentation of the mitochondria.

   c. The fission of mitochondria and the subsequent cleavage of OPA1 is reversible.

   d. The fission and cleavage of OPA1 is regulated by OMA1 and not YME1L1.

   e. It triggers Ca^{2+} total and intracellular mobilization, originating from the Endoplasmic Reticulum (ER) and the mitochondria.

   f. It does not induce rapid ROS production and later ROS production is not causative for cell death.

   g. Bromoxib inhibits significantly three complexes of the electron transport chain (ETC): complex II, III and the ATP-Synthase (complex V).

h. Bromoxib reduces intra cellular ATP-levels by targeting glycolysis and oxidative phosphorylation (OXPHOS).

i. Bromoxib induces breakdown of total cellular respiration as shown in Seahorse analysis.

j. Bromoxib alters intracellular localization of Hexokinase II, but does not reduce its protein levels and does not inhibit its activity.

vi. Bromoxib acts like a protonophore comparable to CCCP.

vii. Bromoxib induces the stabilization of several proteins as analyzed by TPP:

a. Analysis of tubulin proteins: Bromoxib does not disrupt the cell cycle and it does not decrease or increase tubulin polymerization.

b. Analysis of mitochondrial β-oxidation (FAO) proteins:

i. Bromoxib induces the stabilization of a protein cluster mediating FAO in the mitochondria: ACSL4, HADHB, HADHA, ECH1 and ACADVL.

ii. Bromoxib alters the total lipidomics in lymphoma cells and it impairs palmitate oxidation.

6.5.3 Meriolins

i. Meriolin 16 is more cytotoxic than its parental compound Meriolin 31, it induces caspase-3 activation and subsequent PARP1 cleavage more rapid than other Meriolins.

ii. Meriolins (16, 31, 36) do induce irreversible cell death within 5 minutes incubation.

iii. Meriolins (16, 31, 36) do not activate the extrinsic death receptor pathway of apoptosis.

iv. Meriolins (16, 31, 36) activate the intrinsic mitochondria dependent pathway of apoptosis.

a. Meriolin-induced apoptosis is not inhibited in Bcl-2 overexpressing Jurkat cells.

b. Meriolin-induced apoptosis is independent on Bax and Bak.

c. Meriolin-induced apoptosis is dependent on caspase-9 and Apaf-1.

v. Meriolins (16, 31, 36) disrupt the cell cycle.

vi. Meriolin 16 affects the downstream signaling of apoptosis mediating and cell cycle regulating proteins.

vii. Meriolin 16 and 36 inhibit kinases, mainly CDKs with concentrating-dependent selectivity and specificity.

viii. Meriolin 16 and 36 treatment induces p-CHK2 activation and does not induce p-CHK1 activation.

ix. Meriolin 16 treatment results in the failure of phosphorylation at the phosphosite (Ser612) at the main regulator protein of the cell cycle, retinoblastoma protein (Rb).

x. Meriolin 36 treatment results in an increase of protein level of this regulatory phosphosite (Ser612) at the main regulator protein of the cell cycle, retinoblastoma protein (Rb).

xi. Meriolin 16 treatment results in the rapid and complete dephosphorylation of a regulatory and activating phosphosite (Ser2) at the main regulator protein of the transcription, RNA pol II.

xii. Meriolin 36 treatment changes the phosphorylation at Ser2 of RNA pol II only in higher concentrations.

xiii. Meriolin 16 treatment revealed contrary results in the analysis of DNA damage parameters.

xiv. Meriolin 16 and Meriolin 36 were both shown to impair DNA- and RNA-synthesis.

7 Discussion

7.1 Viriditoxin

In our publication [1], the mitochondrial toxicity of VDT was confirmed and the identification of the molecular target was the main goal. The unbiased proteomic approach of TPP identified proteins whose thermal stabilities are impacted upon drug-binding. With mass spectrometry, the affected proteins' thermal profiles were analyzed and respective drug-targets were successfully identified. The destabilized protein candidates were analyzed and discussed in detail in our previous publication [1]. Briefly, VDT destabilized 43 proteins in Ramos cells, 20 of these belong to mitochondrial ribosomes (mitoribosomes). An analysis of the functionality of the mitoribosomes led to the conclusion, that VDT-induced apoptosis primarily was not mediated through the inhibition of mitochondrial protein translation.

Up to that point, the exact molecular target of VDT was still unknown and it was further aimed to address this point via investigation of the stabilized candidates. Thus, in this chapter, the potential of the two stabilized candidate proteins (LRPPRC and GRSF1) will be discussed. The data generated in this work showed, that both proteins colocalize to the mitochondria in HeLa cells. Given the selectivity of VDT in eliminating Ramos and SUPB-15 cells, the protein level analysis of LRPPRC and GRSF1 showed only different effects after 24 h in both cell lines. In Ramos cells for low concentration of VDT (1 µM), a total loss of LRPPRC and GRSF1 was observed, whereas for high concentration of VDT (10 µM) an increase for both protein levels was seen. This is interesting, since different VDT concentrations affect the protein levels distinctly. Exactly this observation was also true for HeLa cells after a shorter time of 4 h incubation with VDT. In HeLa cells an increase in GRSF1 was seen after 4 h and 24 h, whereas no effect on LRPPRC was detected for 4 h. The protein level of LRPPRC remained unchanged in SUPB-15 upon VDT treatment. The types of leukemia may share a common cellular origin *in vivo* (in patients) according to the hematopoiesis but the effect of VDT is probably different for every immortalized cancer cell line. Therefore a common mechanism of VDT across cell lines of Ramos and SUPB-15 can rather be excluded.

Regarding a potential correlation between destabilized and stabilized VDT-targets, there might be an overlap between the destabilized mitoribosomal proteins and mitochondrial mRNA transport and regulation by LRPPRC and GRSF1. It is known, that LRPPRC is involved in mRNA transport and regulation [476] and GRSF1 regulates post-transcriptional mitochondrial (mt) gene expression, required for the mitochondrial ribosome [561]. However, a VDT-mediated effect could be disturbed mitochondrial gene expression with an impaired mt-mRNA-transport to the mitochondrial ribosomes resulting in false or even no assembly of the mitochondrial

ribosomes. In the literature, the mitochondrial RNA metabolism is known to ensure proper expression of genes encoded by the mitochondrial genome, mitochondrial tRNAs and rRNAs [562]. Comparing the mitochondrial and the human genome, there are some differences: The mitochondrial genome does not have introns and mt-mRNAs are not 5'-capped. Also, mt-mRNA stability and translation is regulated different, here LRPPRC is one of the proteins implicated in stability and polyadenylation of mt-mRNAs [562, 563]. It was shown, that LRPPRC is critical in the regulation of mRNA stability in mitochondria and that the loss of LRPPRC leads to a dysregulated mitochondrial translation [563]. Furthermore, in *LRPPRC* knockout heart mitochondria, an increased biogenesis of mitochondrial ribosomes with higher levels of ribosomal proteins (MRPS15, MRPL13 and TFB1M) was observed [563]. Interestingly, we identified MRPS15 and other mitoribosomal small subunit proteins (in total 8) as well as mitoribosomal large subunit proteins (in total 12) as destabilized candidates [1]. An approach to test whether the effect of VDT on the MRPs and LRPPRC is correlated, would be an analysis of the stability of mtDNA-encoded mRNAs. The group of Ruzzenente *et al*. [563], showed, that LRPPRC is crucial for the stability of all mtRNA-encoded mRNAs except mt-ND6. *ND6* is a mitochondrial gene encoding the NADH-ubiquinone oxidoreductase chain 6, a subunit of the NADH dehydrogenase (complex I) located in the inner mitochondrial membrane. Thus, we could analyze in further experiments, if different concentrations and time points of VDT-treatment changes global mRNA levels, with mt-ND6 as negative control. Moreover, the stability of the mRNA stability regulating complex (~250 kDa), namely LRPPRC with SLIRP (SRA stem-loop interacting RNA binding protein), could be analyzed after VDT-treatment with size-exclusion chromatography as shown in [563].

For GRSF1 it is known, that it preferentially binds RNAs transcribed from three genes, the *ND6*, *cytb* and *ND5* mRNA [561]. Additionally, GRSF1 localizes to granules containing newly synthesized RNA in close proximity to mitochondrial nucleoids. It coordinates post-transcriptional mRNA storage and the loss of GRSF1 results in errors in RNA transport onto the mitoribosome with translation defects [561]. The protein was shown to be localized to the mitochondria, which I also showed by immunofluorescence. A visually observable effect of VDT on GRSF1 localization or also granules would probably need a longer VDT exposure, which should be included in further experiments. Since GRSF1 was named together with LRPPRC and SLIRP as a group of proteins involved in mitochondrial RNA metabolism, it would be suggested to analyze LRPPRC and GRSF1 with the same experimental procedures in parallel.

Finally, the targets of VDT are not fully evaluated yet. Therefore, this project and experiments described above will be incorporated in the postdoc project of the author of this thesis incorporated in the RTG 2158 together with Dr. Bhatia (Department of Pediatric Oncology, Hematology & Clinical Immunology). Furthermore, it is intended to further validate and

characterize LRPPRC and GRSF1 as target(s) of VDT and also to test the therapeutic potential of VDT *in vivo* using established mouse models (genetic engineered mouse model (GEMM), patient-derived xenograft model (PDX)) in the RTG 2158, in the research group of Dr. Bhatia.

7.2 Bromoxib

The natural compound P01F08 (Bromoxib) was identified in a screening, of 300 natural compounds, with the objective to identify natural products exhibiting cytotoxic activity against chemotherapy-resistant tumors and microorganisms [441]. In our publication [2], I analyzed the literature of the last 40 years about polybrominated diphenyl ethers (PBDEs), summarizing the bioavailability, structural diversity of natural and synthetic PBDEs with their broad bioactivity against some bacteria, fungi and cancer cells [2]. Furthermore, I validated the time- and concentration-dependent cytotoxicity of P01F08 (Bromoxib) and its apoptosis induction capacity [2]. The results shown above revealed the underlying molecular mechanism with the manifold bioactivity pattern of P01F08, which was then termed Bromoxib. The name 'Brom-ox-ib' originates (i) from its structure as a polybrominated diphenyl ether ('Brom') and (ii, iii) from its oxidative phosphorylation ('ox') inhibitory function ('ib'). In this discussion, three major points will be highlighted: First, the link between its protonophoric characteristics on mitochondria and/or the ER; second, the correlation between the inhibitory effects on the ETC, OXPHOS and glycolysis; and third, the therapeutic potential of targeting the mitochondrial β-oxidation (FAO) in cancer cells.

7.2.1 Bromoxib as a protonophore – are rapid events the trigger of apoptosis?

I showed, that Bromoxib exhibits characteristics comparable to those of CCCP and that their cytotoxicity, caspase-3 activity and apoptosis level are in a similar range. The IC_{50} value of Bromoxib in Ramos cells is 4.98 µM, whereas for CCCP its 4.96 µM. Both agents induce caspase-3 activation in the same kinetics and rate, similar to the apoptosis induction after 24 h. Besides these similar apoptosis-features, Bromoxib induces the breakdown of the mitochondrial membrane potential in the same kinetics as CCCP (within only 5 minutes). In addition to these effects, Bromoxib has the same protonophoric characteristic to induce the reversible cleavage of L-OPA1 into S-OPA1 forms, when the compound is removed, the L-OPA1 forms recover over time. Consequentially, Bromoxib acts like a protonophore similar to CCCP. The CCCP-underlying mechanism responsible for mitochondrial dysfunction is as follows: CCCP is an inhibitor of mitochondrial OXPHOS, since it uncouples the electrochemical proton gradient by transporting protons across the IMM, interfering with the proton gradient [465]. It depolarizes the membrane and reduces the ATP production with affecting cellular metabolism, finally resulting in cell death [463, 465].

One must consider that there are significant distinctions between traditional protonophores such as CCCP and mitochondrial (un-)couplers, which are primarily proteins. The first family

of uncoupling proteins (UCPs), are UCP-1 to UCP-5 of which UCP-1 is localized as a transmembrane protein in the IMM catalyzing the transport of protons across the membrane and thereby uncoupling the mitochondria [490, 564]. The function of UCP-1 is regulated, it is inactivated via the binding of purine nucleotides (GDP) and activated by free fatty acids (FFAs) promoting a UCP-1 dependent proton leak [564-566]. Regarding the exact mechanism of UCP-1, different models exist, which are discussed in a dedicated review [567]. The second family of uncoupling proteins are adenine nucleotide transporter (ANTs), which are also transmembrane proteins that catalyze ATP/ADP exchange across the mitochondrial membrane. Due to the nucleotide-dependent function to export ATP into the cytosol, they have a central role in energy metabolism [568]. Besides that, ANTs were also assumed to exhibit uncoupling properties depending on the transport of fatty acids [569, 570]. However, the initial description of ANTs was restricted as reviewed in the introduction, to its functional involvement in the mPTP induced by Ca^{2+} (**1.3 Intrinsic apoptosis pathway**). The binding of Ca^{2+} to cardiolipin, was thought to be responsible for the ADP/ATP carrier-pore conformation change which the mPTP undergoes upon activation [568, 571]. Brustovetsky and Klingenberg state that the opening of the channel is Ca^{2+} dependent and can be reversibly closed by removal of Ca^{2+} [571]. This is interesting, since both, CCCP and Bromoxib induce the cleavage of L-OPA1 forms with subsequent fragmentation of the mitochondria. This is one common feature of protonophores, which was shown to be reversible since the L-OPA1 forms recovered over time. Further cytotoxicity analyses about the reversibility of Bromoxib showed, that 5 and 15 min Bromoxib treatment with subsequent removal and further 24 h incubation were not sufficient in reducing the cell viability compared to 24 h treatment without removal (data not shown). The correlation between the reversible effects of Bromoxib to the mitochondria with the reversible cytotoxicity leads to the suggestion, that whatever happens within the first up to 15 min of Bromoxib treatment, it seems to be reversible and not sufficient in priming the cells to death. In contrast to other natural product mitotoxins such as Phomoxanthone A, which was shown to disrupt the form and function of IMM with 5 min incubation being sufficient to prime the cells to die [492].

When Bromoxib is incubated for 24 h without removal, the summary of all events induced by the drug are thought to reach a certain threshold with subsequent cell death induction. Therefore, it is assumed, that Bromoxib acts either like a protonophore, shuttling protons across membranes (mitochondria and ER) or it targets specifically an uncoupling protein like UCP-1 or ANT-1. The experimental basis for a protonophoric activity of Bromoxib is given by the rapid breakdown of $\Delta\Psi m$, fission, L-OPA1 cleavage, and dependent on OMA1 and also mobilization of Ca^{2+}. Evidence, that Bromoxib might target an uncoupling protein is based on the observation that it causes the rapid breakdown of $\Delta\Psi m$, induces Ca^{2+} mobilization from two organelles and targets ATP-levels of OXPHOS and glycolysis and last but not least, that Bromoxib treatment results in the stabilization of proteins mediating mitochondrial FAO.

When considering these hypotheses, it appears that Bromoxib exhibits protonophoric characteristics and mediates effects more prone to originate from an uncoupling-protein-targeting like mechanism. Further experiments should include analyses of the protein levels and functionality of UCP-1 and ANT-1 after Bromoxib treatment.

In summary, Bromoxib mimics a concentration-dependent energy demand by stimulating the respiratory chain to operate at maximum capacity in order to meet this artificial metabolic need via rapid oxidation of substrates (which is also shown for FCCP [506]). Examples of substrates that are quickly oxidized to meet elevated metabolic demands include fatty acids, as outlined in the introduction (**1.6.4 Mitochondrial fatty acid β-oxidation**). The connection between Bromoxib and its impact on mitochondrial β-oxidation will be explained in **7.2.3 Bromoxib targets the mitochondrial β-oxidation (FAO)**. It can be concluded, that Bromoxib acts like a protonophore with additional features that will be debated in the following.

It was aimed at unraveling the molecular mechanism of cell death induction by Bromoxib. A known trigger of mitochondrial apoptosis is the rapid break down of ΔΨm with subsequent fission of the mitochondria. As reviewed in the introduction, fission is regulated by the Ca^{2+}-dependent dephosphorylation of DRP1 catalyzed by the phosphatase calcineurin, driving DRP1 association and mitochondrial scission [135]. Bromoxib-induced Ca^{2+} mobilization could be one driver of mitochondrial fission. This should be elucidated in further experiments, by immunoblotting the phosphosite Ser637 whose dephosphorylation is responsible for DRP1 activation [135]. Other regulators of mitochondrial fission are the proteases OMA1 and YME1L1 as reviewed in the introduction (**1.3.1 Mitochondrial dynamics in apoptosis regulation**). Bromoxib induced mitochondrial fragmentation and cleavage of L-OPA1, which was regulated by the IMM metallopeptidase OMA1 and not YME1L1. Both proteases operate under distinct physiological circumstances as described in the following. OMA1 is activated by various homeostatic changes, for example the loss of mitochondrial membrane potential, heat or oxidative stress [136, 572-574]. It converts all L-OPA1 isoforms into the short version, prompting IMM fission and subsequent separation of the mitochondrial network. OMA1 has minimal or no involvement in L-OPA1 processing under normal conditions. YME1L1 is the key protease mediating L-OPA1 processing under non-stress conditions. Its activity generates approximately equal amounts of long and short OPA1 isoforms, which are necessary for achieving an optimal balance between mitochondrial fusion and fission [122, 136, 138, 448, 574]. It can be concluded for Bromoxib, that the underlying initial trigger, for OMA1-dependent cleavage of L-OPA1, is the loss of mitochondrial membrane potential as primary event.

Intrinsic mitochondria dependent apoptosis is closely interconnected with the homeostasis of the mitochondrial network. Thus, the pro-apoptotic proteins Bax and Bak were shown to be primary important in balancing together with DRP1 mitochondrial fission since Bax and Bak promote DRP1 stabilization [145]. Therefore, we collaborated with the RG Garcia-Saéz (CECAD

Cologne) in an external collaboration and they measured the translocation of GFP-tagged Bax and mCherry-tagged SMAC (data not shown). Bromoxib induced the translocation of Bax to the mitochondria within 120 min and the release of pro-apoptotic SMAC was observed also within 120 min. Therefore, a Bax-dependent induction of intrinsic apoptosis was assumed. This is supported since Bromoxib induced caspase-9 dependent intrinsic mitochondrial apoptosis, even in the presence of Bcl-2 overexpression. However, Bromoxib treatment induces rapid effects, which finally led to the induction of intrinsic mitochondrial apoptosis as downstream cascade. The immediate effects, (without any pre-incubation of Bromoxib and readout within 60 min) such as rapid breakdown of ΔΨm, L-OPA1 cleavage, mitochondrial fragmentation, Ca^{2+} release from the ER and mitochondria, the inhibition of ETC complexes II, III and V with the depletion of cellular ATP level and finally the total breakdown of mitochondrial respiration via an uncoupling of the proton gradient, were discussed above and thought to result partially from its protonophoric activity. Thus all events cumulating lead to the transmission and integration of pro-apoptotic stimuli (Bax translocation, Ca^{2+} caused mPTP opening, ΔΨm breakdown) at the mitochondria resulting in the final release of pro-apoptotic factors.

The increase in cytosolic Ca^{2+} serves as an intracellular stimulus for increased permeability of the IMM to solutes with a loss of the ability to synthesize ATP [169]. Bromoxib caused an even higher total Ca^{2+} mobilization than Ionomycin, which is an ionophore known to induce mPTP formation [493]. To determine whether the depletion of Mito-and/or ER Ca^{2+} stores is responsible for the activation of intrinsic mitochondrial apoptosis, the cells could be pre-treated with Cyclosporin A (CsA; binds to CypD and inhibits mPTP opening) [79, 80] followed by treatment with Ionomycin or Bromoxib and the Ca^{2+} mobilization could be measured and also the cell viability (after 24 h) could be determined. This would answer whether Ca^{2+} mobilization is the main underlying reason (and not the breakdown of the proton gradient) activating the apoptosis cascade or an additional trigger. What is also unknown in the storyline, is, whether Bromoxib activates the ER stress pathway next to mitochondrial dependent intrinsic apoptosis, which was briefly introduced in (**1.3.2 Interactions with other organelles – ER-mitochondria interactions**) as unfolded protein response (UPR). Therefore, the effect of Bromoxib on key proteins of the UPR, such as phosphorylation of eIF2α at Ser51 with subsequent activation of the transcription factors ATF4 and CHOP could be analyzed in further experiments via immunoblotting [575, 576].

Following the apoptosis cascade as described, Bromoxib induces as cell permeable small compound the intrinsic mitochondrial dependent apoptosis pathway. From the data it was concluded, that the primary event is the rapid breakdown of mitochondrial membrane potential as trigger for the activation of OMA1-dependent processing of L-OPA1 forms and subsequent fission of the mitochondria. In a similar kinetic (for Bromoxib unidentified) BH3-only proteins inhibit anti-apoptotic Bcl-2 and induce pro-apoptotic Bax (and Bak) to form the MOMP,

releasing pro-apoptotic factors such as SMAC (or cytochrome c). The data allow the assumption that the Ca^{2+}-dependent mPTP opening also occurs, releasing solutes and ions, in addition to the MOMP formed by Bax and Bak. The released pro-apoptotic factor cytochrome c activates and forms together with dATP, Apaf-1 and procaspase-9 the apoptosome, activating caspase-9, which then in turn activates the effector caspases (-3 and -7). Finally, leading to cell shrinkage, chromatin condensation, and fragmentation of the nucleus and blebbing of the membrane with the final formation of apoptotic bodies.

7.2.2 Bromoxib inhibits the ETC, OXPHOS and impairs glycolysis

Bromoxib induces intrinsic mitochondrial apoptosis, with harming the mitochondria as its primary target organelle. In this paragraph, the connection between the effects of Bromoxib on ETC, OXPHOS and glycolysis will be discussed. Bromoxib inhibits complex II, III and V activity, the single inhibition of each complex probably has significant implications for the maintenance of energy balance but it is probably not sufficient causing cell death.

Bromoxib was shown to inhibit the succinate dehydrogenase (SDH) (complex II), which is a crucial element of both the ETC and TCA. Within the TCA cycle, complex II plays a key role in the conversion of succinate to fumarate [577]. In the ETC it serves as an additional gateway for electrons, transferring them through iron-sulfur clusters from succinate to coenzyme Q as reviewed in the introduction. The fact, that Bromoxib inhibits complex II primed me to test other complex II inhibitors on their cytotoxicity, such as Lonidamine [578] and 3-Bromopyruvate [495, 499] showing that none of them reduced the cell viability of HeLa cells (tested up to 30 µM) (in HepG2 cells the IC_{50} value published is 150 µM [579]), whereas in Ramos cells 3-Bromopyruvate exhibited an IC_{50} value of 11.02 µM. In the literature, the subunit D of SDH (SDHD) was shown to be especially important for proper function of total complex II, since it anchors the complex to the IMM and transfers the electrons [577]. In a CRISPR/Cas9-generated knockout of SDHD, the knockout exhibited suppressed mitochondrial respiration, impaired glycolytic capacity, decreased ATP-synthesis with a higher susceptibility to apoptosis [577]. Thus, it seemed likely, that the inhibition of complex II by Bromoxib could result in suppressed mitochondrial respiration and subsequent inhibition of ATP-synthesis. The other two complexes that were inhibited by Bromoxib will also be discussed in their importance for the ETC in the following. Complex III is the coenzyme Q-cytochrome c reductase complex which transfers electrons to cytochrome c, which then moves the electrons to complex IV [580]. Regarding the generation of ROS, complexes I, II and III generate superoxide [581], complex I and II within the mitochondrial matrix and complex III into either the IMS or the matrix [582, 583]. An analysis in cells stably expressing cytosolic- or mitochondria-targeted reporter molecules sensitive for pH and/or H_2O_2 showed that the inhibition of complex I (with Rotenone) and III (with Antimycin A) increased

only cytosolic H_2O_2 levels and did not affect mitochondrial levels [584]. The total and mitochondria-specific lipid peroxidation was not increased as measured by MitoPerOx biosensors and C11-BODIPY$^{581/591}$ [584]. However, an increase in ROS levels was detected and concluded to be less than the stress-inducing level since no oxidative stress and no cell death was induced [584]. In terms of Bromoxib, an analysis of ROS levels showed the loss of fluorescence of the dye for a high concentration of 10 µM and no ROS induction at 1 µM (within 5 and 30 min). H_2DCF-DA is a fluorogenic dye that enables the measurement of peroxyl-, hydroxyl and other ROS species within the cell. The procedure is based on diffusion of the dye into the cell with intracellular deacetylation by esterases to a non-fluorescent compound, which can be oxidized by ROS to 2',7'-dichlorofluorescein (DCF) and is detected at 488/530 nm [585]. Bromoxib does not induce ROS within 5 or 30 min. The cells seem to lose the dye after 30 min Bromoxib treatment, suggesting that Bromoxib somehow opens the cell membrane at high concentrations or increases permeability of the cell membrane. Later occurring ROS events and their influence on cytotoxicity were shown to be not responsible for the toxicity of Bromoxib, since the pre-and co-treatment with the antioxidant and ROS scavenger NAC was not able to reduce the cytotoxicity.

Complex V, the F_1F_0 ATP synthase is the final acceptor of electrons, with pumping of protons from IMS to matrix, generating the proton gradient which finally drives ATP synthesis [321]. Bromoxib inhibited the ATP synthase to a residual activity of 40%, which is thought to be due to an uncoupling of the proton gradient by its protonophoric activity similar to CCCP [586]. However, the cell is significantly harmed by the inhibition of ATP synthase function, which is another lethal event targeting the total mitochondrial metabolism. The effect of Bromoxib on ATP levels was supported by the calculations from OCR measurements (seahorse mito stress test analysis), where the ATP production was reduced to residual 5% after Bromoxib treatment. Additionally, Bromoxib reduced cellular ATP levels, measured with the luminescence based ATP assay (ToxGlo^{TM} assay; Promega). The assay was performed in glucose-supplied medium for the measurement of total ATP generated by mitochondrial OXPHOS and glycolysis. It was also performed in galactose-supplied medium in order to increase cellular oxygen consumption and to increase non mitochondrial ATP production by glycolysis. Bromoxib reduced cellular ATP levels under both conditions as unique feature, since none of the used controls behaved similar. The ATP level under glucose-condition drops because Bromoxib inhibits the ETC and OXPHOS, consequentially no more ATP is synthesized. Why the ATP level under galactose-condition drops was unclear. It was hypothesized that Bromoxib influences non mitochondrial ATP production due to its inhibition of complex II. In the literature a similar phenomenon was described for a compound that inhibits complex II and hexokinase II, a key enzyme of the glycolysis. The compound is 3-Bromopyruvate and it exhibits manifold bioactivity [72, 426, 428, 495-499, 587-589], some of which are very similar to Bromoxib.

A common mechanism of Bromoxib and 3-BP was hypothesized since 3-BP is an inhibitor of complex II inhibiting ETC dependent ATP-levels and glycolytic ATP-levels via its inhibition of HK II. This hypothesis was excluded, since Bromoxib inhibits ETC complex III and V (besides II) and does not inhibit HK II activity, dissimilar to 3-BP. Other HK II inhibitors such as Lonidamine and Clotrimazole were not cytotoxic similar to 3-BP. These three substances did neither induce any caspase-3 activity nor apoptosis (data not shown). Thus, a similar mechanism of Bromoxib to 3-BP was excluded.

Consequentially, the question how Bromoxib influences non mitochondrial ATP-levels remained still unanswered. The current hypothesis is, that Bromoxib damaged the mitochondria to a major extent, that the TCA within the mitochondria cannot be catalyzed. This is supported by the fact, that the succinate dehydrogenase (complex II) is inhibited by Bromoxib and the continuous exchange of FAD/$FADH_2$ substrates between ETC and TCA cannot be maintained.

Another fact supports this hypothesis, because the protein dihydrolipoyl dehydrogenase (DLD) is the most stabilized protein of the TPP analysis with a thermal stabilization (ΔTm) of 11.6 and the highest F-statistic $_{observed}$ of 239.4. Consequentially, it is considered as the primary target of Bromoxib. The methodological approach of TPP aims on identifying proteins by direct binding of the drug to its target resulting in an increased thermal stabilization. Here, DLD was the most stabilized protein upon Bromoxib treatment and it has various functional implications. It is a flavoprotein that functions as an E3 component in complexes with pyruvate dehydrogenase, α-ketoglutarate, α-adipate or branched-chain amino acid dehydrogenase, all localized in the mitochondria matrix. In these complexes it catalyzes the oxidation of dihydrolipiamide and NAD^+ to lipoamide and NADH [590-592]. Interestingly, DLD was identified as a moonlighting protein which are defined as proteins that are able to perform several mechanistically different functions [591]. In the pyruvate dehydrogenase complex, it is involved in regulating the flux of acetyl from pyruvate through acetyl-CoA into the Krebs cycle [590]. DLD participates by reducing NAD^+ to NADH, it facilitates the oxidation of reduced lipoyl moieties, thereby priming them for another round of catalytic reaction [590]. Here the reason for the impact of Bromoxib on the TCA cycle could be found, since a proper supply of acetyl-CoA for the TCA is not mediated if DLD is inhibited by a putative direct binding to Bromoxib. Furthermore, DLD is a component of the α-ketoglutarate dehydrogenase complex, where it is part of one of the main TCA regulating proteins. The reaction catalyzed by the α-ketoglutarate dehydrogenase complex is the conversion of α-ketoglutarate together with NAD^+ and CoA to succinyl-CoA, CO_2 and NADH [593]. The stabilization of DLD upon Bromoxib treatment could be either inhibitory or enhancing its functions. From the cellular effects observed upon Bromoxib incubation it can be concluded, that DLD activity seems to be rather inhibited, since downstream, the cellular non mitochondrial ATP levels are decreased. This is probably due to the inhibition of DLD as one

putative target of Bromoxib and thereby the targeting of TCA regulating enzymes (α-ketoglutarate dehydrogenase or the pyruvate dehydrogenase). To validate this hypothesis further experiments analyzing the metabolic state of the cell should definitely be performed. In the literature it is suggested to measure the auto-fluorescence through imaging of FAD [594], which has a excitation in spectral region shorter than 420 nm [595, 596]. Another experimental approach would be the measurement of TCA metabolites as shown in [597] via LC-MS/MS for anionic and cationic metabolites.

Additionally, glycolysis could also be impaired and be the reason for the drop of ATP-levels. To probe glycolysis, the glycolysis stress test could be performed (measured by seahorse XF analyzer). The glycolysis stress test is a common technique used to investigate glycolysis. During this test, glucose, Oligomycin, and 2-deoxyglucose (2-DG) are sequentially injected through ports while measurements are taken. Glucose is used to fuel glycolysis, and the difference in ECAR before and after addition of glucose provides a parameter for the glycolytic rate. Oligomycin, on the other hand, is an ATP synthase inhibitor, resulting in a decrease in the ATP/ADP ratio, promoting glycolysis. The difference in ECAR before and after Oligomycin injection represents the cell's glycolytic reserve capacity. Finally, 2-DG serves as a baseline ECAR measurement by inhibiting glycolysis. The ECAR after the addition of 2-DG accounts for the cell's non-glycolytic ECAR as reviewed in [598].

7.2.3 Bromoxib targets the mitochondrial β-oxidation (FAO)

Minor ATP synthesis is mediated by glycolysis, the majority is in healthy cells produced in the mitochondria by TCA and OXPHOS. The mitochondrial fatty acid β-oxidation is the most efficient pathway to procure energy in form of ATP. As described in the introduction, free fatty acids are translocated into the mitochondria in order to undergo β-oxidation producing acetyl-CoA, which is fueled into TCA. The TPP identified the FAO-protein-cluster as stabilized target-cluster upon 30 min treatment with Bromoxib. Via immunoblotting, lipidomics and the measurement of fatty acid oxidation this FAO-protein cluster was validated as metabolic target of Bromoxib. Hence, a direct interaction is very unlikely, since five proteins of the whole metabolic pathway were found to be stabilized. Therefore, the stabilization of this protein-cluster will be interpreted and discussed as cellular response to the damage caused by Bromoxib treatment. The question – why does the cell activates selected proteins in the pathway of mitochondrial β-oxidation? – aroused and will be discussed in the following. The most stabilized proteins were ECH1 and ACSL4, followed by HADHA, HADHB and least stabilized ACADVL as seen in the TPP. When looking at the total pathway of FAO, ACSL4 is the primary enzyme catalyzing the activation of the FA with CoA to FA-CoA – thus a very important step in activating the whole process of degrading FAs. Why would the cell

stabilize/activate the FAO within 30 min? It was discussed and concluded in the previous chapters, that Bromoxib depletes the cell of ATP via several rapid mechanisms followed by the final activation of apoptosis. It is thought, that the cell tries to activate FAO as a rapid self-rescue mechanism in order to compensate the increasing high energy demand induced by Bromoxib.

This hypothesis was supported by the data shown in the results chapter. The activation of FAs is mediated by ACSL4 whose protein level is increased after 30 min with an increase of the intramitochondrial metabolization machinery initiated by ECH1, whose protein level is also upregulated significantly. Further supporting evidence is found in the analysis of lipidomics data. Bromoxib induced within 30 min a significant increase in specific glycerophospholipids: LPC, PC, PE and it significantly decreases CLN.

Glycerophospholipids are usually components of cellular or vesicle membranes but also involved in signaling, the most important glycerophospholipids are PC, PE and PI [599, 600]. They regulate cellular signaling via G-protein coupled receptors or ion channels [599]. A significant decrease of CLN upon Bromoxib treatment was observed. CLN is a major component of mitochondrial membranes, especially in the inner membrane, where it mediates membrane protein stability and curvature of the IMM [103, 600]. Studies have demonstrated that CLN is essential for optimal functioning of multiple mitochondrial carrier proteins such as ANT, phosphate carrier (PiC), pyruvate carrier, tricarboxylate carrier and the carnitine/acylcarnitine translocase (CACT) with which it interacts [601, 602]. This is especially interesting, since the ANTs are known to be part of the mPTP, which opens upon increasing Ca^{2+} levels. Bromoxib targets mainly the mitochondria, thus a decrease in CLN levels is not surprising. This phospholipid is especially important for mitochondrial cristae morphology and stability [105, 106]. CLN was found to be prone to peroxidation due to its high content of unsaturated fatty acids [603]. In addition CLN is located in the IMM near the ETC complexes, the main site of ROS production [602]. Paradies *et al*. postulated, that changes in the CLN profile could have a detrimental effect on the function and dynamics of mitochondria [103]. Consequentially, it is assumed, that Bromoxib targets the mitochondrial membrane leading to a decrease of CLN and thereby impairs the function and dynamic of mitochondria.

Bromoxib did not alter levels of glycerides (DGs or TGs). It increased significantly the level of free fatty acids and also the level of free cholesterol (nonglycerides). From these data it is concluded, that Bromoxib destabilizes the metabolic state of the cell and thereby induces the mobilization of free fatty acids (from lipid droplets) in order to degrade them during FAO for ATP production. The free fatty acids are increased upon Bromoxib treatment and get rapidly activated by ACSL4, in order to get transported into the mitochondria. This mechanism is known for tumors, since FAO was widely recognized to act under metabolic stress in order to fuel the tumor proliferation and growth [353].

Along with free fatty acids, also an increase of free cholesterol was found. Cholesterol itself is an important constituent of the cell membrane, thereby it could directly activate oncogenic signaling, i.e. the Hedgehog pathway via G-protein-coupled receptors [604-606]. An increase in free cholesterol might be associated with a loss of membrane integrity due to the protonophoric features of Bromoxib or due to an increase in signaling.

Some tumors are highly dependent on FAO, such as diffuse large B cell lymphoma [607, 608] or prostate cancer [609]. In the literature, pharmacological or genetic inhibition of FAO affected ATP supply and impaired cell proliferation as shown in Burkitt lymphoma [610], glioblastoma [611] and PC3 prostate cancer [609]. The inhibition of FAO (with Etomoxir or Ranolazine) blocked cell proliferation and sensitized leukemia cells to apoptosis induction by ABT-737 (BH3 mimetic, that facilitates the release of Bak from their anti-apoptotic interaction partners) [612]. The FAO inhibition via Etomoxir (blocks entry of FAs into mitochondria by inhibiting CPT1) combined with the pro-apoptotic molecule ABT-737 decreased tumor burden and improved survival significantly in a murine leukemia model (nude mice xenografted with GFP^+/luciferase-bearing MOLM13 human leukemia cells) [612]. Furthermore, these results indicated a close association between FA metabolism, leukemia cell growth and apoptosis [612]. In terms of apoptosis induction, the inhibition of FAO was shown to facilitate Bax and Bak oligomerization and subsequent MOMP opening [612]. The outcomes of this study provided evidence to assess the effectiveness of FAO inhibitors in curing leukemia.

ST1326, also an inhibitor of CPT1, was tested in *in vitro* and *in vivo* models of Burkitt lymphoma, which overexpressed c-myc and exhibited subsequently increased FA metabolism (study performed in Raji cells) [610]. Metabolic studies in Raji cells were conducted and measurement of oxidation of [1-^{14}C]palmitate, distinguishing labeled CO_2 and acid-soluble metabolites derived from acetyl-CoA processing, were performed [610]. Total palmitate oxidation is the sum of the metabolism toward acid-soluble metabolites and CO_2 [610]. Interestingly, the group found [1-^{14}C]palmitate oxidation to be reduced in a dose-dependent manner upon ST1326 treatment in agreement with a reduction of both, the total oxidation as well as CO_2 and acid-soluble metabolites [610]. The effect on the FA oxidation is here mediated due to the decreased activity of CTP1by ST1326 [610]. Furthermore, the cytosolic ATP-levels were not impaired under these conditions supported by the phosphorylation status of the energy sensing kinase Adenosine monophosphate (AMP)-activated kinase (AMPK), which was not phosphorylated [610]. In summary, the group showed, that CPT1 inhibition induced cytotoxicity in Burkitt B cell lymphoma, but the cytotoxicity is not due to the inhibition of energy procuring mechanisms [610].

The measurement of [^{14}C]-CO_2 as total palmitate oxidation and of the [^{14}C]-Acid soluble metabolites as partial palmitate oxidation performed by our collaboration partner (Dr. X. Buqué, RG Aspichueta) revealed that Bromoxib increased the accumulation of acid soluble

metabolites significantly. This result is completely different from that of ST1326 (CPT1 inhibition). It can be concluded from the data described in [610], that an import-inhibition of FAs into the mitochondria by targeting CPT1 activity, is not sufficient for depleting ATP levels and causing cell death in Burkitt lymphoma cells. In accordance with this, Bromoxibs prime target in the FAO might not be in the cytosol, thus ACSL4 stabilization might not be the most prominent effect. However, an upregulation of ACSL4 in chemotherapy-resistant tumors was found to be an acetylated-STAT3-mediated effect resulting in increased phospholipid synthesis [354]. Elevated phospholipid levels in mitochondrial membranes are thought to lead to an increased mitochondrial integrity to overcome chemotherapy-induced apoptosis [354].

Of greater importance is the significant enhancement of FA metabolization within the mitochondrial matrix, as all four enzymes responsible for FAO catalysis within the matrix are stabilized by Bromoxib (with ECH1 being the most stabilized enzyme). It can be concluded, that the accumulation of [^{14}C]-Acid soluble metabolites upon Bromoxib treatment resulted from an increased partial palmitate oxidation within the mitochondrial matrix. Consequentially, the cell stabilizes and upregulates the metabolic pathway of FA utilization in order to compensate the total breakdown of respiration by ETC, OXPHOS, glycolysis and TCA. The interplay between FAO, glycolysis and TCA is mediated by the production of NADH+H$^+$, Acetyl-CoA and $FADH_2$ by FAO as direct supply to the other pathways ensuring extra ATP production and subsequently cancer survival [346]. Bromoxib interferes at every stage of cellular metabolism, in the mitochondrial respiration (ETC and OXPHOS), in glycolysis, in TCA and in FAO.

This rapid survival mechanism is thought to be sensed and activated by AMPK, which is the main energy-sensing kinase in the cell, here further immunoblotting analyses could prove the involvement of AMPK as signaling kinase upon Bromoxib treatment. In more detail, the phosphosite Thr172 of AMPK should be investigated, which gets phosphorylated upon an increased energy demand induced by the drop of ATP levels [610, 613]. Beside the energy homeostasis regulating function, AMPK is involved in protein synthesis and lipid metabolism. Thereby, AMPK plays a major role in cellular processes such as proliferation, autophagy and apoptosis [613, 614].

The final question upon the analysis of Bromoxib is, whether it might be a promising agent for the treatment of leukemia? Generally, Bromoxib was found to be highly and preferably cytotoxic to leukemia and lymphoma cells. Its cytotoxicity was analyzed in malignant cells, primary patient AML samples, compared to healthy peripheral mononuclear blood cells (PBMNCs) [441]. The therapeutic window for Bromoxib of 3.2-fold was observed between malignant cells and their healthy counterparts [441]. So far, these preliminary data for primary malignant cells and healthy cells are promising. Nevertheless, evaluating the safety and cytotoxicity of a substance in the preclinical stage is an essential step in drug development. The *in vitro* assay testing should be extended for this substance and its cytotoxicity should be

tested in a broader screening setup. This should include a higher quantity of PBMNC samples and other healthy control cells for a longer period of incubation to ensure preclinical safety of Bromoxib. The next step in drug development would be animal studies, to fully evaluate the safety and efficacy of Bromoxib *in vivo*. The effects on various organs and systems have to be assessed to determine the appropriate dosing along with the identification of potential toxicities. Additional pharmacokinetic and toxicology studies are indispensable for the final drug development.

The objective of this thesis was to use the natural compound Bromoxib to target the *'deregulation of cellular metabolism'*, which is a key hallmark of cancer.

It was shown that Bromoxib targets predominantly the cellular metabolism by decreasing ATP levels, disturbing Ca^{2+} homeostasis and upregulating FAO in order to compensate the energetic disaster (fully graphical abstract is depicted in **Figure 41**). In the recent years the targeting of FA metabolism in cancer cells gained more and more attention. Malignant cells undergo metabolic reprogramming by altering aerobic glycolysis, upregulating *de novo* lipid synthesis and glutaminolysis, mutating TCA enzymes and also by increasing *de novo* FAO during oncogenesis [615]. Most of the bioenergetic studies focused on the Warburg effect, where cancer cells prefer lactate production from glycolysis in the presence of oxygen, instead of mitochondrial oxidation [415, 616]. The Warburg phenotype provides an advantage for the cell to ensure a fast ATP supply with the production of intermediates and metabolites used for proliferation [617]. Different to glycolysis, FAO enzymes have not been found to be mutated significantly in cancer [615]. Instead, an overexpression of some FAO enzymes was found, such as CPT1 [618] or ACSL [351]. CPT1 overexpression was found to correlate with poor patient outcome in AML [618]. Upstream of FAO c-myc was recognized as a central driver of upregulated FAO [615]. It is worth noting that cancer driven by c-myc seems to exhibit a high level of sensitivity towards inhibition of FAO [516]. The cell sensitivity screening for Bromoxib revealed that SUPB-15 and Ramos cells showed the lowest IC_{50} values. SUPB-15 are B cell acute lymphoblastic leukemia and Ramos cells are B cell Burkitt lymphoma. According to the hematopoiesis of blood cells, they share a common cellular origin [472, 473]. Ramos cells exhibit an overexpression of c-myc [619-621] and SUPB-15 cells an increased stabilization of c-myc [622]. It can be assumed that aberrant c-myc expression could be a reason why Bromoxib predominantly targets these cell lines.

Although Bromoxib has demonstrated its ability to efficiently eliminate cancer cells, it remains uncertain whether its mechanism of action (which involves uncoupling mitochondrial respiration, inhibiting ETC complexes, and disrupting the interplay between TCA, glycolysis, and ETC) differs significantly in healthy cells. Nevertheless, Bromoxib is a promising substance that warrants further investigation to fully evaluate its potential in targeting the hallmark of deregulated metabolism in cancer.

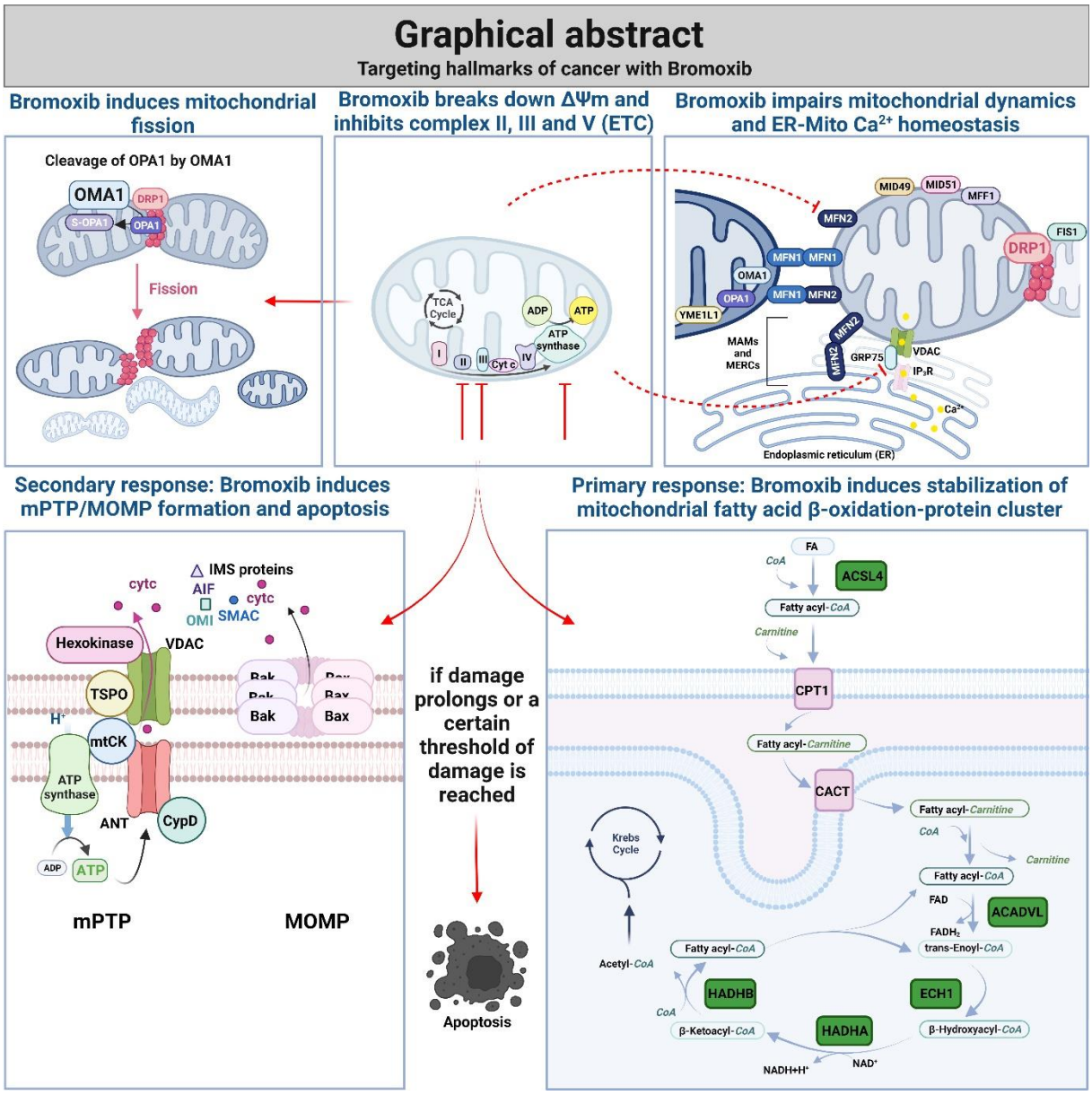

Figure 41 Targeting the hallmarks of cancer with Bromoxib – Graphical abstract displaying the broad bioactivity of Bromoxib as a protonophore capable to induce apoptosis in lymphoma cells. The small natural compound Bromoxib was shown in this thesis to be a protonophore, capable of inducing intrinsic mitochondrial dependent apoptosis. Bromoxib targets mainly the mitochondria, as it induces a rapid total breakdown of the mitochondrial membrane potential, it inhibits complex II, III and V of the ETC and was also shown to impair glycolysis. Furthermore, Bromoxib disturbs total cellular Ca^{2+} homeostasis by inducing Ca^{2+} release from the ER and mitochondria. All these cumulating events lead to the fragmentation of mitochondria, which is a hallmark of apoptosis. Parallel, Bromoxib was shown to rapidly induce the stabilization of a protein cluster mediating the mitochondrial fatty acid β-oxidation as a primary response: ACSL4, ACADVL, ECH1, HADHA and HADHB. The stabilization of this protein cluster is considered as a rapid rescue response of the cell in order to compensate the energetic disaster mediated at the ETC. As a secondary response the mPTP and/or MOMP are opened, releasing pro-apoptotic molecules into the cytosol. Finally, the intrinsic mitochondria dependent apoptosis cascade is activated leading to the destruction of the cancer cell. Bromoxib is considered to target potentially the hallmark 'deregulated cellular metabolism' as it induces an energetic disaster in the cancer cells. (This figure was created with Biorender.com).

7.3 Meriolins

Meriolin derivatives were first synthesized in 2007 [519] and 2008 [524]. Since then this substance class underwent derivatization and optimization in order to enhance their efficacy in cancer therapy. In the present work, the bioactivity of selected Meriolins (16 and 36) was investigated in Burkitt lymphoma and acute T cell leukemia.

The results presented above demonstrate that the distinct bioactivities of Meriolin 16 and 36 can be attributed to their structural differences. Both Meriolins have been characterized in terms of cytotoxicity and apoptosis efficiency. In summary, the Meriolins have been proven to be highly cytotoxic, to induce rapid kinetics of caspase-3 activation via activation of the intrinsic mitochondrial apoptosis pathway in cancer cells. Meriolin 16 and 36 were proven to inhibit kinases, predominantly CDKs. Subsequently, they disrupt the cell cycle and alter protein levels of cell cycle regulating proteins. Hence, the downstream pathway of CDK inhibition was analyzed. Moreover, crosstalk between the cell cycle disruption and occurring DNA- and RNA-damage was demonstrated. In the following, the underlying molecular mechanism of Meriolins will be discussed. It will be focused on the interplay between apoptosis, cell cycle and DNA-damage.

7.3.1 What happens first – Apoptosis induction, cell cycle inhibition or DNA- and RNA-damage?

Interestingly, only 5 min incubation with Meriolins are sufficient to prime lymphoma cells irreversibly to death. In a previous study, Meriolin 31 and 36 were demonstrated to be highly cytotoxic [443]. The new Meriolin derivative Meriolin 16 with its additional methoxy group at the aromatic pyridine ring, was proven in this thesis to be even more cytotoxic than the previously tested derivatives. An addition of a methoxy group can have various effects depending on the position of the substitution at the pyridine ring. This group was added in order to alter its pharmacokinetic properties and enhance its biological activity. Chemically, an additional methoxy group can increase the electron density of the aromatic ring, making the molecule more nucleophilic to finally enhance its potential reactivity in certain chemical reactions. Other effects are an influence on the molecule's polarity and solubility [623]. Beyond that, it was shown that Meriolin 16 exhibits an IC_{50} of 0.04 µM (in lymphoma cells), whereas its parental compound showed an IC_{50} of 0.11 µM [443]. Therefore, the additional methoxy group definitely increased the cytotoxicity of the substance. Regarding the proven irreversibility of all three derivatives, it can be assumed, that whatever target kinase they inhibit within 5 min of incubation, they ultimately induce cell death within 24 h. Potential kinases of the kinome screen that are inhibited upon Meriolin 16 and 36 treatment (in the lower concentration of each Meriolin, with

a residual activity of < 20% and without unspecific inhibition by the cell death inactive Meriolin 17) are shown in **Table 14**. The literature background of these 16 kinases was investigated for their subcellular location and protein function with any involvement in anti-apoptotic and pro-survival pathways by using the data base of human protein atlas [624]. Interestingly, 81.25% of the proteins with a residual activity < 20% were part of the CMGC kinase family, mainly located in the nucleus. The biological function of these kinases can be grouped in cell cycle regulation, transcription regulation via phosphorylation of RNA pol II, dual specificity kinase functions, DNA damage repair and stabilization of the cytoskeleton.

Pro-survival and anti-apoptotic kinase DYRK1A

The only kinase, that exhibits pro-survival and anti-apoptotic regulative function is DYRK1A, according to the database of human protein atlas [624]. In terms of apoptosis, DYRK1A was found to be a negative regulator of the intrinsic apoptotic pathway [625]. DYRK1A phosphorylates caspase-9 on Thr125 and this phosphorylation protects cells from apoptotic death [625, 626]. The inhibition of DYRK1A activity by Harmine (a selective DYRK1A inhibitor [627] used as chemotherapeutic [628-630]) induces caspase-9 activation and leads to massive apoptosis in different cell types [625, 628]. Interestingly, Meriolins and Variolin B were also published in a list of DYRK1A inhibitors, as discussed in the review of Ionescu *et al.* [631]. Earlier, the group of Echalier *et al*. [524] calculated IC_{50} of several Meriolins (and Variolin B) against specific kinases, also DYRK1A (CDK1/Cyclin B, CDK2/Cyclin A, CDK5/p25, CDK9/Cyclin T, GSK-3α/β, CK1 and DYRK1A) [524]. Their top candidate, Meriolin 3 (1b), exhibited inhibitory kinase activity against CDK1/Cyclin B of 0.17 µM, CDK2/Cyclin A of 0.0011 µM, CDK5/p25 of 0.17 µM, CDK9/Cyclin T of 0.006 µM and DYRK1A of 0.029 µM [524].

The Meriolin derivatives investigated in the present work, Meriolin 16 and Meriolin 36, showed inhibitory activity for the same kinases in concentrations of 0.03 µM and 0.3 µM respectively (**Table 14**). Meriolin 16 and Meriolin 36 reduced the kinase activity of these kinases to almost zero % residual activity as shown in **Table 14**. Regarding the binding mode, the Meriolins (3 (1b) and 5 (1e)) were reported to bind to the ATP-binding pocket of the respective kinase, here CDK2 with Cyclin A or E [524]. Echalier *et al*. [524] compared the binding modes published by Bettayeb *et al*.[519] with their own and confirmed that the overall conformation of CDK2/Cyclin A bound to Meriolin 3 and 5 are identical [524]. The pyrrolopyrimidine system together with the pyridine ring (originally of Variolin B) was found to be located between the two lobes of CDK2 [519, 524]. A common feature of kinase inhibitors with a planar ring scaffold is, that the ring system packs against the side chain of Leu134 and Ala31 [524].

Table 14 Kinome profiling results from the kinome screening shown in Table 12 (^{33}PanQinase^{TM}) of Meriolin 36 at 0.3 and Meriolin 16 at 0.03. The results shown here are selected upon (i) no unspecific inhibition of the biological inactive derivative Meriolin 17 and (ii) a residual activity < 20% for the lower tested concentration of Meriolin 16 and 36 to ensure selectivity. (# = kinase number, * the classification of protein kinase families was performed according to [539]: AGC (containing PKA, PKG and PKC families); CAMK (containing Calcium/Calmodulin-dependent protein kinases); CK1 (Casein kinase 1-like); CMGC (containing CDK, MAPK, GSK3 and CLK families); TK (Tyrosine Kinases); TKL (Tyrosine Kinase-like) and STE (Homologs of Yeast Sterile 7, Sterile 11 and Sterile 20 Kinases). Data base research for each kinase (human protein atlas [624]) was performed upon location and function of the protein respectively.

#	Kinase Name	Kinase Family*	36 0.3 µM	16 0.03 µM	Location	Function
49	**CDK19/CycC**	**CMGC**	3	6	Cytosol, nucleoplasm	CDK19 is a component of Mediator co-activator complex required for transcriptional activation by DNA binding transcription factors of genes transcribed by RNA pol II.
50	**CDK2/CycA2**	**CMGC**	1	18	Cytosol, nucleoplasm and centrosome	CDK2 regulates progression through the cell cycle. Its activity is important during G_1 to S phase transition and modulates G_2 progression. Associates with Cyclin A or E.
52	**CDK2/CycE1**	**CMGC**	1	16		
60	**CDK5/p25NCK**	**CMGC**	0	16	Nucleoplasm, plasma membrane	CDK5 does not directly control cell cycle regulation. It is predominantly expressed at high levels in mammalian postmitotic central nervous system. Involved in synaptic plasticity, neuronal migration, cytoskeletal organization, endo- and exocytosis and apoptosis.
61	**CDK5/p35NCK**	**CMGC**	0	7		
66	**CDK8/CycC**	**CMGC**	5	6	Nucleoplasm	CDK8 is a component of the Mediator complex, it acts as a coactivator for nearly all genes transcribed by RNA pol II. The Mediator complex is recruited to promoters and serves as assembly scaffold for the pre-initiation complex with RNA pol II and general transcription factors. CDK8 phosphorylates the CTD of RNA pol II. CDK8 associates with its Cyclin C.
67	**CDK9/CycK**	**CMGC**	2	7	Nucleoplasm, cytoplasmic bodies	CDK9 is involved in the regulation of transcription. It forms the CDK9/Cyclin T complex also called positive transcription elongation factor b (P-TEFb). It phosphorylates the CTD of RNA pol II initiating elongation. P-TEFb is involved in mRNA processing and mRNA export and in cotranscriptional histone modification. CDK9/Cyclin K is a replication stress protein, required for genome integrity maintenance. It promotes cell cycle recovery from replication arrest and limits single stranded DNA amount during replication stress.
68	**CDK9/CycT1**	**CMGC**	1	13		
79	**CLK1**	**CMGC**	4	11	Nucleoplasm, nuclear membrane	CLK1 is a dual specificity kinase phosphorylating serine/threonine and tyrosine-containing substrates.

#	Kinase Name	Kinase Family*	36 0.3 µM	16 0.03 µM	Location	Function
80	**CLK2**	**CMGC**	1	8	Nucleoplasm, nuclear bodies	CLK2 is a dual specificity kinase phosphorylating serine/threonine and tyrosine-containing substrates. Phosphorylates PPP2R5B thereby stimulating the assembly of PP2A phosphatase with the PPP2R5B-AKT1 complex leading to dephosphorylation of AKT1.
82	**CLK4**	**CMGC**	1	3	Actin filaments	CLK4 is a dual specificity kinase phosphorylating serine/threonine and tyrosine-containing substrates.
93	**DYRK1A**	**CMGC**	7	11	Cytosol, Nucleoli fibrillar center	DYRK1A is a dual specificity kinase phosphorylating serine/threonine and tyrosine-containing substrates. Is involved in DSB repair induced by DNA damage. DYRK1A phosphorylates RNF169 and increases its ability to block accumulation of TP53BP1 at the DSB sites. Thereby it promotes HR. It negatively regulates the apoptotic process and has a pro-survival function.
94	**DYRK1B**	**CMGC**	7	8	Nucleoplasm, mitotic chromosome	DYRK1B is a dual specificity kinase phosphorylating serine/threonine and tyrosine-containing substrates. Is crucial for ribosomal DNA DSB repair and maintenance of ribosomal DNA copy numbers.
137	**GSG2**	**OTHER**	2	2	Nucleoplasm	Also named HASPIN, that phosphorylates histone H3 at Thr3 during mitosis. Assumed modulation of AURKB activation and other CPC complex members to maintain chromatic cohesion and cell cycle progression.
163	**LIMK1**	**TKL**	9	10	Nuclear speckles, Cytosol	LIMK1 plays an important role in actin filament dynamics, it stabilizes the actin cytoskeleton.
270	**ROCK2**	**AGC**	1	12	Cytosol	ROCK2 is a key regulator of cell polarity and actin cytoskeleton organization.

Recently, selective DYRK1A inhibitors were developed and their binding mode was investigated (Harmine and Meriolin 3 were also included in the analyses) [632]. They identified two possible binding modes of inhibitors to DYRK1A, a non-classical binding mode and a classical binding mode [632]. Due to the structural differences between Meriolin 16 and 36 I compared the possible binding modes of our Meriolins to their target kinases (CDKs and DYRK1A). Thus, I came up with the hypothesis, that Meriolin 16 and 36 both exhibit different binding modes to their target kinases which might be similar to these shown for DYRK1A. I performed a collaboration with the RG Gohlke (Pablo A. Cea-Medina, Institute for Pharmaceutical and Medicinal Chemistry, Heinrich-Heine University Düsseldorf), who are experts in drug to target modelling. Pablo showed by molecular docking analyses, that Meriolin 16 and 36 have different binding modes (as modelled for CDK1, 2 and 9 – unpublished). Pablo's work supported my hypothesis and he identified one putative binding mode of Meriolin 16 and two putative binding modes of Meriolin 36 to CDKs and performed the following dockings: CDK1 with Cyclin B1, CDK2 with Cyclin E and with Cyclin A2 and also CDK9 with Cyclin T1. However, the CDKs of interest (CDK1, 2 and 9) share a similar binding site, and the inhibition of the kinase by Meriolin 16 or 36 took place via an interaction with the 7-azaindole. Meriolin 16 has one binding mode, whereas 36 has two, a normal and a flipped one (unpublished data – manuscript in preparation).

Meriolin 16 and 36 inhibit the kinases shown in the kinome screening in **Table 13** and the most inhibited kinases are shown in **Table 14** with different selectivity of the Meriolins based on their structural differences. Furthermore, the similarities of the binding modes compared to DYRK1A inhibitors [631, 632] prime the assumption, that DYRK1A might be the pro-survival target kinase targeted by Meriolin 16 and 36 that is responsible for the highly cytotoxic and pro-apoptotic activity of this compound class. In more detail, the selective inhibition of DYRK1A by Harmine was shown to activate caspase-3/-7 and caspase-9 finally resulting in apoptotic cell death as shown in [633]. If Meriolins inhibit DYRK1A and the anti-apoptotic phosphorylation of caspase-9 at Thr125 does not occur, this could prime the cells more rapidly to apoptotic death [625, 626]. Further experiments regarding this link between apoptosis induction and kinase inhibition should be performed. The analysis should include a kinase specific DYRK1A activity assay, to support the inhibition of DYRK1A by Meriolins in a concentration-dependent. Moreover, an immunoblot analysis for Thr125 phosphorylation at caspase-9 should be performed after Meriolin 16 and 36 treatment with their cytotoxic IC_{50} values and the enzymatic IC_{50} values over a time kinetic of 2, 4, 6, 8, 12, 16 and 24 h (as control DYRK1A inhibitors such as Harmine should be included). Interestingly, the Harmine-induced rate of apoptosis determined after 24 h in % [633], is comparable to the rate of apoptosis induced by the Meriolins (16, 31 and 36) investigated in this work, which ranges around 40-60%. In contrast, our derivatives have much

lower IC_{50} values, are faster in terms of capsase-3 activation and PARP1 cleavage, which highlights the diverse bioactivity of this compound class that will be discussed in the following.

Cell cycle arrest, DNA damage and crosstalk to apoptosis

The Meriolin derivatives 16 and 36 were shown in the present work to induce apoptosis and also affect downstream cell cycle regulating proteins. It was focused on the kinase inhibitory pattern of Meriolin 16 and 36 showing that both derivatives inhibit kinases with distinct selectivity and in different concentrations. These results are in concordance with the literature regarding the substance class of Meriolin derivatives, since it was shown over time that these compounds are kinase inhibitors with cytotoxic, anti-proliferative, anti-tumor and pro-apoptotic bioactivity [411, 443, 519, 524, 527, 528, 633]. As discussed in the previous chapter, the differences in bioactivity of both derivatives investigated in the present work relies probably on the structural differences of the derivatives (16 and 36). Furthermore, both derivatives inhibit prevalently CDKs, thereby disrupting the cell cycle regulation, which leads ultimately to cell cycle arrest – which is also a common feature of this substance class [411, 519, 527, 528].

A possible link between CDK inhibition by Meriolins and the morphological changes of the mitochondria during apoptosis induction is, that Meriolins inhibit CDK1, which together with Cyclin B phosphorylates DRP1 (at Ser585 in rat) during mitosis [634]. In the review of Zerihun *et al.* [486] the DRP1-mediated mitochondrial fission protein interactome is summarized, highlighting, that the site of phosphorylation on DRP1 deciphers its activator or inhibitor role referring to fission [486]. Mitochondria are present as long tubular network structures during interphase [634]. In the early mitotic phase the mitochondria are fragmented and redistributed to the daughter cells. DRP1 is directly regulated by the machinery that controls cell cycle progression, which was shown to be dependent on fission regulated by DRP1 phosphorylation by CDK1/Cyclin B [634]. Ser616 and Ser637 are important phosphorylation sites at human DRP1, Ser616 is known to activate fission and Ser637 is inactivating [486, 635]. Some kinases are known to phosphorylate Ser616 such as ROCK, PKC, CDK1, extracellular signal-regulated protein kinase 1/2 (ERK1/2) and calmodulin-dependent protein kinase II (CaMKII) (reviewed in [486]). Interestingly, CDK1 induced phosphorylation on DRP1 has been shown to exhibit a reciprocal effect on oligomerization and translocation to mitochondrial scission sites [636].

Therefore, CDK1 inhibition by Meriolins could impair DRP1 phosphorylation with an impact on mitochondrial fission. This link should be investigated via immunoblotting in future studies. The loss of DRP1 (with siRNA) was linked to mitochondrial hyperfusion with subsequent G_2/M cell cycle arrest and can be found in [637].

The analyses presented in this dissertation are the first approach analyzing the pathways interconnecting cell cycle regulation, checkpoint arrest and DNA damage. The results

presented here lead to the assumption that Meriolins induce a G_2-arrest over time in lymphoma cells. In addition to that they activate apoptosis with the occurrence of DNA damage and a reduction of *de novo* RNA synthesis. It was shown, that both derivatives do not equally target cell cycle regulating pathways. There are obvious concentration-dependent differences between Meriolin 16 and 36 detectable on the protein level (p-CHK2 levels, p-Ser612 Rb, p-Ser2 RNA pol II). In more detail, an inhibition of CDK2 activity prevents cell cycle progression through G_1/S phase and an inhibition of CDK1 impairs progression in G_2/M phase of the cell cycle [528]. Here we show, that a combined inhibition of both main cell cycle regulating CDKs 1 and 2, induces a cell cycle arrest in G_2-phase (depending on the cells phase when treated with Meriolins). The phase arrest in G_2 is supported by the phosphorylation of the checkpoint kinase CHK2 and the absence of a phosphorylation of CHK1. It was reviewed in the introduction, that ATM phosphorylates CHK2 on Thr68 when DNA damage (DSBs) occurs [540]. Meriolin 16 and 36 induced after 8 h treatment, an increase of p-CHK2 levels. They induced no increase of p-CHK1 levels over time. Mechanistically, active CHK2 phosphorylates p53, leading to p21 accumulation to sustain G_2/M arrest [541]. p21 has a cell cycle inhibitory role, is involved in apoptosis and the DNA damage response [638]. Zannini *et al.* [540] reviewed extensively the multiple roles of CHK2 in the nuclear DNA damage response; CHK2 gets activated in the cell cycle checkpoint upon DNA damage, it phosphorylates p53 and CDC25A to induce G_2/M checkpoint activation [540]. In the case of the Meriolins, the increase of p-CHK2 levels could be due to the occurrence of DNA damage starting after 8 h treatment. A possible origination of the DNA damage might be the induction of apoptosis starting rapidly with caspase-3 activation after 2-3 h treatment leading to the destruction of the cell. Immunoblot analyses of my master student Julia Hoppe revealed, that the phosphorylation of p-CHK2 increases up to 200% with the pre- and co-treatment with QVD, assuming that the checkpoint activation is partly originating from caspase-dependent events. Without QVD, the p-CHK2 levels increase up to 1500% for Meriolin 16 and 2000% for Meriolin 36, suggesting that the major part of phosphorylation of CHK2 is probably induced by ATM due to DNA damage occurring during apoptosis. Activated caspases trigger the release of the nuclease Endo G from the mitochondria, which then cleaves chromosomal DNA [639]. Furthermore, activated caspases induce the degradation of nuclear DNA via the cleavage of inhibitor of caspase-activated DNAse (ICAD) and thereby releasing caspase activated DNase (CAD), which forms a scissor-like homodimer in order to cleave double-stranded DNA at nucleosomal linkers [639-643]. In an article by Wang [644], DNA repair is considered as primary response to DNA damage, whereas apoptosis is considered as the secondary response. The first response aims to protect the damaged cell and the second response is activated to protect the whole organism [644]. Here, the guardian of the genome, p53, acts as a central player, which governs the choice between cell cycle arrest and apoptosis [644]. Data generated by my master student Julia Hoppe showed,

that Meriolin treatment induced an increase in p53 protein level after 8 h, which is in concordance with p-CHK2 checkpoint activation (data not shown). This increase is only partially prevented with caspase-inhibition via the pre- and co-treatment of QVD. Probably, DNA damage occurs upon Meriolin treatment, which leads to the activation of ATM, which then phosphorylates CHK2 in order to induce cell cycle arrest in G_2. In addition to that, p53 probably activates apoptosis genes such as Noxa, Puma and Bax [644]. The events of growth arrest and apoptosis are described to be *'distinct, albeit not mutually exclusive'* (*Wang. 2001, S.1047*) [644].

As second mechanism (besides p53), the functional status of Rb protein determines whether a damaged cell commits suicide or undergoes induce cell cycle arrest [644]. In the present work, the phosphorylation of Rb protein at position Ser612 was analyzed, because a G_2-arrest was assumed and this phosphosite is known to be phosphorylated by CDK2/Cyclin A in late S-/G_2-phase [645]. Distinct results were obtained for two derivatives (16 and 36). Meriolin 16 induced in both concentrations (0.1 and 1 µM) the loss of the phosphorylation, whereas Meriolin 36 induced in both concentrations (0.1 and 1 µM) an increase of the phosphorylation at Ser612. This is probably due to the different IC_{50} values, Meriolin 16 exhibits an IC_{50} value which is 4-fold lower (0.04 µM) compared to Meriolin 36 (0.17 µM) in lymphoma cells. It can be concluded, that for Meriolin 16 both concentrations are sufficient in inducing an inhibition of CDK2 *in vivo*, resulting in the failure of phosphorylation at Ser612 of Rb protein. In the case of Meriolin 36, both concentrations were too low to inhibit CDK2 *in vivo*, since the phosphorylation at Ser612 of Rb protein did not decrease. On the contrary, the phosphorylation even increased, suggesting that the cells continued to proliferate and progressed through the cell cycle under these conditions. Therefore, following analyses were performed mainly with the more promising substance, in terms of IC_{50} and also selectivity – Meriolin 16.

In summary, lymphoma cells respond better to Meriolin 16, which was shown to be more cytotoxic. This substance induces caspase-3 activation, intrinsic mitochondrial apoptosis and cell cycle disruption leading to an arrest in G_2 phase. Moreover, Meriolin 16 displays checkpoint activation via p-CHK2 upon apoptosis induction. The G_2-checkpoint activation lead to the investigation of DNA damage upon Meriolin 16 treatment. For Meriolin 16 treatment the phosphorylation of γh2ax occurs in the time window of 3 to 12 h peaking at 6 to 8 h. γh2ax was introduced as a biomarker of DSBs, which gets phosphorylated by either ATM or ATR in order to recruit and direct DNA repair proteins [557]. It is more likely, that the DNA damage (detected by γh2ax via immunoblotting, in the time window of 3 to 12 h) is in concordance with ATM activity and subsequent CHK2 phosphorylation. p-CHK2 then acts either on p53 (activating Puma, Noxa and Bax transcription supporting apoptosis) or on p53 (acting on p21 followed by the induction of G_2 arrest).

Subsequent analyses regarding the impairment of proliferation as measured by EdU incorporation showed, that Meriolin treatment (IC_{25} of 16 and 36) reduced the proliferation to

residual 10%. This result supports the hypothesis, that depending on the dosage of Meriolin treatment, the cells either undergo rapidly apoptosis (probably due to the too high levels of DNA damage) or stop proliferating by entering cell cycle arrest in order to enable repair of the damaged DNA. It is known from the literature, that cells with irreparably damaged DNA rather activate apoptosis to avoid propagation throughout the cell cycle with a potentially detrimental genome [540]. Furthermore, activated CHK2 was observed to induce apoptosis via the phosphorylation and stabilization of E2F-1, which is a transcription factor involved in cell cycle control via its interaction with the Rb protein throughout the cell cycle (CDC2, Cyclin A, Cyclin E [646], Claspin, Rad51ap1, $p27^{Kip1}$ [647]). E2F-1 regulated genes are also pro-apoptotic [540] and the respective E2F-1 induced death effector proteins are: p73, Bad, Bak, Bid, c-FLIP [648], Apaf-1 [649], Puma and Noxa [650], caspase-3/-7/-8 and -9 [651].

The exact mechanism by which the transcription factor E2F-1 exhibits either cell cycle regulative function or pro-apoptotic function was found to be dependent on the total cellular context of p53 activity [652, 653]. In summary, the signaling routes connecting CDK inhibition, cell cycle regulation and arrest, DNA damage and checkpoint activation with the induction of apoptosis all convene at p53. A possible explanation for the crosstalk between cell cycle arrest and apoptosis was provided by the finding that a deregulation of Rb/E2F pathway induces the upregulation of p53-cofactors: apoptosis stimulating proteins of p53 1 and 2 (ASPP1 and 2), junction-mediating and regulatory protein (JMY) and Tumor suppressor p53-induced nuclear protein 1 (TP53INP1) via direct transcriptional mechanisms [653]. Since a *de novo* protein synthesis was not required for the E2F-1-mediated regulation of these genes, it was assumed that they are direct E2F-1 targets [653]. The pro-apoptotic expression of E2F-1 dependent cofactors directs p53 to its pro-apoptotic targets [653] and that might be an explanation for the Meriolin-induced execution of apoptosis even in the presence of anti-apoptotic Bcl-2. Further experiments will include qRT-PCR analyses of Rb-dependent E2F-1 target genes in order to gather insights within the transcriptional level of cells upon Meriolin treatment.

Finally, the interplay of the diverse pathways is thought to involve a number of parallel and also synergistic mechanisms that contribute to the broad bioactivity of Meriolins.

The role of transcription

As mentioned in the introduction, CDK9/Cyclin T is a regulator of transcriptional elongation and termination. Especially at the CTD of RNA pol II, many factors contribute to the regulation of gene expression [544]. CDK9/Cyclin T also termed P-TEFb (positive transcription elongation factor) phosphorylates RNA pol II at Ser2 at its CTD [544, 547-549]. Interestingly, Meriolin 16 induces the decrease of CDK9 and Cyclin T1 levels over time. This is contrary to the stable protein levels of CDK1/Cyclin B1 and CDK2/Cyclin A2. It is known, that the CDK9/Cyclin T1 complex

activity is not regulated periodically throughout the cell cycle as all other CDK/Cyclin complexes are [544, 550, 551]. An essential role for CDK9 has been shown in B cell lymphoma [654], acute myeloid leukemia [655], lung cancer [656], breast cancer [657], prostate cancer [658] and melanoma [659]. Moreover, RNA pol II suppression via CDK9 inhibition was shown to result in a block of transcriptional elongation resulting in oppression of anti-apoptotic short-lived proteins such as Mcl-1, leading to apoptosis in aggressive myc-driven B cell lymphoma *in vivo* [654]. The role of Myc is the binding and recruiting of P-TEFb to its targets in order to activate RNA pol II [660-662]. Therefore, it can be hypothesized that CDK9 inhibition by Meriolin 16 could act as a pharmacological approach to target the transcription of harmful myc-regulated oncogenic effector genes (similar to Dinaciclib, which is a CDK inhibitor in clinical trials [654, 663-666]). In future studies, the effect of Meriolin treatment on myc protein levels should be validated in a time- and concentration-dependent manner. The results for Meriolin 16 showed, that the decrease of RNA pol II total protein is in concordance with the decrease of Mcl-1 and the activation of caspase-3. Furthermore, Meriolin 16 induces the decrease of CDK9/Cyclin T1 along with the loss of phosphorylation Ser2 at RNA pol II. It can be concluded, that Meriolin 16 is a potent inhibitor of the transcriptional function of RNA pol II during elongation. This implicates, that Meriolin 16 treatment not only impairs proliferation, inducing cell cycle arrest and apoptosis, it also reduces the *de novo* RNA synthesis via the inhibition of CDK9 as shown for EU incorporation.

This is a very promising finding which enables to target the hallmark '*sustaining proliferative signaling*' in cancer. Myc acts as transcriptional master regulator in cancer in favor of rapid cell growth, proliferation [418], cell cycle progression, genomic instability [667] and enhanced cellular metabolism [287]. Dysregulation of myc is associated with a negative outcome in diffuse large B-cell lymphoma and there is a lack of effective treatment options for relapsed or refractory diffuse large B cell lymphoma and Burkitt lymphoma [668]. *Myc* overexpression alone was shown to be not causative for lymphoma [59], whereas *myc* translocations as seen in Burkitt lymphoma and other lymphomas was shown to be responsible for their high proliferative nature along with the associated overexpression of Bcl-2 [669, 670]. Meriolin treatment targets probably exactly this Achilles heel in Burkitt B cell lymphoma – myc – as essential driver of rapid proliferation and cell cycle progression. Via the inhibition of RNA pol II function, the transcription of myc-regulated oncogenic effector proteins is inhibited, enabling to efficiently target the hallmark 'sustaining proliferative signaling' with Meriolin treatment.

Another beneficial effect of this inhibitory pathway from CDK9 inhibition to RNA pol II inhibition to inhibition of transcription and the reduction of *de novo* RNA synthesis is, that no dilncRNAs are processed in order to generate DNA damage response RNAs (DDRNAs) [254, 261, 270-273]. Normally, these dilncRNAs enhance together with DDRNAs the DDR foci formation and promote DDR activation and DNA damage repair [270]. Therefore, the loss of RNA pol II function

probably also impairs the efficiency of DNA repair. Generally, the exact cause of DNA damage induced by Meriolins has to be elucidated in further studies together with unraveling the mechanisms of DNA damage repair. Moreover, the impact of RNA pol II inhibition by Meriolins on DNA repair should be investigated. Additionally, the appearance of R-loops could be investigated with the usage of an S9.6 antibody that exhibits high specificity for DNA-RNA hybrids [251]. It can be used to immunoprecipitate R-loops and enabled in previous studies the identification of R-loop-binding proteins [258, 259, 282]. Since R-loops only occur around DSBs during repair processes [251], it first has to be clarified which kind of DNA damage occurs and which mechanism of repair is induced.

A key hallmark of cancer is '*genomic instability and mutation*' that arises upon errors in the DDR and/or increased replication stress resulting from an abnormal high rate of cell division and the related rapid accumulation of aberrations [215]. These errors promote the clonal evolution of cancer cells via the increase of driver alterations such as gene copy-number changes, rearrangements and mutations [215]. However, exactly the same errors also increase and create new vulnerabilities that are relatively specific for cancer cells, which enable the development of new targeted therapies aiming on the cancers Achilles heels. With further analyses regarding the cause of DNA damage and the mechanism of repair, a proper conclusion can be formulated regarding the targeting of the hallmark *'genomic instability and mutation'* in cancer via Meriolins.

The investigation of Meriolins targeting of *'genomic instability and mutation'* will be included in further studies. Finally, Meriolins enable the efficient targeting of *'resisting cell death'* and *'sustaining proliferative signaling'* as hallmarks in Burkitt B cell lymphoma. Meriolins are able to induce apoptosis in the presence of anti-apoptotic Bcl-2, which offers a treatment option for cancers with impaired and/or inhibited apoptosis or even multidrug resistant cancers [371]. Furthermore, they reduce proliferation, induce cell cycle arrest and inhibit RNA pol II dependent transcription. These features enable the targeting of cancer cells with a high oncogene-driven E2F activity inducing aberrant cell proliferation [384] and cancer cells that bypass the DNA damage checkpoints to undergo uninterrupted cell division [175]. Moreover, Meriolins target the CDK-Rb-E2F axis with their CMGC/CDK specific kinase inhibitory profile and their potential as cancer therapeutics should be definitely investigated in further studies including the testing in *in vivo* models of the respective cancer entity. A final graphical abstract that combines all hypotheses discussed above regarding the molecular mechanism of Meriolin derivatives in lymphoma cells is shown in **Figure 42**.

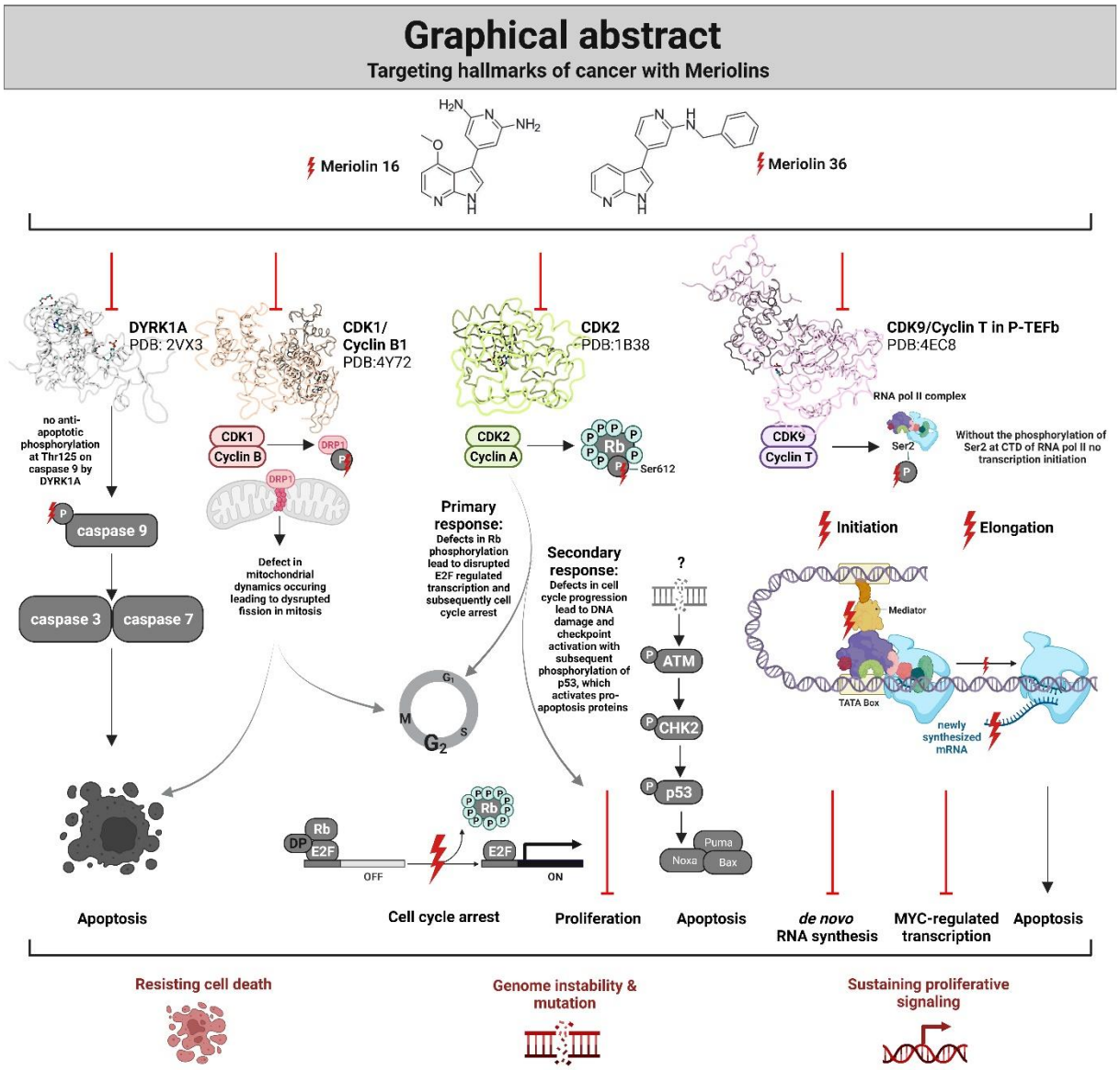

Figure 42 Targeting the hallmarks of cancer with Meriolins – Graphical abstract interconnecting cell cycle inhibition, DNA damage and apoptosis. The Meriolin derivatives Meriolin 16 and 36 are structurally different and were shown to exhibit broad bioactivity in lymphoma cells. This bioactivity includes the inhibition of kinases, prevalently of the CMGC family, such as CDKs (1, 2 and 9) or DYRK1A. An inhibition of DYRK1A could prevent the anti-apoptotic phosphorylation at Thr125 on caspase 9. Thereby apoptosis induction could be supported. CDK1/Cyclin B1 inhibition by Meriolins could lead to the failure of DRP1 phosphorylation, thus a dysregulated mitochondrial fission during mitosis, finally leading to cell cycle arrest or if prolonged to apoptosis. An inhibition of CDK2 in complex with Cyclin E or A (depending on the cell cycle phase) leads as a primary response to the defects in Rb phosphorylation. Dysregulated Rb phosphorylation influences downstream directly E2F-Rb regulated gene transcription, which ultimately leads to cell cycle arrest. As a secondary response, due to the CDK inhibition throughout all phases of the cell cycle, DNA damage occurs, ATM phosphorylates CHK2 and the checkpoint response is activated. This can lead to phosphorylation of p53, which acts on pro-apoptotic proteins such as Noxa, Puma and Bax. Additionally, the inhibition of the transcriptional CDK9 leads to the absence of the phosphorylation of Ser2 at the CTD of RNA pol II, which is needed to initiate the transcription and further perform the elongation step. This leads to the reduction of *de novo* RNA synthesis, along with the inhibition of myc-regulated transcription and finally results in apoptosis. This graphical abstract is based on the underlying molecular mechanistic insights gathered in the presented work and united the working hypotheses discussed in the previous chapter. With the bioactivity displayed by the two Meriolin derivatives 16 and 36 the hallmarks of cancer *'resisting cell death'*, *'genome instability and mutation'* and *'sustaining proliferative signaling'* can be targeted. (The PDB entry of DYRK1A is 2VX3, of CDK1/Cyclin B1 4Y72, of CDK2 1B38 and of CDK9/Cyclin T in P-TEFb complex 4EC8). (This figure was created with Biorender.com).

8 Conclusions and further perspectives

The objective of this thesis was to identify and characterize natural products that are able to induce cell death in chemotherapeutic-resistant tumors. Two natural products, Viriditoxin and Bromoxib, and the semisynthetic Meriolins, were identified to activate intrinsic mitochondria dependent apoptosis through different mechanisms.

Viriditoxin was shown to target the mitochondria and to affect mitoribosomes, whereas the exact target remained unknown. Further experiments characterizing the effect of Viriditoxin on LRPPRC and GRSF1 should be performed. LRPPRC is involved in mRNA transport and regulation [476] and GRSF1 regulates post-transcriptional mitochondrial gene expression, required for the mitochondrial ribosome [561]. Analyzes about a potential correlation between the effect of Viriditoxin on mitoribosomal proteins and LRPPRC and GRSF1 would be an analysis of the stability of mtDNA-encoded RNAs and global mRNA levels. It would also be interesting to analyze the stability of the mRNA stability regulating complex (~250 kDa), namely LRPPRC and GRSF1 with SLIRP (SRA stem-loop interacting RNA binding protein), by size-exclusion chromatography as shown in [563]. With the suggested experiments that were discussed in more detail in the discussion, we could get hands on the target-mediated-effect of Viriditoxin.

Bromoxib, as a small natural compound, was identified in this thesis to act as a protonophore with broad bioactivity. Bromoxib induces the rapid breakdown of the mitochondrial membrane potential, inhibits selectively complex II, III and V of the electron transport chain, it induces total cellular Ca^{2+} mobilization partially from the ER and the mitochondria, with subsequent fission of the mitochondria. The intrinsic mitochondria dependent apoptosis cascade induced by Bromoxib was shown to be dependent on Bcl-2 and caspase-9. This natural compound activates a sequential response. First, it induces an energetic disaster, which is compensated by the stabilization of the mitochondrial fatty acid β-oxidation protein cluster, in order to generate energy rapidly from fatty acids to survive. Then, if the damage prolongs and the signals integrated at the outer mitochondrial membrane of the mitochondria tend to activate the cells suicide program, this is considered as the secondary response. In further experiments, it would be interesting to investigate whether the depletion of mitochondrial and/or ER Ca^{2+} stores is responsible for the activation of intrinsic mitochondrial apoptosis. To address this point, the cells could be pre-treated with Cyclosporin A (binds to Cyclophilin D and inhibits mPTP opening) [79, 80] followed by treatment with Ionomycin or Bromoxib and Ca^{2+} mobilization (and cell viability) could be measured. This would answer the question whether Ca^{2+} mobilization is the main underlying event (and not the breakdown of the proton gradient) activating the apoptosis cascade or whether it is just an additional trigger. In terms of ER stress, the unfolded protein response (UPR) should be investigated. The effect of Bromoxib on key

proteins of the UPR, such as phosphorylation of eIF2α at Ser51 with subsequent activation of the transcription factors ATF4 and CHOP could be analyzed in further experiments via immunoblotting [575, 576]. Regarding the interplay of ETC, TCA and glycolysis, the cells metabolic state should be determined via the measurement of intermediate molecules such as NAD^+/NADH ratio or acetyl-CoA levels. I would be interested in analyzing the effect of Bromoxib on the moonlighting protein DLD, whether Bromoxib impairs DLD protein levels as well as its functionality. To fully validate proteins of the mitochondrial fatty acid β-oxidation protein cluster, Bromoxib-treated samples should be heated up according to the TPP-protocol and the effect of the protein levels should be validated. Bromoxib interferes at every stage of cellular metabolism, in the mitochondrial respiration (ETC and OXPHOS), in glycolysis, in TCA and in FAO. This rapid survival mechanism is sensed and activated by AMPK, as main energy-sensing kinase. Further immunoblotting analyses should include the involvement of AMPK as signaling kinase upon Bromoxib treatment as outlined in the discussion. Although Bromoxib has demonstrated its ability to efficiently eliminate cancer cells, it remains uncertain whether its mechanism of action differs significantly in healthy cells. Nevertheless, Bromoxib is a promising substance that warrants further investigation to fully evaluate its potential in targeting the hallmark of *'deregulated metabolism'* in cancer.

In this thesis, also semisynthetic substances were identified and characterized to induce cell death in cancer. Meriolins (Meriolin 16, 31 and 36) were identified as highly cytotoxic substances with rapid apoptosis induction in leukemia and lymphoma cells. Moreover, Meriolin 16 and 36, were identified as kinase inhibitors with different selectivity and concentration-dependent efficacy. Meriolins were proven to exhibit a dual bioactivity, on the one hand, they induce potentially apoptosis and on the other hand, they inhibit the cell cycle, reduce proliferation, induce DNA damage and reduce *de novo* RNA synthesis.
The Meriolin-induced inhibition of the pro-survival and anti-apoptotic kinase DYRK1A was assumed to provide a potential link between both affected pathways. Further experiments investigating the link between apoptosis induction and kinase inhibition should be performed. These experiments should include a kinase specific DYRK1A activity assay, to support the inhibition of DYRK1A by Meriolins in a concentration-dependent. Moreover, an immunoblot analysis for Thr125 phosphorylation at caspase-9 should be performed after Meriolin 16 and 36 treatment to investigate whether Meriolins inhibit the anti-apoptotic activity of DYRK1A with a downstream effect on caspase-9. Furthermore, the effect of Meriolins on DRP1 induced fission should be investigated via immunoblotting.

In this thesis, Meriolin 16 was demonstrated to be a potent inhibitor of the transcriptional function of RNA pol II during elongation. Meriolin 16 treatment does impair proliferation, induces cell cycle arrest and apoptosis, it also reduces the *de novo* RNA synthesis via the inhibition of CDK9. In terms of the inhibition of *de novo* RNA synthesis, the effect of Meriolin

treatment on myc-regulated genes and myc protein level itself should be validated in a time- and concentration-dependent manner with qRT-PCR and immunoblotting. The results generated in this thesis for Meriolins are very promising. They support the therapeutic potential of these substances to target the hallmark *'sustaining proliferative signaling'* in cancer. With further analyses regarding the cause of DNA damage and the mechanism of repair, a proper conclusion can be formulated regarding the targeting of the hallmark *'genome instability and mutation'* in cancer via Meriolins. In summary, Meriolins target the CDK-Rb-E2F axis with their CMGC/CDK specific kinase inhibitory profile and their potential as cancer therapeutics should be definitely investigated in further studies including the testing in *in vivo* models of the respective cancer entity.

All in all, the results presented in this dissertation underline the importance of natural product research in order to identify new lead structures for further optimization and derivatization in medicinal drug discovery. With Viriditoxin, Bromoxib and Meriolins, three completely different pathways of cell death induction were characterized.

As Hippocrates said *'Nature itself is the best physician'* – the importance of natural product research in medicinal drug discovery is highlighted and emphasizes the potential of nature's own resources in the fight against cancer.

9 References

1. Stuhldreier F, Schmitt L, Lenz T, Hinxlage I, Zimmermann M, Wollnitzke P, Schliehe-Diecks J, Liu Y, Jäger P, Geyh S, et al., *The mycotoxin viriditoxin induces leukemia- and lymphoma-specific apoptosis by targeting mitochondrial metabolism.* **Cell Death Dis** 2022, 13
2. Schmitt L, Hinxlage I, Cea PA, Gohlke H, Wesselborg S, *40 Years of Research on Polybrominated Diphenyl Ethers (PBDEs) - A Historical Overview and Newest Data of a Promising Anticancer Drug.* **Molecules** 2021, 26
3. Elmore S, *Apoptosis: A review of programmed cell death.* **Toxicol Pathol** 2007, 35:495-516
4. Hengartner MO, *The biochemistry of apoptosis.* **Nature** 2000, 407:770-6
5. Metzstein MM, Stanfield GM, Horvitz HR, *Genetics of programmed cell death in C. elegans: Past, present and future.* **Trends Genet** 1998, 14:410-6
6. Kerr JF, Wyllie AH, Currie AR, *Apoptosis: A basic biological phenomenon with wide-ranging implications in tissue kinetics.* **Br J Canc** 1972, 26:239-57
7. Burgoyne LA, *The mechanisms of pyknosis: Hypercondensation and death.* **Exp Cell Res** 1999, 248 1:214-22
8. Bratton DL, Fadok VA, Richter DA, Kailey JM, Guthrie LA, Henson PM, *Appearance of phosphatidylserine on apoptotic cells requires calcium-mediated nonspecific flip-flop and is enhanced by loss of the aminophospholipid translocase.* **J Biol Chem** 1997, 272:26159-65
9. van Engeland M, Nieland LJ, Ramaekers FC, Schutte B, Reutelingsperger CP, *Annexin V-affinity assay: A review on an apoptosis detection system based on phosphatidylserine exposure.* **Cytometry** 1998, 31:1-9
10. Arur S, Uche UE, Rezaul K, Fong M, Scranton V, Cowan AE, Mohler W, Han DK, *Annexin I is an endogenous ligand that mediates apoptotic cell engulfment.* **Dev Cell** 2003, 4:587-98
11. Gardai SJ, McPhillips KA, Frasch SC, Janssen WJ, Starefeldt A, Murphy-Ullrich JE, Bratton DL, Oldenborg PA, Michalak M, Henson PM, *Cell-surface calreticulin initiates clearance of viable or apoptotic cells through trans-activation of LRP on the phagocyte.* **Cell** 2005, 123:321-34
12. Savill J, Fadok V, *Corpse clearance defines the meaning of cell death.* **Nature** 2000, 407:784-8
13. Kurosaka K, Takahashi M, Kobayashi Y, *Activation of extracellular signal-regulated kinase 1/2 is involved in production of CXC-chemokine by macrophages during phagocytosis of late apoptotic cells.* **Biochem Biophys Res Com** 2003, 306:1070-1074
14. Tummers B, Green DR, *Caspase-8: Regulating life and death.* **Immunol Rev** 2017, 277:76-89
15. Cohen GM, *Caspases: The executioners of apoptosis.* **Biochem J** 1997, 326:1-16
16. Cooper DM, *The Balance between Life and Death: Defining a Role for Apoptosis in Aging.* **Exp Pathol** 2012, 2012
17. Lazebnik YA, Kaufmann SH, Desnoyers S, Poirier GG, Earnshaw WC, *Cleavage of poly(ADP-ribose) polymerase by a proteinase with properties like ICE.* **Nature** 1994, 371:346-7
18. Shalini S, Dorstyn L, Dawar S, Kumar S, *Old, new and emerging functions of caspases.* **Cell Death Differ** 2015, 22:526-39
19. Timmer JC, Salvesen GS, *Caspase substrates.* **Cell Death Differ** 2007, 14:66-72
20. Salvesen GS, Dixit VM, *Caspase activation: The induced-proximity model.* **Proc Natl Acad Sci U S A** 1999, 96:10964-10967
21. McIlwain DR, Berger T, Mak TW, *Caspase functions in cell death and disease.* **Cold Spring Harb Perspect Biol** 2013, 5:a008656
22. Julien O, Wells JA, *Caspases and their substrates.* **Cell Death Differ** 2017, 24:1380-1389
23. Thornberry NA, Rano TA, Peterson EP, Rasper DM, Timkey T, Garcia-Calvo M, Houtzager VM, Nordstrom PA, Roy S, Vaillancourt JP, et al., *A Combinatorial Approach Defines Specificities of Members of the Caspase Family and Granzyme B: Functional relationships established for key mediators of apoptosis.* **J Biol Chem** 1997, 272:17907-17911
24. Slee EA, Adrain C, Martin SJ, *Executioner caspase-3, -6, and -7 perform distinct, non-redundant roles during the demolition phase of apoptosis.* **J Biol Chem** 2001, 276:7320-6
25. Turchi JJ, *DNA-Dependent Protein Kinase in Apoptosis.* **Methods Mol Med** 2001, 39:693-700

26. Widłak P, *The DFF40/CAD endonuclease and its role in apoptosis.* **Acta Biochim Pol** 2000, 47:1037-44
27. Tixeira R, Phan TK, Caruso S, Shi B, Atkin-Smith GK, Nedeva C, Chow JDY, Puthalakath H, Hulett MD, Herold MJ, et al., *ROCK1 but not LIMK1 or PAK2 is a key regulator of apoptotic membrane blebbing and cell disassembly.* **Cell Death Differ** 2020, 27:102-116
28. Jänicke RU, Ng P, Sprengart ML, Porter AG, *Caspase-3 is required for alpha-fodrin cleavage but dispensable for cleavage of other death substrates in apoptosis.* **J Biol Chem** 1998, 273:15540-5
29. Green DR, *Caspases and their substrates.* **Cold Spring Harb Perspect Biol** 2022, 14:a041012
30. Zhao H, *Extrinsic and Intrinsic Apoptosis Signal Pathway Review*, in *Apoptosis and Medicine*, Tobias MN, Editor. 2012, IntechOpen: Rijeka. Ch. 1
31. Mohtasham N, Zare Mahmoudabadi R, Mohajertehran F, *Extrinsic and intrinsic pathways of apoptosis and related molecules in ischemic stroke.* **Cent Asian J Med Pharm Sci Innov** 2021, 1:194-204
32. Lavrik I, Golks A, Krammer PH, *Death receptor signaling.* **J Cell Sci** 2005, 118:265-7
33. Sayers TJ, *Targeting the extrinsic apoptosis signaling pathway for cancer therapy.* **Cancer Immunol Immunother** 2011, 60:1173-80
34. Ashkenazi A, Dixit VM, *Death receptors: Signaling and modulation.* **Science** 1998, 281:1305-8
35. Suliman A, Lam A, Datta R, Srivastava RK, *Intracellular mechanisms of TRAIL: Apoptosis through mitochondrial-dependent and -independent pathways.* **Oncogene** 2001, 20:2122-2133
36. Rubio-Moscardo F, Blesa D, Mestre C, Siebert R, Balasas T, Benito A, Rosenwald A, Climent J, Martinez JI, Schilhabel M, et al., *Characterization of 8p21.3 chromosomal deletions in B-cell lymphoma: TRAIL-R1 and TRAIL-R2 as candidate dosage-dependent tumor suppressor genes.* **Blood** 2005, 106:3214-3222
37. Chicheportiche Y, Bourdon PR, Xu H, Hsu Y-M, Scott H, Hession C, Garcia I, Browning JL, *TWEAK, a New Secreted Ligand in the Tumor Necrosis Factor Family That Weakly Induces Apoptosis.* **J Biol Chem** 1997, 272:32401-32410
38. Galluzzi L, Vitale I, Abrams JM, Alnemri ES, Baehrecke EH, Blagosklonny MV, Dawson TM, Dawson VL, El-Deiry WS, Fulda S, et al., *Molecular definitions of cell death subroutines: Recommendations of the Nomenclature Committee on Cell Death 2012.* **Cell Death Differ** 2012, 19:107-120
39. Siegmund D, Mauri D, Peters N, Juo P, Thome M, Reichwein M, Blenis J, Scheurich P, Tschopp J, Wajant H, *Fas-associated Death Domain Protein (FADD) and Caspase-8 Mediate Up-regulation of c-Fos by Fas Ligand and Tumor Necrosis Factor-related Apoptosis-inducing Ligand (TRAIL) via a FLICE Inhibitory Protein (FLIP)-regulated Pathway.* **J Biol Chem** 2001, 276:32585-32590
40. Mahdizadeh SJ, Thomas M, Eriksson LA, *Reconstruction of the Fas-Based Death-Inducing Signaling Complex (DISC) Using a Protein-Protein Docking Meta-Approach.* **J Chem Inf Model** 2021, 61:3543-3558
41. Hughes MA, Powley IR, Jukes-Jones R, Horn S, Feoktistova M, Fairall L, Schwabe JW, Leverkus M, Cain K, MacFarlane M, *Co-operative and Hierarchical Binding of c-FLIP and Caspase-8: A Unified Model Defines How c-FLIP Isoforms Differentially Control Cell Fate.* **Mol Cell** 2016, 61:834-49
42. Scaffidi C, Schmitz I, Krammer PH, Peter ME, *The role of c-FLIP in modulation of CD95-induced apoptosis.* **J Biol Chem** 1999, 274:1541-8
43. Kataoka T, Schröter M, Hahne M, Schneider P, Irmler M, Thome M, Froelich CJ, Tschopp J, *FLIP prevents apoptosis induced by death receptors but not by perforin/granzyme B, chemotherapeutic drugs, and gamma irradiation.* **J Immunol** 1998, 161:3936-42
44. Safa AR, *Roles of c-FLIP in Apoptosis, Necroptosis, and Autophagy.* **J Carcinog Mutagen** 2013, Suppl 6
45. Wei M, Lindsten T, Mootha V, Weiler S, Gross A, Ashiya M, Thompson C, Korsmeyer S, *tBID, a membrane-targeted death ligand, oligomerizes BAK to release cytochrome c.* **Genes Dev** 2000, 14:2060-71
46. Li H, Zhu H, Xu CJ, Yuan J, *Cleavage of BID by caspase 8 mediates the mitochondrial damage in the Fas pathway of apoptosis.* **Cell** 1998, 94:491-501

47. Giacomello M, Pyakurel A, Glytsou C, Scorrano L, *The cell biology of mitochondrial membrane dynamics.* **Nat Rev Mol Cell Biol** 2020, 21:204-224
48. Kalkavan H, Green DR, *MOMP, cell suicide as a BCL-2 family business.* **Cell Death Differ** 2018, 25:46-55
49. Garrido C, Galluzzi L, Brunet M, Puig PE, Didelot C, Kroemer G, *Mechanisms of cytochrome c release from mitochondria.* **Cell Death Differ** 2006, 13:1423-1433
50. Du C, Fang M, Li Y, Li L, Wang X, *Smac, a Mitochondrial Protein that Promotes Cytochrome c–Dependent Caspase Activation by Eliminating IAP Inhibition.* **Cell** 2000, 102:33-42
51. Cain K, *Chemical-induced apoptosis: Formation of the Apaf-1 apoptosome.* **Drug Metab Rev** 2003, 35:337-63
52. Yang QH, Du C, *Smac/DIABLO selectively reduces the levels of c-IAP1 and c-IAP2 but not that of XIAP and livin in HeLa cells.* **J Biol Chem** 2004, 279:16963-70
53. Lorenzo HK, Susin SA, Penninger J, Kroemer G, *Apoptosis inducing factor (AIF): A phylogenetically old, caspase-independent effector of cell death.* **Cell Death Differ** 1999, 6:516-24
54. Li LY, Luo X, Wang X, *Endonuclease G is an apoptotic DNase when released from mitochondria.* **Nature** 2001, 412:95-9
55. Chinnaiyan AM, *The apoptosome: Heart and soul of the cell death machine.* **Neoplasia** 1999, 1:5-15
56. Zou H, Li Y, Liu X, Wang X, *An APAF-1-cytochrome c multimeric complex is a functional apoptosome that activates procaspase-9.* **J Biol Chem** 1999, 274:11549-56
57. Acehan D, Jiang X, Morgan DG, Heuser JE, Wang X, Akey CW, *Three-dimensional structure of the apoptosome: Implications for assembly, procaspase-9 binding, and activation.* **Mol Cell** 2002, 9:423-32
58. Riedl SJ, Salvesen GS, *The apoptosome: Signalling platform of cell death.* **Nat Rev Mol Cell Biol** 2007, 8:405-413
59. Yuan S, Yu X, Topf M, Ludtke SJ, Wang X, Akey CW, *Structure of an Apoptosome-Procaspase-9 CARD Complex.* **Structure** 2010, 18:571-583
60. Qin H, Srinivasula SM, Wu G, Fernandes-Alnemri T, Alnemri ES, Shi Y, *Structural basis of procaspase-9 recruitment by the apoptotic protease-activating factor 1.* **Nature** 1999, 399:549-557
61. Liu X, Kim CN, Yang J, Jemmerson R, Wang X, *Induction of Apoptotic Program in Cell-Free Extracts: Requirement for dATP and Cytochrome c.* **Cell** 1996, 86:147-157
62. Li P, Nijhawan D, Budihardjo I, Srinivasula SM, Ahmad M, Alnemri ES, Wang X, *Cytochrome c and dATP-dependent formation of Apaf-1/caspase-9 complex initiates an apoptotic protease cascade.* **Cell** 1997, 91:479-89
63. Zou H, Henzel WJ, Liu X, Lutschg A, Wang X, *Apaf-1, a human protein homologous to C. elegans CED-4, participates in cytochrome c-dependent activation of caspase-3.* **Cell** 1997, 90:405-13
64. Hill MM, Adrain C, Duriez PJ, Creagh EM, Martin SJ, *Analysis of the composition, assembly kinetics and activity of native Apaf-1 apoptosomes.* **EMBO J** 2004, 23:2134-45
65. Dadsena S, King LE, García-Sáez AJ, *Apoptosis regulation at the mitochondria membrane level.* **Biochim Biophys Acta Biomembr** 2021, 1863:183716
66. Youle RJ, Strasser A, *The BCL-2 protein family: Opposing activities that mediate cell death.* **Nat Rev Mol Cell Biol** 2008, 9:47-59
67. Chipuk JE, Moldoveanu T, Llambi F, Parsons MJ, Green DR, *The BCL-2 Family Reunion.* **Mol Cell** 2010, 37:299-310
68. Bouchier-Hayes L, Lartigue L, Newmeyer D, *Mitochondria: Pharmacological manipulation of cell death.* **J Clin Invest** 2005, 115:2640-7
69. Waseem M, Wang B-D, *Promising Strategy of mPTP Modulation in Cancer Therapy: An Emerging Progress and Future Insight.* **Int J Mol Sci** 2023, 24:5564
70. Bonora M, Giorgi C, Pinton P, *Molecular mechanisms and consequences of mitochondrial permeability transition.* **Nat Rev Mol Cell Biol** 2022, 23:266-285
71. Suh DH, Kim M-k, Kim HS, Chung HH, Song YS, *Mitochondrial permeability transition pore as a selective target for anti-cancer therapy.* **Front Oncol** 2012, 3

72. Mathupala S, Ko YH, Pedersen PL, *Hexokinase II: Cancer's double-edged sword acting as both facilitator and gatekeeper of malignancy when bound to mitochondria.* **Oncogene** 2006, 25:4777-86
73. Naoi M, Wu Y, Shamoto-Nagai M, Maruyama W, *Mitochondria in Neuroprotection by Phytochemicals: Bioactive Polyphenols Modulate Mitochondrial Apoptosis System, Function and Structure.* **Int J Mol Sci** 2019, 20:2451
74. Chipuk JE, Bouchier-Hayes L, Green DR, *Mitochondrial outer membrane permeabilization during apoptosis: the innocent bystander scenario.* **Cell Death Dis** 2006, 13:1396-1402
75. Andrews DW, *The case for brakes: Why restrain the size of Bax and Bak pores in outer mitochondrial membranes?* **Mol Cell** 2022, 82:882-883
76. Zamzami N, Kroemer G, *The mitochondrion in apoptosis: How Pandora's box opens.* **Nat Rev Mol Cell Biol** 2001, 2:67-71
77. Wang C, Youle RJ, *The role of mitochondria in apoptosis.* **Annu Rev Genet** 2009, 43:95-118
78. Bernardi P, Di Lisa F, *The mitochondrial permeability transition pore: Molecular nature and role as a target in cardioprotection.* **J Mol Cell Cardiol** 2015, 78:100-6
79. Broekemeier K, Dempsey M, Pfeiffer D, *Cyclosporin A is a potent inhibitor of the inner membrane permeability transition in liver mitochondria.* **J Biol Chem** 1989, 264:7826-7830
80. Nicolli A, Basso E, Petronilli V, Wenger RM, Bernardi P, *Interactions of Cyclophilin with the Mitochondrial Inner Membrane and Regulation of the Permeability Transition Pore, a Cyclosporin A-sensitive Channel.* **J Biol Chem** 1996, 271:2185-2192
81. Connern CP, Halestrap AP, *Purification and N-terminal sequencing of peptidyl-prolyl cis-trans-isomerase from rat liver mitochondrial matrix reveals the existence of a distinct mitochondrial cyclophilin.* **Biochem J** 1992, 284:381-385
82. Connern CP, Halestrap AP, *Recruitment of mitochondrial cyclophilin to the mitochondrial inner membrane under conditions of oxidative stress that enhance the opening of a calcium-sensitive non-specific channel.* **Biochem J** 1994, 302:321-324
83. Kuwana T, Mackey MR, Perkins G, Ellisman MH, Latterich M, Schneiter R, Green DR, Newmeyer DD, *Bid, Bax, and lipids cooperate to form supramolecular openings in the outer mitochondrial membrane.* **Cell** 2002, 111:331-42
84. Hsu YT, Wolter KG, Youle RJ, *Cytosol-to-membrane redistribution of Bax and Bcl-$_{XL}$ during apoptosis.* **Proc Natl Acad Sci U S A** 1997, 94:3668-72
85. Wolter KG, Hsu YT, Smith CL, Nechushtan A, Xi XG, Youle RJ, *Movement of Bax from the cytosol to mitochondria during apoptosis.* **J Cell Biol** 1997, 139:1281-92
86. Antonsson B, Montessuit S, Sanchez B, Martinou JC, *Bax is present as a high molecular weight oligomer/complex in the mitochondrial membrane of apoptotic cells.* **J Biol Chem** 2001, 276:11615-23
87. Griffiths GJ, Dubrez L, Morgan CP, Jones NA, Whitehouse J, Corfe BM, Dive C, Hickman JA, *Cell damage-induced conformational changes of the pro-apoptotic protein Bak in vivo precede the onset of apoptosis.* **J Cell Biol** 1999, 144:903-14
88. Zong W-X, Lindsten T, Ross A, MacGregor G, Thompson C, *BH3-only proteins that bind pro-survival Bcl-2 family members fail to induce apoptosis in the absence of BAX and BAK.* **Genes Dev** 2001, 15:1481-6
89. Kim H, Rafiuddin-Shah M, Tu HC, Jeffers JR, Zambetti GP, Hsieh JJ, Cheng EH, *Hierarchical regulation of mitochondrion-dependent apoptosis by BCL-2 subfamilies.* **Nat Cell Biol** 2006, 8:1348-58
90. Kim H, Tu H-C, Ren D, Takeuchi O, Jeffers JR, Zambetti GP, Hsieh JJD, Cheng EHY, *Stepwise Activation of BAX and BAK by tBID, BIM, and PUMA Initiates Mitochondrial Apoptosis.* **Mol Cell** 2009, 36:487-499
91. Willis SN, Fletcher JI, Kaufmann T, van Delft MF, Chen L, Czabotar PE, Ierino H, Lee EF, Fairlie WD, Bouillet P, et al., *Apoptosis initiated when BH3 ligands engage multiple Bcl-2 homologs, not Bax or Bak.* **Science** 2007, 315:856-9
92. Edlich F, Banerjee S, Suzuki M, Cleland Megan M, Arnoult D, Wang C, Neutzner A, Tjandra N, Youle Richard J, *Bcl-xl Retrotranslocates Bax from the Mitochondria into the Cytosol.* **Cell** 2011, 145:104-116

93. Schellenberg B, Wang P, Keeble JA, Rodriguez-Enriquez R, Walker S, Owens TW, Foster F, Tanianis-Hughes J, Brennan K, Streuli CH, et al., *Bax exists in a dynamic equilibrium between the cytosol and mitochondria to control apoptotic priming.* **Mol Cell** 2013, 49:959-71

94. Todt F, Cakir Z, Reichenbach F, Youle RJ, Edlich F, *The C-terminal helix of Bcl-xL mediates Bax retrotranslocation from the mitochondria.* **Cell Death Differ** 2013, 20:333-342

95. Leber B, Lin J, Andrews DW, *Embedded together: The life and death consequences of interaction the Bcl-2 family with membranes.* **Apoptosis** 2007, 12:897-911

96. Lovell JF, Billen LP, Bindner S, Shamas-Din A, Fradin C, Leber B, Andrews DW, *Membrane Binding by tBid Initiates an Ordered Series of Events Culminating in Membrane Permeabilization by Bax.* **Cell** 2008, 135:1074-1084

97. Bleicken S, Wagner C, García-Sáez Ana J, *Mechanistic Differences in the Membrane Activity of Bax and Bcl-xL Correlate with Their Opposing Roles in Apoptosis.* **Biophys J** 2013, 104:421-431

98. Subburaj Y, Cosentino K, Axmann M, Pedrueza-Villalmanzo E, Hermann E, Bleicken S, Spatz J, García-Sáez AJ, *Bax monomers form dimer units in the membrane that further self-assemble into multiple oligomeric species.* **Nat Commun** 2015, 6:8042

99. Zhang Z, Subramaniam S, Kale J, Liao C, Huang B, Brahmbhatt H, Condon SG, Lapolla SM, Hays FA, Ding J, et al., *BH3-in-groove dimerization initiates and helix 9 dimerization expands Bax pore assembly in membranes.* **EMBO J** 2016, 35:208-236

100. Tanaka K, Caaveiro JMM, Morante K, González-Mañas JM, Tsumoto K, *Structural basis for self-assembly of a cytolytic pore lined by protein and lipid.* **Nat Commun** 2015, 6:6337

101. Gupta K, Donlan JAC, Hopper JTS, Uzdavinys P, Landreh M, Struwe WB, Drew D, Baldwin AJ, Stansfeld PJ, Robinson CV, *The role of interfacial lipids in stabilizing membrane protein oligomers.* **Nature** 2017, 541:421-424

102. Cowan AD, Smith NA, Sandow JJ, Kapp EA, Rustam YH, Murphy JM, Brouwer JM, Bernardini JP, Roy MJ, Wardak AZ, et al., *BAK core dimers bind lipids and can be bridged by them.* **Nat Struct Mol Biol** 2020, 27:1024-1031

103. Paradies G, Paradies V, Ruggiero FM, Petrosillo G, *Role of Cardiolipin in Mitochondrial Function and Dynamics in Health and Disease: Molecular and Pharmacological Aspects.* **Cells** 2019, 8:728

104. Falabella M, Vernon HJ, Hanna MG, Claypool SM, Pitceathly RDS, *Cardiolipin, Mitochondria, and Neurological Disease.* **Trends Endcrinol Metab** 2021, 32:224-237

105. Ren M, Phoon CK, Schlame M, *Metabolism and function of mitochondrial cardiolipin.* **Prog Lipid Res** 2014, 55:1-16

106. Ikon N, Ryan RO, *Cardiolipin and mitochondrial cristae organization.* **Biochim Biophys Acta Biomembr** 2017, 1859:1156-1163

107. Musatov A, Sedlák E, *Role of cardiolipin in stability of integral membrane proteins.* **Biochimie** 2017, 142:102-111

108. Dudek J, *Role of cardiolipin in mitochondrial signaling pathways.* **Front Cell Dev Biol** 2017, 5:90

109. Ban T, Ishihara T, Kohno H, Saita S, Ichimura A, Maenaka K, Oka T, Mihara K, Ishihara N, *Molecular basis of selective mitochondrial fusion by heterotypic action between OPA1 and cardiolipin.* **Nat Cell Biol** 2017, 19:856-863

110. Schug ZT, Gottlieb E, *Cardiolipin acts as a mitochondrial signalling platform to launch apoptosis.* **Biochim Biophys Acta Biomembr** 2009, 1788:2022-2031

111. Lucken-Ardjomande S, Montessuit S, Martinou J-C, *Contributions to Bax insertion and oligomerization of lipids of the mitochondrial outer membrane.* **Cell Death Differ** 2008, 15:929-937

112. Vogel F, Bornhövd C, Neupert W, Reichert AS, *Dynamic subcompartmentalization of the mitochondrial inner membrane.* **J Cell Biol** 2006, 175:237-47

113. Frey TG, Mannella CA, *The internal structure of mitochondria.* **Trends Biochem Sci** 2000, 25:319-24

114. Scorrano L, Ashiya M, Buttle K, Weiler S, Oakes SA, Mannella CA, Korsmeyer SJ, *A distinct pathway remodels mitochondrial cristae and mobilizes cytochrome c during apoptosis.* **Dev Cell** 2002, 2:55-67

115. Gilkerson RW, Selker JM, Capaldi RA, *The cristal membrane of mitochondria is the principal site of oxidative phosphorylation.* **FEBS Lett** 2003, 546:355-8

116. Kameoka S, Adachi Y, Okamoto K, Iijima M, Sesaki H, *Phosphatidic acid and cardiolipin coordinate mitochondrial dynamics.* **Trends Cell Biol** 2018, 28:67-76

117. Westermann B, *Mitochondrial fusion and fission in cell life and death.* **Nat Rev Mol Cell Biol** 2010, 11:872-884
118. Gilkerson R, De La Torre P, St. Vallier S, *Mitochondrial OMA1 and OPA1 as Gatekeepers of Organellar Structure/Function and Cellular Stress Response.* **Front Cell Dev Biol** 2021, 9
119. Chiu Y-H, Lin S-CA, Kuo C-H, Li C-J, *Molecular Machinery and Pathophysiology of Mitochondrial Dynamics.* **Front Cell Dev Biol** 2021, 9
120. Ishihara N, Eura Y, Mihara K, *Mitofusin 1 and 2 play distinct roles in mitochondrial fusion reactions via GTPase activity.* **J Cell Sci** 2004, 117:6535-46
121. Cipolat S, de Brito OM, Dal Zilio B, Scorrano L, *OPA1 requires mitofusin 1 to promote mitochondrial fusion.* **Proc Natl Acad Sci U S A** 2004, 101:15927-15932
122. Griparic L, Kanazawa T, van der Bliek AM, *Regulation of the mitochondrial dynamin-like protein Opa1 by proteolytic cleavage.* **J Cell Biol** 2007, 178:757-64
123. Frezza C, Cipolat S, De Brito OM, Micaroni M, Beznoussenko GV, Rudka T, Bartoli D, Polishuck RS, Danial NN, De Strooper B, *OPA1 controls apoptotic cristae remodeling independently from mitochondrial fusion.* **Cell** 2006, 126:177-189
124. Cogliati S, Enriquez JA, Scorrano L, *Mitochondrial cristae: Where beauty meets functionality.* **Trends Biochem Sci** 2016, 41:261-273
125. Yamaguchi R, Lartigue L, Perkins G, Scott RT, Dixit A, Kushnareva Y, Kuwana T, Ellisman MH, Newmeyer DD, *Opa1-mediated cristae opening is Bax/Bak and BH3 dependent, required for apoptosis, and independent of Bak oligomerization.* **Mol Cell** 2008, 31:557-569
126. Kalia R, Wang RY-R, Yusuf A, Thomas PV, Agard DA, Shaw JM, Frost A, *Structural basis of mitochondrial receptor binding and constriction by DRP1.* **Nature** 2018, 558:401-405
127. Karren MA, Coonrod EM, Anderson TK, Shaw JM, *The role of Fis1p–Mdv1p interactions in mitochondrial fission complex assembly.* **J Cell Biol** 2005, 171:291-301
128. Smirnova E, Griparic L, Shurland DL, van der Bliek AM, *Dynamin-related protein Drp1 is required for mitochondrial division in mammalian cells.* **Mol Biol Cell** 2001, 12:2245-56
129. Otera H, Wang C, Cleland MM, Setoguchi K, Yokota S, Youle RJ, Mihara K, *Mff is an essential factor for mitochondrial recruitment of Drp1 during mitochondrial fission in mammalian cells.* **J Cell Biol** 2010, 191:1141-58
130. James DI, Parone PA, Mattenberger Y, Martinou JC, *hFis1, a novel component of the mammalian mitochondrial fission machinery.* **J Biol Chem** 2003, 278:36373-9
131. Palmer CS, Osellame LD, Laine D, Koutsopoulos OS, Frazier AE, Ryan MT, *MiD49 and MiD51, new components of the mitochondrial fission machinery.* **EMBO Rep** 2011, 12:565-73
132. Fonseca TB, Sánchez-Guerrero Á, Milosevic I, Raimundo N, *Mitochondrial fission requires DRP1 but not dynamins.* **Nature** 2019, 570:E34-e42
133. Cribbs JT, Strack S, *Reversible phosphorylation of Drp1 by cyclic AMP-dependent protein kinase and calcineurin regulates mitochondrial fission and cell death.* **EMBO Rep** 2007, 8:939-44
134. Chang CR, Blackstone C, *Cyclic AMP-dependent protein kinase phosphorylation of Drp1 regulates its GTPase activity and mitochondrial morphology.* **J Biol Chem** 2007, 282:21583-7
135. Cereghetti GM, Stangherlin A, Martins de Brito O, Chang CR, Blackstone C, Bernardi P, Scorrano L, *Dephosphorylation by calcineurin regulates translocation of Drp1 to mitochondria.* **Proc Natl Acad Sci U S A** 2008, 105:15803-8
136. Baker MJ, Lampe PA, Stojanovski D, Korwitz A, Anand R, Tatsuta T, Langer T, *Stress-induced OMA1 activation and autocatalytic turnover regulate OPA1-dependent mitochondrial dynamics.* **EMBO J** 2014, 33:578-593
137. Ehses S, Raschke I, Mancuso G, Bernacchia A, Geimer S, Tondera D, Martinou JC, Westermann B, Rugarli EI, Langer T, *Regulation of OPA1 processing and mitochondrial fusion by m-AAA protease isoenzymes and OMA1.* **J Cell Biol** 2009, 187:1023-36
138. Head B, Griparic L, Amiri M, Gandre-Babbe S, van der Bliek AM, *Inducible proteolytic inactivation of OPA1 mediated by the OMA1 protease in mammalian cells.* **J Cell Biol** 2009, 187:959-66
139. Cleland MM, Norris KL, Karbowski M, Wang C, Suen DF, Jiao S, George NM, Luo X, Li Z, Youle RJ, *Bcl-2 family interaction with the mitochondrial morphogenesis machinery.* **Cell Death Differ** 2011, 18:235-247
140. Brooks C, Wei Q, Feng L, Dong G, Tao Y, Mei L, Xie Z-J, Dong Z, *Bak regulates mitochondrial morphology and pathology during apoptosis by interacting with mitofusins.* **Proc Natl Acad Sci U S A** 2007, 104:11649-11654

141. Prudent J, Zunino R, Sugiura A, Mattie S, Shore Gordon C, McBride Heidi M, *MAPL SUMOylation of Drp1 Stabilizes an ER/Mitochondrial Platform Required for Cell Death.* **Mol Cell** 2015, 59:941-955
142. Braschi E, Zunino R, McBride HM, *MAPL is a new mitochondrial SUMO E3 ligase that regulates mitochondrial fission.* **EMBO Rep** 2009, 10:748-754
143. Figueroa-Romero C, Iñiguez-Lluhí JA, Stadler J, Chang C-R, Arnoult D, Keller PJ, Hong Y, Blackstone C, Feldman EL, *SUMOylation of the mitochondrial fission protein Drp1 occurs at multiple nonconsensus sites within the B domain and is linked to its activity cycle.* **FASEB J** 2009, 23:3917
144. Karbowski M, Arnoult D, Chen H, Chan DC, Smith CL, Youle RJ, *Quantitation of mitochondrial dynamics by photolabeling of individual organelles shows that mitochondrial fusion is blocked during the Bax activation phase of apoptosis.* **J Cell Biol** 2004, 164:493-499
145. Wasiak S, Zunino R, McBride HM, *Bax/Bak promote sumoylation of DRP1 and its stable association with mitochondria during apoptotic cell death.* **J Cell Biol** 2007, 177:439-450
146. Montessuit S, Somasekharan SP, Terrones O, Lucken-Ardjomande S, Herzig S, Schwarzenbacher R, Manstein DJ, Bossy-Wetzel E, Basañez G, Meda P, et al., *Membrane Remodeling Induced by the Dynamin-Related Protein Drp1 Stimulates Bax Oligomerization.* **Cell** 2010, 142:889-901
147. Pyakurel A, Savoia C, Hess D, Scorrano L, *Extracellular Regulated Kinase Phosphorylates Mitofusin 1 to Control Mitochondrial Morphology and Apoptosis.* **Mol Cell** 2015, 58:244-254
148. Jiang X, Jiang H, Shen Z, Wang X, *Activation of mitochondrial protease OMA1 by Bax and Bak promotes cytochrome c release during apoptosis.* **Proc Natl Acad Sci U S A** 2014, 111:14782-14787
149. Chen X, Cubillos-Ruiz JR, *Endoplasmic reticulum stress signals in the tumour and its microenvironment.* **Nat Rev Cancer** 2021, 21:71-88
150. Rapoport TA, *Protein translocation across the eukaryotic endoplasmic reticulum and bacterial plasma membranes.* **Nature** 2007, 450:663-669
151. Braakman I, Hebert DN, *Protein folding in the endoplasmic reticulum.* **Cold Spring Harb Perspect Biol** 2013, 5:a013201
152. Fagone P, Jackowski S, *Membrane phospholipid synthesis and endoplasmic reticulum function.* **J Lipid Res** 2009, 50:S311-S316
153. Hebert DN, Garman SC, Molinari M, *The glycan code of the endoplasmic reticulum: Asparagine-linked carbohydrates as protein maturation and quality-control tags.* **Trends Cell Biol** 2005, 15:364-370
154. Clapham DE, *Calcium signaling.* **Cell** 2007, 131:1047-1058
155. Jaffe LF, *Sources of calcium in egg activation: A review and hypothesis.* **Dev Biol** 1983, 99:265-276
156. Samtleben S, Jaepel J, Fecher C, Andreska T, Rehberg M, Blum R, *Direct imaging of ER calcium with targeted-esterase induced dye loading (TED).* **J Vis Exp** 2013,
157. Rusiñol AE, Cui Z, Chen MH, Vance JE, *A unique mitochondria-associated membrane fraction from rat liver has a high capacity for lipid synthesis and contains pre-Golgi secretory proteins including nascent lipoproteins.* **J Biol Chem** 1994, 269:27494-502
158. Giacomello M, Pellegrini L, *The coming of age of the mitochondria–ER contact: A matter of thickness.* **Cell Death Differ** 2016, 23:1417-1427
159. De Mario A, Quintana-Cabrera R, Martinvalet D, Giacomello M, *(Neuro)degenerated Mitochondria-ER contacts.* **Biochem Biophys Res Com** 2017, 483:1096-1109
160. Chakrabarti R, Ji WK, Stan RV, de Juan Sanz J, Ryan TA, Higgs HN, *INF2-mediated actin polymerization at the ER stimulates mitochondrial calcium uptake, inner membrane constriction, and division.* **J Cell Biol** 2018, 217:251-268
161. Wong LH, Gatta AT, Levine TP, *Lipid transfer proteins: The lipid commute via shuttles, bridges and tubes.* **Nat Rev Mol Cell Biol** 2019, 20:85-101
162. Janer A, Prudent J, Paupe V, Fahiminiya S, Majewski J, Sgarioto N, Des Rosiers C, Forest A, Lin Z-Y, Gingras A-C, et al., *SLC25A46 is required for mitochondrial lipid homeostasis and cristae maintenance and is responsible for Leigh syndrome.* **EMBO Mol Med** 2016, 8:1019-1038

163. Singaravelu K, Nelson C, Bakowski D, de Brito OM, Ng SW, Di Capite J, Powell T, Scorrano L, Parekh AB, *Mitofusin 2 regulates STIM1 migration from the Ca^{2+} store to the plasma membrane in cells with depolarized mitochondria.* **J Biol Chem** 2011, 286:12189-201
164. Wacquier B, Combettes L, Dupont G, *Cytoplasmic and Mitochondrial Calcium Signaling: A Two-Way Relationship.* **Cold Spring Harb Perspect Biol** 2019, 11
165. Hetz C, Zhang K, Kaufman RJ, *Mechanisms, regulation and functions of the unfolded protein response.* **Nat Rev Mol Cell Biol** 2020, 21:421-438
166. McDonnell SJ, Spiller DG, White MRH, Prior IA, Paraoan L, *ER stress-linked autophagy stabilizes apoptosis effector PERP and triggers its co-localization with SERCA2b at ER-plasma membrane junctions.* **Cell Death Discov** 2019, 5:132
167. Camello-Almaraz C, Gomez-Pinilla PJ, Pozo MJ, Camello PJ, *Mitochondrial reactive oxygen species and Ca^{2+} signaling.* **Am J Physiol Cell Physiol** 2006, 291:C1082-C1088
168. Germain M, Mathai JP, McBride HM, Shore GC, *Endoplasmic reticulum BIK initiates DRP1-regulated remodelling of mitochondrial cristae during apoptosis.* **EMBO J** 2005, 24:1546-56
169. Bernardi P, Rasola A, Forte M, Lippe G, *The Mitochondrial Permeability Transition Pore: Channel Formation by F-ATP Synthase, Integration in Signal Transduction, and Role in Pathophysiology.* **Physiol Rev** 2015, 95:1111-55
170. Gogvadze V, Robertson JD, Zhivotovsky B, Orrenius S, *Cytochrome c release occurs via Ca^{2+}-dependent and Ca^{2+}-independent mechanisms that are regulated by Bax.* **J Cell Biol** 2001, 276:19066-19071
171. Oakes SA, *Endoplasmic Reticulum Stress Signaling in Cancer Cells.* **Am J Pathol** 2020, 190:934-946
172. Szegezdi E, Logue SE, Gorman AM, Samali A, *Mediators of endoplasmic reticulum stress-induced apoptosis.* **EMBO Rep** 2006, 7:880-5
173. Singaravelu K, Devalaraja-Narashimha K, Lastovica B, Padanilam BJ, *PERP, a p53 proapoptotic target, mediates apoptotic cell death in renal ischemia.* **Am J Physiol Renal Physiol** 2009, 296:F847-F858
174. Abreu Velez AM, Howard MS, *Tumor-suppressor Genes, Cell Cycle Regulatory Checkpoints, and the Skin.* **N Am J Med Sci** 2015, 7:176-88
175. Matthews HK, Bertoli C, de Bruin RAM, *Cell cycle control in cancer.* **Nat Rev Mol Cell Biol** 2021,
176. Fischer M, Schade AE, Branigan TB, Müller GA, DeCaprio JA, *Coordinating gene expression during the cell cycle.* **Trends Biochem Sci** 2022, 47:1009-1022
177. Whitfield ML, Sherlock G, Saldanha AJ, Murray JI, Ball CA, Alexander KE, Matese JC, Perou CM, Hurt MM, Brown PO, *Identification of genes periodically expressed in the human cell cycle and their expression in tumors.* **Mol Cell Biol** 2002, 13:1977-2000
178. Nigg EA, *Cyclin-dependent protein kinases: Key regulators of the eukaryotic cell cycle.* **Bioessays** 1995, 17:471-480
179. Fisher RP, *The CDK Network: Linking Cycles of Cell Division and Gene Expression.* **Genes Cancer** 2012, 3:731-8
180. Kovacs LAS, Orlando DA, Haase SB, *Transcription network and cyclin/CDKs: The yin and yang of cell cycle oscillators.* **Cell Cycle** 2008, 7:2626-2629
181. Morgan DO, *The Cell Cycle, Principles of Control*, in *Integ and Comp Biol*. 2007. 794-795
182. Bertoli C, Skotheim JM, de Bruin RA, *Control of cell cycle transcription during G1 and S phases.* **Nat Rev Mol Cell Biol** 2013, 14:518-28
183. Pennycook BR, Barr AR, *Restriction point regulation at the crossroads between quiescence and cell proliferation.* **FEBS Lett** 2020, 594:2046-2060
184. Rubin SM, Sage J, Skotheim JM, *Integrating Old and New Paradigms of G1/S Control.* **Mol Cell** 2020, 80:183-192
185. Trimarchi JM, Lees JA, *Sibling rivalry in the E2F family.* **Nat Rev Mol Cell Biol** 2002, 3:11-20
186. Weinberg R, *The retinoblastoma gene and gene product.* **Cancer Surv** 1992, 12:43-57
187. Narasimha AM, Kaulich M, Shapiro GS, Choi YJ, Sicinski P, Dowdy SF, *Cyclin D activates the Rb tumor suppressor by mono-phosphorylation.* **eLife** 2014, 3:e02872
188. Sanidas I, Morris R, Fella KA, Rumde PH, Boukhali M, Tai EC, Ting DT, Lawrence MS, Haas W, Dyson NJ, *A Code of Mono-phosphorylation Modulates the Function of RB.* **Mol Cell** 2019, 73:985-1000 e6

189. Kõivomägi M, Swaffer MP, Turner JJ, Marinov G, Skotheim JM, *Localized phosphorylation of RNA Polymerase II by G1 cyclin-Cdk promotes cell cycle entry.* **Science** 2021:2021.03.25.436872
190. Aleem E, Arceci RJ, *Targeting cell cycle regulators in hematologic malignancies.* **Front Cell Dev Biol** 2015, 3
191. Ding L, Cao J, Lin W, Chen H, Xiong X, Ao H, Yu M, Lin J, Cui Q, *The Roles of Cyclin-Dependent Kinases in Cell-Cycle Progression and Therapeutic Strategies in Human Breast Cancer.* **Int J Mol Sci** 2020, 21:1960
192. Hochegger H, Takeda S, Hunt T, *Cyclin-dependent kinases and cell-cycle transitions: Does one fit all?* **Nat Rev Mol Cell Biol** 2008, 9:910-916
193. Bury M, Le Calvé B, Ferbeyre G, Blank V, Lessard F, *New Insights into CDK Regulators: Novel Opportunities for Cancer Therapy.* **Trends Cell Biol** 2021, 31:331-344
194. Ma H, Seebacher NA, Hornicek FJ, Duan Z, *Cyclin-dependent kinase 9 (CDK9) is a novel prognostic marker and therapeutic target in osteosarcoma.* **EBioMedicine** 2019, 39:182-193
195. Kolupaeva V, Janssens V, *PP1 and PP2A phosphatases – cooperating partners in modulating retinoblastoma protein activation.* **FEBS J** 2013, 280:627-643
196. Johnson A, Skotheim JM, *Start and the restriction point.* **Curr Opin Cell Biol** 2013, 25:717-23
197. Gavet O, Pines J, *Progressive activation of CyclinB1-Cdk1 coordinates entry to mitosis.* **Dev Cell** 2010, 18:533-543
198. Crncec A, Hochegger H, *Triggering mitosis.* **FEBS Lett** 2019, 593:2868-2888
199. Blethrow JD, Glavy JS, Morgan DO, Shokat KM, *Covalent capture of kinase-specific phosphopeptides reveals Cdk1-cyclin B substrates.* **Proc Natl Acad Sci U S A** 2008, 105:1442-7
200. Dephoure N, Zhou C, Villén J, Beausoleil SA, Bakalarski CE, Elledge SJ, Gygi SP, *A quantitative atlas of mitotic phosphorylation.* **Proc Natl Acad Sci U S A** 2008, 105:10762-7
201. Enserink JM, Kolodner RD, *An overview of Cdk1-controlled targets and processes.* **Cell Div** 2010, 5:1-41
202. Joukov V, De Nicolo A, *Aurora-PLK1 cascades as key signaling modules in the regulation of mitosis.* **Sci Signal** 2018, 11:eaar4195
203. Elledge SJ, *Cell cycle checkpoints: Preventing an identity crisis.* **Science** 1996, 274:1664-72
204. Janssen A, Medema RH, *Genetic instability: Tipping the balance.* **Oncogene** 2013, 32:4459-70
205. Hafner A, Bulyk ML, Jambhekar A, Lahav G, *The multiple mechanisms that regulate p53 activity and cell fate.* **Nat Rev Mol Cell Biol** 2019, 20:199-210
206. Tiwari V, Wilson DM, *DNA Damage and Associated DNA Repair Defects in Disease and Premature Aging.* **Am J Hum Genet** 2019, 105:237-257
207. Lam FC, *The DNA damage response - from cell biology to human disease.* **J Transl Genet Genom** 2022, 6:204-222
208. Hoeijmakers JH, *DNA damage, aging, and cancer.* **N Engl J Med** 2009, 361:1475-85
209. De Bont R, van Larebeke N, *Endogenous DNA damage in humans: A review of quantitative data.* **Mutagenesis** 2004, 19:169-85
210. Lindahl T, *Instability and decay of the primary structure of DNA.* **Nature** 1993, 362:709-15
211. Kirkland D, Kasper P, Martus H-J, Müller L, van Benthem J, Madia F, Corvi R, *Updated recommended lists of genotoxic and non-genotoxic chemicals for assessment of the performance of new or improved genotoxicity tests.* **Mutat Res Genet Toxicol Environ Mutagen** 2016, 795:7-30
212. Hoeijmakers JH, *Genome maintenance mechanisms for preventing cancer.* **Nature** 2001, 411:366-74
213. Harper JW, Elledge SJ, *The DNA damage response: Ten years after.* **Mol Cell** 2007, 28:739-45
214. Chatterjee N, Walker GC, *Mechanisms of DNA damage, repair, and mutagenesis.* **Environ Mol Mutagen** 2017, 58:235-263
215. Pilié PG, Tang C, Mills GB, Yap TA, *State-of-the-art strategies for targeting the DNA damage response in cancer.* **Nat Rev Clin Oncol** 2019, 16:81-104
216. Ciccia A, Elledge SJ, *The DNA damage response: Making it safe to play with knives.* **Mol Cell** 2010, 40:179-204

217. Guirouilh-Barbat J, Lambert S, Bertrand P, Lopez BS, *Is homologous recombination really an error-free process?* **Front Genet** 2014, 5:175
218. Paull TT, Rogakou EP, Yamazaki V, Kirchgessner CU, Gellert M, Bonner WM, *A critical role for histone H2AX in recruitment of repair factors to nuclear foci after DNA damage.* **Curr Biol** 2000, 10:886-95
219. Finzel A, Grybowski A, Strasen J, Cristiano E, Loewer A, *Hyperactivation of ATM upon DNA-PKcs inhibition modulates p53 dynamics and cell fate in response to DNA damage.* **Mol Cell Biol** 2016, 27:2360-2367
220. Lips J, Kaina B, *DNA double-strand breaks trigger apoptosis in p53-deficient fibroblasts.* **Carcinogenesis** 2001, 22:579-585
221. van den Berg J, G. Manjón A, Kielbassa K, Feringa FM, Freire R, Medema RH, *A limited number of double-strand DNA breaks is sufficient to delay cell cycle progression.* **Nucleic Acids Res** 2018, 46:10132-10144
222. Sirbu BM, Cortez D, *DNA damage response: Three levels of DNA repair regulation.* **Cold Spring Harb Perspect Biol** 2013, 5:a012724
223. Vousden KH, Lu X, *Live or let die: The cell's response to p53.* **Nat Rev Cancer** 2002, 2:594-604
224. Schwertman P, Bekker-Jensen S, Mailand N, *Regulation of DNA double-strand break repair by ubiquitin and ubiquitin-like modifiers.* **Nat Rev Mol Cell Biol** 2016, 17:379-394
225. Thorslund T, Ripplinger A, Hoffmann S, Wild T, Uckelmann M, Villumsen B, Narita T, Sixma TK, Choudhary C, Bekker-Jensen S, et al., *Histone H1 couples initiation and amplification of ubiquitin signalling after DNA damage.* **Nature** 2015, 527:389-393
226. Escribano-Díaz C, Orthwein A, Fradet-Turcotte A, Xing M, Young Jordan TF, Tkáč J, Cook Michael A, Rosebrock Adam P, Munro M, Canny Marella D, et al., *A Cell Cycle-Dependent Regulatory Circuit Composed of 53BP1-RIF1 and BRCA1-CtIP Controls DNA Repair Pathway Choice.* **Mol Cell** 2013, 49:872-883
227. Hernández Borrero LJ, El-Deiry WS, *Tumor suppressor p53: Biology, signaling pathways, and therapeutic targeting.* **Biochim Biophys Acta Rev Cancer** 2021, 1876:188556
228. Schuler M, Green D, *Mechanisms of p53-dependent apoptosis.* **Biochem Soc Trans** 2001, 29:684-688
229. Powell SN, Kachnic LA, *Roles of BRCA1 and BRCA2 in homologous recombination, DNA replication fidelity and the cellular response to ionizing radiation.* **Oncogene** 2003, 22:5784-91
230. Huang R, Zhou P-K, *DNA damage repair: Historical perspectives, mechanistic pathways and clinical translation for targeted cancer therapy.* **Signal Transduct Target Ther** 2021, 6:254
231. Garfinkel DJ, Bailis AM, *Nucleotide Excision Repair, Genome Stability, and Human Disease: New Insight from Model Systems.* **J Biomed Biotechnol** 2002, 2:55-60
232. Henning KA, Li L, Iyer N, McDaniel LD, Reagan MS, Legerski R, Schultz RA, Stefanini M, Lehmann AR, Mayne LV, *The Cockayne syndrome group A gene encodes a WD repeat protein that interacts with CSB protein and a subunit of RNA polymerase II TFIIH.* **Cell** 1995, 82:555-564
233. van Gool AJ, Citterio E, Rademakers S, van Os R, Vermeulen W, Constantinou A, Egly J-M, Bootsma D, Hoeijmakers JH, *The Cockayne syndrome B protein, involved in transcription-coupled DNA repair, resides in an RNA polymerase II-containing complex.* **EMBO J** 1997, 16:5955-5965
234. Mellon I, Spivak G, Hanawalt PC, *Selective removal of transcription-blocking DNA damage from the transcribed strand of the mammalian DHFR gene.* **Cell** 1987, 51:241-249
235. Sugasawa K, Ng JM, Masutani C, Iwai S, van der Spek PJ, Eker AP, Hanaoka F, Bootsma D, Hoeijmakers JH, *Xeroderma pigmentosum group C protein complex is the initiator of global genome nucleotide excision repair.* **Mol Cell** 1998, 2:223-232
236. Lindahl T, Wood RD, *Quality control by DNA repair.* **Science** 1999, 286:1897-905
237. Mol CD, Parikh SS, Putnam CD, Lo TP, Tainer JA, *DNA repair mechanisms for the recognition and removal of damaged DNA bases.* **Annu Rev Biophys Biomol Struct** 1999, 28:101-28
238. Jiricny J, *The multifaceted mismatch-repair system.* **Nat Rev Mol Cell Biol** 2006, 7:335-46
239. Fishel R, *Mismatch repair.* **J Biol Chem** 2015, 290:26395-403
240. Umar A, Buermeyer AB, Simon JA, Thomas DC, Clark AB, Liskay RM, Kunkel TA, *Requirement for PCNA in DNA mismatch repair at a step preceding DNA resynthesis.* **Cell** 1996, 87:65-73

241. Knipscheer P, Räschle M, Smogorzewska A, Enoiu M, Ho TV, Schärer OD, Elledge SJ, Walter JC, *The Fanconi anemia pathway promotes replication-dependent DNA interstrand cross-link repair.* **Science** 2009, 326:1698-701

242. Moldovan GL, D'Andrea AD, *How the fanconi anemia pathway guards the genome.* **Annu Rev Genet** 2009, 43:223-49

243. Dronkert ML, Kanaar R, *Repair of DNA interstrand cross-links.* **Mutat Res** 2001, 486:217-247

244. Guainazzi A, Schärer OD, *Using synthetic DNA interstrand crosslinks to elucidate repair pathways and identify new therapeutic targets for cancer chemotherapy.* **Cell Mol Life Sci** 2010, 67:3683-3697

245. Legerski RJ, *Repair of DNA interstrand cross-links during S phase of the mammalian cell cycle.* **Environ Mol Mutagen** 2010, 51:540-551

246. Clauson C, Schärer OD, Niedernhofer L, *Advances in understanding the complex mechanisms of DNA interstrand cross-link repair.* **Cold Spring Harb Perspect Biol** 2013, 5:a012732

247. Hashimoto S, Anai H, Hanada K, *Mechanisms of interstrand DNA crosslink repair and human disorders.* **Genes Environ** 2016, 38:9

248. De Silva IU, McHugh PJ, Clingen PH, Hartley JA, *Defining the roles of nucleotide excision repair and recombination in the repair of DNA interstrand cross-links in mammalian cells.* **Mol Cell Biol** 2000, 20:7980-7990

249. Niedernhofer LJ, Odijk H, Budzowska M, Van Drunen E, Maas A, Theil AF, De Wit J, Jaspers N, Beverloo HB, Hoeijmakers JH, *The structure-specific endonuclease Ercc1-Xpf is required to resolve DNA interstrand cross-link-induced double-strand breaks.* **Mol Cell Biol** 2004, 24:5776-5787

250. McHugh PJ, Sones WR, Hartley JA, *Repair of intermediate structures produced at DNA interstrand cross-links in Saccharomyces cerevisiae.* **Mol Cell Biol** 2000, 20:3425-3433

251. Bader AS, Hawley BR, Wilczynska A, Bushell M, *The roles of RNA in DNA double-strand break repair.* **Br J Canc** 2020, 122:613-623

252. Li L, Monckton EA, Godbout R, *A role for DEAD box 1 at DNA double-strand breaks.* **Mol Cell Biol** 2008, 28:6413-6425

253. Wei W, Ba Z, Gao M, Wu Y, Ma Y, Amiard S, White CI, Danielsen JMR, Yang Y-G, Qi Y, *A role for small RNAs in DNA double-strand break repair.* **Cell** 2012, 149:101-112

254. Francia S, Michelini F, Saxena A, Tang D, de Hoon M, Anelli V, Mione M, Carninci P, d'Adda di Fagagna F, *Site-specific DICER and DROSHA RNA products control the DNA-damage response.* **Nature** 2012, 488:231-235

255. Michalik KM, Böttcher R, Förstemann K, *A small RNA response at DNA ends in Drosophila.* **Nucleic Acids Res** 2012, 40:9596-9603

256. Jain A, Bacolla A, del Mundo IM, Zhao J, Wang G, Vasquez KM, *DHX9 helicase is involved in preventing genomic instability induced by alternatively structured DNA in human cells.* **Nucleic Acids Res** 2013, 41:10345-10357

257. Marin-Vicente C, Domingo-Prim J, Eberle AB, Visa N, *RRP6/EXOSC10 is required for the repair of DNA double-strand breaks by homologous recombination.* **J Cell Sci** 2015, 128:1097-1107

258. Lu W-T, Hawley BR, Skalka GL, Baldock RA, Smith EM, Bader AS, Malewicz M, Watts FZ, Wilczynska A, Bushell M, *Drosha drives the formation of DNA:RNA hybrids around DNA break sites to facilitate DNA repair.* **Nat Commun** 2018, 9:532

259. Cohen S, Puget N, Lin Y-L, Clouaire T, Aguirrebengoa M, Rocher V, Pasero P, Canitrot Y, Legube G, *Senataxin resolves RNA:DNA hybrids forming at DNA double-strand breaks to prevent translocations.* **Nat Commun** 2018, 9:533

260. Hawley BR, Lu W-T, Wilczynska A, Bushell M, *The emerging role of RNAs in DNA damage repair.* **Cell Death Differ** 2017, 24:580-587

261. Michelini F, Jalihal AP, Francia S, Meers C, Neeb ZT, Rossiello F, Gioia U, Aguado J, Jones-Weinert C, Luke B, et al., *From "Cellular" RNA to "Smart" RNA: Multiple Roles of RNA in Genome Stability and Beyond.* **Chem Rev** 2018, 118:4365-4403

262. Adamson B, Smogorzewska A, Sigoillot FD, King RW, Elledge SJ, *A genome-wide homologous recombination screen identifies the RNA-binding protein RBMX as a component of the DNA-damage response.* **Nat Cell Biol** 2012, 14:318-328

263. Paulsen RD, Soni DV, Wollman R, Hahn AT, Yee M-C, Guan A, Hesley JA, Miller SC, Cromwell EF, Solow-Cordero DE, et al., *A Genome-wide siRNA Screen Reveals Diverse Cellular Processes and Pathways that Mediate Genome Stability.* **Mol Cell** 2009, 35:228-239
264. Yin H, Xiong G, Guo S, Xu C, Xu R, Guo P, Shu D, *Delivery of Anti-miRNA for Triple-Negative Breast Cancer Therapy Using RNA Nanoparticles Targeting Stem Cell Marker CD133.* **Mol Ther** 2019, 27:1252-1261
265. Cao F, Wan C, Xie L, Qi H, Shen L, Chen S, Song Z, Fan W, *Localized RNA interference therapy to eliminate residual lung cancer after incomplete microwave ablation.* **Thorac Cancer** 2019, 10:1369-1377
266. Chen X, Mangala LS, Rodriguez-Aguayo C, Kong X, Lopez-Berestein G, Sood AK, *RNA interference-based therapy and its delivery systems.* **Cancer Metastasis Rev** 2018, 37:107-124
267. Zhang C, Zhang B, *RNA therapeutics: Updates and future potential.* **Sci China Life Sci** 2023, 66:12-30
268. Rautela I, Sharma A, Dheer P, Thapliyal P, Sahni S, Sinha VB, Sharma MD, *Extension in the approaches to treat cancer through siRNA system: A beacon of hope in cancer therapy.* **Drug Deliv Transl Res** 2022, 12:1002-1016
269. Berraondo P, Martini PGV, Avila MA, Fontanellas A, *Messenger RNA therapy for rare genetic metabolic diseases.* **Gut** 2019, 68:1323-1330
270. Michelini F, Pitchiaya S, Vitelli V, Sharma S, Gioia U, Pessina F, Cabrini M, Wang Y, Capozzo I, Iannelli F, et al., *Damage-induced lncRNAs control the DNA damage response through interaction with DDRNAs at individual double-strand breaks.* **Nat Cell Biol** 2017, 19:1400-1411
271. Rossiello F, Aguado J, Sepe S, Iannelli F, Nguyen Q, Pitchiaya S, Carninci P, d'Adda di Fagagna F, *DNA damage response inhibition at dysfunctional telomeres by modulation of telomeric DNA damage response RNAs.* **Nat Commun** 2017, 8:13980
272. D'Alessandro G, Whelan DR, Howard SM, Vitelli V, Renaudin X, Adamowicz M, Iannelli F, Jones-Weinert CW, Lee M, Matti V, et al., *BRCA2 controls DNA:RNA hybrid level at DSBs by mediating RNase H2 recruitment.* **Nat Commun** 2018, 9:5376
273. Francia S, *Non-Coding RNA: Sequence-Specific Guide for Chromatin Modification and DNA Damage Signaling.* **Front Genet** 2015, 6
274. Ohle C, Tesorero R, Schermann G, Dobrev N, Sinning I, Fischer T, *Transient RNA-DNA Hybrids Are Required for Efficient Double-Strand Break Repair.* **Cell** 2016, 167:1001-1013.e7
275. Francia S, Cabrini M, Matti V, Oldani A, d'Adda di Fagagna F, *DICER, DROSHA and DNA damage response RNAs are necessary for the secondary recruitment of DNA damage response factors.* **J Cell Sci** 2016, 129:1468-1476
276. Gao M, Wei W, Li M-M, Wu Y-S, Ba Z, Jin K-X, Li M-M, Liao Y-Q, Adhikari S, Chong Z, et al., *Ago2 facilitates Rad51 recruitment and DNA double-strand break repair by homologous recombination.* **Cell Res** 2014, 24:532-541
277. Zhang X, Wan G, Berger FG, He X, Lu X, *The ATM kinase induces microRNA biogenesis in the DNA damage response.* **Mol Cell** 2011, 41:371-383
278. Trabucchi M, Briata P, Garcia-Mayoral M, Haase AD, Filipowicz W, Ramos A, Gherzi R, Rosenfeld MG, *The RNA-binding protein KSRP promotes the biogenesis of a subset of microRNAs.* **Nature** 2009, 459:1010-1014
279. Trabucchi M, Briata P, Filipowicz W, Ramos A, Gherzi R, Rosenfeld MG, *KSRP promotes the maturation of a group of miRNA precuresors.* **Adv Exp Med Biol** 2010:36-42
280. Bian L, Meng Y, Zhang M, Li D, *MRE11-RAD50-NBS1 complex alterations and DNA damage response: Implications for cancer treatment.* **Mol Cancer** 2019, 18:169
281. Lavin MF, Kozlov S, Gatei M, Kijas AW, *ATM-dependent phosphorylation of all three members of the MRN complex: From sensor to adaptor.* **Biomolecules** 2015, 5:2877-2902
282. Cristini A, Groh M, Kristiansen MS, Gromak N, *RNA/DNA Hybrid Interactome Identifies DXH9 as a Molecular Player in Transcriptional Termination and R-Loop-Associated DNA Damage.* **Cell Rep** 2018, 23:1891-1905
283. Ketley Ruth F, Gullerova M, *Jack of all trades? The versatility of RNA in DNA double-strand break repair.* **Essays Biochem** 2020, 64:721-735
284. García-Pichardo D, Cañas JC, García-Rubio ML, Gómez-González B, Rondón AG, Aguilera A, *Histone Mutants Separate R Loop Formation from Genome Instability Induction.* **Mol Cell** 2017, 66:597-609.e5

285. Welty S, Teng Y, Liang Z, Zhao W, Sanders LH, Greenamyre JT, Rubio ME, Thathiah A, Kodali R, Wetzel R, et al., *RAD52 is required for RNA-templated recombination repair in post-mitotic neurons.* **J Biol Chem** 2018, 293:1353-1362
286. Nolfi-Donegan D, Braganza A, Shiva S, *Mitochondrial electron transport chain: Oxidative phosphorylation, oxidant production, and methods of measurement.* **Redox Biol** 2020, 37:101674
287. DeBerardinis RJ, Chandel NS, *Fundamentals of cancer metabolism.* **Sci Adv** 2016, 2:e1600200
288. Pavlova NN, Thompson CB, *The emerging hallmarks of cancer metabolism.* **Cell Metab** 2016, 23:27-47
289. Vasan K, Werner M, Chandel NS, *Mitochondrial Metabolism as a Target for Cancer Therapy.* **Cell Metab** 2020, 32:341-352
290. Barnett JA, *A history of research on yeasts 5: The fermentation pathway.* **Yeast** 2003, 20:509-543
291. Schurr A, Gozal E, *Glycolysis at 75: is it time to tweak the first elucidated metabolic pathway in history?* **Front Neurosci** 2015, 9
292. Li XB, Gu JD, Zhou QH, *Review of aerobic glycolysis and its key enzymes - new targets for lung cancer therapy.* **Thorac Cancer** 2015, 6:17-24
293. Virmani A, Pinto L, Bauermann O, Zerelli S, Diedenhofen A, Binienda ZK, Ali SF, van der Leij FR, *The Carnitine Palmitoyl Transferase (CPT) System and Possible Relevance for Neuropsychiatric and Neurological Conditions.* **Mol Neurobiol** 2015, 52:826-836
294. Patil N, Howe O, Cahill P, Byrne HJ, *Monitoring and modelling the dynamics of the cellular glycolysis pathway: A review and future perspectives.* **Mol Metab** 2022, 66:101635
295. Alabduladhem TO, Bordoni B, *Physiology, Krebs Cycle*, in *StatPearls*. 2022, StatPearls: Treasure Island (FL)
296. Martínez-Reyes I, Diebold LP, Kong H, Schieber M, Huang H, Hensley CT, Mehta MM, Wang T, Santos JH, Woychik R, *TCA cycle and mitochondrial membrane potential are necessary for diverse biological functions.* **Mol Cell** 2016, 61:199-209
297. Martínez-Reyes I, Chandel NS, *Mitochondrial TCA cycle metabolites control physiology and disease.* **Nat Commun** 2020, 11:102
298. Krebs HA, Johnson WA, *Metabolism of ketonic acids in animal tissues.* **J Biochem** 1937, 31:645
299. Sousa JS, D'Imprima E, Vonck J, *Mitochondrial Respiratory Chain Complexes.* **Subcell Biochem** 2018, 87:167-227
300. Siekevitz P, *Powerhouse of the Cell.* **Sci Am** 1957, 197:131-144
301. Mitchell P, *Coupling of phosphorylation to electron and hydrogen transfer by a chemi-osmotic type of mechanism.* **Nature** 1961, 191:144-8
302. Zhao RZ, Jiang S, Zhang L, Yu ZB, *Mitochondrial electron transport chain, ROS generation and uncoupling.* **Int J Mol Med** 2019, 44:3-15
303. Jensen PK, *Antimycin-insensitive oxidation of succinate and reduced nicotinamide-adenine dinucleotide in electron-transport particles I. pH dependency and hydrogen peroxide formation.* **Biochim Biophys Acta** 1966, 122:157-166
304. Vinothkumar KR, Zhu J, Hirst J, *Architecture of mammalian respiratory complex I.* **Nature** 2014, 515:80-84
305. Efremov RG, Sazanov LA, *Structure of the membrane domain of respiratory complex I.* **Nature** 2011, 476:414-420
306. Hirst J, *Towards the molecular mechanism of respiratory complex I.* **Biochem J** 2009, 425:327-39
307. Cecchini G, *Function and structure of complex II of the respiratory chain.* **Annu Rev Biochem** 2003, 72:77-109
308. Sun F, Huo X, Zhai Y, Wang A, Xu J, Su D, Bartlam M, Rao Z, *Crystal Structure of Mitochondrial Respiratory Membrane Protein Complex II.* **Cell** 2005, 121:1043-1057
309. Iverson TM, *Catalytic mechanisms of complex II enzymes: A structural perspective.* **Biochim Biophys Acta Bioenerg** 2013, 1827:648-657
310. Ahmad M, Wolberg A, Kahwaji CI, *Biochemistry, Electron Transport Chain*, in *StatPearls*. 2022, StatPearls: Treasure Island (FL)
311. Schägger H, Link TA, Engel WD, von Jagow G, *Isolation of the eleven protein subunits of the bc1 complex from beef heart.* **Methods Enzymol** 1986, 126:224-37

312. Yang XH, Trumpower BL, *Purification of a three-subunit ubiquinol-cytochrome c oxidoreductase complex from Paracoccus denitrificans.* **J Biol Chem** 1986, 261:12282-9
313. Gao X, Wen X, Esser L, Quinn B, Yu L, Yu CA, Xia D, *Structural basis for the quinone reduction in the bc1 complex: A comparative analysis of crystal structures of mitochondrial cytochrome bc1 with bound substrate and inhibitors at the Qi site.* **Biochem** 2003, 42:9067-80
314. Trumpower BL, *A concerted, alternating sites mechanism of ubiquinol oxidation by the dimeric cytochrome bc(1) complex.* **Biochim Biophys Acta** 2002, 1555:166-73
315. Kadenbach B, Hüttemann M, *The subunit composition and function of mammalian cytochrome c oxidase.* **Mitochondrion** 2015, 24:64-76
316. Tsukihara T, Aoyama H, Yamashita E, Tomizaki T, Yamaguchi H, Shinzawa-Itoh K, Nakashima R, Yaono R, Yoshikawa S, *The whole structure of the 13-subunit oxidized cytochrome c oxidase at 2.8 A.* **Science** 1996, 272:1136-44
317. Konstantinov AA, *Cytochrome c oxidase: Intermediates of the catalytic cycle and their energy-coupled interconversion.* **FEBS Lett** 2012, 586:630-639
318. Sharma V, Wikström M, *The role of the K-channel and the active-site tyrosine in the catalytic mechanism of cytochrome c oxidase.* **Biochim Biophys Acta** 2016, 1857:1111-1115
319. Dickson VK, Silvester JA, Fearnley IM, Leslie AG, Walker JE, *On the structure of the stator of the mitochondrial ATP synthase.* **EMBO J** 2006, 25:2911-8
320. Watt IN, Montgomery MG, Runswick MJ, Leslie AGW, Walker JE, *Bioenergetic cost of making an adenosine triphosphate molecule in animal mitochondria.* **Proc Natl Acad Sci U S A** 2010, 107:16823-16827
321. Jonckheere AI, Smeitink JAM, Rodenburg RJT, *Mitochondrial ATP synthase: Architecture, function and pathology.* **J Inherit Metab Dis** 2012, 35:211-225
322. Campanella M, Parker N, Tan CH, Hall AM, Duchen MR, *IF1: Setting the pace of the F1F0-ATP synthase.* **Trends Cell Biol** 2009, 34:343-350
323. Alavian KN, Beutner G, Lazrove E, Sacchetti S, Park H-A, Licznerski P, Li H, Nabili P, Hockensmith K, Graham M, et al., *An uncoupling channel within the c-subunit ring of the F1/F0/ATP synthase is the mitochondrial permeability transition pore.* **Proc Natl Acad Sci U S A** 2014, 111:10580-10585
324. Azarashvili T, Odinokova I, Bakunts A, Ternovsky V, Krestinina O, Tyynelä J, Saris N-EL, *Potential role of subunit c of F0F1-ATPase and subunit c of storage body in the mitochondrial permeability transition. Effect of the phosphorylation status of subunit c on pore opening.* **Cell Calcium** 2014, 55:69-77
325. Carraro M, Giorgio V, Šileikytė J, Sartori G, Forte M, Lippe G, Zoratti M, Szabò I, Bernardi P, *Channel Formation by Yeast F-ATP Synthase and the Role of Dimerization in the Mitochondrial Permeability Transition.* **J Biol Chem** 2014, 289:15980-15985
326. Carraro M, Checchetto V, Sartori G, Kucharczyk R, di Rago JP, Minervini G, Franchin C, Arrigoni G, Giorgio V, Petronilli V, et al., *High-Conductance Channel Formation in Yeast Mitochondria is Mediated by F-ATP Synthase e and g Subunits.* **Cell Physiol Biochem** 2018, 50:1840-1855
327. Bonora M, Bononi A, De Marchi E, Giorgi C, Lebiedzinska M, Marchi S, Patergnani S, Rimessi A, Suski JM, Wojtala A, et al., *Role of the c subunit of the FO ATP synthase in mitochondrial permeability transition.* **Cell Cycle** 2013, 12:674-683
328. Guo L, Carraro M, Carrer A, Minervini G, Urbani A, Masgras I, Tosatto SCE, Szabò I, Bernardi P, Lippe G, *Arg-8 of yeast subunit e contributes to the stability of F-ATP synthase dimers and to the generation of the full-conductance mitochondrial megachannel.* **J Biol Chem** 2019, 294:10987-10997
329. Giorgio V, von Stockum S, Antoniel M, Fabbro A, Fogolari F, Forte M, Glick GD, Petronilli V, Zoratti M, Szabó I, et al., *Dimers of mitochondrial ATP synthase form the permeability transition pore.* **Proc Natl Acad Sci U S A** 2013, 110:5887-5892
330. Mnatsakanyan N, Llaguno MC, Yang Y, Yan Y, Weber J, Sigworth FJ, Jonas EA, *A mitochondrial megachannel resides in monomeric F1FO ATP synthase.* **Nature Commun** 2019, 10:5823
331. Morciano G, Preti D, Pedriali G, Aquila G, Missiroli S, Fantinati A, Caroccia N, Pacifico S, Bonora M, Talarico A, et al., *Discovery of Novel 1,3,8-Triazaspiro[4.5]decane Derivatives That Target the c Subunit of F1/FO-Adenosine Triphosphate (ATP) Synthase for the Treatment of Reperfusion Damage in Myocardial Infarction.* **J Med Chem** 2018, 61:7131-7143

332. Neginskaya MA, Solesio ME, Berezhnaya EV, Amodeo GF, Mnatsakanyan N, Jonas EA, Pavlov EV, *ATP Synthase C-Subunit-Deficient Mitochondria Have a Small Cyclosporine A-Sensitive Channel, but Lack the Permeability Transition Pore.* **Cell Rep** 2019, 26:11-17.e2

333. Urbani A, Giorgio V, Carrer A, Franchin C, Arrigoni G, Jiko C, Abe K, Maeda S, Shinzawa-Itoh K, Bogers JFM, et al., *Purified F-ATP synthase forms a Ca^{2+}-dependent high-conductance channel matching the mitochondrial permeability transition pore.* **Nat Commun** 2019, 10:4341

334. Pavlov E, Zakharian E, Bladen C, Diao CTM, Grimbly C, Reusch RN, French RJ, *A Large, Voltage-Dependent Channel, Isolated from Mitochondria by Water-Free Chloroform Extraction.* **Biophys J** 2005, 88:2614-2625

335. Kloska A, Węsierska M, Malinowska M, Gabig-Cimińska M, Jakóbkiewicz-Banecka J, *Lipophagy and Lipolysis Status in Lipid Storage and Lipid Metabolism Diseases.* **Int J Mol Sci** 2020, 21:6113

336. Caballero B, *Encyclopedia of human nutrition*. 2012, Elsevier Inc.

337. McGarry JD, Brown NF, *The Mitochondrial Carnitine Palmitoyltransferase System — From Concept to Molecular Analysis.* **Eur J Biochem** 1997, 244:1-14

338. Schreurs M, Kuipers F, Van Der Leij FR, *Regulatory enzymes of mitochondrial β-oxidation as targets for treatment of the metabolic syndrome.* **Obes Rev** 2010, 11:380-388

339. Virmani MA, Cirulli M, *The Role of l-Carnitine in Mitochondria, Prevention of Metabolic Inflexibility and Disease Initiation.* **Int J Mol Sci** 2022, 23:2717

340. Adeva-Andany MM, Carneiro-Freire N, Seco-Filgueira M, Fernández-Fernández C, Mouriño-Bayolo D, *Mitochondrial β-oxidation of saturated fatty acids in humans.* **Mitochondrion** 2019, 46:73-90

341. Rinaldo P, Matern D, Bennett MJ, *Fatty acid oxidation disorders.* **Annu Rev Physiol** 2002, 64:477-502

342. Fahy E, Cotter D, Sud M, Subramaniam S, *Lipid classification, structures and tools.* **Biochim Biophys Acta** 2011, 1811:637-47

343. Magtanong L, Ko PJ, Dixon SJ, *Emerging roles for lipids in non-apoptotic cell death.* **Cell Death Differ** 2016, 23:1099-1109

344. Aloia A, Müllhaupt D, Chabbert CD, Eberhart T, Flückiger-Mangual S, Vukolic A, Eichhoff O, Irmisch A, Alexander LT, Scibona E, *A Fatty Acid Oxidation-dependent Metabolic Shift Regulates the Adaptation of BRAF-mutated Melanoma to MAPK InhibitorsMAPKi Induce Fatty Acid Oxidation in BRAFV600E Melanomas.* **Clin Cancer Res** 2019, 25:6852-6867

345. Camarda R, Zhou AY, Kohnz RA, Balakrishnan S, Mahieu C, Anderton B, Eyob H, Kajimura S, Tward A, Krings G, *Inhibition of fatty acid oxidation as a therapy for MYC-overexpressing triple-negative breast cancer.* **Nat Med** 2016, 22:427-432

346. Carracedo A, Cantley LC, Pandolfi PP, *Cancer metabolism: Fatty acid oxidation in the limelight.* **Nat Rev Cancer** 2013, 13:227-232

347. Chen RR, Yung MM, Xuan Y, Zhan S, Leung LL, Liang RR, Leung TH, Yang H, Xu D, Sharma R, *Targeting of lipid metabolism with a metabolic inhibitor cocktail eradicates peritoneal metastases in ovarian cancer cells.* **Commun Biol** 2019, 2:281

348. Cheng S, Wang G, Wang Y, Cai L, Qian K, Ju L, Liu X, Xiao Y, Wang X, *Fatty acid oxidation inhibitor etomoxir suppresses tumor progression and induces cell cycle arrest via PPARγ-mediated pathway in bladder cancer.* **Clin Sci** 2019, 133:1745-1758

349. Duman C, Yaqubi K, Hoffmann A, Acikgöz AA, Korshunov A, Bendszus M, Herold-Mende C, Liu H-K, Alfonso J, *Acyl-CoA-Binding Protein Drives Glioblastoma Tumorigenesis by Sustaining Fatty Acid Oxidation.* **Cell Metab** 2019, 30:274-289.e5

350. Edmunds LR, Sharma L, Kang A, Lu J, Vockley J, Basu S, Uppala R, Goetzman ES, Beck ME, Scott D, et al., *c-Myc Programs Fatty Acid Metabolism and Dictates Acetyl-CoA Abundance and Fate.* **J Biol Chem** 2014, 289:25382-25392

351. Padanad MS, Konstantinidou G, Venkateswaran N, Melegari M, Rindhe S, Mitsche M, Yang C, Batten K, Huffman KE, Liu J, et al., *Fatty Acid Oxidation Mediated by Acyl-CoA Synthetase Long Chain 3 Is Required for Mutant KRAS Lung Tumorigenesis.* **Cell Rep** 2016, 16:1614-1628

352. He W, Liang B, Wang C, Li S, Zhao Y, Huang Q, Liu Z, Yao Z, Wu Q, Liao W, et al., *MSC-regulated lncRNA MACC1-AS1 promotes stemness and chemoresistance through fatty acid oxidation in gastric cancer.* **Oncogene** 2019, 38:4637-4654

353. Qu Q, Zeng F, Liu X, Wang QJ, Deng F, *Fatty acid oxidation and carnitine palmitoyltransferase I: Emerging therapeutic targets in cancer.* **Cell Death Dis** 2016, 7:e2226-e2226

354. Li YJ, Fahrmann JF, Aftabizadeh M, Zhao Q, Tripathi SC, Zhang C, Yuan Y, Ann D, Hanash S, Yu H, *Fatty acid oxidation protects cancer cells from apoptosis by increasing mitochondrial membrane lipids.* **Cell Rep** 2022, 39:110870
355. Singh KB, Hahm E-R, Kim S-H, Singh SV, *Withaferin A Inhibits Fatty Acid Synthesis in Rat Mammary Tumors.* **Cancer Prev Res** 2023, 16:5-16
356. Liu S, Lai J, Feng Y, Zhuo Y, Zhang H, Chen Y, Li J, Mei X, Zeng Y, Su J, et al., *Acetyl-CoA carboxylase 1 depletion suppresses de novo fatty acid synthesis and mitochondrial beta oxidation in castration-resistant prostate cancer cells.* **J Biol Chem** 2023, 299
357. Zhong L, Li Y, Xiong L, Wang W, Wu M, Yuan T, Yang W, Tian C, Miao Z, Wang T, *Small molecules in targeted cancer therapy: Advances, challenges, and future perspectives.* **Signal Transduct Target Ther** 2021, 6:201
358. Pucci C, Martinelli C, Ciofani G, *Innovative approaches for cancer treatment: Current perspectives and new challenges.* **Ecancermedicalscience** 2019, 13
359. Choudhari AS, Mandave PC, Deshpande M, Ranjekar P, Prakash O, *Phytochemicals in cancer treatment: From preclinical studies to clinical practice.* **Front Pharmacol** 2020, 10:1614
360. Mansoori B, Mohammadi A, Davudian S, Shirjang S, Baradaran B, *The Different Mechanisms of Cancer Drug Resistance: A Brief Review.* **Adv Pharm Bull** 2017, 7:339-348
361. Uramoto H, Tanaka F, *Recurrence after surgery in patients with NSCLC.* **Transl Lung Cancer Res** 2014, 3:242
362. Castells M, Thibault B, Delord J-P, Couderc B, *Implication of tumor microenvironment in chemoresistance: Tumor-associated stromal cells protect tumor cells from cell death.* **Int J Mol Sci** 2012, 13:9545-9571
363. Emran TB, Shahriar A, Mahmud AR, Rahman T, Abir MH, Siddiquee MF-R, Ahmed H, Rahman N, Nainu F, Wahyudin E, et al., *Multidrug Resistance in Cancer: Understanding Molecular Mechanisms, Immunoprevention and Therapeutic Approaches.* **Front Oncol** 2022, 12
364. O'Connor D, Sibson K, Caswell M, Connor P, Cummins M, Mitchell C, Motwani J, Taj M, Vora A, Wynn R, *Early UK experience in the use of clofarabine in the treatment of relapsed and refractory paediatric acute lymphoblastic leukaemia.* **Br J Haematol** 2011, 154:482-485
365. Hanahan D, *Hallmarks of Cancer: New Dimensions.* **Cancer Discov** 2022, 12:31-46
366. Hanahan D, Weinberg RA, *The Hallmarks of Cancer.* **Cell** 2000, 100:57-70
367. Hanahan D, Weinberg RA, *Hallmarks of cancer: The next generation.* **Cell** 2011, 144:646-674
368. Carneiro BA, El-Deiry WS, *Targeting apoptosis in cancer therapy.* **Nat Rev Clin Oncol** 2020, 17:395-417
369. Kurrey NK, Jalgaonkar SP, Joglekar AV, Ghanate AD, Chaskar PD, Doiphode RY, Bapat SA, *Snail and Slug Mediate Radioresistance and Chemoresistance by Antagonizing p53-Mediated Apoptosis and Acquiring a Stem-Like Phenotype in Ovarian Cancer Cells.* **Stem Cells** 2009, 27:2059-2068
370. Teixeira C, Reed JC, Pratt MC, *Estrogen promotes chemotherapeutic drug resistance by a mechanism involving Bcl-2 proto-oncogene expression in human breast cancer cells.* **Cancer Res** 1995, 55:3902-3907
371. Reed JC, *Bcl-2: Prevention of apoptosis as a mechanism of drug resistance.* **Hematol Oncol Clin North Am** 1995, 9:451-474
372. Pearl LH, Schierz AC, Ward SE, Al-Lazikani B, Pearl FM, *Therapeutic opportunities within the DNA damage response.* **Nat Rev Cancer** 2015, 15:166-80
373. Lane DP, *p53, guardian of the genome.* **Nature** 1992, 358:15-16
374. Olivier M, Hollstein M, Hainaut P, *TP53 mutations in human cancers: Origins, consequences, and clinical use.* **Cold Spring Harb Perspect Biol** 2010, 2:a001008
375. Kotler E, Shani O, Goldfeld G, Lotan-Pompan M, Tarcic O, Gershoni A, Hopf TA, Marks DS, Oren M, Segal E, *A Systematic p53 Mutation Library Links Differential Functional Impact to Cancer Mutation Pattern and Evolutionary Conservation.* **Mol Cell** 2018, 71:178-190.e8
376. Zhang J, Stevens MF, Bradshaw TD, *Temozolomide: Mechanisms of action, repair and resistance.* **Curr Mol Pharmacol** 2012, 5:102-14
377. Liu LV, Bell III CB, Wong SD, Wilson SA, Kwak Y, Chow MS, Zhao J, Hodgson KO, Hedman B, Solomon EI, *Definition of the intermediates and mechanism of the anticancer drug bleomycin using nuclear resonance vibrational spectroscopy and related methods.* **Proc Natl Acad Sci U S A** 2010, 107:22419-22424

378. Galluzzi L, Senovilla L, Vitale I, Michels J, Martins I, Kepp O, Castedo M, Kroemer G, *Molecular mechanisms of cisplatin resistance.* **Oncogene** 2012, 31:1869-1883
379. Bukowski K, Kciuk M, Kontek R, *Mechanisms of Multidrug Resistance in Cancer Chemotherapy.* **Int J Mol Sci** 2020, 21:3233
380. Huang D, Duan H, Huang H, Tong X, Han Y, Ru G, Qu L, Shou C, Zhao Z, *Cisplatin resistance in gastric cancer cells is associated with HER2 upregulation-induced epithelial-mesenchymal transition.* **Sci Rep** 2016, 6:1-12
381. Tian H, Gao Z, Li H, Zhang B, Wang G, Zhang Q, Pei D, Zheng J, *DNA damage response – A double-edged sword in cancer prevention and cancer therapy.* **Cancer Lett** 2015, 358:8-16
382. Carrassa L, Colombo I, Damia G, Bertoni F, *Targeting the DNA damage response for patients with lymphoma: Preclinical and clinical evidences.* **Cancer Treat Rev** 2020, 90:102090
383. Deshpande A, Sicinski P, Hinds PW, *Cyclins and cdks in development and cancer: A perspective.* **Oncogene** 2005, 24:2909-15
384. Kent LN, Leone G, *The broken cycle: E2F dysfunction in cancer.* **Nat Rev Cancer** 2019, 19:326-338
385. Malumbres M, Barbacid M, *Cell cycle, CDKs and cancer: A changing paradigm.* **Nat Rev Cancer** 2009, 9:153-66
386. Whittaker SR, Mallinger A, Workman P, Clarke PA, *Inhibitors of cyclin-dependent kinases as cancer therapeutics.* **Pharmacol Ther** 2017, 173:83-105
387. Sherr CJ, Beach D, Shapiro GI, *Targeting CDK4 and CDK6: From discovery to therapy.* **Cancer Discov** 2016, 6:353-367
388. Otto T, Sicinski P, *Cell cycle proteins as promising targets in cancer therapy.* **Nat Rev Cancer** 2017, 17:93-115
389. Klein ME, Kovatcheva M, Davis LE, Tap WD, Koff A, *CDK4/6 inhibitors: The mechanism of action may not be as simple as once thought.* **Cancer Cell** 2018, 34:9-20
390. Lynce F, Shajahan-Haq AN, Swain SM, *CDK4/6 inhibitors in breast cancer therapy: Current practice and future opportunities.* **Pharmacol Ther** 2018, 191:65-73
391. Ma Y, Kurtyka CA, Boyapalle S, Sung S-S, Lawrence H, Guida W, Cress WD, *A small-molecule E2F inhibitor blocks growth in a melanoma culture model.* **Cancer Res** 2008, 68:6292-6299
392. Kurtyka CA, Chen L, Cress WD, *E2F inhibition synergizes with paclitaxel in lung cancer cell lines.* **PLoS One** 2014, 9:e96357
393. Sangwan M, McCurdy SR, Livne-bar I, Ahmad M, Wrana JL, Chen D, Bremner R, *Established and new mouse models reveal E2f1 and Cdk2 dependency of retinoblastoma, and expose effective strategies to block tumor initiation.* **Oncogene** 2012, 31:5019-5028
394. Lan W, Bian B, Xia Y, Dou S, Gayet O, Bigonnet M, Santofimia-Castaño P, Cong M, Peng L, Dusetti N, *E2F signature is predictive for the pancreatic adenocarcinoma clinical outcome and sensitivity to E2F inhibitors, but not for the response to cytotoxic-based treatments.* **Sci Rep** 2018, 8:8330
395. Malumbres M, Harlow E, Hunt T, Hunter T, Lahti JM, Manning G, Morgan DO, Tsai L-H, Wolgemuth DJ, *Cyclin-dependent kinases: A family portrait.* **Nat Cell Biol** 2009, 11:1275-1276
396. Zhang M, Zhang L, Hei R, Li X, Cai H, Wu X, Zheng Q, Cai C, *CDK inhibitors in cancer therapy, an overview of recent development.* **Am J Cancer Res** 2021, 11:1913-1935
397. Lim S, Kaldis P, *Cdks, cyclins and CKIs: Roles beyond cell cycle regulation.* **Development** 2013, 140:3079-3093
398. Meijer L, Borgne A, Mulner O, Chong JP, Blow JJ, Inagaki N, Inagaki M, Delcros JG, Moulinoux JP, *Biochemical and cellular effects of roscovitine, a potent and selective inhibitor of the cyclin-dependent kinases cdc2, cdk2 and cdk5.* **Eur J Biochem** 1997, 243:527-536
399. Cicenas J, Kalyan K, Sorokinas A, Stankunas E, Levy J, Meskinyte I, Stankevicius V, Kaupinis A, Valius M, *Roscovitine in cancer and other diseases.* **Ann Transl Med** 2015, 3
400. Panagiotou E, Gomatou G, Trontzas IP, Syrigos N, Kotteas E, *Cyclin-dependent kinase (CDK) inhibitors in solid tumors: A review of clinical trials.* **Clin Transl Oncol** 2022, 24:161-192
401. Fry DW, Harvey PJ, Keller PR, Elliott WL, Meade M, Trachet E, Albassam M, Zheng X, Leopold WR, Pryer NK, *Specific inhibition of cyclin-dependent kinase 4/6 by PD 0332991 and associated antitumor activity in human tumor xenografts.* **Mol Cancer Ther** 2004, 3:1427-1438

402. Tripathy D, Bardia A, Sellers WR, *Ribociclib (LEE011): Mechanism of Action and Clinical Impact of This Selective Cyclin-Dependent Kinase 4/6 Inhibitor in Various Solid TumorsMechanism of Action and Clinical Impact of Ribociclib.* **Clin Cancer Res** 2017, 23:3251-3262
403. Gelbert LM, Cai S, Lin X, Sanchez-Martinez C, Del Prado M, Lallena MJ, Torres R, Ajamie RT, Wishart GN, Flack RS, *Preclinical characterization of the CDK4/6 inhibitor LY2835219: In-vivo cell cycle-dependent/independent anti-tumor activities alone/in combination with gemcitabine.* **Invest New Drugs** 2014, 32:825-837
404. Poratti M, Marzaro G, *Third-generation CDK inhibitors: A review on the synthesis and binding modes of Palbociclib, Ribociclib and Abemaciclib.* **Eur J Med Chem** 2019, 172:143-153
405. Bacon CW, D'Orso I, *CDK9: A signaling hub for transcriptional control.* **Transcription** 2019, 10:57-75
406. Franco LC, Morales F, Boffo S, Giordano A, *CDK9: A key player in cancer and other diseases.* **J Cell Biol** 2018, 119:1273-1284
407. Anda S, Rothe C, Boye E, Grallert B, *Consequences of abnormal CDK activity in S phase.* **Cell Cycle** 2016, 15:963-973
408. Cherukupalli S, Chandrasekaran B, Aleti RR, Sayyad N, Hampannavar GA, Merugu SR, Rachamalla HR, Banerjee R, Karpoormath R, *Synthesis of 4, 6-disubstituted pyrazolo [3, 4-d] pyrimidine analogues: Cyclin-dependent kinase 2 (CDK2) inhibition, molecular docking and anticancer evaluation.* **J Mol Struct** 2019, 1176:538-551
409. Galbraith MD, Bender H, Espinosa JM, *Therapeutic targeting of transcriptional cyclin-dependent kinases.* **Transcription** 2019, 10:118-136
410. Lukasik PM, Elabar S, Lam F, Shao H, Liu X, Abbas AY, Wang S, *Synthesis and biological evaluation of imidazo[4,5-b]pyridine and 4-heteroaryl-pyrimidine derivatives as anti-cancer agents.* **Eur J Med Chem** 2012, 57:311-322
411. Singh U, Chashoo G, Khan SU, Mahajan P, Nargotra A, Mahajan G, Singh A, Sharma A, Mintoo MJ, Guru SK, et al., *Design of Novel 3-Pyrimidinylazaindole CDK2/9 Inhibitors with Potent In Vitro and In Vivo Antitumor Efficacy in a Triple-Negative Breast Cancer Model.* **J Med Chem** 2017, 60:9470-9489
412. Motati DR, Amaradhi R, Ganesh T, *Azaindole therapeutic agents.* **Bioorg Med Chem** 2020, 28:115830
413. Lunt SY, Vander Heiden MG, *Aerobic glycolysis: meeting the metabolic requirements of cell proliferation.* **Annu Rev Cell Dev Biol** 2011, 27:441-464
414. Loo JM, Scherl A, Nguyen A, Man FY, Weinberg E, Zeng Z, Saltz L, Paty PB, Tavazoie SF, *Extracellular metabolic energetics can promote cancer progression.* **Cell** 2015, 160:393-406
415. Warburg O, *On the origin of cancer cells.* **Science** 1956, 123:309-314
416. Koppenol WH, Bounds PL, Dang CV, *Otto Warburg's contributions to current concepts of cancer metabolism.* **Nat Rev Cancer** 2011, 11:325-337
417. Hu C-J, Wang L-Y, Chodosh LA, Keith B, Simon MC, *Differential Roles of Hypoxia-Inducible Factor 1α (HIF-1α) and HIF-2α in Hypoxic Gene Regulation.* **Mol Cell Biol** 2003, 23:9361-9374
418. Stine ZE, Walton ZE, Altman BJ, Hsieh AL, Dang CV, *MYC, Metabolism, and Cancer.* **Cancer Discov** 2015, 5:1024-1039
419. Kruiswijk F, Labuschagne CF, Vousden KH, *p53 in survival, death and metabolic health: A lifeguard with a licence to kill.* **Nat Rev Mol Cell Biol** 2015, 16:393-405
420. Hensley CT, Wasti AT, DeBerardinis RJ, *Glutamine and cancer: Cell biology, physiology, and clinical opportunities.* **J Clin Invest** 2013, 123:3678-3684
421. Mayers JR, Wu C, Clish CB, Kraft P, Torrence ME, Fiske BP, Yuan C, Bao Y, Townsend MK, Tworoger SS, *Elevation of circulating branched-chain amino acids is an early event in human pancreatic adenocarcinoma development.* **Nat Med** 2014, 20:1193-1198
422. Galluzzi L, Kepp O, Heiden MGV, Kroemer G, *Metabolic targets for cancer therapy.* **Nat Rev Drug Discov** 2013, 12:829-846
423. Altenberg B, Greulich KO, *Genes of glycolysis are ubiquitously overexpressed in 24 cancer classes.* **Genomics** 2004, 84:1014-1020
424. Liu Y, Cao Y, Zhang W, Bergmeier S, Qian Y, Akbar H, Colvin R, Ding J, Tong L, Wu S, *A Small-Molecule Inhibitor of Glucose Transporter 1 Downregulates Glycolysis, Induces Cell-Cycle Arrest, and Inhibits Cancer Cell Growth In Vitro and In VivoA Glut1 Inhibitor Reduces Cancer Growth In Vitro and In Vivo.* **Mol Cancer Ther** 2012, 11:1672-1682

425. Gautier EL, Westerterp M, Bhagwat N, Cremers S, Shih A, Abdel-Wahab O, Lütjohann D, Randolph GJ, Levine RL, Tall AR, *HDL and Glut1 inhibition reverse a hypermetabolic state in mouse models of myeloproliferative disorders.* **J Exp Med** 2013, 210:339-353

426. Ganapathy-Kanniappan S, Geschwind J-FH, Kunjithapatham R, Buijs M, Syed LH, Rao PP, Ota S, Kwak BK, Loffroy R, Vali M, *3-Bromopyruvate induces endoplasmic reticulum stress, overcomes autophagy and causes apoptosis in human HCC cell lines.* **Anticancer Res** 2010, 30:923-935

427. Dwarakanath B, Jain V, *Targeting glucose metabolism with 2-deoxy-D-glucose for improving cancer therapy.* **Future Oncol** 2009, 5:581-585

428. Jae HJ, Chung JW, Park HS, Lee MJ, Lee KC, Kim H-C, Yoon JH, Chung H, Park JH, *The antitumor effect and hepatotoxicity of a hexokinase II inhibitor 3-bromopyruvate: in vivo investigation of intraarterial administration in a rabbit VX2 hepatoma model.* **Korean J Radiol** 2009, 10:596-603

429. Rumsey W, Schlosser C, Nuutinen E, Robiolio M, Wilson D, *Cellular energetics and the oxygen dependence of respiration in cardiac myocytes isolated from adult rat.* **J Biol Chem** 1990, 265:15392-15399

430. Le A, Stine ZE, Nguyen C, Afzal J, Sun P, Hamaker M, Siegel NM, Gouw AM, Kang B-h, Yu S-H, *Tumorigenicity of hypoxic respiring cancer cells revealed by a hypoxia–cell cycle dual reporter.* **Proc Natl Acad Sci U S A** 2014, 111:12486-12491

431. Pollak M, *Overcoming drug development bottlenecks with repurposing: Repurposing biguanides to target energy metabolism for cancer treatment.* **Nat Med** 2014, 20:591-593

432. Stuart SD, Schauble A, Gupta S, Kennedy AD, Keppler BR, Bingham PM, Zachar Z, *A strategically designed small molecule attacks alpha-ketoglutarate dehydrogenase in tumor cells through a redox process.* **Cancer Metab** 2014, 2:1-15

433. Alistar A, Desnoyers R, D'Agostino R, Pasche B, *CPI-613 enhances FOLFIRINOX response rate in stage IV pancreatic cancer.* **Ann Oncol** 2016, 27:vi228

434. Pardee TS, Lee K, Luddy J, Maturo C, Rodriguez R, Isom S, Miller LD, Stadelman KM, Levitan D, Hurd D, *A Phase I Study of the First-in-Class Antimitochondrial Metabolism Agent, CPI-613, in Patients with Advanced Hematologic MalignanciesA Phase I Study of CPI-613.* **Clin Cancer Res** 2014, 20:5255-5264

435. Huang M, Lu J-J, Ding J, *Natural Products in Cancer Therapy: Past, Present and Future.* **Nat Prod Bioprospect** 2021, 11:5-13

436. Newman DJ, Cragg GM, *Natural products as sources of new drugs over the nearly four decades from 01/1981 to 09/2019.* **J Nat Prod** 2020, 83:770-803

437. Huang M-Y, Zhang L-L, Ding J, Lu J-J, *Anticancer drug discovery from Chinese medicinal herbs.* **Chin Med** 2018, 13:1-9

438. Cui Y, Li C, Sang F, Cao W, Qin Z, Zhang P, *Natural products targeting glycolytic signaling pathways-an updated review on anti-cancer therapy.* **Front Pharmacol** 2022, 13:1035882

439. Gao Y, Stuhldreier F, Schmitt L, Wesselborg S, Wang L, Müller WEG, Kalscheuer R, Guo Z, Zou K, Liu Z, et al., *Sesterterpenes and macrolide derivatives from the endophytic fungus Aplosporella javeedii.* **Fitoterapia** 2020, 146:104652

440. Gao Y, Stuhldreier F, Schmitt L, Wesselborg S, Guo Z, Zou K, Mándi A, Kurtán T, Liu Z, Proksch P, *Induction of New Lactam Derivatives From the Endophytic Fungus Aplosporella javeedii Through an OSMAC Approach.* **Front Microbiol** 2020, 11:600983

441. Mayer S, Prechtl M, Liebfried P, Cadeddu RP, Stuhldreier F, Kohl M, Wenzel F, Stork B, Wesselborg S, Proksch P, et al., *First Results from a Screening of 300 Naturally Occurring Compounds: 4,6-dibromo-2-(2',4'-dibromophenoxy)phenol, 4,5,6-tribromo-2-(2',4'-dibromophenoxy)phenol, and 5-epi-nakijinone Q as Substances with the Potential for Anticancer Therapy.* **Mar Drugs** 2019, 17:521-538

442. Drießen D, Dissertation: *Diversitätsorientierte Synthese neuer 7-Azaindol-Derivate gegen Therapie-resistente Tumore und Infektionen.* 2020, Institut für Organische Chemie und Makromolekulare Chemie. Heinrich-Heine-Universität, Düsseldorf

443. Drießen D, Stuhldreier F, Frank A, Stark H, Wesselborg S, Stork B, Muller TJJ, *Novel meriolin derivatives as rapid apoptosis inducers.* **Bioorg Med Chem** 2019, 27:3463-3468

444. Barrera M, Koob S, Dikov D, Vogel F, Reichert AS, *OPA1 functionally interacts with MIC60 but is dispensable for crista junction formation.* **FEBS Lett** 2016, 590:3309-3322

445. Rudner J, Lepple-Wienhues A, Budach W, Berschauer J, Friedrich B, Wesselborg S, Schulze-Osthoff K, Belka C, *Wild-type, mitochondrial and ER-restricted Bcl-2 inhibit DNA damage-induced apoptosis but do not affect death receptor-induced apoptosis.* **J Cell Sci** 2001, 114:4161-4172

446. Manns J, Daubrawa M, Driessen S, Paasch F, Hoffmann N, Loffler A, Lauber K, Dieterle A, Alers S, Iftner T, et al., *Triggering of a novel intrinsic apoptosis pathway by the kinase inhibitor staurosporine: Activation of caspase-9 in the absence of Apaf-1.* **FASEB J** 2011, 25:3250-61

447. Bampton ETW, Goemans CG, Niranjan D, Mizushima N, Tolkovsky AM, *The Dynamics of Autophagy Visualised in Live Cells: from Autophagosome Formation to Fusion with Endo/lysosomes.* **Autophagy** 2005, 1:23-36

448. Anand R, Wai T, Baker MJ, Kladt N, Schauss AC, Rugarli E, Langer T, *The i-AAA protease YME1L and OMA1 cleave OPA1 to balance mitochondrial fusion and fission.* **J Cell Biol** 2014, 204:919-29

449. Soengas MS, Capodieci P, Polsky D, Mora J, Esteller M, Opitz-Araya X, McCombie R, Herman JG, Gerald WL, Lazebnik YA, et al., *Inactivation of the apoptosis effector Apaf-1 in malignant melanoma.* **Nature** 2001, 409:207-11

450. Bradford MM, *A rapid and sensitive method for the quantitation of microgram quantities of protein utilizing the principle of protein-dye binding.* **Anal Biochem** 1976, 72:248-54

451. Laemmli UK, *Cleavage of structural proteins during the assembly of the head of bacteriophage T4.* **Nature** 1970, 227:680-685

452. Weber K, Osborn M, *The reliability of molecular weight determinations by dodecyl sulfate-polyacrylamide gel electrophoresis.* **J Biol Chem** 1969, 244:4406-4412

453. Nicoletti I, Migliorati G, Pagliacci MC, Grignani F, Riccardi C, *A rapid and simple method for measuring thymocyte apoptosis by propidium iodide staining and flow cytometry.* **J Immunol Methods** 1991, 139:271-279

454. Franken H, Mathieson T, Childs D, Sweetman GM, Werner T, Tögel I, Doce C, Gade S, Bantscheff M, Drewes G, et al., *Thermal proteome profiling for unbiased identification of direct and indirect drug targets using multiplexed quantitative mass spectrometry.* **Nat Protoc** 2015, 10:1567-93

455. Folch J, Lees M, Sloane Stanley GH, *A simple method for the isolation and purification of total lipides from animal tissues.* **J Biol Chem** 1957, 226:497-509

456. Ruiz JI, Ochoa B, *Quantification in the subnanomolar range of phospholipids and neutral lipids by monodimensional thin-layer chromatography and image analysis.* **J Lipid Res** 1997, 38:1482-1489

457. Hirschey MD, Shimazu T, Goetzman E, Jing E, Schwer B, Lombard DB, Grueter CA, Harris C, Biddinger S, Ilkayeva OR, et al., *SIRT3 regulates mitochondrial fatty-acid oxidation by reversible enzyme deacetylation.* **Nature** 2010, 464:121-5

458. Vila-Brau A, De Sousa-Coelho AL, Mayordomo C, Haro D, Marrero PF, *Human HMGCS2 regulates mitochondrial fatty acid oxidation and FGF21 expression in HepG2 cell line.* **J Biol Chem** 2011, 286:20423-30

459. Dander E, Fallati A, Starace R, Giussani A, Mauri M, Piazza R, Rizzari C, Biondi A, D'Amico G, *Activina: A Key Factor Mediating Chemoresistance in B-Cell Type Acute Lymphoblastic Leukemia.* **Blood** 2022, 140:6002-6003

460. Wang X, Lou K, Song X, Ma H, Zhou X, Xu H, Wang W, *Mebendazole is a potent inhibitor to chemoresistant T cell acute lymphoblastic leukemia cells.* **Toxicol Appl Pharmacol** 2020, 396:115001

461. Omura S, Iwai Y, Hirano A, Nakagawa A, Awaya J, Tsuchya H, Takahashi Y, Masuma R, *A new alkaloid AM-2282 OF Streptomyces origin. Taxonomy, fermentation, isolation and preliminary characterization.* **J Antibiot** 1977, 30:275-82

462. Eskandari E, Eaves CJ, *Paradoxical roles of caspase-3 in regulating cell survival, proliferation, and tumorigenesis.* **J Cell Biol** 2022, 221

463. Koncha RR, Ramachandran G, Sepuri NBV, Ramaiah KVA, *CCCP-induced mitochondrial dysfunction - characterization and analysis of integrated stress response to cellular signaling and homeostasis.* **FEBS J** 2021, 288:5737-5754

464. Lim ML, Minamikawa T, Nagley P, *The protonophore CCCP induces mitochondrial permeability transition without cytochrome c release in human osteosarcoma cells.* **FEBS Lett** 2001, 503:69-74

465. Kwon D, Park E, Sesaki H, Kang SJ, *Carbonyl cyanide 3-chlorophenylhydrazone (CCCP) suppresses STING-mediated DNA sensing pathway through inducing mitochondrial fission.* **Biochem Biophys Res Com** 2017, 493:737-743

466. Stuhldreier F, Dissertation: *Identification of apoptosis-inducing natural products and derivatives for the elimination of tumor cells.* 2021, Institute for Molecular Medicine I. Heinrich Heine University, Düsseldorf

467. Savitski MM, Reinhard FB, Franken H, Werner T, Savitski MF, Eberhard D, Martinez Molina D, Jafari R, Dovega RB, Klaeger S, et al., *Tracking cancer drugs in living cells by thermal profiling of the proteome.* **Science** 2014, 346:1255784

468. Škrtić M, Sriskanthadevan S, Jhas B, Gebbia M, Wang X, Wang Z, Hurren R, Jitkova Y, Gronda M, Maclean N, *Inhibition of mitochondrial translation as a therapeutic strategy for human acute myeloid leukemia.* **Cancer Cell** 2011, 20:674-688

469. Schimmer AD, Škrtić M, *Therapeutic potential of mitochondrial translation inhibition for treatment of acute myeloid leukemia.* **Expert Rev Hematol** 2012, 5:117-119

470. Saavedra E, *Energy metabolism in tumor cells.* **FEBS J** 2007, 274:13931418

471. Steliarova-Foucher E, Colombet M, Ries LA, Moreno F, Dolya A, Bray F, Hesseling P, Shin HY, Stiller CA, Bouzbid S, *International incidence of childhood cancer, 2001–10: A population-based registry study.* **Lancet Oncol** 2017, 18:719-731

472. Davis KL, *Understanding the hematopoietic factory during acute lymphoblastic leukemia.* **Pediatr Res** 2022, 91:1023-1024

473. Zhang Y, Gao S, Xia J, Liu F, *Hematopoietic Hierarchy - An Updated Roadmap.* **Trends Cell Biol** 2018, 28:976-986

474. THPA. *The human protein atlas*. Version: 22.0, Atlas updated: 2022-12-07, Access Date 20.10.2022; Available from: https://www.proteinatlas.org/

475. Zhou J, Zhang F, Hou X, Zhang N, *Downregulation of LRPPRC induces apoptosis in prostate cancer cells through the mitochondria-mediated pathway.* **Cancer Biother Radiopharm** 2014, 29:345-50

476. Cui J, Wang L, Ren X, Zhang Y, Zhang H, *LRPPRC: A Multifunctional Protein Involved in Energy Metabolism and Human Disease.* **Front Physiol** 2019, 10

477. Aibara S, Singh V, Modelska A, Amunts A, *Structural basis of mitochondrial translation.* **eLife** 2020, 9:e58362

478. De Silva D, Tu Y-T, Amunts A, Fontanesi F, Barrientos A, *Mitochondrial ribosome assembly in health and disease.* **Cell Cycle** 2015, 14:2226-2250

479. Khotimchenko R, Bryukhovetskiy I, Khotimchenko M, Khotimchenko Y, *Bioactive Compounds with Antiglioma Activity from Marine Species.* **Biomedicines** 2021, 9:886

480. Carté B, Faulkner DJ, *Polybrominated diphenyl ethers from Dysidea herbacea, Dysidea chlorea and Phyllospongia foliascens.* **Tetrahedron** 1981, 37:2335-2339

481. Fu X, Schmitz FJ, *New brominated diphenyl ether from an unidentified species of Dysidea sponge. 13C NMR data for some brominated diphenyl ethers.* **J Nat Prod** 1996, 59:1102-3

482. Fu X, Schmitz FJ, Govindan M, Abbas SA, Hanson KM, Horton PA, Crews P, Laney M, Schatzman RC, *Enzyme inhibitors: New and known polybrominated phenols and diphenyl ethers from four Indo-Pacific Dysidea sponges.* **J Nat Prod** 1995, 58:1384-91

483. Liu H, Lohith K, Rosario M, Pulliam TH, O'Connor RD, Bell LJ, Bewley CA, *Polybrominated Diphenyl Ethers: Structure Determination and Trends in Antibacterial Activity.* **J Nat Prod** 2016, 79:1872-1876

484. Burden DA, Kingma PS, Froelich-Ammon SJ, Bjornsti M-A, Patchan MW, Thompson RB, Osheroff N, *Topoisomerase II - Etoposide interactions direct the formation of drug-induced enzyme-DNA cleavage complexes.* **J Biol Chem** 1996, 271:29238-29244

485. Park YS, Choi SE, Koh HC, *PGAM5 regulates PINK1/Parkin-mediated mitophagy via DRP1 in CCCP-induced mitochondrial dysfunction.* **Toxicol Lett** 2018, 284:120-128

486. Zerihun M, Sukumaran S, Qvit N, *The Drp1-Mediated Mitochondrial Fission Protein Interactome as an Emerging Core Player in Mitochondrial Dynamics and Cardiovascular Disease Therapy.* **Int J Mol Sci** 2023, 24:5785

487. Del Dotto V, Fogazza M, Carelli V, Rugolo M, Zanna C, *Eight human OPA1 isoforms, long and short: What are they for?* **Biochim Biophys Acta Bioenerg** 2018, 1859:263-269

488. Xiao X, Hu Y, Quirós PM, Wei Q, López-Otín C, Dong Z, *OMA1 mediates OPA1 proteolysis and mitochondrial fragmentation in experimental models of ischemic kidney injury.* **Am J Physiol Renal Physiol** 2014, 306:F1318-26

489. MacVicar T, Langer T, *OPA1 processing in cell death and disease - the long and short of it.* **J Cell Sci** 2016, 129:2297-306

490. Demine S, Renard P, Arnould T, *Mitochondrial Uncoupling: A Key Controller of Biological Processes in Physiology and Diseases.* **Cells** 2019, 8

491. Kazak L, Chouchani ET, Stavrovskaya IG, Lu GZ, Jedrychowski MP, Egan DF, Kumari M, Kong X, Erickson BK, Szpyt J, et al., *UCP1 deficiency causes brown fat respiratory chain depletion and sensitizes mitochondria to calcium overload-induced dysfunction.* **Proc Natl Acad Sci U S A** 2017, 114:7981-7986

492. Böhler P, Stuhldreier F, Anand R, Kondadi AK, Schlütermann D, Berleth N, Deitersen J, Wallot-Hieke N, Wu W, Frank M, et al., *The mycotoxin phomoxanthone A disturbs the form and function of the inner mitochondrial membrane.* **Cell Death Dis** 2018, 9:286-303

493. Gao J, Sana R, Calder V, Calonge M, Lee W, Wheeler LA, Stern ME, *Mitochondrial Permeability Transition Pore in Inflammatory Apoptosis of Human Conjunctival Epithelial Cells and T Cells: Effect of Cyclosporin A.* **Invest Ophthalmol Vis Sci** 2013, 54:4717-4733

494. Marroquin LD, Hynes J, Dykens JA, Jamieson JD, Will Y, *Circumventing the Crabtree Effect: Replacing Media Glucose with Galactose Increases Susceptibility of HepG2 Cells to Mitochondrial Toxicants.* **Toxicol Sci** 2007, 97:539-547

495. Fan T, Sun G, Sun X, Zhao L, Zhong R, Peng Y, *Tumor Energy Metabolism and Potential of 3-Bromopyruvate as an Inhibitor of Aerobic Glycolysis: Implications in Tumor Treatment.* **Cancers** 2019, 11:317

496. Cardaci S, Desideri E, Ciriolo MR, *Targeting aerobic glycolysis: 3-bromopyruvate as a promising anticancer drug.* **J Bioenerg Biomembr** 2012, 44:17-29

497. Nakano A, Miki H, Nakamura S, Harada T, Oda A, Amou H, Fujii S, Kagawa K, Takeuchi K, Ozaki S, et al., *Up-regulation of hexokinaseII in myeloma cells: targeting myeloma cells with 3-bromopyruvate.* **J Bioenerg Biomembr** 2012, 44:31-8

498. Skaripa-Koukelli I, Hauton D, Walsby-Tickle J, Thomas E, Owen J, Lakshminarayanan A, Able S, McCullagh J, Carlisle RC, Vallis KA, *3-Bromopyruvate-mediated MCT1-dependent metabolic perturbation sensitizes triple negative breast cancer cells to ionizing radiation.* **Cancer Metab** 2021, 9:37

499. Rai Y, Yadav P, Kumari N, Kalra N, Bhatt AN, *Hexokinase II inhibition by 3-bromopyruvate sensitizes myeloid leukemic cells K-562 to anti-leukemic drug, daunorubicin.* **Biosci Rep** 2019, 39

500. Chopineaux-Courtois V, Reymond F, Bouchard G, Carrupt P-A, Testa B, Girault HH, *Effects of Charge and Intramolecular Structure on the Lipophilicity of Nitrophenols.* **J Am Chem Soc** 1999, 121:1743-1747

501. *Ion transport across energy conserving membranes*, in *Bioenergetics 2*, Nicholls DG,Ferguson SJ, Editors. 1992, Academic Press. 22-37

502. Hards K, McMillan DGG, Schurig-Briccio LA, Gennis RB, Lill H, Bald D, Cook GM, *Ionophoric effects of the antitubercular drug bedaquiline.* **Proc Natl Acad Sci U S A** 2018, 115:7326-7331

503. Miyahara K, Takano N, Yamada Y, Kazama H, Tokuhisa M, Hino H, Fujita K, Barroga E, Hiramoto M, Handa H, et al., *BRCA1 degradation in response to mitochondrial damage in breast cancer cells.* **Sci Rep** 2021, 11:8735

504. Rado M, Flepisi B, Fisher D, *The Effect of Normoxic and Hypoxic U-87 Glioblastoma Paracrine Secretion on the Modulation of Brain Endothelial Cells.* **Cells** 2022, 11

505. Jelluma N, Yang X, Stokoe D, Evan GI, Dansen TB, Haas-Kogan DA, *Glucose Withdrawal Induces Oxidative Stress followed by Apoptosis in Glioblastoma Cells but not in Normal Human Astrocytes.* **Mol Cancer Res** 2006, 4:319-330

506. Catarinella G, Nicoletti C, Bracaglia A, Procopio P, Salvatori I, Taggi M, Valle C, Ferri A, Canipari R, Puri PL, et al., *SerpinE1 drives a cell-autonomous pathogenic signaling in Hutchinson–Gilford progeria syndrome.* **Cell Death Dis** 2022, 13:737

507. Childs D, Bach K, Franken H, Anders S, Kurzawa N, Bantscheff M, Savitski MM, Huber W, *Nonparametric Analysis of Thermal Proteome Profiles Reveals Novel Drug-binding Proteins.* **Mol Cell Proteomics** 2019, 18:2506-2515

508. Tusher VG, Tibshirani R, Chu G, *Significance analysis of microarrays applied to the ionizing radiation response.* **Proc Natl Acad Sci U S A** 2001, 98:5116-21
509. Uniprot. *Uniprot*. updated: Release 2023_01, Access Date 22.03.2023; Available from: https://www.uniprot.org/
510. THPA. *The human protein atlas*. Version: 22.0, Atlas updated: 2022-12-07, Access Date 22.03.2023; Available from: https://www.proteinatlas.org/
511. Jordan MA, *Mechanism of action of antitumor drugs that interact with microtubules and tubulin.* **Curr Med Chem Anticancer Agents** 2002, 2:1-17
512. Perez EA, *Microtubule inhibitors: Differentiating tubulin-inhibiting agents based on mechanisms of action, clinical activity, and resistance.* **Mol Cancer Ther** 2009, 8:2086-95
513. Cortazar P, Justice R, Johnson J, Sridhara R, Keegan P, Pazdur R, *US Food and Drug Administration approval overview in metastatic breast cancer.* **J Clin Oncol** 2012, 30:1705-11
514. Blajeski AL, Phan VA, Kottke TJ, Kaufmann SH, *G(1) and G(2) cell-cycle arrest following microtubule depolymerization in human breast cancer cells.* **J Clin Invest** 2002, 110:91-9
515. Koundouros N, Poulogiannis G, *Reprogramming of fatty acid metabolism in cancer.* **Br J Canc** 2020, 122:4-22
516. Chen M, Huang J, *The expanded role of fatty acid metabolism in cancer: New aspects and targets.* **Precis Clin Med** 2019, 2:183-191
517. Farese RV, Walther TC, *Lipid droplets finally get a little RESPECT.* **Cell** 2009, 139:855-860
518. Yen C-LE, Stone SJ, Koliwad S, Harris C, Farese RV, *Thematic review series: Glycerolipids, DGAT enzymes and triacylglycerol biosynthesis.* **J Lipid Res** 2008, 49:2283-2301
519. Bettayeb K, Tirado OM, Marionneau-Lambot S, Ferandin Y, Lozach O, Morris JC, Mateo-Lozano S, Drueckes P, Schachtele C, Kubbutat MH, et al., *Meriolins, a new class of cell death inducing kinase inhibitors with enhanced selectivity for cyclin-dependent kinases.* **Cancer Res** 2007, 67:8325-34
520. Franco LH, Joffé EB, Puricelli L, Tatian M, Seldes AM, Palermo JA, *Indole alkaloids from the tunicate Aplidium meridianum.* **J Nat Prod** 1998, 61:1130-2
521. Walker SR, Carter EJ, Huff BC, Morris JC, *Variolins and Related Alkaloids.* **Chem Rev** 2009, 109:3080-3098
522. Trimurtulu G, Faulkner DJ, Perry NB, Ettouati L, Litaudon M, Blunt JW, Munro MHG, Jameson GB, *Alkaloids from the antarctic sponge Kirkpatrickia varialosa. Part 2: Variolin A and N(3')-methyl tetrahydrovariolin B.* **Tetrahedron** 1994, 50:3993-4000
523. Perry NB, Ettouati L, Litaudon M, Blunt JW, Munro MHG, Parkin S, Hope H, *Alkaloids from the antarctic sponge Kirkpatrickia varialosa.: Part 1: Variolin b, a new antitumour and antiviral compound.* **Tetrahedron** 1994, 50:3987-3992
524. Echalier A, Bettayeb K, Ferandin Y, Lozach O, Clement M, Valette A, Liger F, Marquet B, Morris JC, Endicott JA, et al., *Meriolins (3-(pyrimidin-4-yl)-7-azaindoles): Synthesis, kinase inhibitory activity, cellular effects, and structure of a CDK2/cyclin A/meriolin complex.* **J Med Chem** 2008, 51:737-51
525. Kruppa M, Müller TJJ, *A Survey on the Synthesis of Variolins, Meridianins, and Meriolins - Naturally Occurring Marine (aza)Indole Alkaloids and Their Semisynthetic Derivatives.* **Molecules** 2023, 28:947
526. Skowron MA, Vermeulen M, Winkelhausen A, Becker TK, Bremmer F, Petzsch P, Schonberger S, Calaminus G, Kohrer K, Albers P, et al., *CDK4/6 inhibition presents as a therapeutic option for paediatric and adult germ cell tumours and induces cell cycle arrest and apoptosis via canonical and non-canonical mechanisms.* **Br J Cancer** 2020, 123:378-391
527. Chashoo G, Singh U, Singh PP, Mondhe DM, Vishwakarma RA, *A Marine-based Meriolin (3-Pyrimidinylazaindole) Derivative (4ab) Targets PI3K/AKT/mTOR Pathway Inducing Cell Cycle Arrest and Apoptosis in Molt-4 Cells.* **Clin Cancer Drugs** 2019, 6:33-40
528. Jarry M, Lecointre C, Malleval C, Desrues L, Schouft MT, Lejoncour V, Liger F, Lyvinec G, Joseph B, Loaec N, et al., *Impact of meriolins, a new class of cyclin-dependent kinase inhibitors, on malignant glioma proliferation and neo-angiogenesis.* **Neuro Oncol** 2014, 16:1484-98
529. Thatikonda T, Singh U, Ambala S, Vishwakarma RA, Singh PP, *Metal free C-H functionalization of diazines and related heteroarenes with organoboron species and its application in the synthesis of a CDK inhibitor, meriolin 1.* **Org Biomol Chem** 2016, 14:4312-20

530. Kim G, McKee AE, Ning Y-M, Hazarika M, Theoret M, Johnson JR, Xu QC, Tang S, Sridhara R, Jiang X, *FDA Approval Summary: Vemurafenib for Treatment of Unresectable or Metastatic Melanoma with the BRAFV600E MutationVemurafenib for Advanced Melanoma with BRAFV600E Mutation.* **Clin Cancer Res** 2014, 20:4994-5000
531. Tap WD, Gelderblom H, Palmerini E, Desai J, Bauer S, Blay J-Y, Alcindor T, Ganjoo K, Martín-Broto J, Ryan CW, *Pexidartinib versus placebo for advanced tenosynovial giant cell tumour (ENLIVEN): A randomised phase 3 trial.* **Lancet Glob** 2019, 394:478-487
532. Foote KM, Nissink JWM, McGuire T, Turner P, Guichard S, Yates JWT, Lau A, Blades K, Heathcote D, Odedra R, et al., *Discovery and Characterization of AZD6738, a Potent Inhibitor of Ataxia Telangiectasia Mutated and Rad3 Related (ATR) Kinase with Application as an Anticancer Agent.* **J Med Chem** 2018, 61:9889-9907
533. Smits VAJ, Cabrera E, Freire R, Gillespie DA, *Claspin - checkpoint adaptor and DNA replication factor.* **FEBS J** 2019, 286:441-455
534. Seshacharyulu P, Pandey P, Datta K, Batra SK, *Phosphatase: PP2A structural importance, regulation and its aberrant expression in cancer.* **Cancer Lett** 2013, 335:9-18
535. Grallert A, Boke E, Hagting A, Hodgson B, Connolly Y, Griffiths JR, Smith DL, Pines J, Hagan IM, *A PP1-PP2A phosphatase relay controls mitotic progression.* **Nature** 2015, 517:94-98
536. Zarkowska T, Mittnacht S, *Differential Phosphorylation of the Retinoblastoma Protein by G1/S Cyclin-dependent Kinases.* **J Biol Chem** 1997, 272:12738-12746
537. Sellckchem. Access Date 15.03.2023; Available from: Selleckchem.com
538. Leroux AE, Schulze JO, Biondi RM, *AGC kinases, mechanisms of regulation and innovative drug development.* **Semin Cancer Biol** 2018, 48:1-17
539. Manning G, Whyte DB, Martinez R, Hunter T, Sudarsanam S, *The protein kinase complement of the human genome.* **Science** 2002, 298:1912-34
540. Zannini L, Delia D, Buscemi G, *CHK2 kinase in the DNA damage response and beyond.* **J Mol Cell Biol** 2014, 6:442-57
541. Hirao A, Kong Y-Y, Matsuoka S, Wakeham A, Ruland Jr, Yoshida H, Liu D, Elledge SJ, Mak TW, *DNA damage-induced activation of p53 by the checkpoint kinase Chk2.* **Science** 2000, 287:1824-1827
542. Rawlinson R, Massey AJ, *γH2AX and Chk1 phosphorylation as predictive pharmacodynamic biomarkers of Chk1 inhibitor-chemotherapy combination treatments.* **BMC Cancer** 2014, 14:483
543. Adams PD, Li X, Sellers WR, Baker KB, Leng X, Harper JW, Taya Y, Kaelin WG, *Retinoblastoma Protein Contains a C-terminal Motif That Targets It for Phosphorylation by Cyclin-cdk Complexes.* **Mol Cell Biol** 1999, 19:1068-1080
544. Anshabo AT, Milne R, Wang S, Albrecht H, *CDK9: A Comprehensive Review of Its Biology, and Its Role as a Potential Target for Anti-Cancer Agents.* **Front Oncol** 2021, 11
545. Sims RJ, Belotserkovskaya R, Reinberg D, *Elongation by RNA polymerase II: The short and long of it.* **Genes Dev** 2004, 18:2437-2468
546. Saunders A, Core LJ, Lis JT, *Breaking barriers to transcription elongation.* **Nat Rev Mol Cell Biol** 2006, 7:557-567
547. Ni Z, Schwartz BE, Werner J, Suarez J-R, Lis JT, *Coordination of transcription, RNA processing, and surveillance by P-TEFb kinase on heat shock genes.* **Mol Cell** 2004, 13:55-65
548. Shim EY, Walker AK, Shi Y, Blackwell TK, *CDK-9/cyclin T (P-TEFb) is required in two postinitiation pathways for transcription in the C. elegans embryo.* **Genes Dev** 2002, 16:2135-46
549. Czudnochowski N, Bösken CA, Geyer M, *Serine-7 but not serine-5 phosphorylation primes RNA polymerase II CTD for P-TEFb recognition.* **Nat Commun** 2012, 3:842
550. Grana X, De Luca A, Sang N, Fu Y, Claudio P, Rosenblatt J, Morgan D, Giordano A, *PITALRE, a nuclear CDC2-related protein kinase that phosphorylates the retinoblastoma protein in vitro.* **Proc Natl Acad Sci U S A** 1994, 91:3834-3838
551. Garriga J, Bhattacharya S, Calbó J, Marshall RM, Truongcao M, Haines DS, Grana X, *CDK9 is constitutively expressed throughout the cell cycle, and its steady-state expression is independent of SKP2.* **Mol Cell Biol** 2003, 23:5165-5173
552. Tesauro C, Simonsen AK, Andersen MB, Petersen KW, Kristoffersen EL, Algreen L, Hansen NY, Andersen AB, Jakobsen AK, Stougaard M, et al., *Topoisomerase I activity and sensitivity to camptothecin in breast cancer-derived cells: A comparative study.* **BMC Cancer** 2019, 19:1158

553. Agudelo D, Bourassa P, Bérubé G, Tajmir-Riahi H-A, *Intercalation of antitumor drug doxorubicin and its analogue by DNA duplex: Structural features and biological implications.* **Int J Biol Macromol** 2014, 66:144-150

554. Nelson EM, Tewey KM, Liu LF, *Mechanism of antitumor drug action: Poisoning of mammalian DNA topoisomerase II on DNA by 4'-(9-acridinylamino)-methanesulfon-m-anisidide.* **Proc Natl Acad Sci U S A** 1984, 81:1361-1365

555. Gewirtz D, *A critical evaluation of the mechanisms of action proposed for the antitumor effects of the anthracycline antibiotics adriamycin and daunorubicin.* **Biochem Pharmacol** 1999, 57:727-741

556. Al-Aamri HM, Ku H, Irving HR, Tucci J, Meehan-Andrews T, Bradley C, *Time dependent response of daunorubicin on cytotoxicity, cell cycle and DNA repair in acute lymphoblastic leukaemia.* **BMC Cancer** 2019, 19:179

557. Kuo LJ, Yang LX, *Gamma-H2AX - a novel biomarker for DNA double-strand breaks.* **In Vivo** 2008, 22:305-9

558. Cuadrado M, Gutierrez-Martinez P, Swat A, Nebreda AR, Fernandez-Capetillo O, *p27Kip1 stabilization is essential for the maintenance of cell cycle arrest in response to DNA damage.* **Cancer Res** 2009, 69:8726-32

559. Abbastabar M, Kheyrollah M, Azizian K, Bagherlou N, Tehrani SS, Maniati M, Karimian A, *Multiple functions of p27 in cell cycle, apoptosis, epigenetic modification and transcriptional regulation for the control of cell growth: A double-edged sword protein.* **DNA Repair (Amst)** 2018, 69:63-72

560. Lassmann M, Hänscheid H, Gassen D, Biko J, Meineke V, Reiners C, Scherthan H, *In vivo formation of gamma-H2AX and 53BP1 DNA repair foci in blood cells after radioiodine therapy of differentiated thyroid cancer.* **J Nucl Med** 2010, 51:1318-25

561. Antonicka H, Sasarman F, Nishimura T, Paupe V, Shoubridge Eric A, *The Mitochondrial RNA-Binding Protein GRSF1 Localizes to RNA Granules and Is Required for Posttranscriptional Mitochondrial Gene Expression.* **Cell Metab** 2013, 17:386-398

562. Nicholls TJ, Rorbach J, Minczuk M, *Mitochondria: Mitochondrial RNA metabolism and human disease.* **Int J Biochem Cell Biol** 2013, 45:845-849

563. Ruzzenente B, Metodiev MD, Wredenberg A, Bratic A, Park CB, Cámara Y, Milenkovic D, Zickermann V, Wibom R, Hultenby K, et al., *LRPPRC is necessary for polyadenylation and coordination of translation of mitochondrial mRNAs.* **EMBO J** 2012, 31:443-56

564. Jacobsson A, Stadler U, Glotzer M, Kozak L, *Mitochondrial uncoupling protein from mouse brown fat. Molecular cloning, genetic mapping, and mRNA expression.* **J Biol Chem** 1985, 260:16250-16254

565. Strieleman PJ, Schalinske KL, Shrago E, *Fatty acid activation of the reconstituted brown adipose tissue mitochondria uncoupling protein.* **J Biol Chem** 1985, 260:13402-13405

566. Rial E, Poustie A, Nicholls DG, *Brown-adipose-tissue mitochondria: The regulation of the 32 000-Mr uncoupling protein by fatty acids and purine nucleotides.* **Eur J Biochem** 1983, 137:197-203

567. Crichton PG, Lee Y, Kunji ERS, *The molecular features of uncoupling protein 1 support a conventional mitochondrial carrier-like mechanism.* **Biochimie** 2017, 134:35-50

568. Brenner C, Subramaniam K, Pertuiset C, Pervaiz S, *Adenine nucleotide translocase family: Four isoforms for apoptosis modulation in cancer.* **Oncogene** 2011, 30:883-895

569. Andreyev AY, Bondareva TO, Dedukhova VI, Mokhova EN, Skulachev VP, Tsofina LM, Volkov NI, Vygodina TV, *The ATP/ADP-antiporter is involved in the uncoupling effect of fatty acids on mitochondria.* **Eur J Biochem** 1989, 182:585-592

570. Sparks LM, Gemmink A, Phielix E, Bosma M, Schaart G, Moonen-Kornips E, Jörgensen JA, Nascimento EB, Hesselink MK, Schrauwen P, *ANT1-mediated fatty acid-induced uncoupling as a target for improving myocellular insulin sensitivity.* **Diabetologia** 2016, 59:1030-1039

571. Brustovetsky N, Klingenberg M, *Mitochondrial ADP/ATP carrier can be reversibly converted into a large channel by Ca^{2+}.* **Biochemistry** 1996, 35:8483-8488

572. Bohovych I, Donaldson G, Christianson S, Zahayko N, Khalimonchuk O, *Stress-triggered activation of the metalloprotease Oma1 involves its C-terminal region and is important for mitochondrial stress protection in yeast.* **J Biol Chem** 2014, 289:13259-13272

573. Zhang K, Li H, Song Z, *Membrane depolarization activates the mitochondrial protease OMA1 by stimulating self-cleavage.* **EMBO Rep** 2014, 15:576-585

574. Levytskyy RM, Bohovych I, Khalimonchuk O, *Metalloproteases of the Inner Mitochondrial Membrane.* **Biochemistry** 2017, 56:4737-4746

575. Rozpedek W, Pytel D, Mucha B, Leszczynska H, Diehl JA, Majsterek I, *The Role of the PERK/eIF2α/ATF4/CHOP Signaling Pathway in Tumor Progression During Endoplasmic Reticulum Stress.* **Curr Mol Med** 2016, 16:533-44

576. Muaddi H, Majumder M, Peidis P, Papadakis AI, Holcik M, Scheuner D, Kaufman RJ, Hatzoglou M, Koromilas AE, *Phosphorylation of eIF2α at serine 51 is an important determinant of cell survival and adaptation to glucose deficiency.* **Mol Biol Cell** 2010, 21:3220-31

577. Bandara AB, Drake JC, Brown DA, *Complex II subunit SDHD is critical for cell growth and metabolism, which can be partially restored with a synthetic ubiquinone analog.* **BMC Cell Biol** 2021, 22:35

578. Guo L, Shestov AA, Worth AJ, Nath K, Nelson DS, Leeper DB, Glickson JD, Blair IA, *Inhibition of Mitochondrial Complex II by the Anticancer Agent Lonidamine.* **J Biol Chem** 2016, 291:42-57

579. Pereira Da Silva Ana P, El-Bacha T, Kyaw N, Dos Santos Reinaldo S, Da-Silva Wagner S, Almeida Fabio CL, Da Poian Andrea T, Galina A, *Inhibition of energy-producing pathways of HepG2 cells by 3-bromopyruvate1.* **Biochem J** 2009, 417:717-726

580. Chandel NS, *Mitochondrial complex III: An essential component of universal oxygen sensing machinery?* **Respir Physiol Neurobiol** 2010, 174:175-81

581. Murphy MP, *How mitochondria produce reactive oxygen species.* **Biochem J** 2009, 417:1-13

582. Brand MD, *The sites and topology of mitochondrial superoxide production.* **Exp Gerontol** 2010, 45:466-472

583. Muller FL, Liu Y, Van Remmen H, *Complex III releases superoxide to both sides of the inner mitochondrial membrane.* **J Biol Chem** 2004, 279:49064-49073

584. Forkink M, Basit F, Teixeira J, Swarts HG, Koopman WJH, Willems P, *Complex I and complex III inhibition specifically increase cytosolic hydrogen peroxide levels without inducing oxidative stress in HEK293 cells.* **Redox Biol** 2015, 6:607-616

585. Hans C, Saini R, Sachdeva MUS, Sharma P, *2',7'-Dichlorofluorescein (DCF) or 2',7'-dichlorodihydrofluorescein diacetate (DCFH2-DA) to measure reactive oxygen species in erythrocytes.* **Biomed Pharmacother** 2021, 138:111512

586. Wang Y, Hou Q, Xiao G, Yang S, Di C, Si J, Zhou R, Ye Y, Zhang Y, Zhang H, *Selective ATP hydrolysis inhibition in F1Fo ATP synthase enhances radiosensitivity in non-small-cell lung cancer cells (A549).* **Oncotarget** 2017, 8

587. Jardim-Messeder D, Moreira-Pacheco F, *3-Bromopyruvic Acid Inhibits Tricarboxylic Acid Cycle and Glutaminolysis in HepG2 Cells.* **Anticancer Res** 2016, 36:2233-41

588. Chen Z, Zhang H, Lu W, Huang P, *Role of mitochondria-associated hexokinase II in cancer cell death induced by 3-bromopyruvate.* **Biochim Biophys Acta** 2009, 1787:553-60

589. Ayat M, *3-bromopyruvate as a Promising Treatment for Hematological Cancer.* **Cancer Res Treat** 2018, 6:12-17

590. Ciszak EM, Makal A, Hong YS, Vettaikkorumakankauv AK, Korotchkina LG, Patel MS, *How dihydrolipoamide dehydrogenase-binding protein binds dihydrolipoamide dehydrogenase in the human pyruvate dehydrogenase complex.* **J Biol Chem** 2006, 281:648-55

591. Babady NE, Pang YP, Elpeleg O, Isaya G, *Cryptic proteolytic activity of dihydrolipoamide dehydrogenase.* **Proc Natl Acad Sci U S A** 2007, 104:6158-63

592. Ambrus A, Adam-Vizi V, *Human dihydrolipoamide dehydrogenase (E3) deficiency: Novel insights into the structural basis and molecular pathomechanism.* **Neurochem Int** 2018, 117:5-14

593. Massey V, *The composition of the ketoglutarate dehydrogenase complex.* **Biochim Biophys Acta** 1960, 38:447-460

594. Bartolome F, Abramov A, *Measurement of Mitochondrial NADH and FAD Autofluorescence in Live Cells.* **Methods Mol Biol** 2015, 1264:263-70

595. Islam SDM, Susdorf T, Penzkofer A, Hegemann P, *Fluorescence quenching of flavin adenine dinucleotide in aqueous solution by pH dependent isomerisation and photo-induced electron transfer.* **Chem Phys** 2003, 295:137-149

596. Gorbunova IA, Danilova MK, Sasin ME, Belik VP, Golyshev DP, Vasyutinskii OS, *Determination of quantum yield of NADH and FAD in alcohol-water solutions: The analysis of radiative and nonradiative relaxation pathways.* **Chem Phys** 2022,

597. Hara Y, Kume S, Kataoka Y, Watanabe N, *Changes in TCA cycle and TCA cycle-related metabolites in plasma upon citric acid administration in rats.* **Heliyon** 2021, 7:e08501

598. TeSlaa T, Teitell MA, *Techniques to monitor glycolysis.* **Methods Enzymol** 2014, 542:91-114

599. Mukhopadhyay TK, Trauner D, *Concise Synthesis of Glycerophospholipids.* **J Org Chem** 2022,

600. Hishikawa D, Hashidate T, Shimizu T, Shindou H, *Diversity and function of membrane glycerophospholipids generated by the remodeling pathway in mammalian cells.* **J Lipid Res** 2014, 55:799-807

601. Klingenberg M, *Cardiolipin and mitochondrial carriers.* **Biochim Biophys Acta** 2009, 1788:2048-2058

602. Paradies G, Paradies V, De Benedictis V, Ruggiero FM, Petrosillo G, *Functional role of cardiolipin in mitochondrial bioenergetics.* **Biochim Biophys Acta Bioenerg** 2014, 1837:408-417

603. Paradies G, Petrosillo G, Paradies V, Ruggiero FM, *Role of cardiolipin peroxidation and Ca^{2+} in mitochondrial dysfunction and disease.* **Cell Calcium** 2009, 45:643-650

604. Huang P, Nedelcu D, Watanabe M, Jao C, Kim Y, Liu J, Salic A, *Cellular cholesterol directly activates smoothened in hedgehog signaling.* **Cell** 2016, 166:1176-1187. e14

605. Guixà-González R, Albasanz JL, Rodriguez-Espigares I, Pastor M, Sanz F, Martí-Solano M, Manna M, Martinez-Seara H, Hildebrand PW, Martín M, *Membrane cholesterol access into a G-protein-coupled receptor.* **Nat Commun** 2017, 8:14505

606. Luchetti G, Sircar R, Kong JH, Nachtergaele S, Sagner A, Byrne EF, Covey DF, Siebold C, Rohatgi R, *Cholesterol activates the G-protein coupled receptor Smoothened to promote Hedgehog signaling.* **eLife** 2016, 5:e20304

607. Caro P, Kishan AU, Norberg E, Stanley IA, Chapuy B, Ficarro SB, Polak K, Tondera D, Gounarides J, Yin H, *Metabolic signatures uncover distinct targets in molecular subsets of diffuse large B cell lymphoma.* **Cancer Cell** 2012, 22:547-560

608. Monti S, Savage KJ, Kutok JL, Feuerhake F, Kurtin P, Mihm M, Wu B, Pasqualucci L, Neuberg D, Aguiar RC, *Molecular profiling of diffuse large B-cell lymphoma identifies robust subtypes including one characterized by host inflammatory response.* **Blood** 2005, 105:1851-1861

609. Liu Y, *Fatty acid oxidation is a dominant bioenergetic pathway in prostate cancer.* **Prostate Cancer Prostatic Dis** 2006, 9:230-234

610. Pacilli A, Calienni M, Margarucci S, D'Apolito M, Petillo O, Rocchi L, Pasquinelli G, Nicolai R, Koverech A, Calvani M, *Carnitine-acyltransferase system inhibition, cancer cell death, and prevention of myc-induced lymphomagenesis.* **J Natl Cancer Inst** 2013, 105:489-498

611. Zhao Y, Butler EB, Tan M, *Targeting cellular metabolism to improve cancer therapeutics.* **Cell Death Dis** 2013, 4:e532-e532

612. Samudio I, Harmancey R, Fiegl M, Kantarjian H, Konopleva M, Korchin B, Kaluarachchi K, Bornmann W, Duvvuri S, Taegtmeyer H, *Pharmacologic inhibition of fatty acid oxidation sensitizes human leukemia cells to apoptosis induction.* **J Clin Invest** 2010, 120:142-156

613. Hardie DG, Ross FA, Hawley SA, *AMPK: A nutrient and energy sensor that maintains energy homeostasis.* **Nat Rev Mol Cell Biol** 2012, 13:251-262

614. Mihaylova MM, Shaw RJ, *The AMPK signalling pathway coordinates cell growth, autophagy and metabolism.* **Nat Cell Biol** 2011, 13:1016-1023

615. Ma Y, Temkin SM, Hawkridge AM, Guo C, Wang W, Wang XY, Fang X, *Fatty acid oxidation: An emerging facet of metabolic transformation in cancer.* **Cancer Lett** 2018, 435:92-100

616. Warburg O, *On respiratory impairment in cancer cells.* **Science** 1956, 124:269-270

617. Vander Heiden MG, Cantley LC, Thompson CB, *Understanding the Warburg effect: The metabolic requirements of cell proliferation.* **Science** 2009, 324:1029-1033

618. Shi J, Fu H, Jia Z, He K, Fu L, Wang W, *High expression of CPT1A predicts adverse outcomes: A potential therapeutic target for acute myeloid leukemia.* **EBioMedicine** 2016, 14:55-64

619. Habel ME, Jung D, *c-Myc over-expression in Ramos Burkitt's lymphoma cell line predisposes to iron homeostasis disruption in vitro.* **Biochem Biophys Res Com** 2006, 341:1309-16

620. Winkler R, Mägdefrau A-S, Piskor E-M, Kleemann M, Beyer M, Linke K, Hansen L, Schaffer A-M, Hoffmann ME, Poepsel S, et al., *Targeting the MYC interaction network in B-cell lymphoma via histone deacetylase 6 inhibition.* **Oncogene** 2022, 41:4560-4572

621. Seitz V, Butzhammer P, Hirsch B, Hecht J, Gütgemann I, Ehlers A, Lenze D, Oker E, Sommerfeld A, von der Wall E, et al., *Deep Sequencing of MYC DNA-Binding Sites in Burkitt Lymphoma.* **PLoS One** 2011, 6:e26837

622. Malempati S, Tibbitts D, Cunningham M, Akkari Y, Olson S, Fan G, Sears RC, *Aberrant stabilization of c-Myc protein in some lymphoblastic leukemias.* **Leukemia** 2006, 20:1572-81

623. Murrell JN, *The Electronic Spectrum of Aromatic Molecules VI: The Mesomeric Effect.* **Proc Phys Soc** 1955, 68:969

624. THPA. *The human protein atlas*. Version: 22.0, Atlas updated: 2022-12-07, Access Date 18.04.2023; Available from: https://www.proteinatlas.org/

625. Laguna A, Aranda S, Barallobre MJ, Barhoum R, Fernández E, Fotaki V, Delabar JM, de la Luna S, de la Villa P, Arbonés ML, *The Protein Kinase DYRK1A Regulates Caspase-9-Mediated Apoptosis during Retina Development.* **Dev Cell** 2008, 15:841-853

626. Seifert A, Clarke PR, *p38alpha- and DYRK1A-dependent phosphorylation of caspase-9 at an inhibitory site in response to hyperosmotic stress.* **Cell Signal** 2009, 21:1626-33

627. Bain J, Plater L, Elliott M, Shpiro N, Hastie CJ, McLauchlan H, Klevernic I, Arthur JS, Alessi DR, Cohen P, *The selectivity of protein kinase inhibitors: A further update.* **Biochem J** 2007, 408:297-315

628. Seifert A, Allan LA, Clarke PR, *DYRK1A phosphorylates caspase 9 at an inhibitory site and is potently inhibited in human cells by harmine.* **FEBS J** 2008, 275:6268-80

629. Coulthard CE, Levene HH, Pyman FL, *The chemotherapy of derivatives of harmine and harmaline.* **Biochem J** 1933, 27:727-39

630. Sanchez-Ramos JR, *Banisterine and Parkinson's disease.* **Clin Neuropharmacol** 1991, 14:391-402

631. Ionescu A, Dufrasne F, Gelbcke M, Jabin I, Kiss R, Lamoral-Theys D, *DYRK1A Kinase Inhibitors with Emphasis on Cancer.* **Mini Rev Med Chem** 2012, 12:1315-1329

632. Lee Walmsley D, Murray JB, Dokurno P, Massey AJ, Benwell K, Fiumana A, Foloppe N, Ray S, Smith J, Surgenor AE, et al., *Fragment-Derived Selective Inhibitors of Dual-Specificity Kinases DYRK1A and DYRK1B.* **J Med Chem** 2021, 64:8971-8991

633. Uhl KL, Schultz CR, Geerts D, Bachmann AS, *Harmine, a dual-specificity tyrosine phosphorylation-regulated kinase (DYRK) inhibitor induces caspase-mediated apoptosis in neuroblastoma.* **Cancer Cell Int** 2018, 18:82

634. Taguchi N, Ishihara N, Jofuku A, Oka T, Mihara K, *Mitotic phosphorylation of dynamin-related GTPase Drp1 participates in mitochondrial fission.* **J Biol Chem** 2007, 282:11521-9

635. Chang CR, Blackstone C, *Dynamic regulation of mitochondrial fission through modification of the dynamin-related protein Drp1.* **Ann NY Acad Sci** 2010, 1201:34-39

636. Cho B, Choi SY, Cho HM, Kim HJ, Sun W, *Physiological and pathological significance of dynamin-related protein 1 (drp1)-dependent mitochondrial fission in the nervous system.* **Exp Neurobiol** 2013, 22:149-157

637. Qian W, Choi S, Gibson GA, Watkins SC, Bakkenist CJ, Van Houten B, *Mitochondrial hyperfusion induced by loss of the fission protein Drp1 causes ATM-dependent G2/M arrest and aneuploidy through DNA replication stress.* **J Cell Sci** 2012, 125:5745-5757

638. Shamloo B, Usluer S, *p21 in Cancer Research.* **Cancers** 2019, 11

639. He B, Lu N, Zhou Z, *Cellular and nuclear degradation during apoptosis.* **Curr Opin Cell Biol** 2009, 21:900-12

640. Enari M, Sakahira H, Yokoyama H, Okawa K, Iwamatsu A, Nagata S, *A caspase-activated DNase that degrades DNA during apoptosis, and its inhibitor ICAD.* **Nature** 1998, 391:43-50

641. Liu X, Zou H, Slaughter C, Wang X, *DFF, a heterodimeric protein that functions downstream of caspase-3 to trigger DNA fragmentation during apoptosis.* **Cell** 1997, 89:175-184

642. Woo E-J, Kim Y-G, Kim M-S, Han W-D, Shin S, Robinson H, Park S-Y, Oh B-H, *Structural mechanism for inactivation and activation of CAD/DFF40 in the apoptotic pathway.* **Mol Cell** 2004, 14:531-539

643. Hanus J, Kalinowska-Herok M, Widlak P, *The major apoptotic endonuclease DFF40/CAD is a deoxyribose-specific and double-strand-specific enzyme.* **Apoptosis** 2008, 13:377-382

644. Wang JYJ, *DNA damage and apoptosis.* **Cell Death Differ** 2001, 8:1047-1048

645. Hattori T, Uchida C, Takahashi H, Yamamoto N, Naito M, Taya Y, *Distinct and Site-Specific Phosphorylation of the Retinoblastoma Protein at Serine 612 in Differentiated Cells.* **PLoS One** 2014, 9:e86709

646. DeGregori J, Kowalik T, Nevins JR, *Cellular Targets for Activation by the E2F1 Transcription Factor Include DNA Synthesis- and G1/S-Regulatory Genes.* **Mol Cell Biol** 1995, 15:4215-4224

647. Iwanaga R, Komori H, Ishida S, Okamura N, Nakayama K, Nakayama KI, Ohtani K, *Identification of novel E2F1 target genes regulated in cell cycle-dependent and independent manners.* **Oncogene** 2006, 25:1786-1798

648. Stanelle J, Stiewe T, Theseling CC, Peter M, Pützer BM, *Gene expression changes in response to E2F1 activation.* **Nucleic Acids Res** 2002, 30:1859-67

649. Moroni MC, Hickman ES, Lazzerini Denchi E, Caprara G, Colli E, Cecconi F, Müller H, Helin K, *Apaf-1 is a transcriptional target for E2F and p53.* **Nat Cell Biol** 2001, 3:552-8

650. Hershko T, Ginsberg D, *Up-regulation of Bcl-2 homology 3 (BH3)-only proteins by E2F1 mediates apoptosis.* **J Biol Chem** 2004, 279:8627-34

651. Nahle Z, Polakoff J, Davuluri RV, McCurrach ME, Jacobson MD, Narita M, Zhang MQ, Lazebnik Y, Bar-Sagi D, Lowe SW, *Direct coupling of the cell cycle and cell death machinery by E2F.* **Nat Cell Biol** 2002, 4:859-64

652. Stanelle J, Pützer BM, *E2F1-induced apoptosis: Turning killers into therapeutics.* **Trends Mol Med** 2006, 12:177-185

653. Hershko T, Chaussepied M, Oren M, Ginsberg D, *Novel link between E2F and p53: Proapoptotic cofactors of p53 are transcriptionally upregulated by E2F.* **Cell Death Differ** 2005, 12:377-383

654. Gregory GP, Hogg SJ, Kats LM, Vidacs E, Baker AJ, Gilan O, Lefebure M, Martin BP, Dawson MA, Johnstone RW, et al., *CDK9 inhibition by dinaciclib potently suppresses Mcl-1 to induce durable apoptotic responses in aggressive MYC-driven B-cell lymphoma in vivo.* **Leukemia** 2015, 29:1437-1441

655. Boffo S, Damato A, Alfano L, Giordano A, *CDK9 inhibitors in acute myeloid leukemia.* **J Exp Clin Cancer Res** 2018, 37

656. Shan B, Zhuo Y, Chin D, Morris CA, Morris GF, Lasky JA, *Cyclin-dependent Kinase 9 Is Required for Tumor Necrosis Factor-α-stimulated Matrix Metalloproteinase-9 Expression in Human Lung Adenocarcinoma Cells.* **J Biol Chem** 2005, 280:1103-1111

657. Sengupta S, Biarnes MC, Jordan VC, *Cyclin dependent kinase-9 mediated transcriptional de-regulation of cMYC as a critical determinant of endocrine-therapy resistance in breast cancers.* **Breast Cancer Res Treat** 2014, 143:113-124

658. Rahaman MH, Kumarasiri M, Mekonnen LB, Yu M, Diab S, Albrecht H, Milne RW, Wang S, *Targeting CDK9: A promising therapeutic opportunity in prostate cancer.* **Endocr Relat** 2016, 23:T211-T226

659. Abdullah C, Wang X, Becker D, *Expression analysis and molecular targeting of cyclin-dependent kinases in advanced melanoma.* **Cell Cycle** 2011, 10:977-988

660. Kanazawa S, Soucek L, Evan G, Okamoto T, Peterlin BM, *c-Myc recruits P-TEFb for transcription, cellular proliferation and apoptosis.* **Oncogene** 2003, 22:5707-5711

661. Gargano B, Amente S, Majello B, Lania L, *P-TEFb is a crucial co-factor for Myc transactivation.* **Cell Cycle** 2007, 6:2031-2037

662. Cowling VH, Cole MD, *The Myc transactivation domain promotes global phosphorylation of the RNA polymerase II carboxy-terminal domain independently of direct DNA binding.* **Mol Cell Biol** 2007, 27:2059-2073

663. Parry D, Guzi T, Shanahan F, Davis N, Prabhavalkar D, Wiswell D, Seghezzi W, Paruch K, Dwyer MP, Doll R, *Dinaciclib (SCH 727965), a Novel and Potent Cyclin-Dependent Kinase InhibitorSCH 727965 CDK Inhibitor.* **Mol Cancer Ther** 2010, 9:2344-2353

664. Murphy AG, Zahurak M, Shah M, Weekes CD, Hansen A, Siu LL, Spreafico A, LoConte N, Anders NM, Miles T, *A Phase I Study of Dinaciclib in Combination With MK-2206 in Patients With Advanced Pancreatic Cancer.* **Clin Transl Sci** 2020, 13:1178-1188

665. Chien AJ, Gliwa AS, Rahmaputri S, Dittrich HF, Majure MC, Rugo HS, Melisko ME, Munster PN, Park JW, Moasser MM, *A phase Ib trial of the cyclin-dependent kinase inhibitor dinaciclib (dina) in combination with pembrolizumab (P) in patients with advanced triple-negative breast cancer (TNBC) and response correlation with MYC-overexpression.* **J Clin Oncol** 2020, 38:1076-1076

666. Zhang H, Chu T, Zheng J, Teng Y, Ma R, Zou L, Zhao H, *Sensitization of cervical cancer cells to radiation by the cyclin-dependent kinase inhibitor dinaciclib.* **Med Oncol** 2022, 40:68

667. Cai Q, Medeiros LJ, Xu X, Young KH, *MYC-driven aggressive B-cell lymphomas: Biology, entity, differential diagnosis and clinical management.* **Oncotarget** 2015, 6

668. Savage KJ, Johnson NA, Ben-Neriah S, Connors JM, Sehn LH, Farinha P, Horsman DE, Gascoyne RD, *MYC gene rearrangements are associated with a poor prognosis in diffuse large B-cell lymphoma patients treated with R-CHOP chemotherapy.* **Blood** 2009, 114:3533-3537

669. Klapproth K, Wirth T, *Advances in the understanding of MYC-induced lymphomagenesis.* **Br J Haematol** 2010, 149:484-97

670. Ott G, Rosenwald A, Campo E, *Understanding MYC-driven aggressive B-cell lymphomas: Pathogenesis and classification.* **Blood** 2013, 122:3884-91

10 Appendix

10.1 List of figures

10.2 List of tables

10.3 Licensing and Copyright

10.3.1 This dissertation

Schmitt, Laura (2023) *Elimination of chemotherapeutic-resistant tumors by natural product-induced cell death*. Heinrich Heine University, Düsseldorf.

10.3.2 Publications within this dissertation

1.) The mycotoxin viriditoxin induces leukemia- and lymphoma-specific apoptosis by targeting mitochondrial metabolism

Stuhldreier F*, **Schmitt L***, Lenz T, Hinxlage I, Zimmermann M, Wollnitzke P, Schliehe-Diecks J, Liu Y, Jäger P, Geyh S, Teusch N, Peter C, Bhatia S, Haas R, Levkau B, Reichert A, Stühler K, Proksch P, Stork B, Wesselborg S. The mycotoxin viriditoxin induces leukemia- and lymphoma-specific apoptosis by targeting mitochondrial metabolism. *Cell Death and Disease*. 2022, *equally contributing first authors, doi: 10.1038/s41419-022-05356-w

2.) Years of research on polybrominated diphenyl ethers (PBDEs) – A historical overview and newest data of a promising anticancer drug

Schmitt L, Hinxlage I, A Cea P, Gohlke H, Wesselborg S. 40 Years of research on polybrominated diphenyl ethers (PBDEs) – A historical overview and newest data of a promising anticancer drug. *Molecules*. 2021, doi: 10.3390/molecules26040995

10.3.3 Figures created with BioRender.com

Confirmation of publication and licensing rights given by Science Suite Inc. (49 Spadina Ave. Suite 2000, Toronto ON M5V 2J1 Canada)

It has been confrmed that Laura Schmitt has been granted a license to use the BioRender content, including icons, templates and other original artwork, appearing in the figures listed in her dissertation in **Table 15** (**10.1 List of figures** comprising Figures 1-11, 41 and 42) completed to BioRender's Academic License Terms. This license permits BioRender content to be sublicensed for use in journal publications. All rights and ownership of BioRender content are reserved by BioRender. All completed graphics are accompanied by the following citation: “Created with BioRender.com”.

Table 15 List of figures that were created with BioRender.com for this dissertation. Shown is the number and the respective confirmation of publication and licensing as depicted by an individual agreement number.

Figure number	Agreement number
Figure 1	FK259PHU28
Figure 2	TS259PJCAQ
Figure 3	OQ259PKJIU
Figure 4	SN259PQ9YD
Figure 5	SM259PQTHY
Figure 6	HG259PRH0E
Figure 7	NI259PRV7D
Figure 8	CP259PS761
Figure 9	OI259PTLJB
Figure 10	QD259PUAB7
Figure 11	CV259PUJ92
Figure 42	WQ259Q6T0T
Figure 42	EG25A46FMN

11 Danksagung

Das Titelblatt trägt meinen Namen, es waren jedoch viele Personen am Entstehen dieser Dissertation beteiligt, denen ich an dieser Stelle danken möchte. Ohne deren Unterstützung hätte sie in dieser Form nicht realisiert werden können. Für die vielfältig erfahrene Hilfe möchte ich mich an dieser Stelle sehr herzlich bedanken.

Einen besonderen Dank möchte ich meinem Doktorvater Prof. Dr. Sebastian Wesselborg aussprechen. Er hat meine Forschungsprojekte mit fortwährendem Interesse und großem Engagement unterstützt. Ich danke ihm für sein stets offenes Ohr, für die kritischen und konstruktiven Diskussionen, die vertrauensvolle Betreuung, sowie die kontinuierliche Förderung meiner fachlichen Weiterbildung und die Ermutigung zur akademischen Karriere.
Gleichermaßen danke ich ebenso Prof. Dr. Gerhard Fritz, der meine Doktorarbeit als zweiter Gutachter betreut hat, für die spannenden und bereichernden Besprechungen.

Für vielfältige methodische Unterstützung im Rahmen gemeinsamer Kooperationen oder Laborrotationen bedanke ich mich bei Thomas Lenz, Dr. Philipp Wollnitzke, Dr. Xabier Buqué, Pablo Cea-Medina, André Wolsing und Lena Schumacher.
Mein Dank gilt auch Dr. Martina Holz und dem Graduiertenkolleg 2158, welches meine wissenschaftliche Laufbahn während des PhD, im Rahmen zahlreicher Veranstaltungen, Konferenzen sowie eines Auslandsaufenthaltes maßgeblich unterstützt und geformt hat.

Des Weiteren danke ich den Mitgliedern des Instituts für Molekulare Medizin I. Mein besonderer Dank gilt meinen Kolleginnen Ilka Hinxlage, Lea Esser, Karina Krings, Julia Hoppe, Seda Akgün und Céline David, die mit ihrer Warmherzigkeit und Fürsorglichkeit sowie den zahlreichen fachlichen Diskussionen einen erheblichen Beitrag zu der angenehmen Arbeitsatmosphäre beigetragen haben. Ich empfinde es als großes Privileg die Zeit der Dissertation mit Kolleginnen, die zu Freundinnen wurden, verbracht zu haben.

Mein besonderer Dank gilt schließlich meiner besten Freundin Sara und vor allem meinem Freund Chris, die mich beide mit ihrem Zuspruch, Verständnis und vor allem mit ihrem Rückhalt unterstützt haben.

Der größte Dank gebührt jedoch meiner Familie, meinen Eltern Bernd und Barbara Schmitt und meinem Bruder Sebastian, die immer an mich geglaubt haben und ohne deren unermüdliche Unterstützung die vorliegende Dissertation nicht möglich gewesen wäre.

Euch ist diese Dissertation gewidmet.